# Analysis of Piled Rafts by the Program *ELPLA*

**2017**

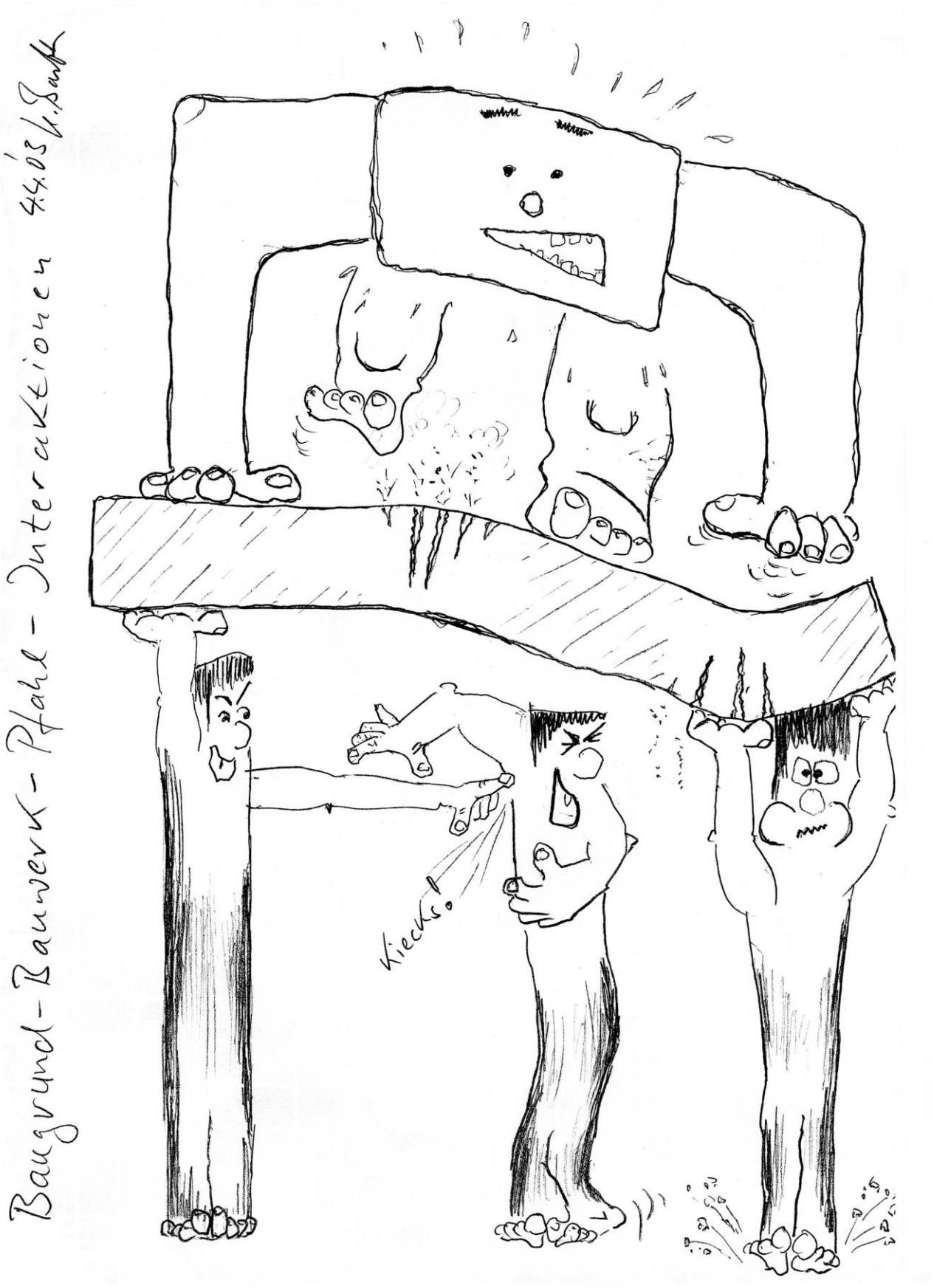
Baugrund - Bauwerk - Pfahl - Interaktionen 4.4.03 V. Sauth
Kiecks!

## Analysis of Piled Rafts

### Preface

Today, nearly every engineering office has its own computer programs for the analysis and design of piled rafts. Furthermore, most of the available programs under Windows are user-friendly and give very excellent output graphics with colors. Consequently, theoretically a secretary not an engineer can use them. But the problem here is how can man control the data and check the results.

The purpose of this book is to present methods, equations, procedures and techniques used in the formulation of the computer analysis of piled rafts. These items are coded in the program *ELPLA*.

This book contains many practical problems which are analyzed in details by using the program *ELPLA*. It is important for the engineer to be familiar with this information when carrying out computer analysis of piled rafts. An understanding of these concepts will be of great benefit in carrying out the computer analysis, resolving difficulties and judging the acceptability of the results. Three familiar types of subsoil models (standard models) for piled raft analyses are considered. The models are Simple Assumption Model, *Winkler*'s Model and Continuum Model. In the analysis, rafts are treated as elastic or rigid. In this book the Finite Element-Method was used to analyze the raft, in which plate bending elements represent the raft according to the two-dimensional nature of foundation. The development of the finite element equations for plate elements is well documented in standard textbooks such as *Schwarz* (1984) and *Zienkiewicz/ Cheung* (1970). Therefore, it is not duplicated in this book.

Program authors: *M. El Gendy*
*A. El Gendy*


GEOTEC Software Inc.
PO Box 14001 Richmond Road PO, Calgary AB, Canada T3E 7Y7
Tele.:+1(587) 332-3323
geotec@geotecsoftware.com
www.geotecsoftware.com

# Chapter 1

# Models for analyzing piled raft

Table of contents Page

**1 Models for analyzing piled raft** 1- 3

1.1 Introduction 1- 3

1.2 Description of the numerical calculation methods 1- 4
1.2.1 Linear contact pressure - Simple assumption model (method 1) 1- 6
1.2.2 Modulus of subgrade reaction - Winkler's model (methods 2 and 3) 1- 8
1.2.3 Modulus of compressibility method - Continuum model (methods 4 to 9) 1-11

1.3 Test example: Verifying forces in piles of a pile group 1-12
1.3.1 Description of the problem 1-12
1.3.2 Hand calculation of pile forces 1-13
1.3.3 Pile forces by *ELPLA* 1-15

1.4 References 1-17

# 1 Models for analyzing piled raft

## 1.1 Introduction

This chapter describes the most common practical models used in the analysis of foundations. Piled raft is a raft on piles that transmits its loads to the soil. It must include often considerable moments and forces. In times, when there no computers were available, simplified methods were used considering as low as possible computation effort to receive the results with acceptable accuracy. The computers whose programming and memory possibilities are developed increasingly caused a revolution of the calculation practice. Now the programming and extensive computation effort can expand considerably to achieve the results as perfect as possible to the reality. These methods are considered particularly for the analysis of mostly deformation-sensitive large structures.

The subsoil models for analysis of pile foundation (standard models) can be divided into three main groups:

A Simple assumption model
B *Winkler*'s model
C Continuum model

Simple assumption model does not consider the interaction between the foundation and the soil. The model assumes a linear distribution of contact pressures beneath the foundation. *Winkler*'s model is the oldest and simplest one that considers the interaction between the foundation and the soil. The model represents the soil or piles as elastic springs. Continuum model is the complicated one. The model considers also the interaction between all foundation elements and soil. It represents the soil as a layered continuum medium or isotropic elastic half-space soil medium.

Although Continuum model provides a better physical representation of the supporting soil, it has remained unfamiliar, because of its mathematical difficulties where an application of this model requires extensive calculations. Practical application for this model is only possible if a computer program or appropriate tables or charts are available. These tables and charts are limited to certain problems.

For this purpose, a general computerized mathematical solution based on Finite elements-method was developed to represent an analysis for pile foundations on the real subsoil model. The solution can analyze foundations of any shape considering holes within the foundation and the interaction of external foundations. This mathematical solution is coded in the program *ELPLA*. The developed computer program *ELPLA* also can analyze different types of subsoil models, especially the three-dimensional Continuum model that considers any number of irregular layers.

In this book, the three standard soil models are described through 9 different numerical calculation methods. The methods graduate from the simplest one to the more complicated one covering the analysis of most common pile foundation problems that may be found in the practice.

## 1.2 Description of the numerical calculation methods

According to the three standard soil models (simple assumption model, *Winkler*'s model, Continuum model), nine numerical calculation methods are considered to analyze the raft as shown in Figure 1-1 und Table 1-1.

Table 1-1 Numerical calculation methods

| Method No. | Method |
|---|---|
| 1 | Linear contact pressure<br>(Simple assumption model) |
| 2 | Constant modulus of subgrade reaction<br>(*Winkler*'s model) |
| 3 | Variable modulus of subgrade reaction<br>(*Winkler*'s model) |
| 4 | Modification of modulus of subgrade reaction by iteration<br>(*Winkler*'s model/ Continuum model) |
| 5 | Modulus of compressibility method for elastic raft on half-space soil medium (Isotopic elastic half-space soil medium - Continuum model) |
| 6 | Modulus of compressibility method for elastic raft on layered soil medium<br>(Solving system of linear equations by iteration)<br>(Layered soil medium - Continuum model) |
| 7 | Modulus of compressibility method for elastic raft on layered soil medium<br>(Solving system of linear equations by elimination)<br>(Layered soil medium - Continuum model) |
| 8 | Modulus of compressibility method for rigid piled raft on layered soil medium<br>(Layered soil medium - Continuum model) |
| 9 | Modulus of compressibility method for rigid free-standing piled raft on layered soil medium<br>(Layered soil medium - Continuum model)<br>(elastische Schichten - Kontinuummodell) |

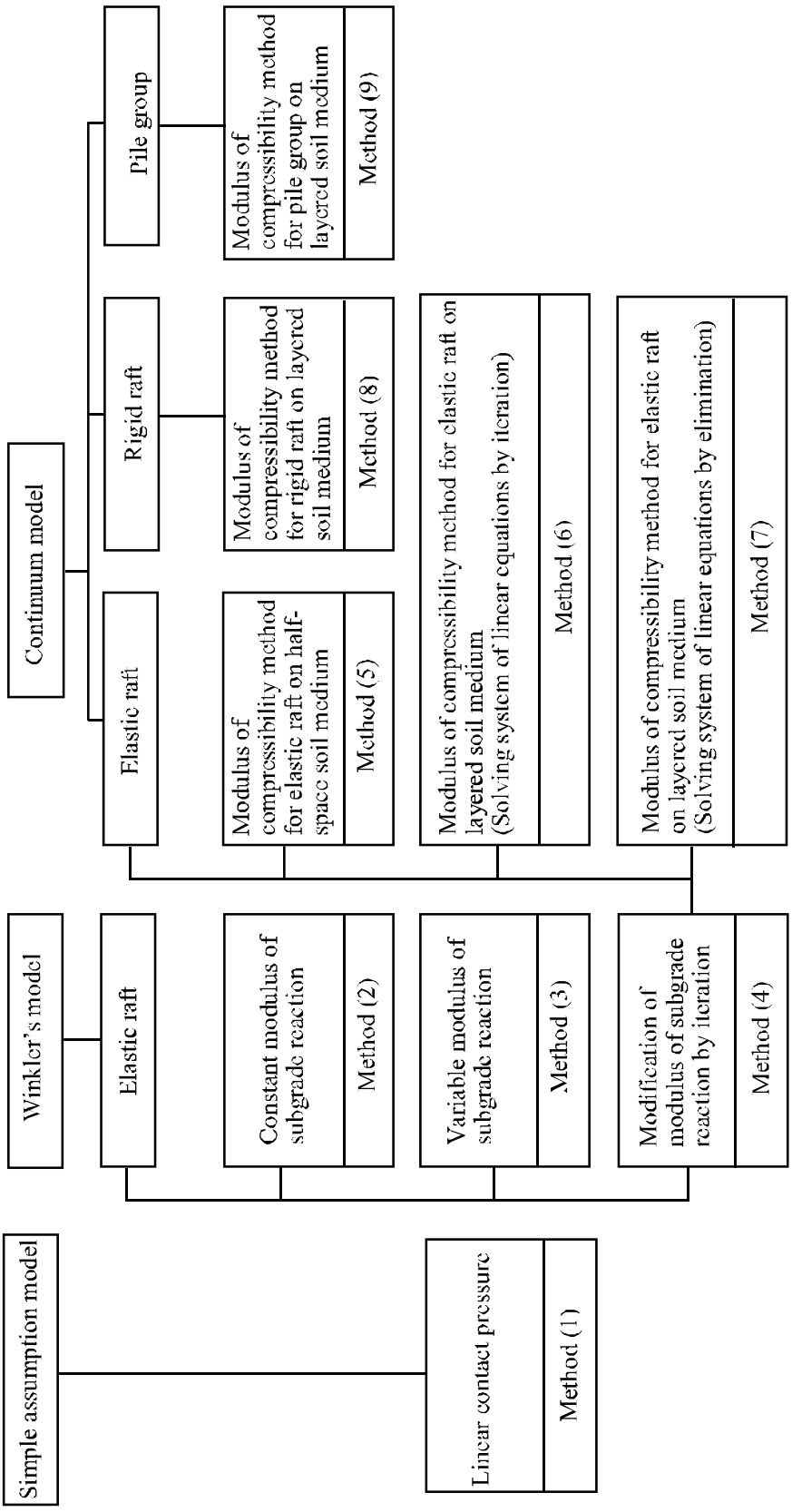


Figure 1-1 Numerical calculation methods of rafts (methods 1 to 9) in program *ELPLA*

Today, the Finite elements-method is the most powerful procedure available in many complex problems. It can be applied to nearly all engineering problems, especially in structure analysis problems. In this book, the Finite elements-method is used to analyze the raft for all numerical calculation methods except Modulus of compressibility method for rigid piled raft on layered soil medium (method 8), which does not obey the elasticity rules. In the Finite elements-analysis, the raft is represented by rectangular plate bending elements according to the two dimensional nature of foundation. Each node of plate or grid elements has three degrees of freedom, vertical displacement $w$ and two rotations $\theta_x$ and $\theta_y$ about $x$- and $y$-axis, respectively. The development of the finite element equations is well documented in standard textbooks. Therefore, it is not duplicated in this book. The reader can see as an example that of *Zienkiewicz/ Cheung* (1970) or *Schwarz* (1984) for further information on the development of finite element equations.

To formulate the equations of the numerical calculation methods both the raft and the contact area of the supporting medium are divided into rectangular or triangular elements. Compatibility between the raft, piles and the soil medium in vertical direction is considered for all methods except Linear contact pressure method (method 1). The fundamental formulation of equilibrium equation for the raft can be described in general form through the following Eq. (1.1):

$$[k_p]\{\delta\} = \{F\} \tag{1.1}$$

where the vector of forces $\{F\}$ contains the action and reaction forces acting on the raft. In principle for all calculation methods, the action forces are known and equal to the applied forces on the raft, while the reaction forces (contact forces) are required to be found according to each soil model.

According to subsoil models (Simple assumption model, *Winkler*'s model, Continuum model), 9 numerical calculation methods are considered to find the contact pressures, and hence to analyze the raft. The next pages describe the interaction between the raft and subsoil medium in these methods.

### 1.2.1 Linear contact pressure - Simple assumption model (method 1)

This method is the simplest one for determination of the pile forces. The assumption of this method is that there is no compatibility between the pile foundation deflection and the soil settlement. In the method, it is assumed that pile forces are distributed linearly on the bottom of the raft (statically determined) as shown in Figure 1-12, in which the resultant of soil reactions coincides with the resultant of applied loads.

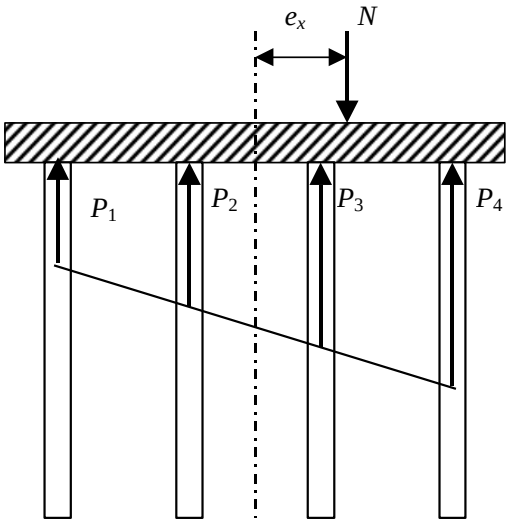


Figure 1-2 Pile force distribution for Simple assumption model

In the general case of a foundation with an arbitrary unsymmetrical shape and loading with $M_x$ and $M_y$, based on *Navier's* solution the pile force $P_i$ at any point $i$ from the geometry centroid on the bottom of the foundation is given by:

$$P_i = \frac{N}{n} + \frac{M_y I_x - M_x I_{xy}}{I_x I_y - I_{xy^2}} x_i + \frac{M_x I_y - M_y I_{xy}}{I_x I_y - I_{xy^2}} y_i \tag{1.2}$$

where $I_x = \sum_1^n y_i^2$, $I_y = \sum_1^n x_i^2$ und $I_{xy} = \sum_1^n x_i \; y_i$

and:

| | |
|---|---|
| $P_i$ | Force in pile $i$ [kN] |
| $N$ | Sum of all vertical applied loads on the pile cap [kN] |
| $x_i$ | Coordinate of pile $i$ from the centroidal axis $x$ [m] |
| $y_i$ | Coordinate of pile $i$ from the centroidal axis $y$ [m] |
| $M_x$ | Moment due to $N$ about the $x$-axis, $M_x = N\, e_y$ [kN.m] |
| $M_y$ | Moment due to $N$ about the $y$-axis, $M_y = N\, e_x$ [kN.m] |
| $e_x$ | Eccentricity measured from the centroidal axis $x$ [m] |
| $e_y$ | Eccentricity measured from the centroidal axis $y$ [m] |
| $n$ | Number of piles under the pile cap [-] |

For a foundation of rectangular shape, there are two axes of symmetry and $I_{xy} = 0$. Therefore, the pile force $P_i$ of Eq. (1.2) reduces to:

$$P_i = \frac{N}{n} + \frac{M_y}{I_y} x_i + \frac{M_x}{I_x} y_i \tag{1.3}$$

For strip pile foundation, the pile forces can be obtained from:

$$P_i = \frac{N}{n} + \frac{M_y}{I_y} x_i \tag{1.4}$$

while for a foundation without moments or without eccentricity about both axes the pile force $P_i$ will be uniform under the foundation and is given by:

$$P_i = \frac{N}{n} \tag{1.5}$$

#### *1.2.1.1 System of equations of Linear contact pressure method*

The foundation can be analyzed by working out the soil reactions at the different nodal points of the Finite elements-mesh. This is done by obtaining the pile force $P_i$ from Eq. (1.2).

Considering the entire foundation, the foundation will deflect under the action of the total external forces $\{F\}$ due to known applied loads $\{P\}$ and the known soil reactions $\{Q\}$, where:

$$\{F\} = \{P\} - \{Q\} \tag{1.6}$$

The equilibrium of the system is expressed by the following matrix equation:

$$[k_p]\{\delta\} = \{P\} - \{Q\} \tag{1.7}$$

where:
$\{Q\}$ Vector of pile forces
$\{P\}$ Load vector from applied forces and moments on the foundation
$\{\delta\}$ Deformation vector
$[k_p]$ Plate stiffness matrix

#### *1.2.1.2 Equation solver of Linear contact pressure method*

As the plate stiffness matrix $[k_p]$ in Equation (1.7) is a diagonal matrix, the system of linear equations (1.7) is solved by Banded coefficients-technique. The unknown variables are the nodal displacements $w_i$ and the nodal rotations $\theta_{xi}$ and $\theta_{yi}$ about the *x*- and *y*-directions.

### 1.2.2 Modulus of subgrade reaction-Winkler's model (methods 2 and 3)

The oldest method for the analysis of foundation on elastic medium is the modulus of subgrade reaction, which was proposed by *Winkler* (1867). The assumption of this method is that the soil model or piles are represented by elastic springs as shown in Figure 1-3 according to *Poulos* (1994). The settlement $s_i$ of the soil medium or the pile at any point *i* on the surface are directly proportional to the contact force or pile reaction $Q_i$.

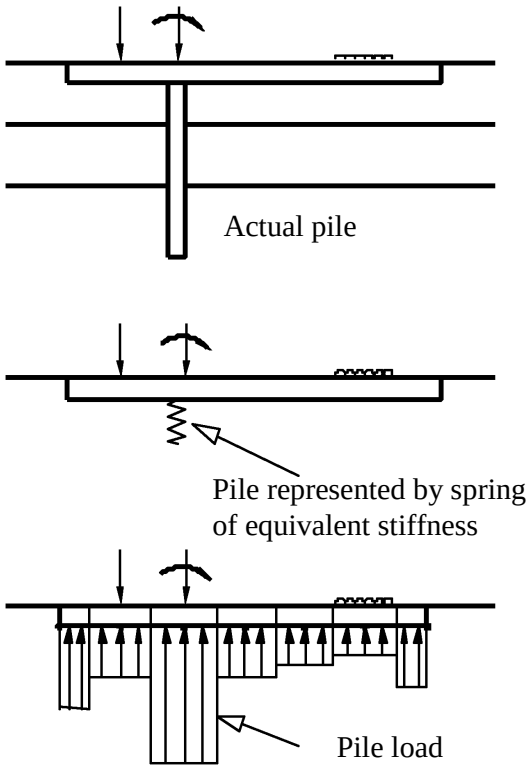


Figure 1-3 Simplified representation of pile for *Winkler's model* after *Poulos* (1994)

### *1.2.2.1 System of equations of Modulus of subgrade reaction*

For a node *i* on the Finite elements-mesh, the contact force or the pile reaction $Q_i$ is given by:

$$Q_i = k_i \, s_i \tag{1.8}$$

where:
$Q_i$ Contact force or the pile reaction on a node *i* [kN]
$k_i$ Soil stiffness or pile stiffness at node *i* [kN/m]

Considering the entire foundation, Eq. (1.8) can be rewritten in matrix form as:

$$\begin{Bmatrix} Q_1 \\ Q_2 \\ Q_3 \\ \dots \\ \dots \\ Q_n \end{Bmatrix} = \begin{bmatrix} k_1 & 0 & 0 & \dots & \dots & 0 \\ 0 & k_2 & 0 & \dots & \dots & 0 \\ 0 & 0 & k_3 & \dots & \dots & 0 \\ \dots & \dots & \dots & \dots & \dots & \dots \\ \dots & \dots & \dots & \dots & \dots & \dots \\ 0 & 0 & 0 & \dots & \dots & k_n \end{bmatrix} \begin{Bmatrix} s_1 \\ s_2 \\ s_3 \\ \dots \\ \dots \\ s_n \end{Bmatrix} \tag{1.9}$$

Eq. (1.9) is rewritten in a simple form as:

$$\{Q\} = [k_s]\{s\} \tag{1.10}$$

where:
$\{Q\}$ Vector of contact forces and pile reactions
$\{s\}$ Settlement vector
$[k_s]$ Stiffness matrix of the soil and piles

The foundation will deflect under the action of the total external forces $\{F\}$ due to known applied loads $\{P\}$ and the unknown soil reactions $\{Q\}$, where:

$$\{F\} = \{P\} - \{Q\} \tag{1.11}$$

The equilibrium of the raft-pile-soil system is expressed by the following matrix equation:

$$[k_p]\{\delta\} = \{P\} - \{Q\} \tag{1.12}$$

Eq. (1.10) for *Winkler's* model can be substituted into Eq. (1.12) as:

$$[k_p]\{\delta\} = \{P\} - [k_s]\{s\} \tag{1.13}$$

Considering the compatibility of deformation between the plate and the soil medium, where the soil settlement $s_i$ is equal to the plate deflection $w_i$, Eq. (1.13) becomes:

$$[[k_p] + [k_s]]\{\delta\} = \{P\} \tag{1.14}$$

Equation (1.14) shows that the stiffness matrix of the whole raft-pile-soil system is the sum of the plate and the soil stiffness matrices, $[k_p] + [k_s]$.

#### *1.2.2.2 Equation solver of Modulus of subgrade reaction*

It should be noticed that the soil stiffness matrix $[k_s]$ is a purely diagonal matrix for *Winkler's* model (methods 2 and 3). Therefore, the total stiffness matrix for the plate and the soil is a banded matrix. Then, the system of linear equations (1.14) is solved by Banded coefficients-technique. Since the total stiffness matrix is a banded matrix, the equation solver (1.14) takes short computation time by applying these methods 2 and 3.

The unknown variables in Eq. (1.14) are the nodal displacements $w_i$ ($w_i = s_i$) and the nodal rotations $\theta_{xi}$ and $\theta_{yi}$ about *x*- and *y*-directions. After solving the system of linear equation (1.14), substituting the obtained settlements $s_i$ in Eq. (1.10), gives the unknown contact forces and pile reactions $Q_i$.

### 1.2.3 Modulus of compressibility method - Continuum model (methods 4 to 9)

Continuum model was first proposed by *Ohde* (1942), which based on the settlement will occur not only under the loaded area but also outside. Otherwise, the settlement at any nodal point is affected by the forces at all the other nodal points. Figure 1-4 shows Continuum model applied for pile foundation according to *Liang*/ *Chen* (2004).

Continuum model assumes continuum behavior of the soil, where the soil is represented as isotropic elastic half-space medium or layered medium. Consequently, this model overcomes the assumption of *Winkler's* model, which does not take into account the interaction between the different points of the soil medium. Representation of soil as a continuum medium is more accurate as it realized the interaction among the different points of the continuum medium. However, it needs mathematical analysis that is more complex.

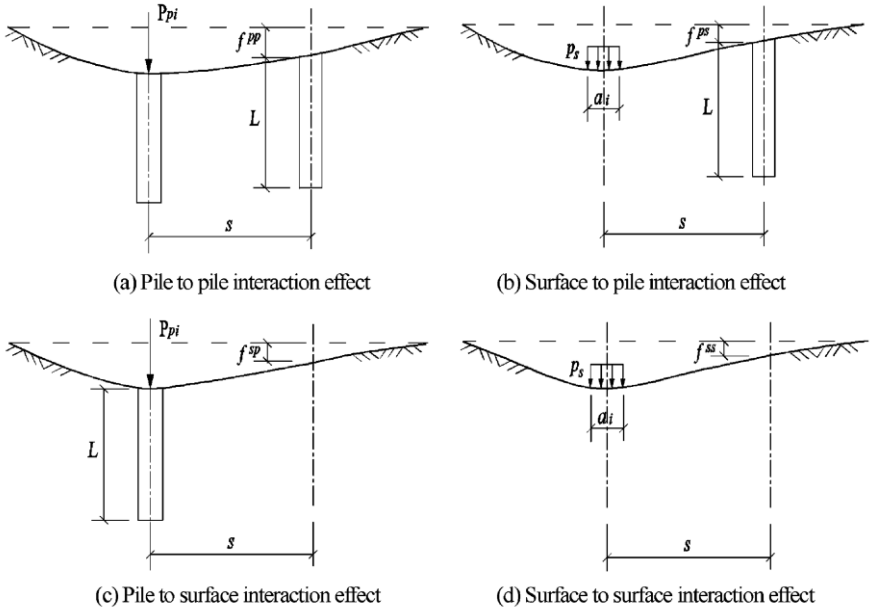


Figure 1-4 Continuum model after *Liang*/ *Chen* (2004)

#### *1.2.3.1 Methods for analyzing piled raft for Continuum model*

The behavior of the pile-soil system can be examined by considering linearly or nonlinearly analysis according to the following three different methods:

- **L**inear analysis of **p**iled **r**aft, termed LPR
- **N**onlinear analysis of **p**iled **r**aft using **h**yperbolic function, termed NPRH
- **N**onlinear analysis of **p**iled **r**aft using **D**IN 4014, termed NPRD

The next chapters describe methods for analyzing piled raft for Continuum model.

## 1.3 Test example: Verifying forces in piles of a pile group

The numerical modeling described in this chapter was implemented in the program *ELPLA*. To verify and evaluate the numerical modeling, a comparison was carried out, in which results from *ELPLA* were compared with those from existing methods of analysis.

### 1.3.1 Description of the problem

To verify the mathematical model of *ELPLA* for determining pile forces of pile groups under a pile cap, results of a pile group obtained by *Bakhoum* (1992), Example 5.19, page 592 are compared with those obtained by *ELPLA*.

A pile cap on 24 vertical piles is considered as shown in Figure 1-5. It is required to determine the force in each pile of the group due to a vertical load of $N$ = 8000 [kN] acting on the pile cap with eccentricities $e_x$ = 1.4 [m] and $e_y$ = 1.8 [m] in both $x$- and $y$-directions.

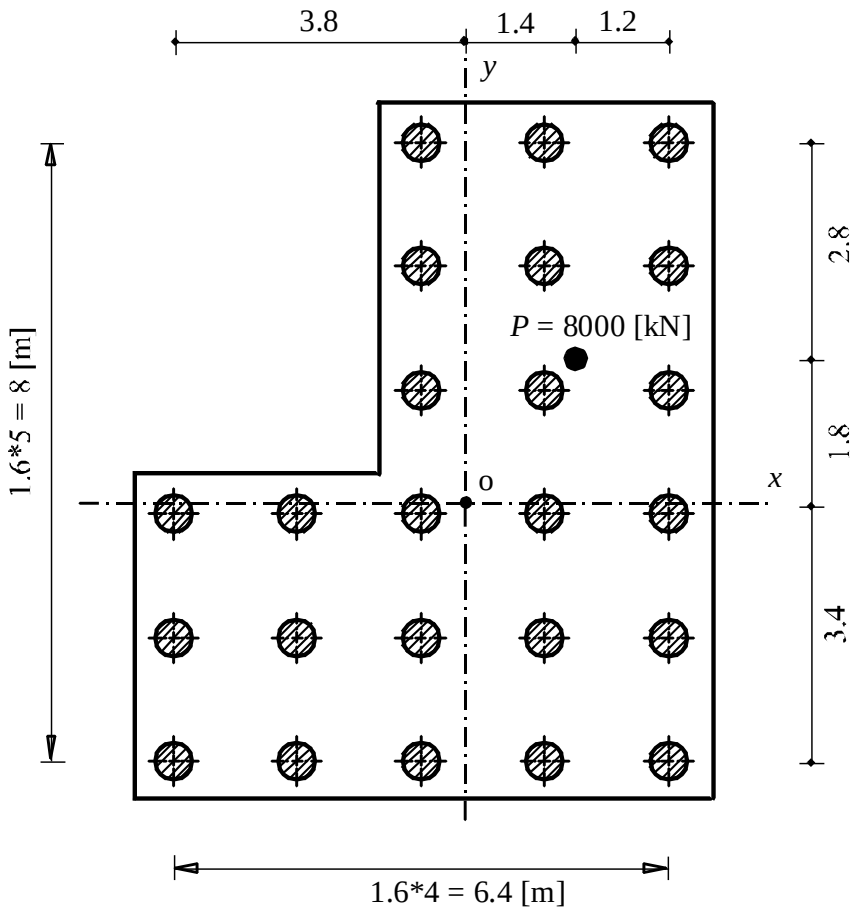


Figure 1-5 Pile cap dimensions and pile arrangements

### 1.3.2 Hand calculation of pile forces

According to *Bakhoum* (1992), the force in each pile in the pile group can be obtained by hand calculation as follows:

**Step 1: Compute moments**

$$M_x = 8000 * 1.8 = 14400\,[\text{kN.m}]$$
$$M_y = 8000 * 1.4 = 11200\,[\text{kN.m}] \qquad (1.15)$$

**Step 2: Compute properties $I_x$, $I_y$ and $I_{xy}$**

Determining properties of $I_x$, $I_y$ and $I_{xy}$ are listed in Table 1-2.

Table 1-2 Properties $I_x$, $I_y$ and $I_{xy}$

| Pile number | $x_i$ [m] | $y_i$ [m] | $x_i^2$ [m$^2$] | $y_i^2$ [m$^2$] | $x_i\, y_i$ [m$^2$] |
|---|---|---|---|---|---|
| 1 | -3.8 | -3.4 | 14.44 | 11.56 | 12.92 |
| 2 | -2.2 | -3.4 | 4.84 | 11.56 | 7.48 |
| 3 | -0.6 | -3.4 | 0.36 | 11.56 | 2.04 |
| 4 | 1.0 | -3.4 | 1.00 | 11.56 | -3.40 |
| 5 | 2.6 | -3.4 | 6.76 | 11.56 | -8.84 |
| 6 | -3.8 | -1.8 | 14.44 | 3.24 | 6.84 |
| 7 | -2.2 | -1.8 | 4.84 | 3.24 | 3.96 |
| 8 | -0.6 | -1.8 | 0.36 | 3.24 | 1.08 |
| 9 | 1.0 | -1.8 | 1.00 | 3.24 | -1.08 |
| 10 | 2.6 | -1.8 | 6.76 | 3.24 | -4.68 |
| 11 | -3.8 | -0.2 | 14.44 | 0.04 | 0.76 |
| 12 | -2.2 | -0.2 | 4.84 | 0.04 | 0.44 |
| 13 | -0.6 | -0.2 | 0.36 | 0.04 | 0.12 |
| 14 | 1.0 | -0.2 | 1.00 | 0.04 | -0.20 |
| 15 | 2.6 | -0.2 | 6.76 | 0.04 | -0.52 |
| 16 | -0.6 | 1.4 | 0.36 | 1.96 | -0.84 |
| 17 | 1.0 | 1.4 | 1.00 | 1.96 | 1.40 |
| 18 | 2.6 | 1.4 | 6.76 | 1.96 | 3.64 |
| 19 | -0.6 | 3.0 | 0.36 | 9.00 | -1.80 |
| 20 | 1.0 | 3.0 | 1.00 | 9.00 | 3.00 |
| 21 | 2.6 | 3.0 | 6.76 | 9.00 | 7.80 |
| 22 | -0.6 | 4.6 | 0.36 | 21.16 | -2.76 |
| 23 | 1.0 | 4.6 | 1.00 | 21.16 | 4.60 |
| 24 | 2.6 | 4.6 | 6.76 | 21.16 | 11.96 |
| 3 | | | $I_y$ = 106.56 | $I_x$ = 170.56 | $I_{xy}$ = 43.2 |

**Step 3: Compute pile force**

The force $P_i$ in any pile $i$ at location ($x_i$, $y_i$) from the geometry centroid is obtained from:

$$P_i = \frac{N}{n} + \frac{M_y I_x - M_x I_{xy}}{I_x I_y - I_{xy}^2} x_i + \frac{M_x I_y - M_y I_{xy}}{I_x I_y - I_{xy}^2} y_i$$

$$P_i = \frac{8000}{24} + \frac{(11200)(170.56) - (14400)(43.2)}{(170.56)(106.56) - (43.2)^2} x_i + \frac{(14400)(106.56) - (11200)(43.2)}{(170.56)(106.56) - (43.2)^2} y_i \qquad (1.16)$$

$$P_i = 333.333 + 78.988\, x_i + 64.421\, y_i$$

### 1.3.3 Pile forces by *ELPLA*

The available method "Linear Contact pressure 1" in *ELPLA* is used to determine the force in each pile in the pile group. A net of equal square elements is chosen. Each element has a side of 1.6 [m]. The pile forces obtained by *ELPLA* are compared with those obtained by *Bakhoum* (1992) in Table 1-3. It is obviously from this table that pile forces obtained by *ELPLA* are equal to those obtained by hand calculation.

Table 1-3 Comparison of pile forces obtained by *ELPLA* and those of *Bakhoum* (1992)

| Pile number | *Bakhoum* (1992) | | | | | | *ELPLA* |
|---|---|---|---|---|---|---|---|
| | $x_i$ [m] | $y_i$ [m] | $N/n$ [kN] | 78.988 $x_i$ [kN] | 64.421 $y_i$ [kN] | $P_i$ [kN] | $P_i$ [kN] |
| 1 | -3.8 | -3.4 | 333.33 | -300.16 | -219.03 | -185.86 | -185.85 |
| 2 | -2.2 | -3.4 | 333.33 | -173.77 | -219.03 | -59.47 | -59.47 |
| 3 | -0.6 | -3.4 | 333.33 | -47.39 | -219.03 | 66.91 | 66.91 |
| 4 | 1.0 | -3.4 | 333.33 | 78.99 | -219.03 | 193.29 | 193.29 |
| 5 | 2.6 | -3.4 | 333.33 | 205.37 | -219.03 | 319.67 | 319.67 |
| 6 | -3.8 | -1.8 | 333.33 | -300.16 | -115.96 | -82.79 | -82.78 |
| 7 | -2.2 | -1.8 | 333.33 | -173.77 | -115.96 | 43.50 | 43.60 |
| 8 | -0.6 | -1.8 | 333.33 | -47.39 | -115.96 | 169.98 | 169.98 |
| 9 | 1.0 | -1.8 | 333.33 | 78.99 | -115.96 | 296.36 | 296.36 |
| 10 | 2.6 | -1.8 | 333.33 | 205.37 | -115.96 | 422.74 | 422.72 |
| 11 | -3.8 | -0.2 | 333.33 | -300.16 | -12.88 | 20.29 | 20.29 |
| 12 | -2.2 | -0.2 | 333.33 | -173.77 | -12.88 | 146.68 | 146.67 |
| 13 | -0.6 | -0.2 | 333.33 | -47.39 | -12.88 | 273.06 | 273.06 |
| 14 | 1.0 | -0.2 | 333.33 | 78.99 | -12.88 | 399.44 | 399.44 |
| 15 | 2.6 | -0.2 | 333.33 | 205.37 | -12.88 | 525.82 | 525.82 |
| 16 | -0.6 | 1.4 | 333.33 | -47.39 | 90.19 | 376.13 | 376.13 |
| 17 | 1.0 | 1.4 | 333.33 | 78.99 | 90.19 | 502.51 | 502.51 |
| 18 | 2.6 | 1.4 | 333.33 | 205.37 | 90.19 | 628.89 | 628.89 |
| 19 | -0.6 | 3.0 | 333.33 | -47.39 | 193.26 | 479.20 | 479.20 |
| 20 | 1.0 | 3.0 | 333.33 | 78.99 | 193.26 | 605.58 | 605.59 |
| 21 | 2.6 | 3.0 | 333.33 | 205.37 | 193.26 | 731.96 | 731.97 |
| 22 | -0.6 | 4.6 | 333.33 | -47.39 | 296.34 | 582.28 | 582.28 |
| 23 | 1.0 | 4.6 | 333.33 | 78.99 | 296.34 | 708.66 | 708.66 |
| 24 | 2.6 | 4.6 | 333.33 | 205.37 | 296.34 | 835.04 | 835.04 |

## 1.4 References

[1] *Bakhoum, M.* (1992): Structural Mechanics
Cairo, Egypt

[2] *Liang, F./ Chen, L.* (2004): A modified variational approach for the analysis of piled raft foundation
Mechanics Research Communications 31, 593-604

[3] *Ohde, J.* (1942): Die Berechnung der Sohldruckverteilung unter Gründungskörpern
Der Bauingenieur, Heft 14/16, S. 99 bis 107 - Heft 17/18 S. 122 bis 127

[4] *Poulos, H.* (1994): An Approximation numerical analysis of pile-raft interaction
Int. J. Numer. Anal. Meth. Geomech., 18, 73-92

[5] *Schwarz, H.* (1984): Methode der finiten Elemente
Teubner-Verlag, Stuttgart

[6] *Winkler, E.* (1867): Die Lehre von der Elastizität und Festigkeit
Dominicus, Prag

[7] *Zienkiewicz, O./ Cheung, Y.* (1970): The Finite Element Method in Structural and Continuum Mechanics
McGraw-Hill, England

# Chapter 2

# Numerical modeling single pile, pile groups and piled raft

Table of contents Page

**2 Numerical modeling single pile, pile groups and piled raft** 2- 3

2.1 Introduction 2- 3

2.2 Modeling single pile 2- 5
2.2.1 Soil flexibility for single pile 2- 5
2.2.2 Determining flexibility coefficients 2- 7
2.2.3 Elastic analysis of single pile 2-13
2.2.4 Rigid analysis of single pile 2-14

2.3 Modeling pile groups (free-standing rigid raft) 2-16
2.3.1 Soil stiffness for pile groups 2-16
2.3.2 Analysis of pile groups 2-19

2.4 Modeling piled raft 2-24
2.4.1 Soil stiffness for piled raft 2-24
2.4.2 Analysis of piled flexible raft 2-27
2.4.3 Analysis of piled rigid raft 2-28
2.4.4 Analysis of piled elastic raft 2-29

2.5 Nonlinear analysis 2-30
2.5.1 Nonlinear rigid analysis of single pile 2-30
2.5.2 Nonlinear analysis of pile groups, elastic piled raft and rigid piled raft 2-32
2.5.3 Iterative Procedure 2-32

2.6 Numerical Examples 2-35
2.6.1 Test Example: Evaluation of settlement influence factor $I_1$ for a single pile 2-35
2.6.2 Case study: Piled raft of *Torhaus* 2-38

2.7 References 2-48

# 2 Numerical modeling single pile, pile groups and piled raft

## 2.1 Introduction

Analyzing piled raft is a complex task because it is a three-dimensional problem including many capabilities. The main capabilities that must be considered in the analysis are: the interaction between all piled raft and soil elements, taking into account the actual loading and geometry of the piled raft, representing the soil by a real model and treating the problem as nonlinear analysis. Considering all these capabilities requires great experience and effort. Besides, such a problem requires long computational time where huge size soil matrix is required for a large piled raft due to discretized nodes along piles and under the raft. For this reason many authors suggested simplified methods in recent years to reduce the size of analysis.

*Clancy/* R*andolph* (1993) and (1994) developed the hybrid layer method to reduce the computing effort. *Ta/ Small* (1997) approximated the surface displacement of the soil by a polynomial instead of generating flexibility factors, but the rafts have to be square and of equal size. *Russo* (1998) presented an approximate numerical method for the analysis of piled raft where piles were modeled as interactive linear or non-linear springs. He used the interaction factor method and a preliminary BEM to model pile to pile interaction. *Poulos* (1999) described an approximate analysis for the response of a pile group. The analysis uses a simplified form of boundary element analysis to obtain single pile responses and interaction factors, and employs various simplifying assumptions to facilitate the computational process. *Lee/ Xiao* (2001) presented a simplified analytical method for nonlinear analysis of the behavior of pile groups using a hyperbolic approach to describe the nonlinear relation between the shaft stress and displacement. They developed the method for pile groups under both rigid and flexible pile cap based on the load-transfer function. *Kitiyodom/ Matsumoto* (2002) and (2003) developed a simplified method of numerical analysis of piled raft using a hybrid mode. The raft is modeled as a thin plate, the piles as elastic beams and the soil as springs. *Mendonça/ Paiva* (2003) presented BEM/ FEM formulation for the analysis of piled raft in which each pile is represented by a single element with three nodal points and the shear force along the shaft is approximated by a quadratic function. The soil is considered as half-space medium. *Jeong et al.* (2003) proposed a simple algorithm to analyze laterally loaded three-dimensional pile groups using beam column method. *Liang/ Chen* (2004) presented a modified variational approach for analyzing piled raft by a simplified analytical solution to evaluate the pile-soil interaction. They applied the approach on piled rigid and flexible rafts resting on homogeneous soil. *Wong/ Poulos* (2005) developed approximations for the settlement interaction factors between dissimilar piles via an extensive parametric study. *Lutz et al.* (2006) presented a simple method to estimate the load settlement behavior of piled raft based on the theory of elasticity and solutions for calculation of ultimate limit state. Most of the simplified analyses carried out by the methods mentioned previously approximated the soil model. However, several methods are available for analyzing this complex problem by a full three-dimensional analysis but they are time consuming even for fast computers of today.

In standard methods of analyzing piled raft based on elasticity theory, the entire soil stiffness matrix of the piled raft is assembled due to all elements of piles and raft. Then, settlements of piled raft elements are obtained directly by solving the global equations. Based on elasticity theory *El Gendy* (2007) presented more efficient analysis of single pile, pile group and piled raft by using composed coefficient technique to reduce the size of entire soil stiffness matrix. In the technique, the pile is treated as a rigid member having a uniform settlement on its nodes. This assumption enables to assemble pile coefficients in composed coefficients. It can be easily modeling the nonlinear response of single pile, pile groups or piled raft. The composed coefficient technique makes the size of the soil stiffness matrix of the piled raft equivalent to that of the raft alone without piles. The proposed analysis reduces considerably the number of equations that need to be solved. Raft can be analyzed as flexible, rigid or elastic on continuum soil medium. The advantage of the analysis is that there is no approximation when generating the flexibility coefficients of the soil. In the analysis a full interaction among piled raft elements is taken into account by generating the entire flexibility matrix of the piled raft. Using the composed coefficient technique enables to apply the nonlinear response of the pile by a hyperbolic relation between the load and settlement of the pile. *El Gendy* (2007) introduced also a direct hyperbolic function for nonlinear analysis of a single pile. Besides, an iteration method is developed to solve the system of nonlinear equations of pile groups or piled raft. This chapter presents numerical modeling single pile, pile groups and piled raft according to *El Gendy* (2007).

## 2.2 Modeling single pile

To carry out the analysis, a composed coefficient or modulus *ks* [kN/m] representing the linear soil stiffness of the pile is determined. The modulus *ks* is a parameter used in both linear and nonlinear analysis of the pile. It is defined as the ratio between the applied force on the pile head *Ph* [kN] and the pile settlement *wo* [m]. The modulus *ks* is not a soil constant, it depends on pile load, pile geometry and stratification of the soil. It is analogous to the modulus of subgrade reaction of the raft on *Winkler's* soil medium (*Winkler* (1867)), which is the ratio between the average contact pressure and the settlement under the characteristic point on the raft. This section describes a method to obtain the modulus *ks* from the rigid analysis of the pile.

### 2.2.1 Soil flexibility for single pile

In the analysis, the pile is divided into a number of shaft elements with *m* nodes, each acted upon by a uniform shear stress $qs_j$ [kN/m$^2$] and a circular base having a uniform stress *qb* [kN/m$^2$] as shown in Figure 2-1a. To carry out the analysis, pile shaft elements are represented by line elements as indicated in Figure 2-1b. All stresses acting on shaft elements are replaced by a series of concentrated forces acting on line nodes. The shear force on node *j* may be expressed as:

$$Qs_j = 2\pi r_o \frac{l_{j-1} + l_j}{2} qs_j \tag{2.1}$$

while the force on the pile base may be expressed as:

$$Qb = \pi r_o^2 qb \tag{2.2}$$

where:

| | |
|---|---|
| *j* - 1 and *j* | Node number of element *j* |
| $Qs_j$ | Shear force on node *j* [kN] |
| *Qb* | Force on the base [kN] |
| $r_o$ | Radius of the pile [m] |
| $l_j$ | Length of the element *j* [m] |

To consider the interaction between pile and soil, the soil is represented as layered medium or isotropic elastic half-space medium. Considering a typical node *i* as shown in Figure 2-1b, the settlement $s_i$ of the soil adjacent to the node *i* due to shear forces $Qs_j$ on all *m* nodes and due to the base force *Qb* is expressed as:

$$s_i = \sum_{j=1}^{m} f_{i,j} Qs_j + f_{i,b} Qb \tag{2.3}$$

where:

| | |
|---|---|
| $f_{i,j}$ | Flexibility coefficient of node *i* due to a unit shear force on a node shaft *j* [m/kN] |
| $f_{i,b}$ | Flexibility coefficient of node *i* due to a unit force on the base *b* [m/kN] |

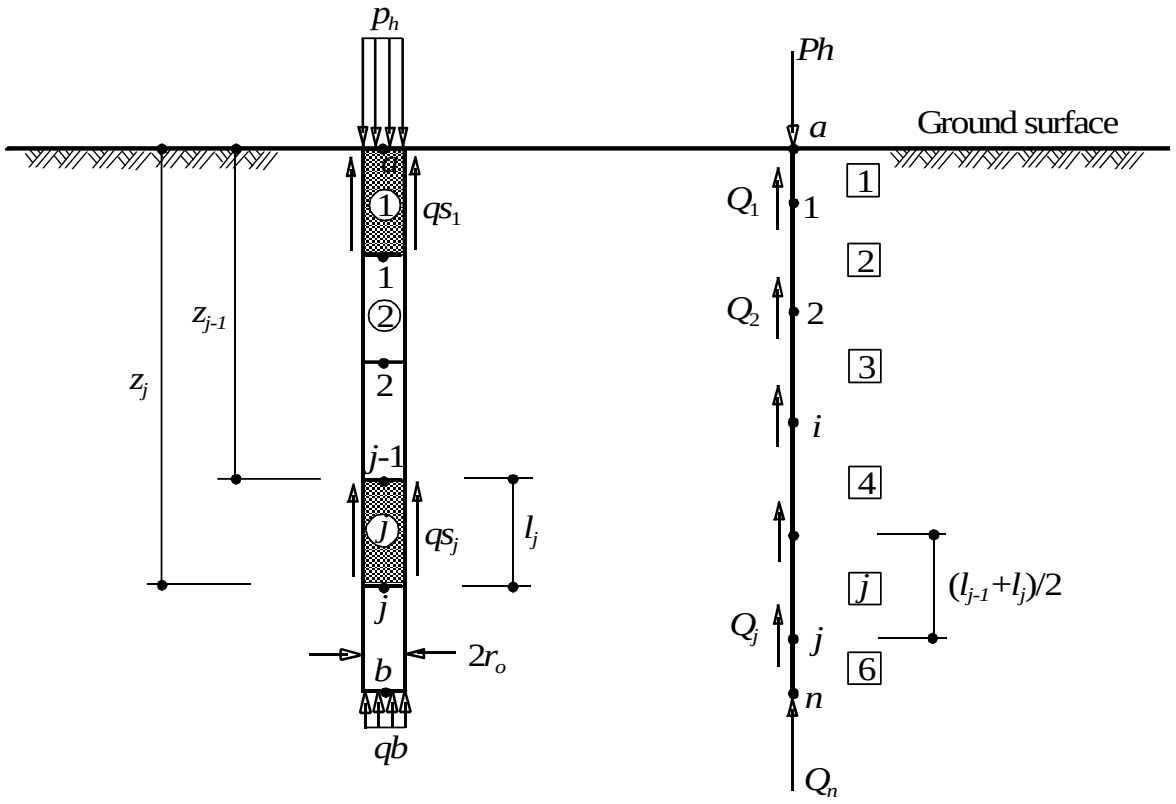


a) Pile shaft elements b) Pile line elements

Figure 2-1 Pile geometry and elements

As a special case of Eq. (2.3) and by changing the index *i* to *b*, the settlement of the base $s_b$ may be expressed as:

$$s_b = \sum_{j=1}^{m} f_{b,j} Qs_j + f_{b,b} Qb \tag{2.4}$$

where:

$f_{b,j}$ Flexibility coefficient of the base *b* due to a unit shear force on a node shaft *j* [m/kN]

$f_{b,b}$ Flexibility coefficient of the base *b* due to a unit force on the base *b* [m/kN]

Equations (2.3) and (2.4) for the settlement of the soil adjacent to all nodes of the pile may be rewritten in general form as:

$$w_i = \sum_{j=1}^{n} I_{i,j} Q_j \tag{2.5}$$

where:

$Q_j$ Contact force on node $j$ [kN]. $Q_j$ represents the shear forces $Qs_j$ on the shaft nodes or a base force $Qb$

$w_i$ Settlement on node $i$ [m]. $w_i$ represents the settlement $s_j$ on a shaft node $j$ or settlement $s_b$ on the base

$n$ Total number of contact nodes, $n = m + 1$

$I_{i,j}$ Flexibility coefficient of node $i$ due to a unit force on node $j$ [m/kN]. $I_{i,j}$ represents the coefficient $f_{i,j}$, $f_{i,b}$, $f_{b,j}$ or $f_{b,b}$. These coefficients can be evaluated from elastic theory using *Mindlin's* solution. Closed form equations for these coefficients are described in the next paragraph

### 2.2.2 Determining flexibility coefficients

In 1936 *Mindlin* presented a mathematical solution for determining stresses and displacements in soil due to a point load acting beneath the surface of semi-infinite mass. The solution is often employed in the numerical analysis of piled foundations and may have other applications in geotechnical engineering such as study the interaction between foundations and ground anchors or buried structures.

Pioneer authors of piled raft such as *Poulos/ Davis* (1968) and *Butterfield/ Banerjee* (1971) integrated numerically coefficients of flexibility using *Mindlin's* solution (*Mindlin* (1936)). Analysis of piled raft using integrated numerical coefficients leads to significant computations, especially in large pile group problems. An analytical derivation of coefficients of flexibility using *Mindlin's* solution is presented.

#### *2.2.2.1 Flexibility coefficient $f_{i,b}$ of a node i due to a unit force on the base b*

To avoid the significant computations when applying *Mindlin's* solution to determine the flexibility coefficients for nodes located outside the base, circular load at the base is replaced by an equivalent point load. In this case the flexibility coefficient can be obtained directly from *Mindlin's* solution for determining the displacement $w_{ij}$ [m] at point $i$ due to a point load $Q_j$ [kN] acting at point $j$ beneath the surface of a semi-infinite mass (Figure 2-2). According to *Mindlin's* solution the displacement $w_{ij}$ can be expressed as:

$$w_{ij} = f_{ij} Q_j \tag{2.6}$$

where $f_{ij}$ is given by *Mindlin's* solution as:

$$f_{ij} = \frac{1}{16\pi G_s (1-\nu_s)} \left( \frac{3-4\nu_s}{R_1} + \frac{8(1-\nu_s)^2 - (3-4\nu_s)}{R_2} + \frac{(z-c)^2}{R_1^3} + \frac{(3-4\nu_s)(z+c)^2 - 2cz}{R_2^3} + \frac{6cz(z+c)^2}{R_2^5} \right) \tag{2.7}$$

where:

$R_1 = \sqrt{r^2 + (z-c)^2}$, $R_2 = \sqrt{r^2 + (z+c)^2}$ and

$c$ Depth of the point load $Q_j$ [kN] from the surface [m]
$z$ Depth of the studied point $i$ from the surface [m]
$r$ Radial distance between points $i$ and $j$ [m]
$z\text{-}c$ Vertical distance between points $i$ and $j$ [m]
$z+c$ Vertical distance between points $i$ and $k$ [m]
$f_{ij}$ Displacement factor of point $i$ due to a unit load at point $j$ [m/kN]
$G_s$ Shear modulus of the soil [kN/m$^2$]

$$G_s = \frac{E_s}{2\,(1+\nu_s)}$$

$E_s$ Modulus of elasticity of the soil [kN/m$^2$]
$v_s$ *Poisson's* ratio of the soil [-]

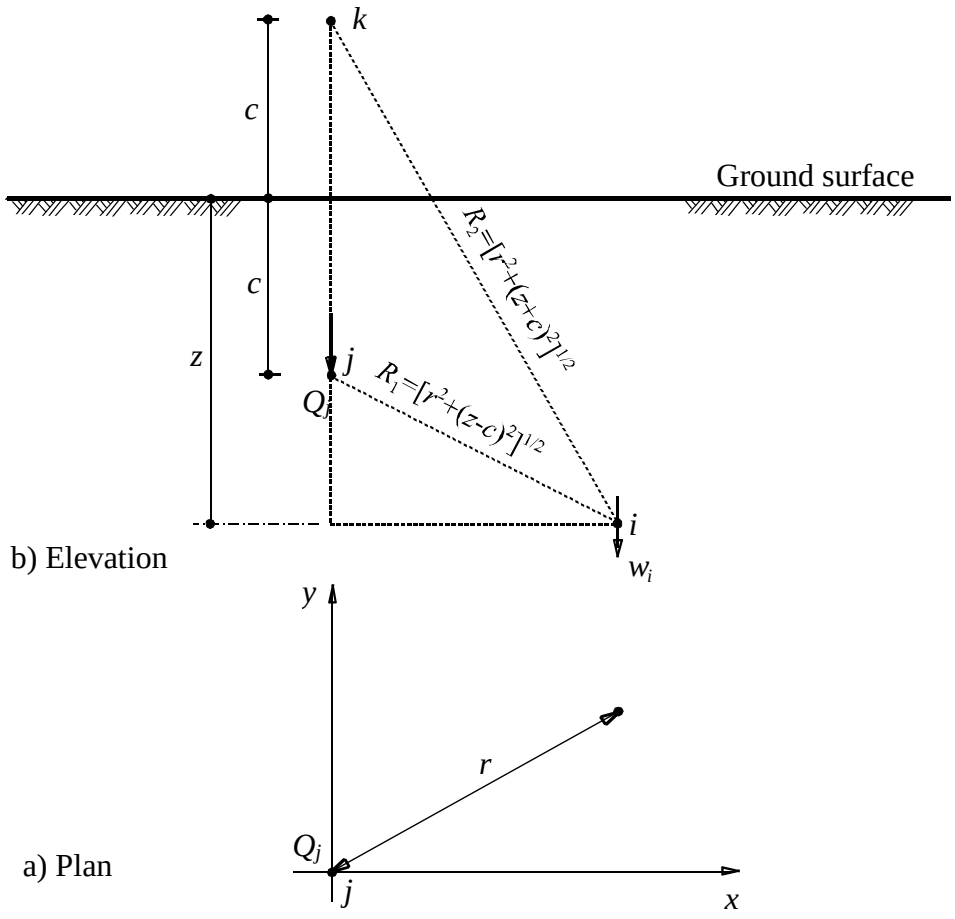


Figure 2-2 Geometry of *Mindlin's* problem

Now, the flexibility coefficient $f_{i,\,b}$ [m/kN] of node $i$ due to a unit force $Q_b$ = 1 [kN] acting on the base $b$ is equal to the displacement factor $f_{ij}$. In Eq (2.7), $r$ is the radial distance between the pile of point $i$ and the pile of the base $b$. For the pile of the studied base $b$, $r$ is equal to the radius of the base $r_o$.

### *2.2.2.2 Flexibility coefficient $f_{b,b}$ of the base b due to a unit force on the base itself*

The base *b* of the pile has a circular loaded area of radius $r_o$ [m] and a uniform load $q = Q_b / \pi r_o^2$ [kN/m$^2$] as shown in Figure 2-3. The flexibility coefficient $f_{b,b}$ [m/kN] at the base center *b* due to a unit load $Q_b$ = 1 [kN] at the base itself can be obtained from:

$$f_{b,b} = \frac{1}{\pi r_o^2} \int_0^{2\pi} \int_0^{r_o} f_{ij}\, r\, dr\, d\theta \tag{2.8}$$

The integration of the flexibility coefficient can be obtained analytically as:

$$f_{b,b} = \frac{1}{8\pi r_o^2 G_s (1-\nu_s)} \left( (3-4\nu_s)\, r_o + \left[ 8(1-\nu_s)^2 - (3-4\nu_s) \right] \left[ \sqrt{r_o^2 + 4c^2} - 2c \right] + \left[ 4c^2 (3-4\nu_s) - 2c^2 \right] \left[ \frac{1}{2c} - \frac{1}{\sqrt{r_o^2 + 4c^2}} \right] + \left[ 1 - \frac{8c^4}{\left( r_o^2 + 4c^2 \right)^{3/2}} \right] \right) \tag{2.9}$$

The flexibility coefficient $f_{b,b}$ may be multiplied by a factor π/4 to take the effect of base rigidity. This factor is the ratio of the surface displacement of a rigid circle on the surface of a half-space to the center displacement of a corresponding uniformly loaded circle.

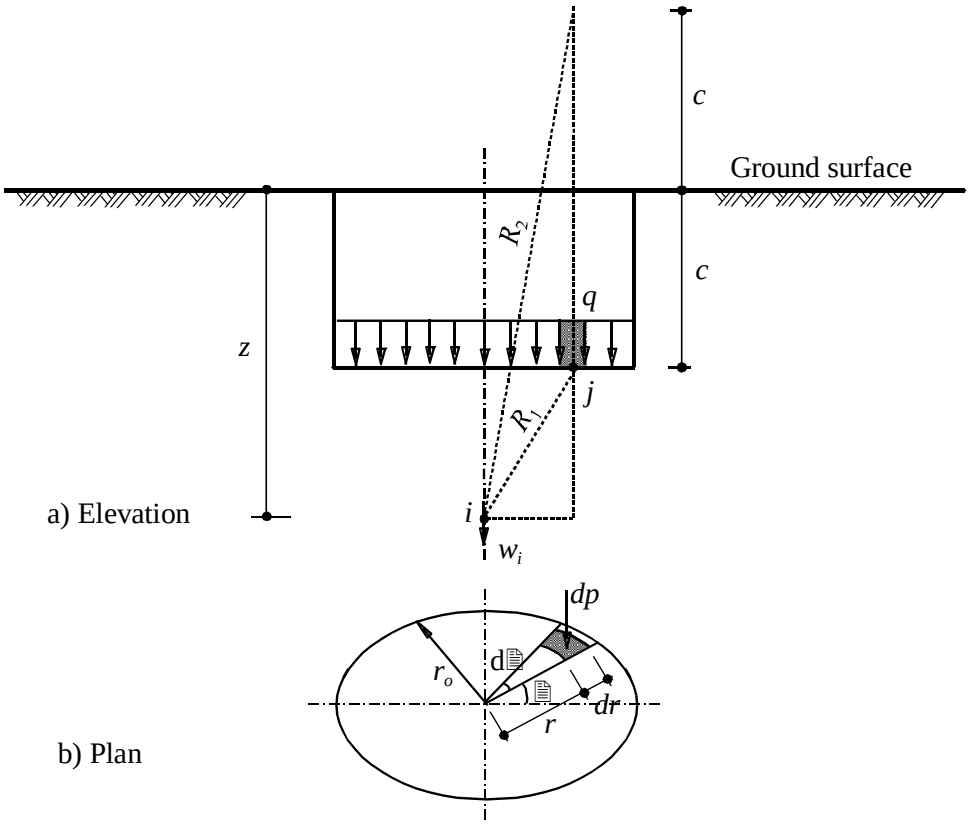


Figure 2-3 Geometry of circular loaded area for finding displacement at the center

### *2.2.2.3 Flexibility coefficient $f_{i,j}$ of node i due to a unit shear force on a node shaft j*

To avoid the significant computations when applying *Mindlin's* solution to determine the flexibility coefficients due to shaft stress, the shaft stress is replaced by an equivalent line load. The shaft element *j* of the pile has a length *l* [m] and a line load $T = Q_j / l$ [kN/m] as shown in Figure 2-4. The flexibility coefficient $f_{i,j}$ [m/kN] at the point *i* due to a unit load $Q_j = 1$ [kN] at a shaft element *j* can be obtained from:

$$f_{i,j} = \frac{1}{l}\int_{l_1}^{l_2} f_{ij}\, dc \tag{2.10}$$

The integration yields to:

$$f_{i,j} = \frac{1}{16\,\pi\, l\, G_s\,(1-\nu_s)}\left(I_1 + I_2 + I_3 + I_4 + I_5\right) \tag{2.11}$$

where terms $I_1$ to $I_5$ are given by:

$$I_1 = (3-4\,\nu_s)\ln\left[\frac{\sqrt{r_1^2+(z-l_2)^2}-(z-l_2)}{\sqrt{r_1^2+(z-l_1)^2}-(z-l_1)}\right] \tag{2.12}$$

$$I_2 = \left[8\,(1-\nu_s)^2-(3-4\,\nu_s)\right]\ln\left[\frac{\sqrt{r_1^2+(z+l_2)^2}+(z+l_2)}{\sqrt{r_1^2+(z+l_1)^2}+(z+l_1)}\right] \tag{2.13}$$

$$I_3 = \ln\left[\frac{\sqrt{r_1^2+(z-l_2)^2}-(z-l_2)}{\sqrt{r_1^2+(z-l_1)^2}-(z-l_1)}\right] + \frac{z-l_2}{\sqrt{r_1^2+(z-l_2)^2}} - \frac{z-l_1}{\sqrt{r_1^2+(z-l_1)^2}} \tag{2.14}$$

$$\begin{aligned} I_4 = {} & (3-4\,\nu_s)\left(\ln\left[\frac{\sqrt{r_1^2+(z+l_2)^2}+(z+l_2)}{\sqrt{r_1^2+(z+l_1)^2}+(z+l_1)}\right] - \frac{(z+l_2)}{\sqrt{r_1^2+(z+l_2)^2}} + \frac{(z+l_1)}{\sqrt{r_1^2+(z+l_1)^2}}\right) \\ & -2\,z\left(\frac{1}{\sqrt{r_1^2+(z+l_1)^2}} - \frac{1}{\sqrt{r_1^2+(z+l_2)^2}} + \frac{z\,(z+l_1)}{r_1^2\sqrt{r_1^2+(z+l_1)^2}} - \frac{z\,(z+l_2)}{r_1^2\sqrt{r_1^2+(z+l_2)^2}}\right) \end{aligned} \tag{2.15}$$

$$I_5 = \frac{6\,z\left[r_1^4 - z\,(z+l_2)^3\right]}{3\,r_1^2\left[r_1^2+(z+l_2)^2\right]^{3/2}} - \frac{6\,z\left[r_1^4 + z\,(z+l_1)^3\right]}{3\,r_1^2\left[r_1^2+(z+l_2)^2\right]^{3/2}} - \frac{6\,z}{\sqrt{r_1^2+(z+l_2)^2}} + \frac{6\,z}{\sqrt{r_1^2+(z+l_1)^2}} \tag{2.16}$$

where:

$l_1$ Start depth of the line load $T$ or the shear stress $\tau$ from the surface [m]
$l_2$ End depth of the line load $T$ or the shear stress $\tau$ from the surface [m]
$l$ Length of the line load $T$ or the shear stress $\tau$ [m]
$r_1$ Radial distance between point $i$ and $j$ [m]

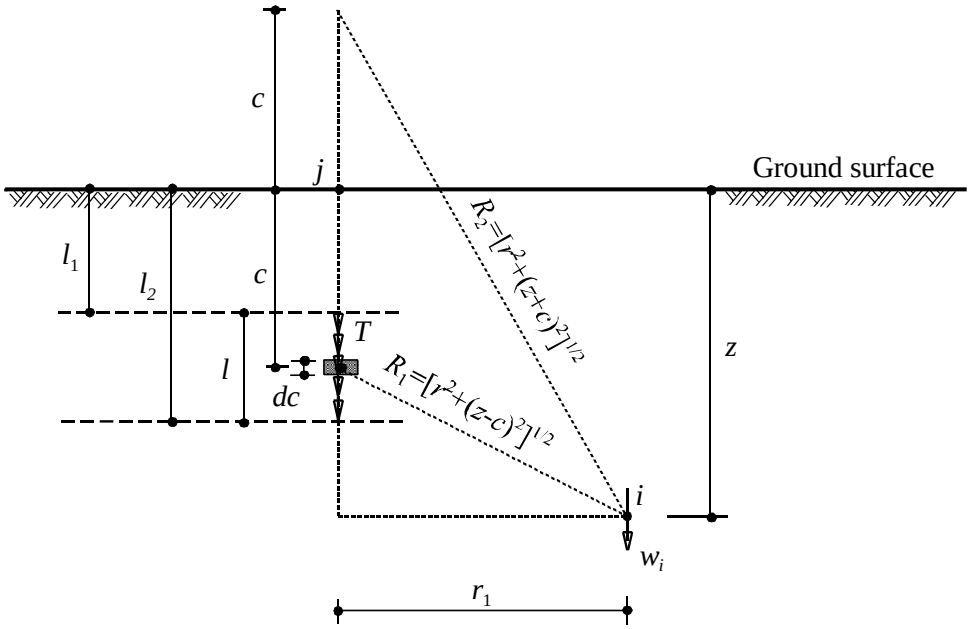


Figure 2-4 Geometry of the line load

### *2.2.2.4 Flexibility coefficient $f_{b,j}$ of the base b due to a unit shear force on a node shaft j*

The base $b$ of the pile has a radius $r_o$ [m], while the shaft element $j$ has a length $l$ [m] and a shear stress $\tau = Q_j / 2\,\pi\, r_o\, l$ [kN/m$^2$] as shown in Figure 2-5. The flexibility coefficient $f_{b,j}$ [m/kN] at the base center $b$ due to a unit load $Q_j = 1$ [kN] at a shaft element $j$ can be obtained from:

$$f_{b,j} = \frac{1}{2\,\pi\, l} \int_0^{2\pi} \int_{l_1}^{l_2} f_{ij}\, dc\, d\theta \tag{2.17}$$

The integration yields to:

$$f_{b,j} = \frac{1}{16\,\pi\, l\, G_s\,(1-\nu_s)} \left(J_1 + J_2 + J_3 + J_4 + J_5\right) \tag{2.18}$$

Replacing $r_1$ by $r_o$ in Eqns (2.12) to (2.16) gives terms $J_1$ to $J_5$.

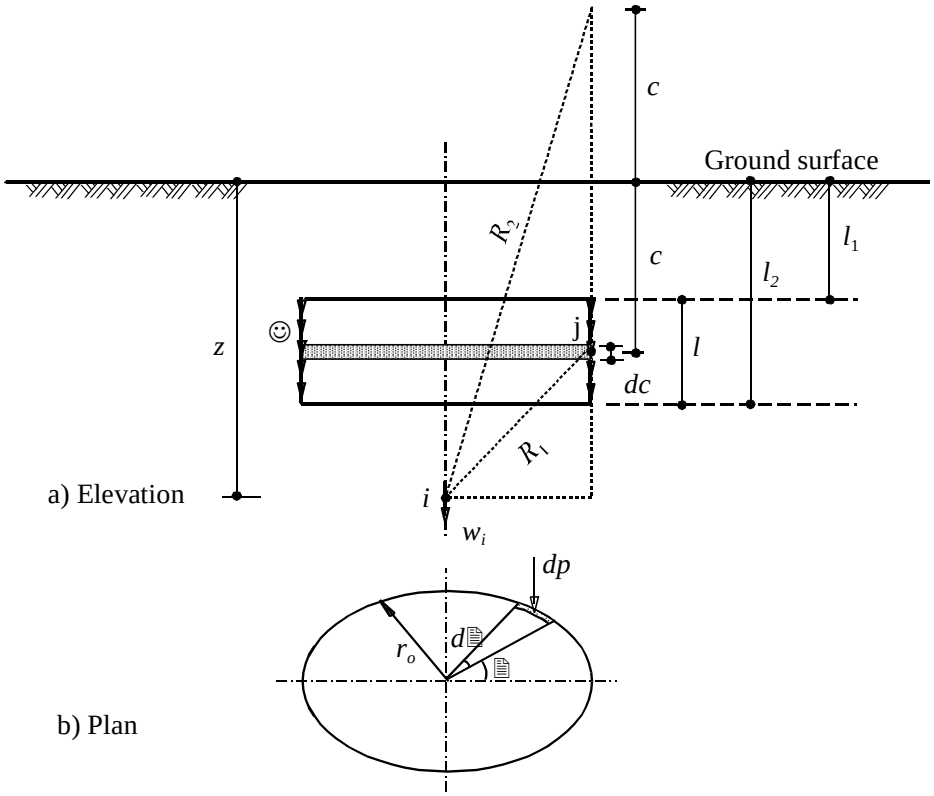


Figure 2-5 Geometry of cylindrical surface stress for finding the displacement at the center

### *2.2.2.5 Multi-layered soil*

Flexibility coefficients described previously can be applied only for isotropic elastic half-space soil medium. For finite layer, flexibility coefficients may be obtained as described by *Poulos/ Davis* (1968). As an example, for a point *k* in a layer of depth *h*, the flexibility coefficient is then:

$$f_{k,j}(h) = f_{k,j}(\infty) - f_{h,j}(\infty) \tag{2.19}$$

where:

$f_{k,j}(h)$ Flexibility coefficient for a point *k* in a layer of depth *h* due to a unit load on point *j* [m/kN]

$f_{k,j}(\infty)$ Flexibility coefficient for a point *k* due to a unit load on point *j* in a semi-infinite mass [m/kN]

$f_{h,j}(\infty)$ Flexibility coefficient for a point within the semi-infinite mass directly beneath *k*, at a depth *h* below the surface due to a unit load on point *j* [m/kN]

### 2.2.3 Elastic analysis of single pile

#### *2.2.3.1 Soil settlement*

Equation (2.5) for settlements of the soil adjacent to all nodes of the pile may be written in a matrix form as:

$$\{w\} = [Is]\{Q\} \tag{2.20}$$

where:
$\{w\}$ $n$ settlement vector
$\{Q\}$ $n$ contact force vector
$[Is]$ $n * n$ soil flexibility matrix

Inverting the soil flexibility matrix in Eq. (2.20), leads to:

$$\{Q\} = [ks]\{w\} \tag{2.21}$$

where $[ks]$ is $n * n$ soil stiffness matrix, $[ks] = [Is]^{-1}$.

Equation (2.21) may be modified as:

$$\begin{Bmatrix} 0 \\ Qs_1 \\ Qs_2 \\ Qs_3 \\ \dots \\ Qb \end{Bmatrix} = \begin{bmatrix} 0 & 0 & 0 & 0 & 0 & 0 \\ 0 & k_{1,1} & k_{1,2} & k_{1,3} & \dots & k_{1,n} \\ 0 & k_{2,1} & k_{2,1} & k_{2,1} & \dots & k_{2,n} \\ 0 & k_{3,1} & k_{3,1} & k_{3,1} & \dots & k_{3,n} \\ 0 & \dots & \dots & \dots & \dots & \dots \\ 0 & k_{n,1} & k_{n,1} & k_{n,1} & \dots & k_{n,n} \end{bmatrix} \begin{Bmatrix} 0 \\ s_1 \\ s_2 \\ s_3 \\ \dots \\ sb \end{Bmatrix} \tag{2.22}$$

Equation (2.22) is rewritten in a compacted matrix form as:

$$\{Qs\} = [ke]\{s\} \tag{2.23}$$

where:
$\{s\}$ $n + 1$ settlement vector, $\{s\} = \{o, s1, s2, s3, \dots, sn, sb\}^T$
$\{Qs\}$ $n + 1$vector of contact forces on the pile, $\{Q\} = \{o, Qs1, Qs2, Qs3, \dots, Qsn, Qb\}^T$
$[ke]$ $n + 1 * n + 1$ soil stiffness matrix

#### *2.2.3.2 Pile displacement*

The finite element method is used for analyzing the pile. Only the axial compression of the pile is considered in determining displacements of pile elements. The beam stiffness matrix of the pile element $i$ can be expressed as:

$$[kp]_i = \frac{Ep \cdot Ap_i}{l_i} \begin{bmatrix} 1 & -1 \\ -1 & 1 \end{bmatrix} \tag{2.24}$$

where:
*Ep* Modulus of Elasticity of the pile material [kN/m$^2$]
$Ap_i$ Cross-section area of the pile element *i* [m$^2$]
$l_i$ Length of the pile element *i* [m]

According to the principal of the finite element method, the assembled axial stiffness matrix equation for the pile can be written as:

$$[kp]\{\delta\} = \{P\} - \{Qs\} \tag{2.25}$$

where:
$\{\delta\}$ $n + 1$ Displacement vector
$\{P\}$ $n + 1$ vector of applied load on the pile, $\{P\} = \{Ph, o, o, o, \ldots, o\}^T$
$[kp]$ $n + 1 * n + 1$ beam stiffness matrix

Substituting Eq. (2.23) in Eq (2.25) leads to:

$$[kp]\{\delta\} = \{P\} - [ke]\{s\} \tag{2.26}$$

Assuming full compatibility between pile displacement $\delta_i$ and soil settlement $s_i$, the following equation can be obtained:

$$[[kp] + [ke]]\{\delta\} = \{P\} \tag{2.27}$$

Solving the above system of linear equations gives the displacement at each node, which is equal to the soil settlement at that node. Substituting soil settlements from Eq. (2.27) in Eq. (2.23), gives contact forces on the pile.

### 2.2.4 Rigid analysis of single pile

For a rigid pile, the settlement will be uniform. Therefore, the unknowns of the problem are *n* contact forces $Q_j$ and the rigid body translation *wo*. The derivation of the uniform settlement for the rigid pile can be carried out by equating the settlement $w_i$ in Eq. (2.5) by a uniform translation *wo* at all nodes on the pile. Expanding Eq. (2.5) for all nodes yields to:

$$\left.\begin{aligned} w_1 = wo = I_{1,1}Q_1 + I_{1,2}Q_1 + I_{1,3}Q_1 + \ldots + I_{1,n}Q_n \\ w_2 = wo = I_{2,1}Q_1 + I_{2,2}Q_1 + I_{2,3}Q_1 + \ldots + I_{2,n}Q_n \\ w_3 = wo = I_{3,1}Q_1 + I_{3,2}Q_1 + I_{3,3}Q_1 + \ldots + I_{3,n}Q_n \\ \ldots \\ w_n = wo = I_{n,1}Q_1 + I_{n,2}Q_1 + I_{n,3}Q_1 + \ldots + I_{n,n}Q_n \end{aligned}\right\} \tag{2.28}$$

Contact forces can be written as a function in terms $k_{i,j}$ of the soil stiffness matrix [*ks*] as:

$$\left.\begin{aligned} Q_1 &= k_{1,1}wo + k_{1,2}wo + k_{1,3}wo + ... + k_{1,n}wo \\ Q_2 &= k_{2,1}wo + k_{2,2}wo + k_{2,3}wo + ... + k_{2,n}wo \\ Q_3 &= k_{3,1}wo + k_{3,2}wo + k_{3,3}wo + ... + k_{3,n}wo \\ &... \\ Q_n &= k_{n,1}wo + k_{n,2}wo + k_{n,3}wo + ... + k_{n,n}wo \end{aligned}\right\} \tag{2.29}$$

Carrying out the summation of all contact forces leads to:

$$\sum_{i=1}^{n} Q_i = wo \sum_{i=1}^{n}\sum_{j=1}^{n} k_{i,j} \tag{2.30}$$

Equation (2.30) may be rewritten as:

$$Ph = ks\, wo \tag{2.31}$$

where the applied force *Ph* [kN] is the sum of all contact forces $Q_i$:

$$Ph = \sum_{i=1}^{n} Q_i \tag{2.32}$$

while the composed coefficient *ks* [kN/m] is the sum of all coefficients of the soil stiffness matrix [*ks*]:

$$ks = \sum_{i=1}^{n}\sum_{j=1}^{n} k_{i,j} \tag{2.33}$$

Eq. (2.31) gives the linear relation between the applied load on the pile head and the uniform settlement *wo*, which is analogous to *Hook's* law. Therefore, the composed coefficient *ks* may be used to determine the total soil stiffness adjacent to the pile. In case of analysis of a single pile, it is easy to determine the contact forces $Q_i$. Substituting the value of *wo* from Eq. (2.31) in Eq. (2.29) gives Eq. (2.34) in *n* unknown contact forces $Q_i$ as:

$$Q_i = \frac{Ph \sum_{j=1}^{n} k_{i,j}}{ks} \tag{2.34}$$

Equation (2.34) of contact forces on the rigid pile is found to be independent on the Modulus of elasticity of the soil $E_s$ in case of isotropic elastic half-space soil medium.

## 2.3 Modeling pile groups (free-standing rigid raft)

The composed coefficient technique is first used to perform a linear analysis of pile groups. Then it is extended to include the nonlinearity effect. The next paragraphs present the formulation of composed coefficients for pile groups to generate a soil stiffness matrix of composed coefficients.

### 2.3.1 Soil stiffness for pile groups

Deriving equations for free-standing raft on piles requires taking into account the interaction effect among the pile groups. For doing that, the simple free-standing raft on pile groups shown in Figure 2-6 as an example is considered, having $n_p = 4$ piles and total nodes of $n = 23$.

The relation between pile settlement and contact force on pile groups shown in Figure 2-6 can be expressed in matrix form as:

$$\left\{\begin{Bmatrix} w_1 \\ \dots \\ w_6 \end{Bmatrix}_1 \begin{Bmatrix} w_7 \\ \dots \\ w_{12} \end{Bmatrix}_2 \begin{Bmatrix} w_{13} \\ \dots \\ w_{17} \end{Bmatrix}_3 \begin{Bmatrix} w_{18} \\ \dots \\ w_{23} \end{Bmatrix}_4\right\} = \begin{bmatrix} I_{1,1} & \dots & I_{1,6} & I_{1,7} & \dots & I_{1,12} & I_{1,13} & \dots & I_{1,17} & I_{1,18} & \dots & I_{1,23} \\ \dots & \dots & \dots & \dots & \dots & \dots & \dots & \dots & \dots & \dots & \dots & \dots \\ I_{6,1} & \dots & I_{6,6} & I_{6,7} & \dots & I_{6,12} & I_{6,13} & \dots & I_{6,17} & I_{6,18} & \dots & I_{6,23} \\ I_{7,1} & \dots & I_{7,6} & I_{7,7} & \dots & I_{7,12} & I_{7,13} & \dots & I_{7,17} & I_{7,18} & \dots & I_{7,23} \\ \dots & \dots & \dots & \dots & \dots & \dots & \dots & \dots & \dots & \dots & \dots & \dots \\ I_{12,1} & \dots. & I_{12,6} & I_{12,7} & \dots & I_{12,12} & I_{12,13} & \dots & I_{12,17} & I_{12,18} & \dots & I_{12,23} \\ I_{13,1} & \dots & I_{13,6} & I_{13,7} & \dots & I_{13,12} & I_{13,13} & \dots & I_{13,17} & I_{13,18} & \dots & I_{13,23} \\ \dots & \dots & \dots & \dots & \dots & \dots & \dots & \dots & \dots & \dots & \dots & \dots \\ I_{17,1} & \dots & I_{17,6} & I_{17,7} & \dots & I_{17,12} & I_{17,13} & \dots & I_{17,17} & I_{17,18} & \dots & I_{17,23} \\ I_{18,1} & \dots & I_{18,6} & I_{18,7} & \dots & I_{18,12} & I_{18,13} & \dots & I_{18,17} & I_{18,18} & \dots & I_{18,23} \\ \dots & \dots & \dots & \dots & \dots & \dots & \dots & \dots & \dots & \dots & \dots & \dots \\ I_{23,1} & \dots & I_{23,6} & I_{23,7} & \dots & I_{23,12} & I_{23,13} & \dots & I_{23,17} & I_{23,18} & \dots & I_{23,23} \end{bmatrix} \left\{\begin{Bmatrix} Q_1 \\ \dots \\ Q_6 \end{Bmatrix}_1 \begin{Bmatrix} Q_7 \\ \dots \\ Q_{12} \end{Bmatrix}_2 \begin{Bmatrix} Q_{13} \\ \dots \\ Q_{17} \end{Bmatrix}_3 \begin{Bmatrix} Q_{18} \\ \dots \\ Q_{23} \end{Bmatrix}_4\right\} \tag{2.35}$$

Inverting the total flexibility matrix in Eq. (2.35), gives the total soil stiffness matrix of the system of the pile groups as:

$$\begin{Bmatrix} \begin{Bmatrix} Q_1 \\ \dots \\ Q_6 \end{Bmatrix}_1 \\ \begin{Bmatrix} Q_7 \\ \dots \\ Q_{12} \end{Bmatrix}_2 \\ \begin{Bmatrix} Q_{13} \\ \dots \\ Q_{17} \end{Bmatrix}_3 \\ \begin{Bmatrix} Q_{18} \\ \dots \\ Q_{23} \end{Bmatrix}_4 \end{Bmatrix} = \begin{bmatrix} k_{1,1} & \dots & k_{1,6} & k_{1,7} & \dots & k_{1,12} & k_{1,13} & \dots & k_{1,17} & k_{1,18} & \dots & k_{1,23} \\ \dots & \dots & \dots & \dots & \dots & \dots & \dots & \dots & \dots & \dots & \dots & \dots \\ k_{6,1} & \dots & k_{6,6} & k_{6,7} & \dots & k_{6,12} & k_{6,13} & \dots & k_{6,17} & k_{6,18} & \dots & k_{6,23} \\ k_{7,1} & \dots & k_{7,6} & k_{7,7} & \dots & k_{7,12} & k_{7,13} & \dots & I_{7,17} & k_{7,18} & \dots & k_{7,23} \\ \dots & \dots & \dots & \dots & \dots & \dots & \dots & \dots & \dots & \dots & \dots & \dots \\ k_{12,1} & \dots. & k_{12,6} & k_{12,7} & \dots & k_{12,12} & k_{12,13} & \dots & k_{12,17} & k_{12,18} & \dots & k_{12,23} \\ k_{13,1} & \dots & k_{13,6} & k_{13,7} & \dots & k_{13,12} & k_{13,13} & \dots & k_{13,17} & k_{13,18} & \dots & k_{13,23} \\ \dots & \dots & \dots & \dots & \dots & \dots & \dots & \dots & \dots & \dots & \dots & \dots \\ k_{17,1} & \dots & k_{17,6} & k_{17,7} & \dots & k_{17,12} & k_{17,13} & \dots & k_{17,17} & k_{17,18} & \dots & k_{17,23} \\ k_{18,1} & \dots & k_{18,6} & k_{18,7} & \dots & k_{18,12} & k_{18,13} & \dots & k_{18,17} & k_{18,18} & \dots & k_{18,23} \\ \dots & \dots & \dots & \dots & \dots & \dots & \dots & \dots & \dots & \dots & \dots & \dots \\ k_{23,1} & \dots & k_{23,6} & k_{23,7} & \dots & k_{23,12} & k_{23,13} & \dots & k_{23,17} & k_{23,18} & \dots & k_{23,23} \end{bmatrix} \begin{Bmatrix} \begin{Bmatrix} w_1 \\ \dots \\ w_6 \end{Bmatrix}_1 \\ \begin{Bmatrix} w_7 \\ \dots \\ w_{12} \end{Bmatrix}_2 \\ \begin{Bmatrix} w_{13} \\ \dots \\ w_{17} \end{Bmatrix}_3 \\ \begin{Bmatrix} w_{18} \\ \dots \\ w_{23} \end{Bmatrix}_4 \end{Bmatrix} \tag{2.36}$$

where $k_{i,j}$ [kN/ m] is stiffness coefficient of the soil stiffness matrix.

Due to the high rigidity of the pile in its length direction, the settlement in every pile itself is considered as uniform. This assumption can establish the relationship between the uniform pile settlement and the force on the pile head in the pile groups. It can be done by equating all settlements in each pile by a uniform settlement.

Carrying out the summation of rows and columns corresponding to pile *i* in Eq. (2.36) leads to:

$$\begin{Bmatrix} \begin{Bmatrix} \sum_{i=1}^{6} Q_i \end{Bmatrix}_1 \\ \begin{Bmatrix} \sum_{i=7}^{12} Q_i \end{Bmatrix}_2 \\ \begin{Bmatrix} \sum_{i=13}^{17} Q_i \end{Bmatrix}_3 \\ \begin{Bmatrix} \sum_{i=18}^{23} Q_i \end{Bmatrix}_4 \end{Bmatrix} = \begin{bmatrix} \sum_{i=1}^{6}\sum_{j=1}^{6} k_{i,j} & \sum_{i=1}^{6}\sum_{j=7}^{12} k_{i,j} & \sum_{i=1}^{6}\sum_{j=13}^{17} k_{i,j} & \sum_{i=1}^{6}\sum_{j=18}^{23} k_{i,j} \\ \sum_{i=7}^{12}\sum_{j=1}^{6} k_{i,j} & \sum_{i=7}^{12}\sum_{j=7}^{12} k_{i,j} & \sum_{i=7}^{12}\sum_{j=13}^{17} k_{i,j} & \sum_{i=7}^{12}\sum_{j=18}^{23} k_{i,j} \\ \sum_{i=13}^{17}\sum_{j=1}^{6} k_{i,j} & \sum_{i=13}^{17}\sum_{j=7}^{12} k_{i,j} & \sum_{i=13}^{17}\sum_{j=13}^{17} k_{i,j} & \sum_{i=13}^{17}\sum_{j=18}^{23} k_{i,j} \\ \sum_{i=18}^{23}\sum_{j=1}^{6} k_{i,j} & \sum_{i=18}^{23}\sum_{j=7}^{12} k_{i,j} & \sum_{i=18}^{23}\sum_{j=13}^{17} k_{i,j} & \sum_{i=18}^{23}\sum_{j=18}^{23} k_{i,j} \end{bmatrix} \begin{Bmatrix} \{ wo_1 \}_1 \\ \{ wo_2 \}_2 \\ \{ wo_3 \}_3 \\ \{ wo_4 \}_4 \end{Bmatrix} \tag{2.37}$$

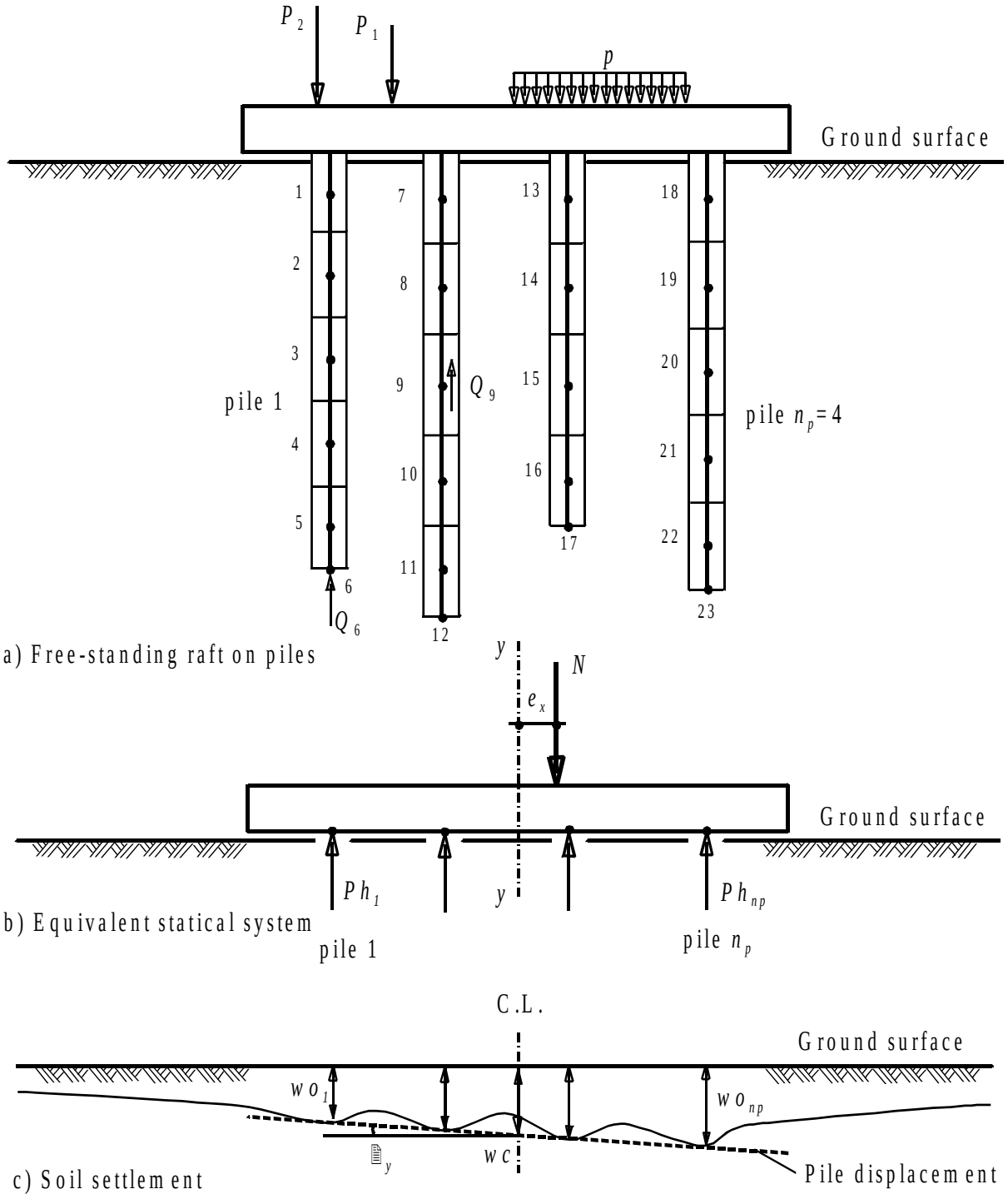


Figure 2-6 Modeling free-standing raft on pile groups

Accordingly, Eq. (2.37) can be rewritten for the simple pile groups in Figure 2-6 in composed coefficients as:

$$\begin{Bmatrix} Ph_1 \\ Ph_2 \\ Ph_3 \\ Ph_4 \end{Bmatrix} = \begin{bmatrix} K_{1,1} & K_{1,2} & K_{1,3} & K_{1,4} \\ K_{2,1} & K_{2,2} & K_{2,3} & K_{2,4} \\ K_{3,1} & K_{3,2} & K_{3,3} & K_{2,4} \\ K_{4,1} & K_{4,2} & K_{4,3} & K_{2,4} \end{bmatrix} \begin{Bmatrix} wo_1 \\ wo_2 \\ wo_3 \\ wo_4 \end{Bmatrix} \tag{2.38}$$

where:

$wo_i$ Settlement in pile $i$ [m]

$K_{i,j}$ Composed coefficient [kN/m]. In general $K_{i,j} = \sum_{n=n1}^{n2} \sum_{m=m1}^{m2} k_{n,m}$

$Ph_i$ Force on the head of pile $i$, which is equal to the summation of all contact forces in that pile [kN]. In general $Ph_i = \sum_{n=n1}^{n2} Q_n$

$n1 = 1 + \sum_{l=1}^{i-1} nn(l)$, $n2 = \sum_{l=1}^{i} nn(l)$, $m1 = 1 + \sum_{l=1}^{j-1} nn(l)$ and $m2 = \sum_{l=1}^{j} nn(l)$

$nn(l)$ Number of nodes in pile $l$

### 2.3.2 Analysis of pile groups

In general case of a completely rigid raft, the linear settlement of the raft at any point is defined by the vertical displacement $wc$ of the center and by two rotations $\theta_x$ and $\theta_y$ about $x$-and $y$-axes, respectively. The settlement of the pile $i$, having coordinates $x_i$ and $y_i$ referred to the center, must be compatible with the raft settlement at that point. Determining values of displacement $wc$ and rotations $\theta_x$ and $\theta_y$ allows to find the unknown pile head forces and settlements.

#### *2.3.2.1 Case of uniform settlement ($e_x = 0$ and $e_y = 0$)*

For a free-standing raft with a centric load, the settlement will be uniform. Therefore, unknowns of the problem are reduced to $n_p$ pile head forces $Ph_i$ and the rigid body translation $wc$ on all piles. The derivation of the uniform settlement for the rigid free-standing raft can be carried out by equating the settlement $wo_i$ by a uniform translation $wc$ at all piles in the pile groups. Expanding Eq. (2.38) for all piles yields to:

$$\left.\begin{aligned} Ph_1 &= K_{1,1}wc + K_{1,2}wc + K_{1,3}wc + ... + K_{1,n_p}wc \\ Ph_2 &= K_{2,1}wc + K_{2,2}wc + K_{2,3}wc + ... + K_{2,n_p}wc \\ Ph_3 &= K_{3,1}wc + K_{3,2}wc + K_{3,3}wc + ... + K_{3,n_p}wc \\ &... \\ Ph_{n_p} &= K_{n_p,1}wc + K_{n_p,2}wc + K_{n_p,3}wc + ... + K_{n_p,n_p}wc \end{aligned}\right\} \tag{2.39}$$

Carrying out the summation of all forces on pile heads, leads to:

$$\sum_{i=1}^{n_p} Ph_i = wc \sum_{i=1}^{n_p} \sum_{j=1}^{n_p} K_{i,j} \tag{2.40}$$

Equation (2.40) may be rewritten in a simple form as:

$$N = Ks\ wc \tag{2.41}$$

where the resultant force $N$ is the sum of all forces $Ph_i$ on pile heads:

$$N = \sum_{i=1}^{n_p} Ph_i \tag{2.42}$$

while the modulus $Ks$ is the sum of all terms $K_{i,j}$:

$$Ks = \sum_{i=1}^{n_p} \sum_{j=1}^{n_p} K_{i,j} \tag{2.43}$$

Equation (2.41) gives the linear relation between the applied resultant force $N$ on the pile groups and the uniform settlement $wc$, which is analogous to *Hook's* low. The modulus $Ks$ is the total soil stiffness of the pile groups.

Substituting the value of $wc$ in Eq. (2.39), gives Eq. (2.44) in $n_p$ unknown pile head forces $Ph_i$.

$$Ph_i = wc \sum_{j=1}^{n_p} K_{i,j} \tag{2.44}$$

Equation (2.44) represents the linear relation between the force on the pile head and its settlement in the pile groups and can be rewritten in a simplified form as:

$$Ph_i = ks_i\ wc \tag{2.45}$$

where $ks_i$ [kN/m] is the Modulus of soil stiffness adjacent to the pile $i$ in the pile groups. It is given by:

$$ks_i = \sum_{j=1}^{n_p} K_{i,j} \tag{2.46}$$

#### *2.3.2.2 Case of single eccentric load ($e_x \neq 0$)*

Due to the raft rigidity, the following linear relation expresses the settlement $wo_i$ at a pile $i$ that has a distance $x_i$ from the geometry centroid in the case of single eccentric load in $x$-axis:

$$wo_i = wc + x_i \tan\theta_y \tag{2.47}$$

where $\theta_y$ [Grad] is the rotation angle of the raft about $y$-axis.

Similarly to the procedures of derivation *wc*, the expansion of forces on pile heads in Eq. (2.39) becomes:

$$\left.\begin{aligned} Ph_1 &= K_{1,1}\, wo_1 + K_{1,2}\, wo_2 + K_{1,3}\, wo_3 + ... + K_{1,n_p}\, wo_{n_p} \\ Ph_2 &= K_{2,1}\, wo_1 + K_{2,2}\, wo_2 + K_{2,3}\, wo_3 + ... + K_{2,n_p}\, wo_{n_p} \\ Ph_3 &= K_{3,1}\, wo_1 + K_{3,2}\, wo_2 + K_{3,3}\, wo_3 + ... + K_{3,n_p}\, wo_{n_p} \\ &... \\ Ph_{n_p} &= K_{n_p,1}\, wo_1 + K_{n_p,2}\, wo_2 + K_{n_p,3}\, wo_3 + ... + K_{n_p,n_p}\, wo_{n_p} \end{aligned}\right\} \tag{2.48}$$

Multiplying both sides of a row $i$ in Eq. (2.48) by $x_i$, gives the following system of linear equations:

$$\left.\begin{aligned} Ph_1\, x_1 &= x_1 K_{1,1}\, wo_1 + x_1 K_{1,2}\, wo_2 + x_1 K_{1,3}\, wo_3 + ... + x_1 K_{1,n_p}\, wo_{n_p} \\ Ph_2\, x_2 &= x_2 K_{2,1}\, wo_1 + x_2 K_{2,2}\, wo_2 + x_2 K_{2,3}\, wo_3 + ... + x_2 K_{2,n_p}\, wo_{n_p} \\ Ph_3\, x_3 &= x_3 K_{3,1}\, wo_1 + x_3 K_{3,2}\, wo_2 + x_3 K_{3,3}\, wo_3 + ... + x_3 K_{3,n_p}\, wo_{n_p} \\ &... \\ Ph_{n_p}\, x_{n_p} &= x_{n_p} K_{n_p,1}\, wo_1 + x_{n_p} K_{n_p,2}\, wo_2 + x_{n_p} K_{n_p,3}\, wo_3 + ... + x_{n_p} K_{n_p,n_p}\, wo_{n_p} \end{aligned}\right\} \tag{2.49}$$

To eliminate the contact forces from Eq. (2.49), carry out the summation of all $Ph_i\, x_i$ as follows:

$$\sum_{i=1}^{n_p} Ph_i\, x_i = \sum_{i=1}^{n_p} x_i \sum_{j=1}^{n_p} K_{i,j}\, wo_j \tag{2.50}$$

Substituting Eq. (2.47) in Eq. (2.50) gives:

$$\sum_{i=1}^{n_p} Ph_i\, x_i = \sum_{i=1}^{n_p} x_i \sum_{j=1}^{n_p} K_{i,j} \left(wc + x_j \tan\theta_y\right) \tag{2.51}$$

But the moment due to resultant $N$ about the $y$-axis must be equal to the sum of moments due to forces on pile heads $Ph_i$ about that axis:

$$N\, e_x = Ph_1\, x_1 + Ph_2\, x_2 + Ph_3\, x_3 + ... + Ph_{n_p}\, x_{n_p} = \sum_{i=1}^{n_p} Ph_i\, x_i \tag{2.52}$$

Substituting Eq. (2.51) in Eq. (2.52) eliminates the forces on pile heads from Eq. (2.52) and gives the rigid rotation $\theta_y$ about *y*-axis from:

$$\tan\theta_y = \frac{N\, e_x - wc \sum_{i=1}^{n_p} x_i \sum_{j=1}^{n_p} K_{i,j}}{\sum_{i=1}^{n_p} x_i \sum_{j=1}^{n_p} K_{i,j}\, x_j} \tag{2.53}$$

Substituting the value of $\tan\theta_y$ in Eq. (2.47) gives the $n_p$ unknown settlements $wo_i$. Then, substituting the value of $wo_i$ in Eq. (2.48), gives the $n_p$ unknown forces on pile heads $Ph_i$:

$$Ph_i = wc \sum_{j=1}^{n_p} K_{i,j} + \tan\theta_y \sum_{j=1}^{n_p} x_i\, K_{i,j} \tag{2.54}$$

The stiffness $ks_i$ of the soil adjacent to the pile *i* in the pile group is given by:

$$ks_i = \frac{Ph_i}{wc + x_i \tan\theta_y} \tag{2.55}$$

#### *2.3.2.3 Case of single eccentric load ($e_y \neq 0$)*

The settlement $wo_i$ at pile *i* that has a distance $y_i$ from the geometry centroid in the case of single eccentric load in *y*-axis is given by:

$$wo_i = wc + y_i \tan\theta_x \tag{2.56}$$

The derivation of the free-standing rigid raft in the case of an eccentric load in *y*-axis can be carried out in a similar manner to the above procedures, which leads to the following Eq. (2.57) in the rotation $\theta_x$ about *x*-axis:

$$\tan\theta_x = \frac{N\, e_y - wc \sum_{i=1}^{n_p} y_i \sum_{j=1}^{n_p} K_{i,j}}{\sum_{i=1}^{n} y_i \sum_{j=1}^{n_p} K_{i,j}\, y_j} \tag{2.57}$$

while the force on the pile head is given by:

$$Ph_i = wc \sum_{j=1}^{n_p} K_{i,j} + \tan\theta_x \sum_{j=1}^{n_p} y_i\, K_{i,j} \tag{2.58}$$

and the soil stiffness $ks_i$ adjacent to the pile *i* in the pile groups is given by:

$$ks_i = \frac{Ph_i}{wc + y_i \tan\theta_x} \tag{2.59}$$

***General case of double eccentric load ($e_x \neq 0$ and $e_y \neq 0$)***

The settlement $wo_i$ in the general case of an eccentric load at any pile $i$ that has coordinates $x_i$ and $y_i$ from the geometry centroid is given by:

$$wo_i = wc + x_i \tan\theta_y + y_i \tan\theta_x \tag{2.60}$$

while the force on the pile head is given by:

$$Ph_i = wc \sum_{j=1}^{n_p} K_{i,j} + \tan\theta_y \sum_{j=1}^{n_p} x_i K_{i,j} + \tan\theta_x \sum_{j=1}^{n_p} y_i K_{i,j} \tag{2.61}$$

and the soil stiffness $ks_i$ adjacent to the pile $i$ in the pile groups is given by:

$$ks_i = \frac{Ph_i}{wc + x_i \tan\theta_y + y_i \tan\theta_x} \tag{2.62}$$

Once settlements $wo_i$ on piles are determined, the contact forces along the pile shaft and on the pile base can be obtained from Eq. (2.35).

## 2.4 Modeling piled raft

### 2.4.1 Soil stiffness for piled raft

For a complete analysis of piled raft foundation, pile-soil-raft and raft-soil-raft interactions must be taken into account in addition to pile-soil-pile interaction. To illustrate how to formulate the composed coefficient technique for piled raft, the simple piled raft shown in Figure 2-7 is considered, having $n_p = 4$ piles and a total $n_{pr} = 33$ contact nodes of raft and piles with the soil. If the raft is analyzed alone without piles, the number of its nodes will be $n_r = 14$. In the analysis, the contact area is divided for the raft into triangular and/ or rectangular elements, while that for pile shafts into cylindrical elements and that for pile bases into circular elements. The contact pressure under the raft, on pile shafts or on pile bases is represented by a series of contact forces on nodes. For the set of 33 nodes of the piled raft, the relation between soil settlements and contact forces is expressed as:

$$\begin{Bmatrix} w_1 \\ w_2 \\ \begin{Bmatrix} w_3 \\ \dots \\ w_8 \end{Bmatrix}_{p1} \\ w_9 \\ w_{10} \\ \begin{Bmatrix} w_{11} \\ \dots \\ w_{16} \end{Bmatrix}_{p2} \\ .. \\ w_{33} \end{Bmatrix} = \begin{bmatrix} I_{1,1} & I_{1,2} & I_{1,3} & \dots & I_{1,8} & I_{1,9} & I_{1,10} & I_{1,11} & \dots & I_{1,16} & \dots & I_{1,33} \\ I_{2,1} & I_{2,2} & I_{2,3} & \dots & I_{2,8} & I_{2,9} & I_{2,10} & I_{2,11} & \dots & I_{2,16} & \dots & I_{2,33} \\ I_{3,1} & I_{3,2} & I_{3,3} & \dots & I_{3,8} & I_{3,9} & I_{3,10} & I_{3,11} & \dots & I_{3,16} & \dots & I_{3,33} \\ \dots & \dots & \dots & \dots & \dots & \dots & \dots & \dots & \dots & \dots & \dots & \dots \\ I_{8,1} & I_{8,2} & I_{8,3} & \dots & I_{8,8} & I_{8,9} & I_{8,10} & I_{8,11} & \dots & I_{8,16} & \dots & I_{8,33} \\ I_{9,1} & I_{9,2} & I_{9,3} & \dots & I_{9,8} & I_{9,9} & I_{9,10} & I_{9,11} & \dots & I_{9,16} & \dots & I_{9,33} \\ I_{10,1} & I_{10,2} & I_{10,3} & \dots & I_{10,8} & I_{10,9} & I_{10,10} & I_{10,11} & \dots & I_{10,16} & \dots & I_{10,33} \\ I_{11,1} & I_{11,2} & I_{11,3} & \dots & I_{11,8} & I_{11,9} & I_{11,10} & I_{11,11} & \dots & I_{11,16} & \dots & I_{11,33} \\ \dots & \dots & \dots & \dots & \dots & \dots & \dots & \dots & \dots & \dots & \dots & \dots \\ I_{16,1} & I_{16,2} & I_{16,3} & \dots & I_{16,8} & I_{16,9} & I_{16,10} & I_{16,11} & \dots & I_{16,16} & \dots & I_{16,33} \\ \dots & \dots & \dots & \dots & \dots & \dots & \dots & \dots & \dots & \dots & \dots & \dots \\ I_{33,1} & I_{33,2} & I_{33,3} & \dots & I_{33,8} & I_{33,9} & I_{33,10} & I_{33,11} & \dots & I_{33,16} & \dots & I_{33,33} \end{bmatrix} \begin{Bmatrix} Q_1 \\ Q_2 \\ \begin{Bmatrix} Q_3 \\ \dots \\ Q_8 \end{Bmatrix}_{p1} \\ Q_9 \\ Q_{10} \\ \begin{Bmatrix} Q_{11} \\ \dots \\ Q_{16} \end{Bmatrix}_{p2} \\ .. \\ Q_{33} \end{Bmatrix} \tag{2.63}$$

where *p1, p2, …* are numbers of the piles.

The total flexibility matrix in Eq. (2.63) can be inverted to give the relationship between contact forces and nodal settlements as follows:

$$\begin{Bmatrix} Q_1 \\ Q_2 \\ \begin{Bmatrix} Q_3 \\ \dots \\ Q_8 \end{Bmatrix}_{p1} \\ Q_9 \\ Q_{10} \\ \begin{Bmatrix} Q_{11} \\ \dots \\ Q_{16} \end{Bmatrix}_{p2} \\ .. \\ Q_{33} \end{Bmatrix} = \begin{bmatrix} k_{1,1} & k_{1,2} & k_{1,3} & \dots & k_{1,8} & k_{1,9} & k_{1,10} & k_{1,11} & \dots & k_{1,16} & \dots & k_{1,33} \\ k_{2,1} & k_{2,2} & k_{2,3} & \dots & k_{2,8} & k_{2,9} & k_{2,10} & k_{2,11} & \dots & k_{2,16} & \dots & k_{2,33} \\ k_{3,1} & k_{3,2} & k_{3,3} & \dots & k_{3,8} & k_{3,9} & k_{3,10} & k_{3,11} & \dots & k_{3,16} & \dots & k_{3,33} \\ \dots & \dots & \dots & \dots & \dots & \dots & \dots & \dots & \dots & \dots & \dots & \dots \\ k_{8,1} & k_{8,2} & k_{8,3} & \dots & k_{8,8} & k_{8,9} & k_{8,10} & k_{8,11} & \dots & k_{8,16} & \dots & k_{8,33} \\ k_{9,1} & k_{9,2} & k_{9,3} & \dots & k_{9,8} & k_{9,9} & k_{9,10} & k_{9,11} & \dots & k_{9,16} & \dots & k_{9,33} \\ k_{10,1} & k_{10,2} & k_{10,3} & \dots & k_{10,8} & k_{10,9} & k_{10,10} & k_{10,11} & \dots & k_{10,16} & \dots & k_{10,33} \\ k_{11,1} & k_{11,2} & k_{11,3} & \dots & k_{11,8} & k_{11,9} & k_{11,10} & k_{11,11} & \dots & k_{11,16} & \dots & k_{11,33} \\ \dots & \dots & \dots & \dots & \dots & \dots & \dots & \dots & \dots & \dots & \dots & \dots \\ k_{16,1} & k_{16,2} & k_{16,3} & \dots & k_{16,8} & k_{16,9} & k_{16,10} & k_{16,11} & \dots & k_{16,16} & \dots & k_{16,33} \\ \dots & \dots & \dots & \dots & \dots & \dots & \dots & \dots & \dots & \dots & \dots & \dots \\ k_{33,1} & k_{33,2} & k_{33,3} & \dots & k_{33,8} & k_{33,9} & k_{33,10} & k_{33,11} & \dots & k_{33,16} & \dots & k_{33,33} \end{bmatrix} \begin{Bmatrix} w_1 \\ w_2 \\ \begin{Bmatrix} w_3 \\ \dots \\ w_8 \end{Bmatrix}_{p1} \\ w_9 \\ w_{10} \\ \begin{Bmatrix} w_{11} \\ \dots \\ w_{16} \end{Bmatrix}_{p2} \\ .. \\ w_{33} \end{Bmatrix} \tag{2.64}$$

As indicated before, equating settlements of all nodes on each pile by a uniform settlement and carrying out the summation of rows and columns related to that pile in Eq. (2.64), gives the composed coefficients with the force on the pile head $Ph_i$ and its corresponding settlement $wo_i$ as follows:

$$\begin{Bmatrix} Q_1 \\ Q_2 \\ \left\{ \sum_{i=3}^{8} Q_i \right\}_{p1} \\ Q_9 \\ Q_{10} \\ \left\{ \sum_{i=11}^{16} Q_i \right\}_{p2} \\ \dots \\ Q_{33} \end{Bmatrix} = \begin{bmatrix} k_{1,1} & k_{1,2} & \sum_{j=3}^{8} k_{1,j} & k_{1,9} & k_{1,10} & \sum_{j=11}^{16} k_{1,j} & \dots & k_{1,33} \\ k_{2,1} & k_{2,2} & \sum_{j=3}^{8} k_{2,j} & k_{2,9} & k_{2,10} & \sum_{j=11}^{16} k_{2,j} & \dots & k_{2,33} \\ \sum_{i=3}^{8} k_{i,1} & \sum_{i=3}^{8} k_{i,2} & \sum_{i=3}^{8}\sum_{j=3}^{8} k_{i,j} & \sum_{i=3}^{8} k_{i,9} & \sum_{i=3}^{8} k_{i,10} & \sum_{i=3}^{8}\sum_{j=11}^{16} k_{i,j} & \dots & \sum_{i=3}^{8} k_{i,33} \\ k_{9,1} & k_{9,2} & \sum_{j=3}^{8} k_{9,j} & k_{9,9} & k_{9,10} & \sum_{j=11}^{16} k_{9,j} & \dots & k_{9,33} \\ k_{10,1} & k_{10,2} & \sum_{j=3}^{8} k_{10,j} & k_{10,9} & k_{10,10} & \sum_{j=11}^{16} k_{10,j} & \dots & k_{10,33} \\ \sum_{i=11}^{16} k_{i,1} & \sum_{i=11}^{16} k_{i,2} & \sum_{i=11}^{16}\sum_{j=3}^{8} k_{i,j} & \sum_{i=11}^{16} k_{i,9} & \sum_{i=11}^{16} k_{i,10} & \sum_{i=11}^{16}\sum_{j=11}^{16} k_{i,j} & \dots & \sum_{i=11}^{16} k_{i,33} \\ \dots & \dots & \dots & \dots & \dots & \dots & \dots & \dots \\ k_{33,1} & k_{33,2} & \sum_{j=3}^{8} k_{33,j} & k_{33,9} & k_{33,10} & \sum_{j=11}^{16} k_{33,j} & \dots & k_{33,33} \end{bmatrix} \begin{Bmatrix} w_1 \\ w_2 \\ \{ wo_1 \}_{p1} \\ w_9 \\ w_{10} \\ \{ wo_2 \}_{p2} \\ \dots \\ w_{33} \end{Bmatrix} \tag{2.65}$$

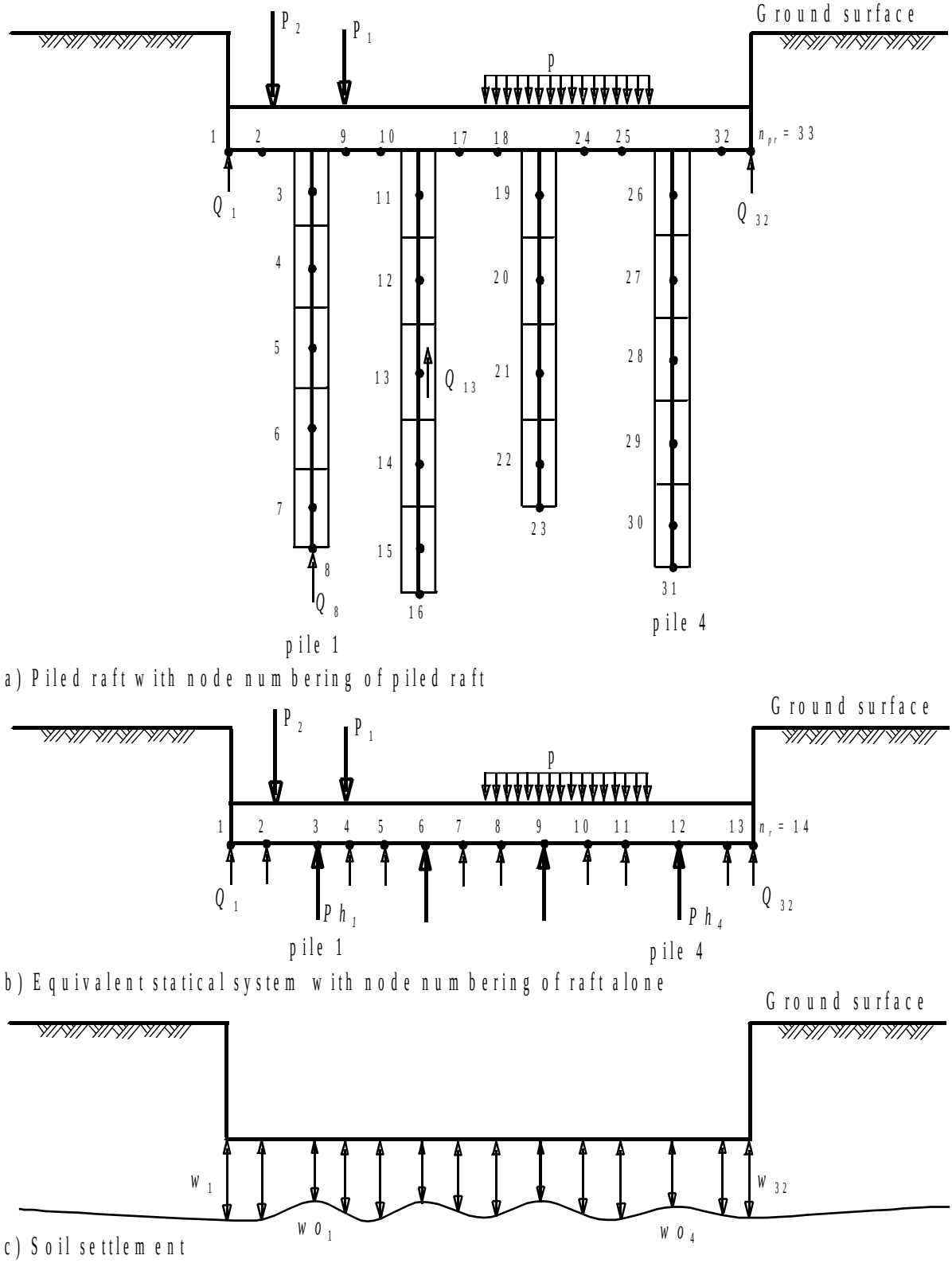


Figure 2-7 Modeling piled raft

Accordingly, the total stiffness matrix of the piled raft of size [$n_{pr}$ * $n_{pr}$] is reduced to [$n_r$ * $n_r$]. It means that the composed coefficient technique makes the size of the soil stiffness matrix of the piled raft problem equivalent to that of the raft problem alone without piles.

Now, Eq. (2.65) can be rewritten in composed coefficients as:

$$\begin{Bmatrix} Q_1 \\ Q_2 \\ Ph_1 \\ Q_9 \\ Q_{10} \\ Ph_2 \\ \cdots \\ Q_{33} \end{Bmatrix} = \begin{bmatrix} k_{1,1} & k_{1,2} & K_{1,p1} & k_{1,9} & k_{1,10} & K_{1,p2} & \cdots & k_{133} \\ k_{2,1} & k_{2,2} & K_{2,p1} & k_{2,9} & k_{2,10} & K_{2,p2} & \cdots & k_{2,33} \\ K_{p1,1} & K_{p1,2} & K_{p1,p1} & K_{p1,9} & K_{p1,10} & K_{p1,p2} & \cdots & K_{p2,33} \\ k_{9,1} & k_{9,2} & K_{9,p1} & k_{9,9} & k_{9,10} & K_{9,p2} & \cdots & k_{9,33} \\ k_{10,1} & k_{10,2} & K_{10,p1} & k_{10,9} & k_{10,10} & K_{10,p2} & \cdots & k_{10,33} \\ K_{p2,1} & K_{p2,2} & K_{p2,p1} & K_{p2,9} & K_{p2,10} & K_{p2,p2} & \cdots & K_{p2,33} \\ \cdots & \cdots & \cdots & \cdots & \cdots & \cdots & \cdots & \cdots \\ k_{33,1} & k_{33,2} & K_{33,p1} & k_{33,9} & k_{33,10} & K_{33,p2} & \cdots & k_{33,33} \end{bmatrix} \begin{Bmatrix} w_1 \\ w_2 \\ wo_1 \\ w_9 \\ w_{10} \\ wo_2 \\ \cdots \\ w_{33} \end{Bmatrix} \tag{2.66}$$

where $K_{pi,\,pj}$, $K_{i,\,pj}$ and $K_{pi,\,j}$ [kN/m] are composed coefficients of the piled raft.

Based on Eq. (2.66), the relationship between settlements and contact forces of the piled raft can be written in general compacted matrix form as:

$$\{Q\} = [kb]\{w\} \tag{2.67}$$

where:
$\{w\}$ $n_r$ settlement vector
$\{Q\}$ $n_r$ contact force vector
$[kb]$ $n_r$ * $n_r$ soil stiffness matrix of the piled raft

For simplicity of the formulation, in next paragraphs the settlement on either raft node or pile head is donated by $w_i$, while the contact force on either raft node or pile head is donated by $Q_i$.

### 2.4.2 Analysis of piled flexible raft

In case of analyzing full flexible raft, the contact force vector $\{Q\}$ on raft nodes is known. Only settlements are required. The advantage of the composed coefficient technique is that the composed soil stiffness matrix can be inverted to get a composed flexibility matrix.

Accordingly, a relationship between contact forces under the flexible raft besides forces on pile heads and nodal settlements is expressed as:

$$\{w\} = [Cb]\{Q\} \tag{2.68}$$

where $[Cb]$ is $n_r$ *$n_r$ flexibility matrix of the piled raft, $[Cb] = [kb]^{-1}$.

### 2.4.3 Analysis of piled rigid raft

For piled rigid raft, unknowns of the interaction problem are $n_r$ contact forces $Q_i$, the rigid body translation of the piled raft $wc$, and the rigid body rotations $\theta_x$ and $\theta_y$ of the piled raft about axes of geometry centroid. These are determined by considering $n_r$ compatibility equations of rigid piled raft deflection and the displacement of subsoil at $n_r$ nodal points in addition to the three equations of overall equilibrium.

Due to the piled raft rigidity, the following linear relation (plane translation) expresses the settlement $w_i$ at either a node in the raft or a pile that has coordinates ($x_i$, $y_i$) from the geometry centroid:

$$w_i = wc + x_i \tan\theta_y + y_i \tan\theta_x \tag{2.69}$$

Equation (2.69) is rewritten in matrix form for the entire piled raft system as:

$$\{w\} = [X]^T \{\Delta\} \tag{2.70}$$

where:
$\{\Delta\}$ 3 vector of translation $wc$ and rotations $\tan\theta_y$ and $\tan\theta_x$
$[X]^T$ 3 * $n_r$ matrix of {1, $x_i$, $y_i$ }. $x_i$, $y_i$ are coordinates of node $i$

For equilibrium the following conditions must be satisfied:

- The resultant due to external vertical forces acting on the raft must be equal to the sum of contact forces and pile loads
- The moment due to that resultant about either $x$-axis or $y$-axis must be equal to the sum of moments due to contact forces and pile loads about that axis

Assuming $Q_i$ is a symbol representing either pile load $Ph_i$ or contact force $Q_i$ on the mesh, gives:

$$\left.\begin{aligned} N &= Q_1 + Q_2 + Q_3 + ... + Q_n \\ N \,.\, e_x &= Q_1 \,.\, x_1 + Q_2 \,.\, x_2 + Q_3 \,.\, x_3 + ... + Q_n \,.\, x_n \\ N \,.\, e_y &= Q_1 \,.\, y_1 + Q_2 \,.\, y_2 + Q_3 \,.\, y_3 + ... + Q_n \,.\, y_n \end{aligned}\right\} \tag{2.71}$$

where:
$N$ Resultant of applied loads acting on the raft [kN]
$N\,e_x$ Moment due to resultant about $x$-axis, $M_x = N\,e_x$ [kN.m]
$N\,e_y$ Moment due to resultant about $y$-axis, $M_y = N\,e_y$ [kN.m]
$e_x$, $e_y$ Eccentricities of the resultant about $x$- and $y$-axes [m]
$x_i$, $y_i$ Coordinates of the load $Q_i$ [m]

Equation (2.71) is rewritten for the entire piled raft foundation in matrix form as:

$$\{N\} = [X]\{Q\} \tag{2.72}$$

where:
$\{N\}$ 3 vector of resultant and moments of applied loads acting on the piled raft

Substituting Eqns (2.67) and (2.70) in Eq. (2.72), gives the following linear system of equations of the piled rigid raft:

$$\{N\} = [X][kb][X]^T \{\Delta\} \tag{2.73}$$

Solving the above system of linear equations, gives *wc*, tan $\theta_x$, and tan $\theta_y$. Substituting these values in Eq. (2.70) gives the *n* settlements.

Substituting Eq. (2.70) in Eq. (2.67), gives the following equation to find the *n* unknown pile loads and contact forces.

$$\{Q\} = [kb][X]^T \{\Delta\} \tag{2.74}$$

### 2.4.4 Analysis of piled elastic raft

It is possible to treat the raft as an elastic plate on rigid piles. From the finite element analysis of the plate, the equilibrium of the raft is expressed as:

$$[kr]\{\delta\} = \{P\} - \{Q\} \tag{2.75}$$

where:
$\{P\}$ $3 * n_r$ vector of applied loads and moments on the raft nodes
$[kr]$ $3\ n_r * 3\ n_r$ plate stiffness matrix
$\{\delta\}$ $3 * n_r$ deformation vector of the raft

In the case of analyzing an elastic raft on pile groups, the elastic shortening of the pile may be added to the pile settlement in Eq. (2.68). The elastic shortening of the pile *i* is expressed as:

$$\Delta_i = \frac{Ph_i\, l_i}{Ep_i\, Ap_i} \tag{2.76}$$

where:
$\Delta_i$ Elastic shortening of pile *i* [m]
$l_i$ Length of pile *i* [m]
$Ap_i$ Cross-section area of pile *i* [$m^2$]
$Ep_i$ Modulus of elasticity of the material of pile *i* [$kN/m^2$]

Equation (2.76) is written for the entire piled raft in matrix form as:

$$\{wp\} = [Cp]\{Ph\} \tag{2.77}$$

where:
$\{wp\}$ Elastic shortening vector
$[Cp]$ Elastic pile matrix, which is a diagonal matrix
$\{Ph\}$ Vector of forces on pile heads

To take the effect of pile shortening into account, the elastic coefficient of the pile *i* in the matrix [*Cp*] is added to the flexibility coefficient of that pile in the matrix [*Cb*] in Eq. (2.68) as follows:

$$\{w\} = [\,[Cb] + [Cp]\,]\{Q\} \tag{2.78}$$

Inverting the total flexibility matrix [[*Cb*] + [*Cp*]] gives also the total stiffness matrix of piled raft [*kp*] with the effect of pile stiffness due to its elastic material.

$$\{Q\} = [kp]\{w\} \tag{2.79}$$

where [*kp*] is $n_r * n_r$ stiffness matrix of the piled raft with the effect of pile elastic material, $[kp] = [[Cb] + [Cp]]^{-1}$.

Substituting Eq. (2.79) in Eq (2.75) leads to:

$$[kr]\{\delta\} = \{P\} - [kp]\{w\} \tag{2.80}$$

Considering compatibility between piled raft displacement $\delta_i$ and soil settlement $s_i$, the following linear system of equations of the piled elastic raft can be obtained:

$$[\,[kp] + [kr]\,]\{\delta\} = \{P\} \tag{2.81}$$

Solving the above system of linear equations gives the displacement at each node of the raft, which is equal to the soil settlement at that node. Substituting soil settlements from Eq. (2.81) in Eq. (2.66), gives contact forces on the raft and forces on pile heads.

Once settlements on piles $wo_i$ are determined in the above three cases of piled rafts, the individual forces along the pile shaft and on the pile base can be obtained from Eq. (2.64).

## 2.5 Nonlinear analysis

### 2.5.1 Nonlinear rigid analysis of single pile

Nonlinear analysis is an important consideration since piles may be loaded close to their full capacity, even under working condition. The nonlinear relation between the load and settlement of a pile may be determined by considering a hyperbolic relation between load and settlement. Figure 2-8 shows a typical nonlinear curve of load-settlement for a wide range of soils. The curve can be approximated through a hyperbolic interpolation formula where several equation forms are available to verify this curve.

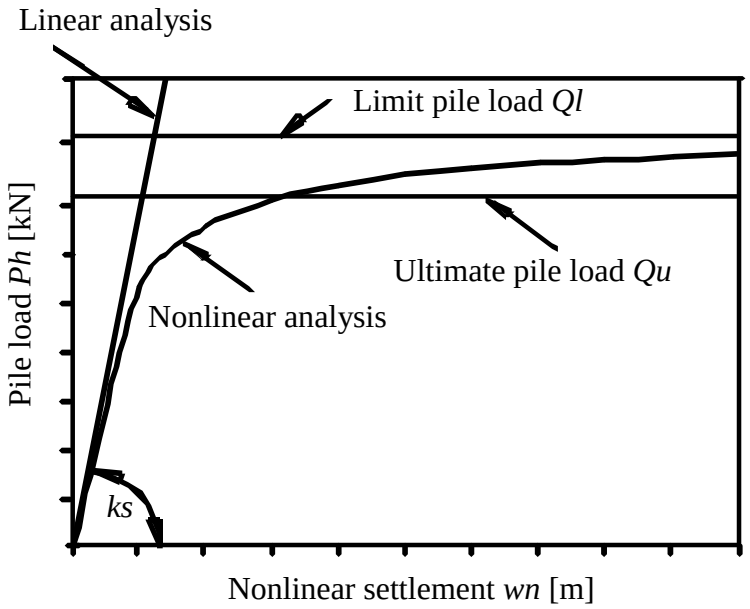


Figure 2-8 Load-settlement curve of a single pile (hyperbolic relation)

Many methods were developed to study pile-soil systems with nonlinear response using a hyperbolic relation between the load and settlement. *Fleming* (1992) developed a method to analyze and predict load-deformation behavior of a single pile using two hyperbolic functions describing the shaft and base performance individually under applied load. Analyzing nonlinear behavior by hyperbolic function was used by *Mandolini/ Viggiani* (1997) for pile groups and was used by *Russo* (1998) for piled raft. They considered piles as nonlinear interacting springs based on the method of interaction factors. *Basile* (1999) assumed, *Young's* modulus of the soil varies with the stress level at the pile-soil interface using a hyperbolic stress-strain relationship.

Available nonlinear analysis of foundation on *Winkler's* soil medium was presented by *Baz* (1987) for grid and by *Hasnien* (1993) for raft. *El Gendy* (1999) extended this analysis to be applicable for raft on continuum soil medium. The composed coefficient technique described in the previous sections enables to apply this analysis on pile problems.

The nonlinear behavior of the pile head force-settlement at the piled raft-soil interface may be represented as:

$$Ph = \frac{wn}{\frac{1}{ks} + \frac{wn}{Ql}} \tag{2.82}$$

where:
*wn* Nonlinear settlement of the pile [m]
*Ql* Limit pile load [kN]

In Figure 2-8 and Eq. (2.82) the initial tangent modulus for single pile is easily obtained from linear analysis of the pile, which is equal to the modulus of soil stiffness *ks*. The limit pile load *Ql* is a geometrical parameter of the hyperbolic relation. In some cases the value of *Ql* is different from the actual ultimate pile load. For a single pile, the force on the pile head *Ph* is known. Therefore, Eq. (2.82) gives directly the nonlinear settlement of the pile *wn*.

### 2.5.2 Nonlinear analysis of pile groups, elastic piled raft and rigid piled raft

The nonlinear analysis of the piled raft is also based on the hyperbolic relation presented in section 2.5.1. The initial tangent modulus of the hyperbolic relation may be obtained from the linear analysis of the piled raft as:

$$ks_i = \frac{Ph_i^o}{wo_i^o} \tag{2.83}$$

where:
$Ph_i^o$ Force on the pile head obtained from the linear analysis [kN]
$wo_i^o$ Pile settlement obtained from the linear analysis [m]
*i* Pile number
*o* Index, denotes the first analysis in the iteration (linear analysis)

### 2.5.3 Iterative Procedure

An iteration method is presented to solve the system of nonlinear equations of the piled raft. The main idea of this method is that the stiffness matrix [*kb*] for rigid raft or [*kp*] for elastic raft is converted to a diagonal stiffness matrix [*ke*]. Stiffness coefficients of this matrix, which represent nodal raft stiffness and pile stiffness coefficients, are determined from the contact force and its corresponding settlement. Only the pile stiffness is modified at each cycle from the iteration process. Using the equivalent diagonal matrix, equations of the piled raft are solved for each iteration cycle until the compatibility between raft, piles and soil is achieved.

Figure 2-9 shows the iteration cycle and the flow chart of the iteration process. The iteration process can be described in the following steps:

1 Carry out the linear analysis of the piled raft by solving system of linear Eqns (2.73) or (2.81) whichever is applicable, to get the settlements $\{w\}$

2 Find the nodal contact forces $\{Q\}$ due to the computed settlements from Eq. (2.74) for rigid raft and from Eq. (2.79) for elastic raft

3 From the computed settlements and contact forces, determine the nodal stiffness at all nodes on the raft and on pile heads from:

$$ke_i = \frac{Q_i}{w_i} \tag{2.84}$$

4 Modify the pile stiffness by:

$$ke_i = \frac{1}{\frac{1}{ks_i} + \frac{w_i}{Ql_i}} \tag{2.85}$$

5 Convert the soil stiffness matrix (matrix [*kb*] or matrix [*kp*]) to equivalent diagonal stiffness matrix [*ke*]. This matrix can be generated from nodal raft stiffness computed in step 3 and pile stiffness computed in step 4

6 Replace the full matrix by diagonal matrix [*ke*]. Then, carry out the nonlinear analysis of the piled raft to get the settlements $\{w\}$

7 Compute the contact force under the raft and force on pile head by:

$$Q_i = ke_i w_i \tag{2.86}$$

8 Compare the settlement from cycle *i* with that of cycle *I* - 1 to find the accuracy of the solution

The steps 3 to 8 are repeated until the accuracy reaches a specified tolerance ε, which means that a sufficient compatibility between settlements of piles, raft and soil are achieved at the piles-raft-soil interface. However, in this analysis the nonlinear response is applied only on piles, it can be easily added the nonlinear response of the raft as indicated by *El Gendy* (1999) to the piled raft system.

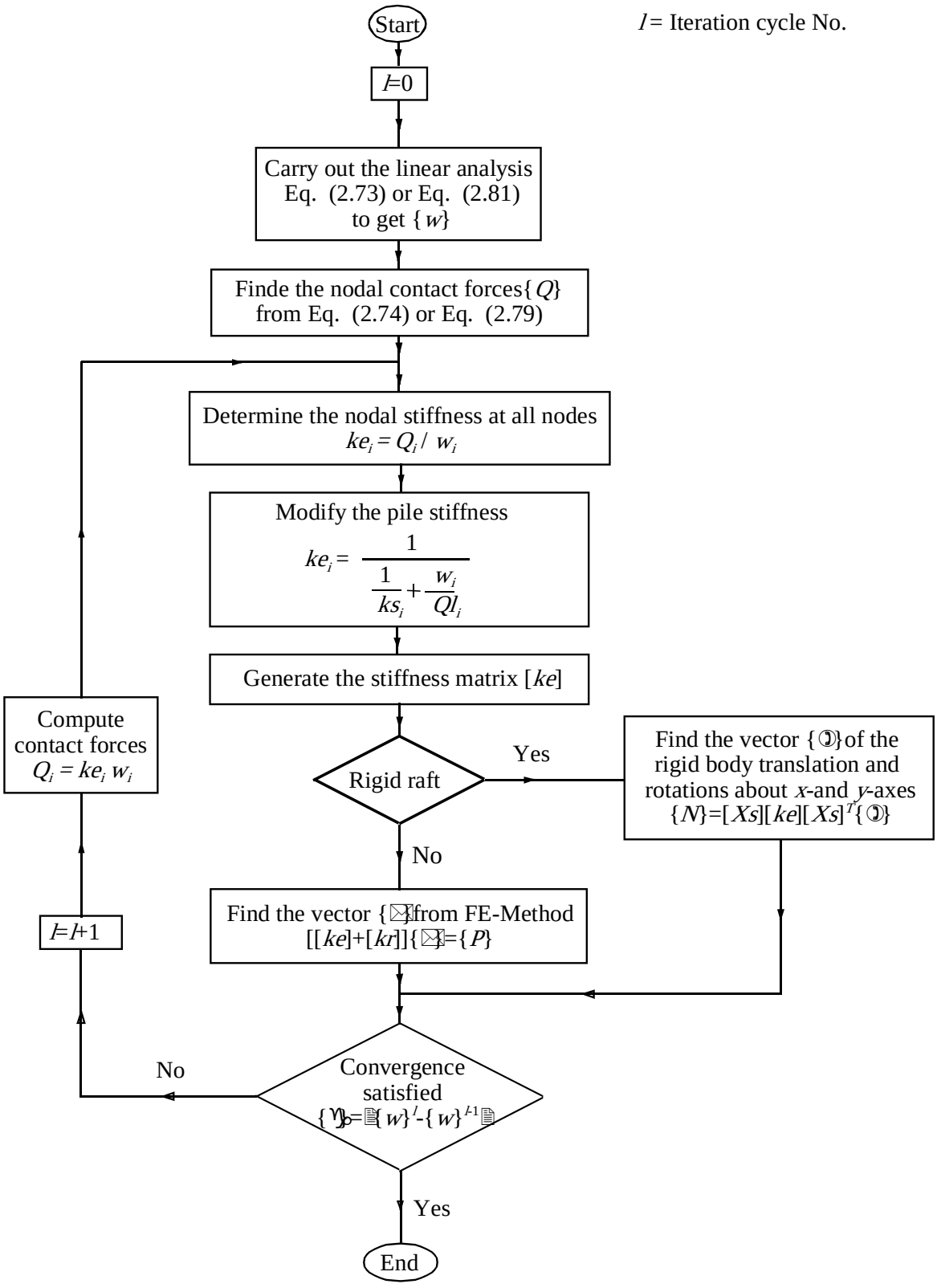


Figure 2-9 Flow chart of the iteration process

## 2.6 Numerical Examples

The numerical modeling of single pile, pile groups and piled raft described in this chapter was implemented in the program *ELPLA*. To verify and evaluate the numerical modeling, a series of comparison were carried out in which results from *ELPLA* were compared with those from existing methods of analysis.

### 2.6.1 Test Example: Evaluation of settlement influence factor $I_1$ for a single pile

Most of piled raft analyses apply a numerical integration using *Mindlin's* solution to determine flexibility coefficients of piles. Applying a numerical integration in the piled raft analysis, leads to significant computations, especially in large piled raft problems. In this case study closed form equations derived from *Mindlin's* solution are used in all computations. To verify these equations for determining flexibility coefficients, the settlement influence factors $I_1$ for a single pile obtained by *Poulos* (1968) and *Poulos/ Davis* (1968) are compared with those obtained by closed form equations listed in chapter 1.

From the analysis of a single pile carried out by *Poulos/ Davis* (1968), the settlement $s_1$ [m] of a single pile is expressed as:

$$s_1 = \frac{P}{L\,E_s} I_1 \tag{2.87}$$

where:

$P$ Load on the pile head [kN]
$L$ Pile length [m]
$E_s$ *Young's* modulus of the surrounding soil mass [kN/m$^2$]
$I_1$ Settlement influence factor for a single pile [-]

A pile of length $L$ = 12.5 [m] is chosen. The pile is divided into 10 elements, each 1.25 [m]. Load on the pile head $P$ and *Young's* modulus of the surrounding soil mass $E_s$ are chosen to make the term $P/E_s$ of Eq. (2.87) equal to unit. Thus, load on the pile head is chosen to be $P$ = 5000 [kN], while *Young's* modulus of the surrounding soil mass is chosen to be $E_s$ = 5000 [kN/m$^2$]. The settlement influence factor $I_1$ is determined at different values of $h/L$ and $L/d$, where $h$ [m] is the thickness of the soil layer and $d$ [m] is the pile diameter.

The settlement influence factors $I_1$ of a single pile published by *Poulos* (1968) in Table 1 in his paper are compared with those obtained from the closed form equations. The factors are tabulated in Table 2-1 and Table 2-2 for two different values of *Poisson's* ratio of the soil $\nu_s$. From these tables, it can be observed that the settlement influence factors obtained by closed form equations (chapter 1) at different soil layers and pile diameters are nearly equal to those obtained by *Poulos* (1968) with maximum difference of $\Delta$ = 2.78 [%].

Flexibility coefficients determined from numerical integration are also available in *ELPLA*. Table 2-3 and Table 2-4 list the settlement influence factors $I_1$ when using numerical integration. The tables show that settlement influence factors determined from closed form equation and those determined from numerical integration are nearly the same.

Table 2-1 Settlement influence factors $I_1$ [-] for a single pile
Using closed from equations, *Poisson's* ratio of the soil $\nu_s = 0.5$ [-]

| *h/L* | *Poulos* (1968) | | | *ELPLA* | | | Max. Diff. Δ [%] |
|---|---|---|---|---|---|---|---|
| | *L/d* | | | *L/d* | | | |
| | 10 | 25 | 100 | 10 | 25 | 100 | |
| ∞ | 1.41 | 1.86 | 2.54 | 1.44 | 1.88 | 2.56 | 2.13 |
| 5 | 1.31 | 1.76 | 2.44 | 1.34 | 1.77 | 2.47 | 1.23 |
| 2.5 | 1.20 | 1.64 | 2.31 | 1.22 | 1.65 | 2.33 | 1.67 |
| 1.5 | 0.98 | 1.42 | 2.11 | 0.99 | 1.43 | 2.12 | 1.02 |
| 1.2 | 0.72 | 1.18 | 1.89 | 0.74 | 1.19 | 1.90 | 2.78 |

Table 2-2 Settlement influence factors $I_1$ [-] for a single pile
Using closed from equations, *Poisson's* ratio of the soil $\nu_s = 0.0$ [-]

| *h/L* | *Poulos* (1968) | | | *ELPLA* | | | Max. Diff. Δ [%] |
|---|---|---|---|---|---|---|---|
| | *L/d* | | | *L/d* | | | |
| | 10 | 25 | 100 | 10 | 25 | 100 | |
| ∞ | 1.16 | 1.47 | 1.95 | 1.17 | 1.48 | 1.94 | 0.86 |
| 5 | 1.07 | 1.37 | 1.86 | 1.08 | 1.38 | 1.86 | 0.93 |
| 2.5 | 0.96 | 1.27 | 1.75 | 0.98 | 1.28 | 1.74 | 2.08 |
| 1.5 | 0.80 | 1.11 | 1.58 | 0.81 | 1.12 | 1.59 | 1.25 |
| 1.2 | 0.62 | 0.94 | 1.44 | 0.62 | 0.94 | 1.42 | 1.39 |

Table 2-3 Settlement influence factors $I_1$ [-] for a single pile
Using numerical integration, *Poisson's* ratio of the soil $\nu_s = 0.5$ [-]

| *h/L* | *Poulos* (1968) | | | *ELPLA* | | | Max. Diff. Δ [%] |
|---|---|---|---|---|---|---|---|
| | *L/d* | | | *L/d* | | | |
| | 10 | 25 | 100 | 10 | 25 | 100 | |
| ∞ | 1.41 | 1.86 | 2.54 | 1.42 | 1.84 | 2.51 | 1.18 |
| 5 | 1.31 | 1.76 | 2.44 | 1.31 | 1.74 | 2.42 | 0.82 |
| 2.5 | 1.20 | 1.64 | 2.31 | 1.19 | 1.62 | 2.30 | 1.22 |
| 1.5 | 0.98 | 1.42 | 2.11 | 0.97 | 1.40 | 2.08 | 1.42 |
| 1.2 | 0.72 | 1.18 | 1.89 | 0.72 | 1.16 | 1.86 | 1.59 |

Table 2-4 Settlement influence factors $I_1$ [-] for a single pile
Using numerical integration, *Poisson's* ratio of the soil $\nu_s = 0.0$ [-]

| *h/L* | *Poulos* (1968) | | | *ELPLA* | | | Max. Diff. Δ [%] |
|---|---|---|---|---|---|---|---|
| | *L/d* | | | *L/d* | | | |
| | 10 | 25 | 100 | 10 | 25 | 100 | |
| ∞ | 1.16 | 1.47 | 1.95 | 1.15 | 1.45 | 1.91 | 2.09 |
| 5 | 1.07 | 1.37 | 1.86 | 1.06 | 1.36 | 1.82 | 2.15 |
| 2.5 | 0.96 | 1.27 | 1.75 | 0.96 | 1.26 | 1.72 | 1.71 |
| 1.5 | 0.80 | 1.11 | 1.58 | 0.79 | 1.09 | 1.55 | 1.90 |
| 1.2 | 0.62 | 0.94 | 1.44 | 0.61 | 0.92 | 1.40 | 2.78 |

### 2.6.2 Case study: Piled raft of *Torhaus*

*Torhaus* is the first building in Germany with a foundation designed as a piled raft, Figure 2-10. The building lies in Frankfurt city in Germany. It is 130 [m] high and rests on two separate piled rafts, where a street passes under the building. Measured instruments were installed inside the foundation to record piled raft settlement and stress. Many authors studied the foundation of the *Torhaus* and applied their analysis methods on piled raft. Some of them are *Sommer et al.* (1985), *Sommer* (1989) and *Reul/ Randolph* (2003).

Figure 2-10 *Torhaus* (http://www.fussballportal.de/images/wm/fra_torhaus.jpg)

Figure 2-12 shows a layout of *Torhaus* with piled rafts. The building has no underground floors. The foundation is two separate equal piled rafts with rectangular shape areas, each of 17.5 [m] × 24.5 [m] sides. The distance between the two rafts is 10 [m]. The rafts are founded at a depth 3.0 [m] under the ground surface. The estimated total load on each raft is 200 [MN]. Raft thickness is 2.5 [m]. A total of 42 bored piles with a length of $l$ = 20 [m] and diameter of $D$ = 0.9 [m] are located under each raft. The pile spacing varies from 3.5 $D$ to 3.0 $D$. The subsoil at the location of the building consists of gravel and sand up to 5.5 [m] below the ground surface, followed by layers of Frankfurt clay extending to great depth. The groundwater level lies below rafts.

The building was constructed between 1983 and 1986, the recorded maximum settlement at the raft middle in 1988 was about 12 [cm] according to *Sommer* (1989). If *Torhaus* stands on a raft only, the expected settlement would be about 26 [cm], based on geotechnical studies according to *Sommer et al.* (1985). Therefore, to reduce the settlement, piled rafts were considered. Using available data and results of *Torhaus* piled rafts, which have been discussed in details in the previous references, the present piled raft analysis is evaluated and verified for analyzing a piled raft.

#### *2.6.2.1 Soil properties*

*Young's modulus*
According to *Reul/ Randolph* (2003), *Young's* modulus of the sand with gravel layer under the rafts is $E$ = 75000 [kN/m$^2$]. *Young's* modulus for reloading is taken to be $W = 3\,E$. Based on the back analysis after *Amann et al.* (1975), the distribution of modulus of compressibility for loading of Frankfurt clay with depth is defined by the following empirical formula:

$$E_s = E_{so}\left(1 + 0.35\,z\right) \tag{2.88}$$

while that for reloading is:

$$W_s = 70\left[\mathrm{MN/m^2}\right] \tag{2.89}$$

where:
$E_s$ Modulus of compressibility for loading [MN/m$^2$]
$W_s$ Modulus of compressibility for reloading [MN/m$^2$]
$E_{so}$ Initial modulus of compressibility, $E_{so}$= 7 [MN/m$^2$]
$z$ Depth measured from the clay surface, [m]

*Undrained cohesion and limit pile load*
The undrained cohesion $c_u$ of Frankfurt clay increases with depth from $c_u$ = 100 [kN/m$^2$] to $c_u$ = 400 [kN/m$^2$] in 70 [m] depth under the clay surface according to *Sommer/ Katzenbach* (1990). *Russo* (1998) suggested a limiting shaft friction not less than 180 [kN/m$^2$] meeting undrained shear strength of 200 [kN/m$^2$]. To carry out the present analysis a limit shaft friction of $\tau$ = 180 [kN/m$^2$] is assumed, which gives a limit pile load of $Ql$ = 10 [MN] where it is calculated from:

$$Ql = \tau * \pi * D * l = 180 * \pi * 0.9 * 20 = 10179\,[\mathrm{kN}] = 10\,[\mathrm{MN}] \tag{2.90}$$

where:
$Q_l$ Limit pile load, [MN]
$\tau$ Limit shaft friction, $\tau$ = 180 [kN/m$^2$]
$D$ Pile diameter, [m]
$l$ Pile length, [m]

*Poisson's ratio*
*Poisson's* ratio of the soil is taken to be $\nu_s$ = 0.25 [-].

To carry out the analysis, the subsoil under the raft is considered as indicated in the boring log of Figure 2-11 that consists of 13 soil layers. The total depth under the ground surface is taken to be 113 [m].

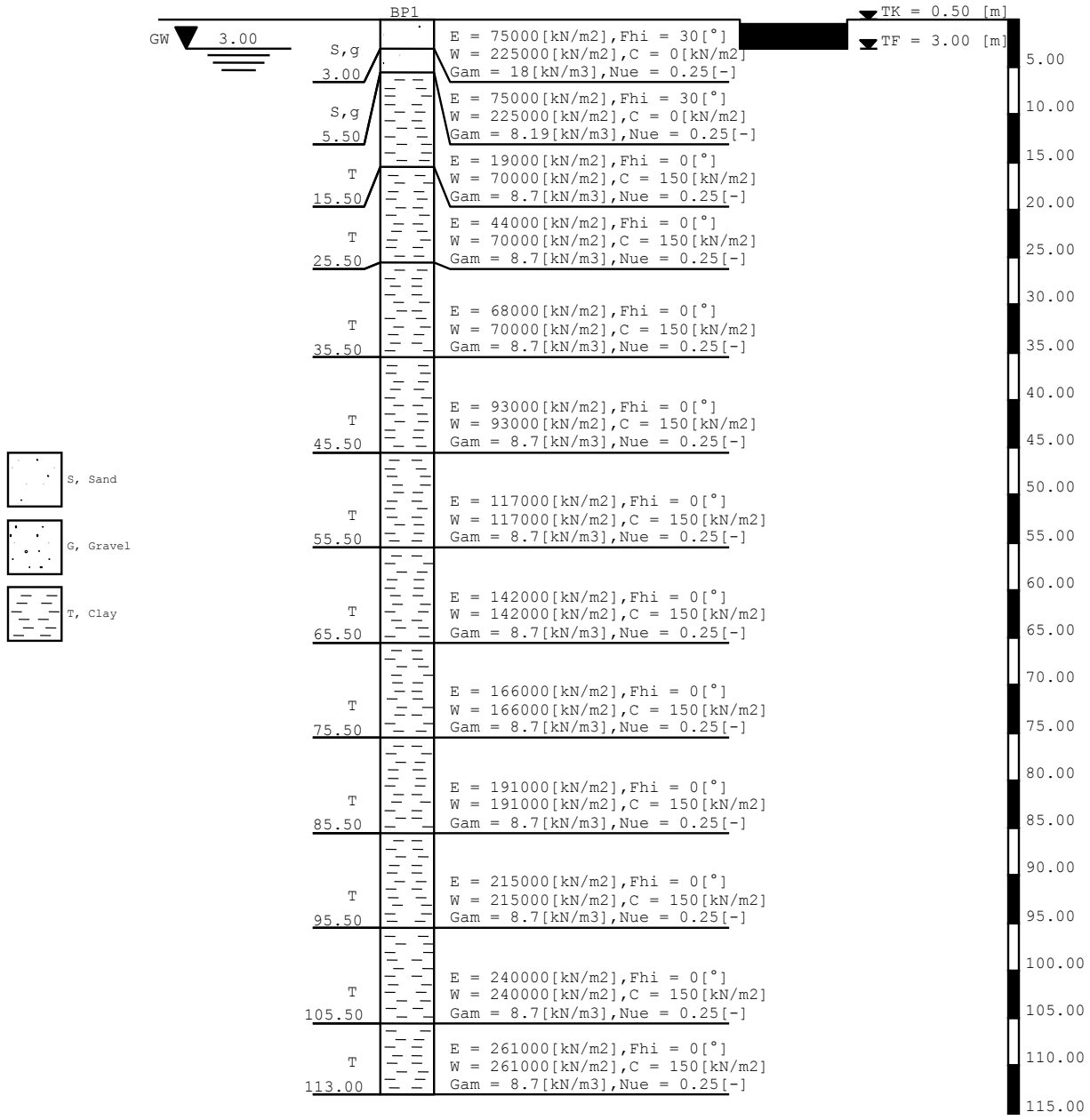


Figure 2-11 Boring log

### *2.6.2.2 Raft and pile material*

Raft has the following material parameters:

| | | | |
|---|---|---|---|
| *Young's* modulus | $E_b$ | $= 3.4 * 10^7$ | [kN/m$^2$] |
| *Poisson's* ratio | $\nu_b$ | $= 0.2$ | [-] |
| Unit weight | $\gamma_b$ | $= 25$ | [kN/m$^3$] |

while piles have the following material parameters:

| | | | |
|---|---|---|---|
| *Young's* modulus | $E_b$ | $= 2.35 * 10^7$ | [kN/m$^2$] |
| Unit weight | $\gamma_b$ | $= 25$ | [kN/m$^3$] |

### *2.6.2.3 Analysis of the piled raft*

Comparisons are carried out to evaluate the nonlinear analysis of piled elastic raft using composed coefficient technique. Here results of three-dimensional finite element analysis and field measurements are compared with those obtained by the present analysis. In the comparisons the present analysis is termed NPRH.

The raft is divided into rectangular elements as shown in Figure 2-13. Element sizes in *x*-direction for a single raft are 1.75 + 10 * 1.4 + 1.75 = 17.5 [m], while those in *y*-direction are 14 * 1.75 = 24.5 [m]. Piles are divided into line elements with 2.0 [m] in length. The raft is considered to be elastic plate supported on rigid piles. The effective depth of the soil layers under the raft is taken to be $H$ = 110 [m] as assumed by three-dimensional finite element analysis.

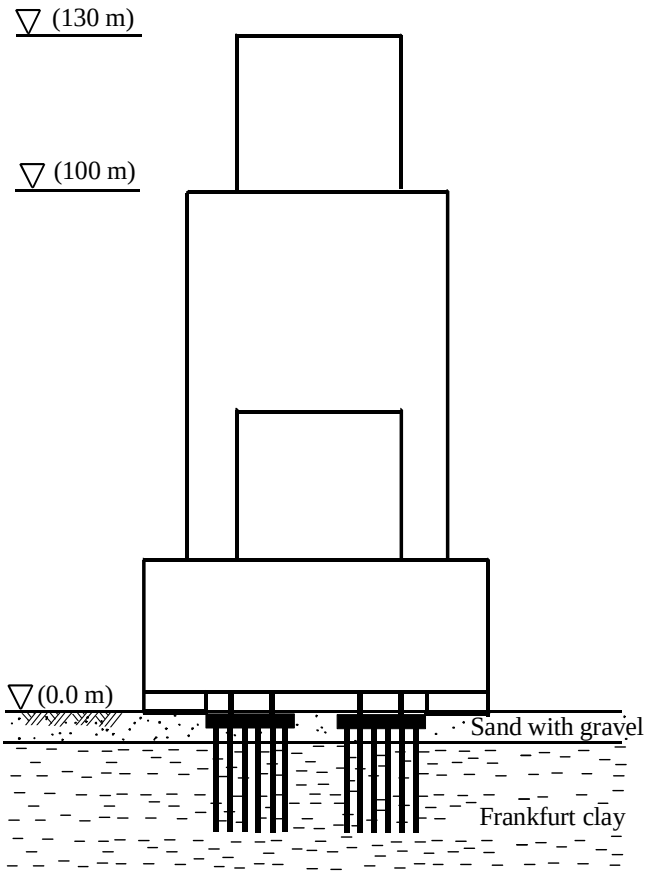


Figure 2-12 Layout of *Torhaus* with piled rafts

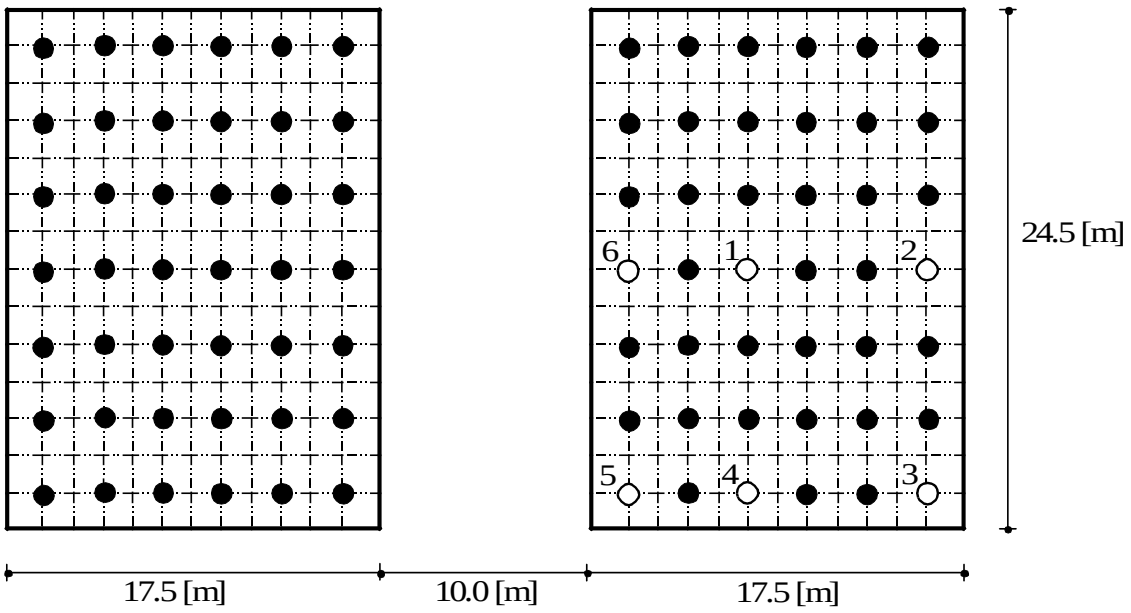


Figure 2-13 Mesh of *Torhaus* piled rafts with piles

#### *2.6.2.4 Comparison with three-dimensional finite element analysis and field measurements*

*Reul/ Randolfph* (2003) analyzed *Torhaus* piled rafts using three dimensional finite element model and compared their results with those obtained by field measurements according to *Sommer* (1989). For reducing the computational effort and time, they took the advantage of the symmetry in shape, soil and load geometry about both *x*- and *y*-axes to carry out the analysis for a quarter of a piled raft. In NPRH the two piled rafts are analyzed together to take the interaction among all elements of piled rafts. A linear analysis is carried out first to obtain the initial modulus of subgrade reaction. In this primary analysis the effect of reloading is taken into account. For the nonlinear analysis, the accuracy number is chosen to be 0.0002 [m]. Seven cycles in few minutes are required to obtain the nonlinear analysis of the piled rafts together. This is related to using composed coefficient technique that reduced the size of soil stiffness matrix from [1314 * 1314] to [390 * 390]. Accordingly, the total number of equations was reduced to 1170, where $n_{pr}$ = 1314, $n_r$ = 390 and number of unknown per node is 3 (3 $n_r$ = 1170).

Table 2-5 lists results of central settlement and bearing factor of piled raft obtained by NPRH and those obtained by *Reul/ Randolph* (2003) using three-dimensional finite element analysis. Also, the table includes the measured results presented by *Sommer* (1989). Figure 2-14 and Figure 2-15 compare loads on piles 1 to 6 (Figure 2-13) obtained by NPRH with those obtained by *Reul/ Randolph* (2003) using three-dimensional finite element analysis and with measured pile loads presented by *Sommer* (1989).

Table 2-5 Comparison between results obtained by 3D FE-Analysis and field measurements with those obtained by NPRH

| Type of analysis | Measurement | 3D FE-Analysis | NPRH |
|---|---|---|---|
| Central settlement $s_{center}$ [cm] | 12.4 | 9.6 | 11.2 |
| Bearing factor $\alpha_{kpp}$ [%] | 67 | 76 | 64 |

Table 2-5 shows that settlement and bearing factor of piled raft for NPRH is are in good agreement with field measurements. Results of pile loads in Figure 2-14 and Figure 2-15 are in good agreement with both those of three-dimensional finite element analysis and field measurements. Three-dimensional finite element analysis gave a relatively big difference in the bearing factor compared with that of field measurement and NPRH.

This case study shows that NPRH is not only an acceptable method to analyze piled raft but also a practical one for analyzing large piled raft problems. Besides the analysis gives good agreement with measured results, it takes less computational time and less effort for generating input data compared with other complicated models using three dimensional finite element analysis.

### *2.6.2.5 Comparing among different analysis types*

To show the difference between results when analyzing piled raft of *Torhous* linearly and nonlinearly as piled elastic raft or piled rigid raft, piled raft of *Torhous* is analyzed four times as follows:

- Linear piled rigid raft
- Nonlinear piled rigid raft
- Linear piled elastic raft
- Nonlinear piled elastic raft

For the four analysis types, Table 2-6 shows central settlement and bearing factor of piled raft, while Figure 2-16 and Figure 2-17 show loads on piles 1 to 6. In general, it can be noticed from Table 2-6 and these figures that:

*Settlement*
- Settlement from nonlinear analysis for piled rigid raft or piled elastic raft is greater than that obtained from linear analysis
- The nonlinear settlement exceeds linear settlement by 48 [%] for piled rigid raft and by 29 [%] for piled elastic raft
- For a single analysis, either linear or nonlinear, the difference in settlement obtained from analyzing piled rigid raft or piled elastic raft is small. This means any of the analysis can be used for estimating the settlement

*Bearing factor of piled raft*
- Bearing factor of piled raft from nonlinear analysis is less than that obtained from linear analysis
- Bearing factor of piled raft from nonlinear analysis decreases by 13 [%] for analyzing piled rigid raft and by 15 [%] for piled elastic raft

*Force on pile head*
- Using nonlinear analysis redistributes pile loads by increasing values of inner piles (piles 1 and 6) and decreasing values of edge piles (piles 2, 3, 4 and 5)
- Total pile loads of piled rigid raft are greater than those of piled elastic raft
- Pile loads for edge piles of piled rigid raft are greater than those of piled elastic raft and vice verse for inner piles

Table 2-6 Comparison between results of different analysis types

| Type of analysis | Piled rigid raft | | Piled elastic raft | |
|---|---|---|---|---|
| | Linear | Nonlinear | Linear | Nonlinear |
| Central settlement $s_{center}$ [cm] | 7.0 | 13.4 | 8.0 | 11.2 |
| Bearing factor $\alpha_{kpp}$ [%] | 88 | 77 | 75 | 64 |

Applying different analysis types on piled raft of *Torhous* shows that the nonlinear analysis of piled elastic raft is the acceptable analysis type, where its results are in agreement with measured values.

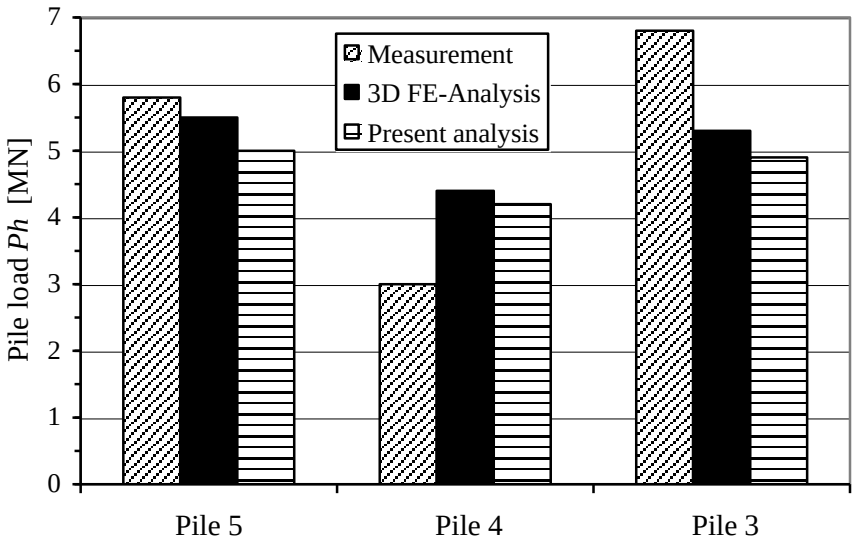


Figure 2-14 Comparison between pile loads obtained by 3D FE-Analysis and field measurements with those obtained by NPRH (Piles 3, 4 and 5)

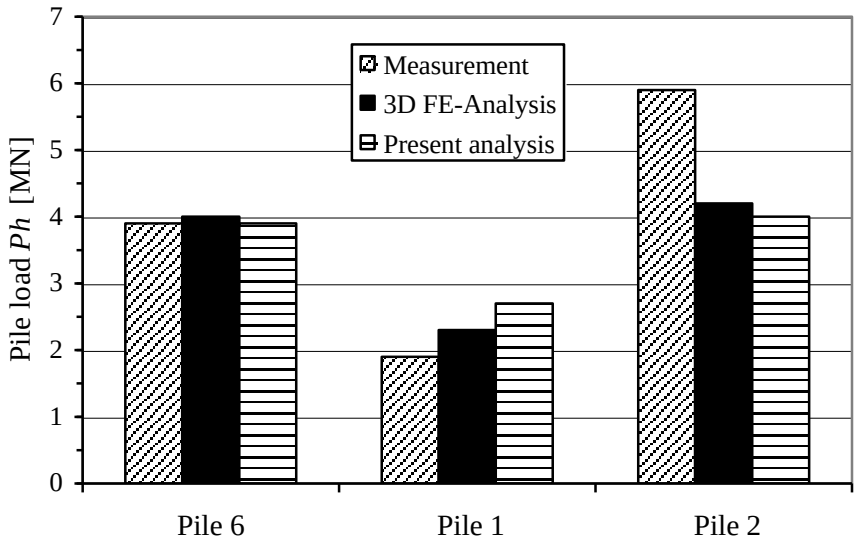


Figure 2-15 Comparison between pile loads obtained by 3D FE-Analysis and field measurements with those obtained by NPRH (Piles 1, 2 and 6)

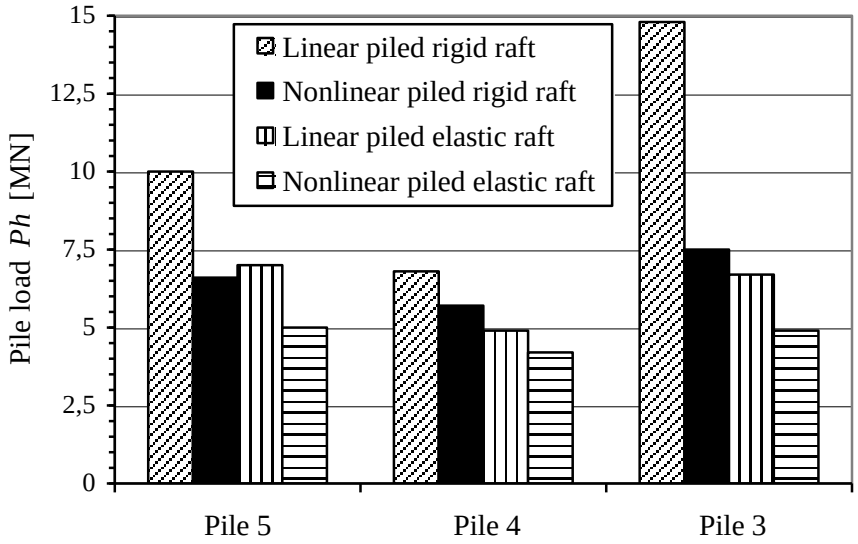


Figure 2-16 Comparison between pile loads of different analysis types (Piles 3, 4 and 5)

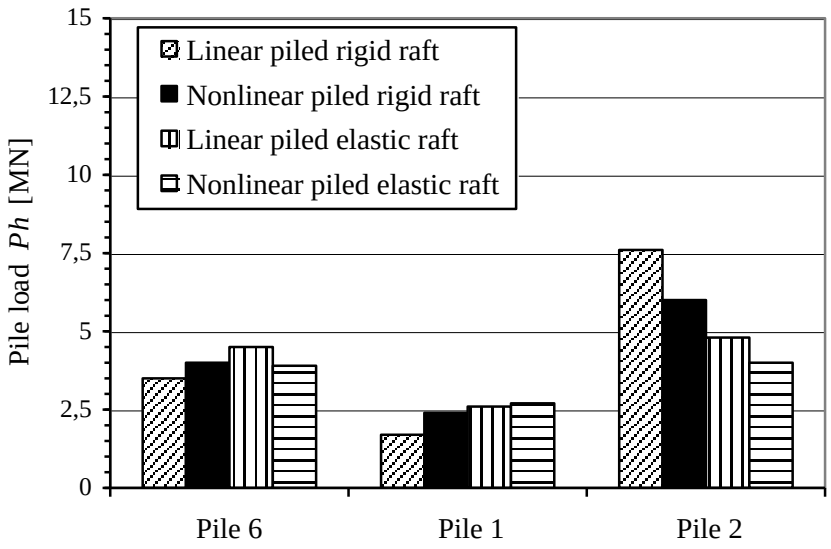


Figure 2-17 Comparison between pile loads of different analysis types (Piles 1, 2 and 6)

## 2.7 References


[1] *Amann, P./ Breth, H./ Stroh, D.* (1975): Verformungsverhalten des Baugrundes beim Baugrubenaushub und anschließendem Hochhausbau am Beispiel des Frankfurter Ton Mitteilungen der Versuchsanstalt für Bodenmechanik und Grundbau der Technischen Hochschule Darmstadt, Heft 15

[2] *Basile, F.* (1999): Non-linear analysis of pile groups
Proc. Instn Civ. Engrs Geotech. Engng. 137, 105-115

[3] *Baz, O.* (1987): Plates on nonlinear subgrade
Master Thesis, Mansoura University, Egypt

[4] *Butterfield, R./ Banerjee, K.* (1971): The elastic analysis of compressible piles and pile group
Géotechnique, 21, No. 1, 43-60

[5] *Clancy, P./ Randolph, M.* (1993): An approximate analysis procedure for piled raft foundation
Int. J. Numer. Anal. Meth. Geomech., 17 (12), 849-869

[6] *Clancy, P./ Randolph, M.* (1994): Simple design tools for piled raft foundation
Géotechnique, Vol. 46, No. 2, pp. 313-328

[7] *Fleming, W.* (1992): A new method for single pile settlement predication and analysis
Géotechnique, Vol. 42, No. 3, 411-425

[8] *El Gendy, M.* (1999): An iterative procedure for foundation-superstructure interaction problem
Port-Said Engineering Research journal, Vol. 3, No. I, pp. 1-19, Egypt

[9] *El Gendy, M.* (2007): Formulation of a composed coefficient technique for analyzing large piled raft
Scientific Bulletin, Faculty of Engineering, Ain Shams University, Cairo, Egypt. Vol. 42, No. 1, March 2007, pp. 29-56

[10] *Hasnien, M.* (1993): Finite element analysis of mat resting on nonlinear elastic medium
M. Sc. Thesis, Ain Shams University, Faculty of Engineering, Egypt

[11] *Jeong, S./ Won, J./ Lee, J.* (2003): Simplified 3D analysis of laterally loaded Pile Groups *TRB* Annual Meeting

[12] *Kany, M./ El Gendy, M./ El Gendy, A.* (2007): Analysis and design of foundations by the Program ELPLA
GEOTEC Software, Zirndorf

[13] *Kitiyodom, P./ Matsumoto, T.* (2002): A simplified analysis method for piled raft and pile group foundation with batter Piles
Int. J. Numer. Anal. Meth. Geomech., 26, 1349-1369

[14] *Kitiyodom, P./ Matsumoto, T.* (2003): A simplified analysis method for piled raft foundations in non-homogeneous soils
Int. J. Numer. Anal. Meth. Geomech., 27, 85-109

[15] *Lee, K./ Xiao, Z.* (2001): A simplified nonlinear approach for pile group settlement analysis in multilayered soils
Can. Geotech. *J.,* 38, 1063-1080

[16] *Liang, F./ Chen, L.* (2004): A modified variational approach for the analysis of piled raft foundation
Mechanics Research Communications 31, 593-604

[17] *Lutz, B./ El-Mossallamy, Y./ Richter, Th.* (2006): Ein einfaches, für die Handberechnung geeignetes Berechnungsverfahren zur Abschätzung des globalen Last-Setzungsverhaltens von Kombinierten Pfahl-Plattengründungen
Bauingenieur, Band 81, 61-66

[18] *Mandolini, A./ Viggiani, C.* (1997): Settlement of piled foundations
Géotechnique, Vol. 47, No. 4, 791-816

[19] *Mendonça, A./ Paiva, J.* (2003): An elastostatic FEM/BEM analysis of vertically loaded raft and piled raft foundation
Engineering Analysis with Boundary Elements, 27, 919-933

[20] *Mindlin, R. D.* (1936): Force at a Point in the interior of a semi-infinite solid
Physic 8, 195

[21] *Poulos, H.* (1968): Analysis of the settlement of pile groups
Géotechnique, Vol. 18, 449-471

[22] *Poulos, H.* (1999): Approximate computer analysis of pile groups subjected to loads and ground movements
Int. J. Numer. Anal. Meth. Geomech., 23, 1021-1041

[23] *Poulos, H./ Davis, E.* (1968): The settlement behaviour of single axially loaded incompressible piles and piers
Géotechnique, Vol. 18, 351-371

[24] *Reul, O./ Randolph, M.F.* (2003): Piled rafts in overconsolidated clay: comparison of in situ measurements and numerical analyses
Géotechnique Vol. 53, No. 3, 301-315

[25] *Russo, G.* (1998): Numerical analysis of piled rafts
Int. J. Numer. Anal. Meth. Geomech., 22, 477-493

[26] *Sommer, H.* (1989): Entwicklung der Hochhausgründungen in Frankfurt/ Main
Festkolloquium 20 Jahre Grundbauinstitut, 47-62, Darmstadt

[27] *Sommer, H./ Katzenbach, R.* (1990): Last-Verformungsverhalten des Messeturmes Frankfurt/ Main
Vorträge der Baugrundtagung 1990 in Karlsruhe, Seite 371-380

[28] *Sommer, H./ Wittmann, P./ Ripper, P.* (1985): Piled raft foundation of a tall building in Frankfurt clay
Proc. 11th Int. Conf. Soil Mech. Found. Engng, San Francisco 4, 2253-2257

[29] *Ta, L./ Small, J.* (1997): An approximation for analysis of raft and piled raft foundation
Computer and Geotechnics, Vol. 20, No. 2, pp. 105-123

[30] *Winkler, E.* (1867): Die Lehre von der Elastizität und Festigkeit
Dominicus, Prag

[31] *Wong, S./ Poulos, H.* (2005): Approximate pile-to-pile interaction factors between two dissimilar piles
Computer and Geotechnics 32, 613-618

# Chapter 3

# Empirical with numerical modeling pile group and piled raft

Table of Contents Page

**3 Empirical with numerical modeling pile group and piled raft** 3- 3

3.1 Introduction 3- 3

3.2 Numerical Modeling 3- 4
3.2.1 Pile-pile interaction 3- 4
3.2.2 Pile-raft interaction 3-12
3.2.3 Raft-pile interaction 3-13
3.2.4 Raft-soil interaction 3-15
3.2.5 Formulation of soil equations 3-16
3.2.6 Analysis of rigid piled raft 3-19
3.2.7 Analysis of rigid pile group or flexible raft on rigid pile group 3-22
3.2.8 Analysis of elastic piled raft 3-22
3.2.9 Iteration method 3-23

3.3 Case study: *Messeturm* piled raft 3-25
3.3.1 Description of the problem 3-25
3.3.2 Analysis of the piled raft 3-27
3.3.3 Soil properties 3-30

3.4 References 3-34

# 3 Empirical with numerical modeling pile group and piled raft

## 3.1 Introduction

Many authors have studied pile-soil system with nonlinear response using theoretical relations between load and settlement. *Mandolini/ Viggiani* (1997), (1998) and *Russo* (1998) considered piles as nonlinear interacting springs based on the method of interaction factors. In their analysis, the no-linearity is essentially concentrated at the pile-soil interface, while the interaction between other elements (pile-pile, pile-raft and raft-pile interactions) may be represented by a linear model. The nonlinear soil-pile response is represented by an expression corresponding to a hyperbolic load-settlement relationship for the single pile. The hyperbolic relation is based on a function having a maximum value for the pile capacity. The maximum value is intended only as a geometrical parameter of the hyperbola fitting the load-settlement curve in the load range of interest. In some cases, this value may significantly differ from the actual failure load (*Mandolini/ Viggiani* (1997)).

*Basile* (1999), (2003) had used a nonlinear model that follows the well-established hyperbolic relationship between soil stress and strain. This model was proposed by *Duncan/ Chang* (1970), which assumes that soil modulus of elasticity varies with the stress level at the pile-soil interface. The hyperbolic curve fitting for this model depends on some constants, which are difficult to be evaluated. The best way to determine these constants is by fitting the load-deformation curve with the data from the full-scale pile load test.

*Witzel/ Kempfert* (2005) presented empirical relations to predict load-settlement behavior for precast driven piles using field test data. Also, most national codes such as German standard DIN 4014 [5] and Egyptian standard ECP [7] present empirical relations for load-settlement of piles based on situ statistical results. Therefore, *El Gendy et al.* (2006) developed a mixed technique containing empirical and mathematical models for analyzing pile group and piled raft. The technique depends on load-settlement curve obtained from field measurements or empirical relations; a nonlinear analysis of combined piled-raft is presented to take into account the actual response of subsoil behavior. In the analysis, each pile is treated as two units, shaft and base, having a uniform settlement along the pile shaft and in the pile base. This assumption enables modeling the nonlinear behavior of combined piled-raft. The nonlinear response of the pile is based on the DIN 4014 empirical relation of load-settlement curve. Connecting empirical and theoretical procedures, a method termed NPRD for **n**onlinear analysis of combined **p**iled-**r**aft using **D**IN 4014 is developed. The procedure meets the requirements of the KPP-guideline [23], section 6, to a computation model. The efficiency of NPRD is demonstrated in a comparison computation of Frankfurt *Messeturm* with the results of different authors. The method was implemented in the program *ELPLA* [8].

## 3.2 Numerical Modeling

In the analysis of the numerical model, the self-settlement of a pile is determined from DIN 4014 [5] load-settlement relationship while the settlement due to pile-pile, pile-raft and raft-soil interactions is determined numerically using flexibility coefficients. Full compatibility between settlements of piles, raft and soil is achieved at pile-raft-soil interface.

### 3.2.1 Pile-pile interaction

DIN 4014 [5] presents pile load in two components: tip force on the base of the pile and skin friction force acting along the pile shaft. Therefore, two flexibility matrices for pile-pile interaction without the effect of pile itself are determined. The first matrix represents the influence of unit tip forces, while the other represents the influence of unit skin forces.

#### *3.2.1.1 Settlement along the pile shaft $Sbs_{i,j}$* **[m]** *due to a tip force $Qb_j$* **[kN]**

To formulate equations of the method, a system of two piles of different lengths is considered as shown in Figure 3-1. The actual tip stress $qb_j$ [kN/m$^2$] on the base of the pile $j$ is replaced by an equivalent tip force $Qb_j$ [kN]. The pile $i$ of a length $l_i$ [m] is subdivided into $m$ elements of equal length $\Delta l$ [m]. First, the settlement in a shaft element $k$ of the pile $i$ that is influenced by a tip force $Qb_j$ acting on the base of the pile $j$ is determined. Then, a uniform settlement along the pile shaft due to this tip force can be calculated numerically by integrating settlements for the individual elements.

According to *Mindlin's* solution (1936) the settlement $Sbs_{k,j}$ in a point $k$ at a depth $z$ from the surface due to a tip force $Qb_j$ on the base of pile $j$ is given by:

$$Sbs_{k,j} = f_{k,j}\, Qb_j \tag{3.1}$$

where $f_{k,j}$ is given by *Mindlin's* solution as:

$$f_{k,j} = \frac{1}{16\,\pi\, G_s\,(1-\nu_s)}\left(\frac{3-4\,\nu_s}{R_1} + \frac{8\,(1-\nu_s)^2 - (3-4\nu_s)}{R_2}\right.$$
$$\left. + \frac{(z-c)^2}{R_1^3} + \frac{(3-4\,\nu_s)(z+c)^2 - 2cz}{R_2^3} + \frac{6\,c\,z\,(z+c)^2}{R_2^5}\right) \tag{3.2}$$

where:

$R_1 = \sqrt{r^2 + (z-c)^2}$, $R_2 = \sqrt{r^2 + (z+c)^2}$ and

$c$ Depth of the point load $Qb_j$ from the surface [m]
$z$ Depth of the studied point $k$ from the surface [m]
$r$ Radial distance between points $k$ and $j$ [m]
$f_{k,j}$ Flexibility coefficient of point $k$ due to a unit load at point $j$ [m/kN]
$G_s$ Shear modulus of the soil [kN/m$^2$], $G_s = 0.5\, E_s / (1+ \nu_s)$
$E_s$ Elasticity modulus of the soil [kN/m$^2$]
$\nu_s$ *Poisson's* ratio of the soil [-]

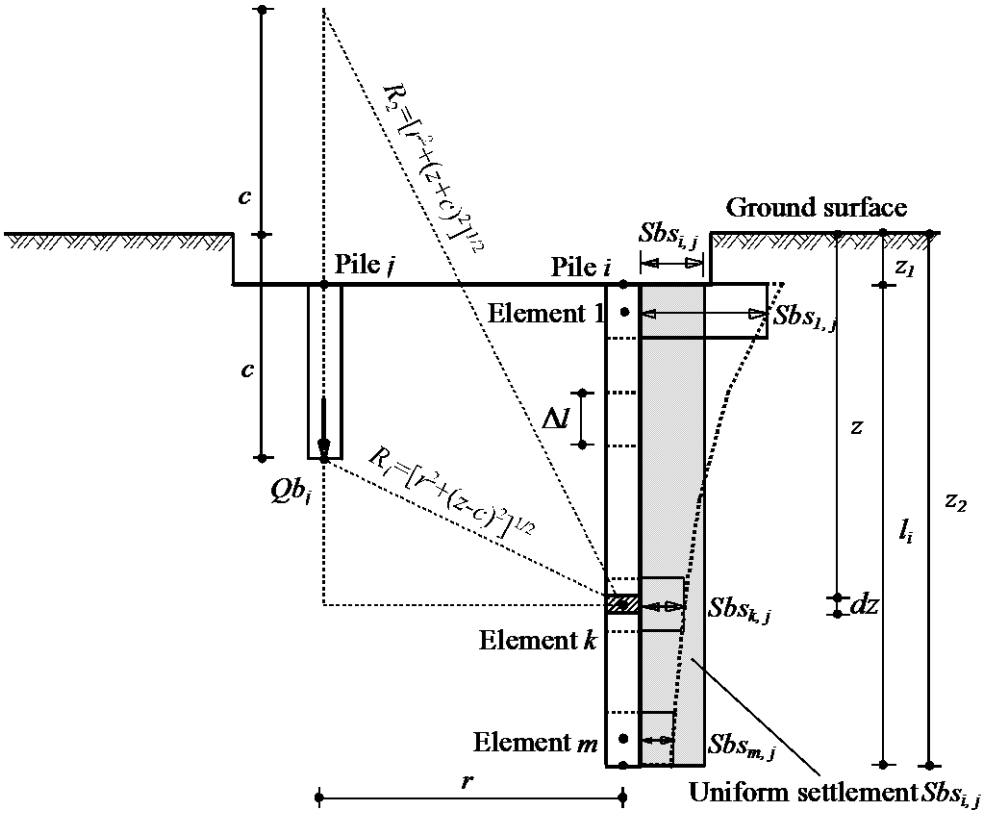


Figure 3-1 Settlement $Sbs_{k,j}$ in a pile element $k$ due to a tip force $Qb_j$ on the base of pile $j$

Then the uniform settlement $Sbs_{i,j}$ along the shaft of pile $i$ due to a tip force $Qb_j$ on the base of pile $j$ can be obtained from:

$$Sbs_{i,j} = \frac{1}{l_i} \int_{z_1}^{z_2} Sbs_{k,j}\, dz \tag{3.3}$$

Although Eq. (3.3) can be integrated analytically for $z$ but a numerical integration is used to allow analyzing pile passing through multi-layered soil as described later. Substituting Eq. (3.1) in Eq. (3.3) and applying numerical integration using the rectangular rule, leads to:

$$Sbs_{i,j} = \frac{Qb_j\, \Delta l}{l_i} \left( f_{1,j} + f_{2,j} + f_{3,j} + f_{4,j} + ... + f_{m,j} \right) \tag{3.4}$$

Equation (3.4) is written in a simplified form as:

$$Sbs_{i,j} = F_{i,j}\, Qb_j \tag{3.5}$$

where $F_{i,j}$ [m/kN] is the shaft flexibility coefficient of pile $i$ due to a tip force $Qb_j$ on the base of pile $j$.

The shaft flexibility coefficient $F_{i,j}$ is expressed as:

$$F_{i,j} = \frac{\Delta l}{l_i}\left( f_{1,j} + f_{2,j} + f_{3,j} + f_{4,j} + ... + f_{m,j} \right) \tag{3.6}$$

#### *3.2.1.2 Settlement in the pile base $Sbb_{i,j}$ [m] due to a tip force $Qb_j$ [kN]*

The settlement $Sbb_{i,j}$ in the base of the pile $i$ due to a tip force $Qb_j$ on the base of pile $j$ is expressed as:

$$Sbb_{i,j} = F_{b,j}\, Qb_j \tag{3.7}$$

where $F_{b,j}$ [m/kN] is the base flexibility coefficient of pile $i$ due to a tip force $Qb_j$ on the base of pile $j$. The base flexibility coefficient is determined from Eq. (3.2) by putting $z = z_2$, where $z_2$ [m] is the base depth of pile $i$ from the ground surface.

#### *3.2.1.3 Settlement in the pile $Sb_{i,j}$ [m] due to a tip force $Qb_j$ [kN]*

From the assumption that the pile has a uniform settlement in all its nodes, settlement along the shaft is the same as that in the base. Now, the settlement in the pile $i$ can be represented by one value $Sb_{i,j}$, which is the average of shaft and base settlements of the pile due to the tip force $Qb_j$ on the base of the pile $j$. Taking the average of settlements in Eqns (3.5) and (3.7) gives the settlement in the pile by:

$$Sb_{i,j} = Fb_{i,j}\, Qb_j \tag{3.8}$$

where $Fb_{i,j} = 0.5\ (F_{i,j} + F_{b,j})$ is the flexibility coefficient of pile $i$ due to a tip force $Qb_j$ on the base of pile $j$ [m/kN].

#### *3.2.1.4 Settlement in the pile $Sb_i$ [m] due to all tip forces*

For a group of $n_p$ piles, the settlement $Sb_i$ in a pile $i$ is attributed to settlements caused by all tip forces acting on $n_p$ piles except pile $i$. Then, settlement $Sb_i$ is given by:

$$Sb_i = S\, b_{i,1} + Sb_{i,2} + Sb_{i,3} + ... + Sb_{i,n} = \sum_{j=1}^{n} Fb_{i,j}\, Qb_j \,, i \neq j \tag{3.9}$$

For a pile group of $n_p$ piles, Eq. (3.9) can be written in matrix form as:

$$\{Sb\} = [Fb]\{Qb\} \tag{3.10}$$

where:
$\{Sb\}$ $n_p$ vector of settlements in piles due to tip forces on pile bases
$\{Qb\}$ $n_p$ vector of tip forces on pile bases
$[Fb]$ $n_p * n_p$ matrix of pile flexibility coefficients due to unit tip forces on piles, $Fb_{i,i} = 0$

### *3.2.1.5 Settlement along the pile shaft* $Sss_{i,j}$ [m] *due to a skin friction force* $Qs_j$ [kN]

Figure 3-2 shows a system of two piles where a shaft element *k* of a pile *i* is influenced by a skin friction $\tau s_j$ [kN/m$^2$] acting on the shaft perimeter of a pile *j* with a diameter $d_j$ [m] and a length $l_j$ [m]. Using DIN 4014 [5], the skin friction along the shaft perimeter of pile *j* is represented by a total skin friction force $Qs_j$ [kN] = $\pi\ d_j\ l_j\ \tau s_j$. To avoid extensive computations when applying *Mindlin's* solution to determine flexibility coefficients due to shaft stress along the pile shaft, the shaft stress $\tau s_j$ is replaced by an equivalent line load $T$ [kN/m] = $Qs_j / l_j$ acting on the axis of the pile. The settlement $Sss_{k,j}$ in a point *k* at a depth *z* from the surface due to a total skin force $Qs_j$ on a pile *j* is expressed as:

$$Sss_{k,j} = I_{k,j}\, Qs_j \tag{3.11}$$

where $I_{k,j}$ [m/kN] is the flexibility coefficient of point *k* due to the total skin friction force $Qs_j$ on pile *j*. This flexibility coefficient is determined from Eq. (3.2) by integrating the coefficient of point load $dQs_j = T\ dc$ over the length of pile *j*. The flexibility coefficient $I_{k,j}$ of the point *k* due to a unit skin force on pile *j* can be obtained from:

$$I_{k,j} = \frac{1}{l_j}\int_{c_1}^{c_2} f_{k,j}\, dc \tag{3.12}$$

The integration yields to:

$$I_{k,j} = \frac{1}{16\,\pi\, l_j\, G_s\,(1-\nu_s)}\left(I_1 + I_2 + I_3 + I_4 + I_5\right) \tag{3.13}$$

where terms $I_1$ to $I_5$ are given by:

$$I_1 = (3-4\,\nu_s)\ln\left[\frac{\sqrt{r^2+(z-c_2)^2}-(z-c_2)}{\sqrt{r^2+(z-c_1)^2}-(z-c_1)}\right] \tag{3.14}$$

$$I_2 = \left[8\,(1-\nu_s)^2-(3-4\,\nu_s)\right]\ln\left[\frac{\sqrt{r^2+(z+c_2)^2}+(z+c_2)}{\sqrt{r^2+(z+c_1)^2}+(z+c_1)}\right] \tag{3.15}$$

$$I_3 = \ln\left[\frac{\sqrt{r^2+(z-c_2)^2}-(z-c_2)}{\sqrt{r^2+(z-c_1)^2}-(z-c_1)}\right] + \frac{z-c_2}{\sqrt{r^2+(z-c_2)^2}} - \frac{z-c_1}{\sqrt{r^2+(z-c_1)^2}} \tag{3.16}$$

$$I_4 = (3 - 4\,\nu_s)\left( \ln\left[ \frac{\sqrt{r^2 + (z + c_2)^2} + (z + c_2)}{\sqrt{r^2 + (z + c_1)^2} + (z + c_1)} \right] - \frac{(z + c_2)}{\sqrt{r^2 + (z + c_2)^2}} \right.$$

$$\left. + \frac{(z + c_1)}{\sqrt{r^2 + (z + c_1)^2}} \right) - 2\,z \left( \frac{1}{\sqrt{r^2 + (z + c_1)^2}} - \frac{1}{\sqrt{r^2 + (z + c_2)^2}} \right. \tag{3.17}$$

$$\left. + \frac{z\,(z + c_1)}{r^2 \sqrt{r^2 + (z + c_1)^2}} - \frac{z\,(z + c_2)}{r^2 \sqrt{r^2 + (z + c_2)^2}} \right)$$

$$I_5 = \frac{6\,z\left[r^4 - z\,(z + c_2)^3\right]}{3\,r^2\left[r^2 + (z + c_2)^2\right]^{3/2}} - \frac{6\,z\left[r^4 + z\,(z + c_1)^3\right]}{3\,r^2\left[r^2 + (z + c_2)^2\right]^{3/2}} \tag{3.18}$$

$$- \frac{6\,z}{\sqrt{r^2 + (z + c_2)^2}} + \frac{6\,z}{\sqrt{r^2 + (z + c_1)^2}}$$

where:

$c_1$ Start depth of the line load $T$ from the surface [m]
$c_2$ End depth of the line load $T$ from the surface [m]
$l_j$ Length of the line load $T$ [m]
$r$ Radial distance between point $k$ and $j$ [m]

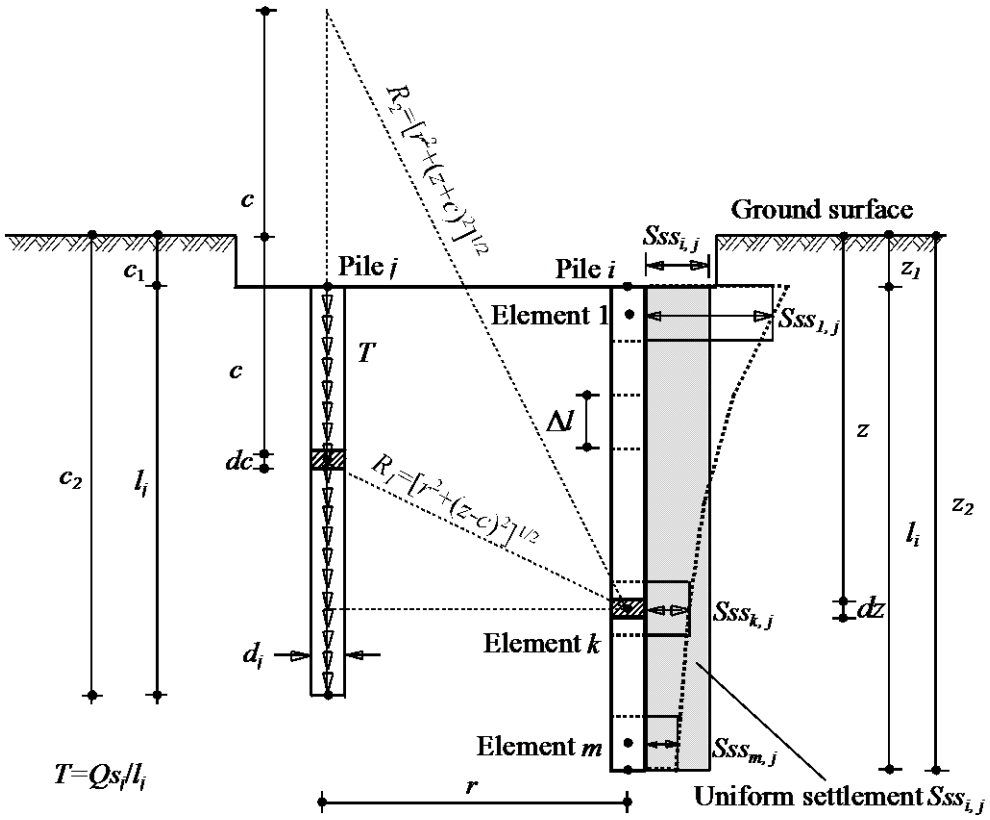


Figure 3-2 Settlement $Sss_{k,j}$ in a pile element $k$ due to a skin force $Qs_j = T_j\, l_j$ on pile $j$

The uniform settlement $Sss_{i,j}$ along the shaft of pile $i$ due to a skin force $Qs_j$ on pile $j$ can be obtained by using the same approach used for determining the uniform settlement due to a tip force on the base. Similarly to Eq. (3.5), the uniform settlement $Sss_{i,j}$ is given by:

$$Sss_{i,j} = L_{i,j}\, Qs_j \tag{3.19}$$

where $L_{i,j}$ [m/kN] is the shaft flexibility coefficient of pile $i$ due to a skin force $Qs_j$ on pile $j$. The shaft flexibility coefficient $L_{i,j}$ is expressed as:

$$L_{i,j} = \frac{\Delta l}{l_i}\left( I_{1,j} + I_{2,j} + I_{3,j} + I_{4,j} + ... + I_{m,j} \right) \tag{3.20}$$

#### *3.2.1.6 Settlement in the pile base $Ssb_{i,j}$ [m] due to a skin force $Qs_j$ [kN]*

The settlement $Ssb_{i,j}$ in the base of the pile $i$ due to a skin force $Qs_j$ on pile $j$ is expressed as:

$$Ssb_{i,j} = L_{b,j}\, Qs_j \tag{3.21}$$

where $L_{b,j}$ [m/kN] is the base flexibility coefficient of pile $i$ due to a skin force $Qs_j$ on pile $j$. The base flexibility coefficient is determined from Eq. (3.11) by putting $z = z_2$.

#### *3.2.1.7 Settlement in the pile $Ss_{i,j}$* **[m]** *due to a skin force $Qs_j$* **[kN]**

Similarly to Eq. (3.8), the settlement in the pile is obtained from:

$$Ss_{i,j} = Is_{i,j}\, Qs_j \tag{3.22}$$

where $Is_{i,j} = 0.5\,(L_{i,j} + L_{b,j})$ is the flexibility coefficient of pile *i* due to a skin force $Qs_j$ on pile *j* [m/kN].

#### *3.2.1.8 Settlement in the pile $Ss_i$* **[m]** *due to all skin forces*

Again and similar to Eq. (3.10), the settlement $Ss_i$ for a pile group of $n_p$ piles is given in matrix form by:

$$\{Ss\} = [Is]\{Qs\} \tag{3.23}$$

where:
$\{Ss\}$ $n_p$ vector of settlements in piles due to skin forces on piles
$[Is]$ $n_p * n_p$ matrix of pile flexibility coefficients due to unit skin forces on piles, $Is_{i,i} = 0$
$\{Qs\}$ $n_p$ vector of skin forces on piles

#### *3.2.1.9 Self-settlement of the pile $Sv_i$* **[m]**

According to DIN 4014 [5], the self-settlement of the pile is determined from the empirical nonlinear relation between the load and settlement of a single pile as indicated in Figure 3-3. From this figure, the relation between the self-settlement in the pile and its load can be expressed as:

$$Sv_i = \frac{1}{\tan k_i}\, Qp_i = Cp_i\, Qp_i \tag{3.24}$$

where:
$Sv_i$ Self-settlement of pile *i* [m]
$Qp_i$ Load on pile *i*, $Qp_i = Qb_i + Qs_i$ [kN]
$\tan k_i$ Ratio between the load on pile and the settlement [kN/m]
$Cp_i$ Flexibility coefficient of pile *i* due to a unit load on it, $Cp_i = 1/\tan k_i$, [m/kN]

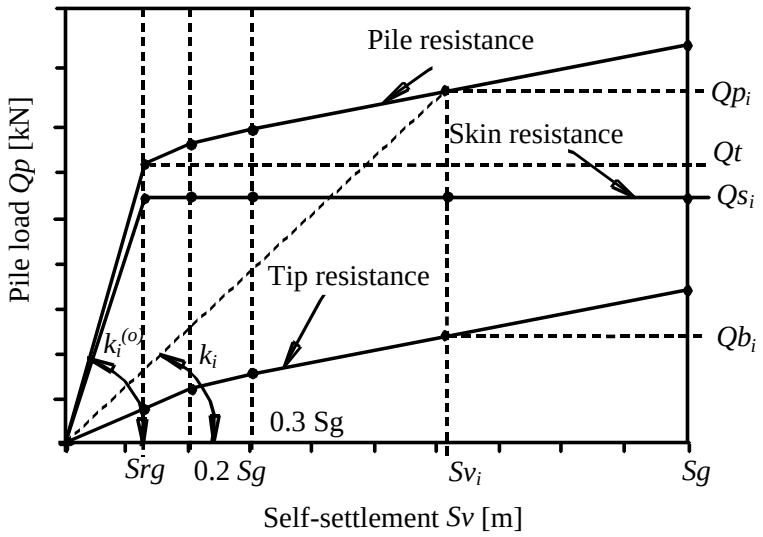


Figure 3-3 Load-settlement curve of a single pile according to DIN 4014 [5]

For a pile group of $n_p$ piles, Eq. (3.24) can be written in matrix form as:

$$\{Sv\} = [Cp]\{Qp\} \tag{3.25}$$

where:
$\{Sv\}$ $n_p$ vector of self-settlements in piles
$[Cp]$ $n_p * n_p$ diagonal matrix of flexibility coefficients due to unit pile loads
$\{Qp\}$ $n_p$ vector of pile loads

Equation (3.25) may be written in another form as:

$$\{Qp\} = [Kp]\{Sv\} \tag{3.26}$$

where $[Kp] = [Cp]^{-1}$ is a diagonal matrix of dimension $[n_p * n_p]$ representing soil stiffness due to pile self-settlements. The matrix coefficients are obtained from ($\tan k_i$).

In the nonlinear analysis of pile group or piled raft, it is required to assess an initial value for the flexibility coefficient $Cp_i$ to start the computation. This value may be estimated from the ratio between pile load $Qt$ and settlement $Srg$ as indicated in Figure 3-3 and Eq. (3.27). It is clear from Figure 3-3 that for a relative light applied load on the raft, i.e. $Qp \leq Qt$, the analysis can be carried out by this initial value without modification.

$$Cp_i^{(o)} = \frac{1}{\tan k_i^{(o)}} \tag{3.27}$$

where:
$\tan k_i^{(o)}$ Ratio between $Qt$ and $Srg$ [kN/m]
$Cp_i^{(o)}$ Initial flexibility coefficient of pile $i$ due to a unit load on it [m/kN]
$Srg$ Settlement at ultimate skin friction [m]
$Qt$ Pile load corresponding to $Srg$ [kN]

### 3.2.2 Pile-raft interaction

In the analysis, both the raft and the contact area of the supporting medium are divided into elements. For each node in the elements, the contact pressure area around this node may take different shapes according to the natural geometry of the elements around the node. The contact pressure $qr_j$ [kN/m$^2$] at the area around a node $j$ on the raft is replaced by an equivalent contact force $Qr_j$ [kN]. Figure 3-4 shows a shaft element $k$ of a pile $i$ that is influenced by a contact force $Qr_j$ acting on the raft at node $j$.

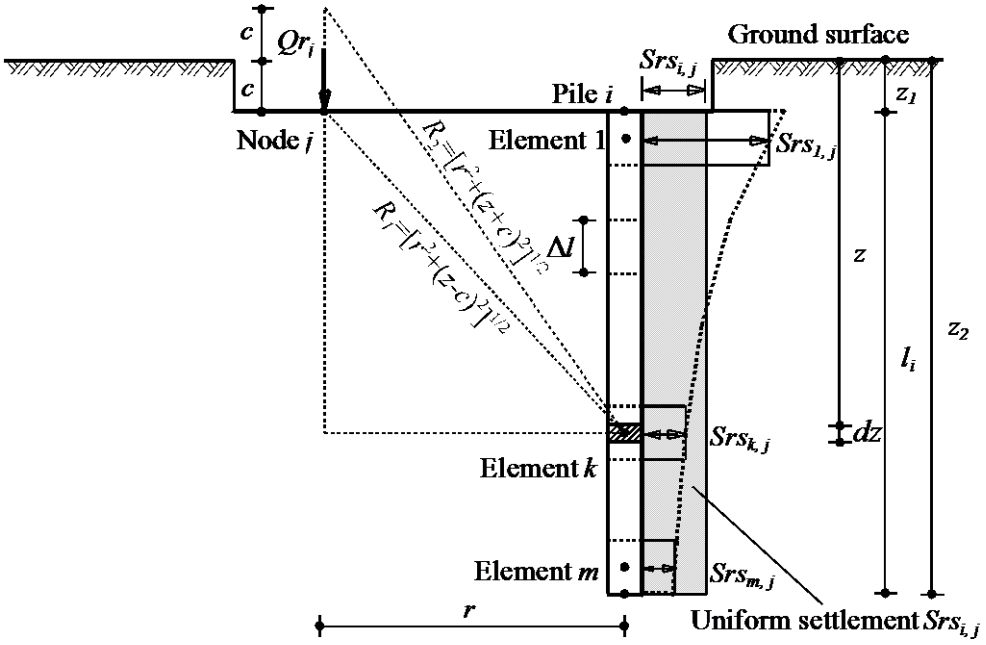


Figure 3-4 Settlement $Srs_{k,j}$ in a pile element $k$ due to a contact force $Qr_j$

Using the same approach described in section 3.2.1 with the same equations, a settlement $Srs_{k,j}$ in a pile element $k$ due to a contact force $Qr_j$ is determined. Then, a uniform settlement $Srs_{i,j}$ along the shaft of pile $i$ can be obtained using numerical integration as the same manner in Eqns (3.3) to (3.5). Finally, settlement $Srb_{i,j}$ in the base of the pile $i$ due to contact force $Qr_j$ is obtained as the same manner in Eq. (3.7). Taking the average of settlements $Srs_i$, and $Srb_{i,j}$, gives the settlement in the pile by:

$$Sr_{i,j} = Jr_{i,j}\, Qr_j \tag{3.28}$$

where $Jr_i$, is the flexibility coefficient of pile $i$ due to a contact force $Qr_j$ on node $j$ on the raft [m/kN].

For a pile group of $n_p$ piles, settlements in piles due to contact forces are expressed as:

$$\{Sr\} = [Jr]\{Qr\} \tag{3.29}$$

where:
$\{Sr\}$ $n_p$ vector of settlements in piles due to contact forces on the raft
$[Jr]$ $n_p$* $n_r$ matrix of pile flexibility coefficients due to unit contact forces
$\{Qr\}$ $n_r$ vector of contact forces on the raft

Now the total settlement in a pile *i* due to all forces in the system of piled raft foundation is given by:

$$\{Sp\} = \{Sb\} + \{Ss\} + \{Sv\} + \{Sr\} \tag{3.30}$$

Substituting Eqns (3.10), (3.23), (3.25) and (3.29) in Eq. (3.30), gives:

$$\{Sp\} = [Fb]\{Qb\} + [Is]\{Qs\} + [Cp]\{Qp\} + [Jr]\{Qr\} \tag{3.31}$$

where:
$\{Sp\}$ $n_p$ vector of total settlements in piles due to all forces in the system of piled raft foundation

### 3.2.3 Raft-pile interaction

Figure 3-5 and Figure 3-6 show the raft-pile interaction for both pile base and shaft. Referring to Figure 3-5, the settlement $Wb_{i,j}$ [m] in a node *i* on the raft due to a tip force $Qb_j$ on the base of pile *j* is given by:

$$Wb_{i,j} = Cb_{i,j}\, Qb_j \tag{3.32}$$

while the settlement $Wb_{i,j}$ [m] in a node *i* on the raft due to a skin force $Qs_j$ on pile *j* as shown in Figure 3-6 is given by:

$$Ws_{i,j} = Cs_{i,j}\, Qs_j \tag{3.33}$$

where $Cb_{i,j}$ [m/kN] is the flexibility coefficient of node *i* due to a tip force $Qb_j$ on the base of pile *j* and $Cs_{i,j}$ [m/kN] is the flexibility coefficient of node *i* due to a skin force $Qs_j$ on pile *j*. The flexibility coefficients $Cb_{i,j}$ and $Cs_{i,j}$ are obtained directly from Eq. (3.2) and Eq. (3.13), respectively.

For a raft of $n_r$ nodes Eq. (3.32) can be written in matrix form as:

$$\{Wb\} = [Cb]\{Qb\} \tag{3.34}$$

where:
$\{Wb\}$ $n_r$ vector of settlements in raft nodes due to base forces
$[Cb]$ $n_r$* $n_p$ matrix of raft flexibility coefficients due to unit tip forces on piles

Similarly, Eq. (3.33) for the raft is written as:

$$\{Ws\} = [Cs]\{Qs\} \tag{3.35}$$

where:
{*Ws*} $n_r$ vector of settlements in raft nodes due to skin forces
[*Cs*] $n_r$* $n_p$ matrix of raft flexibility coefficients due to unit skin forces on piles

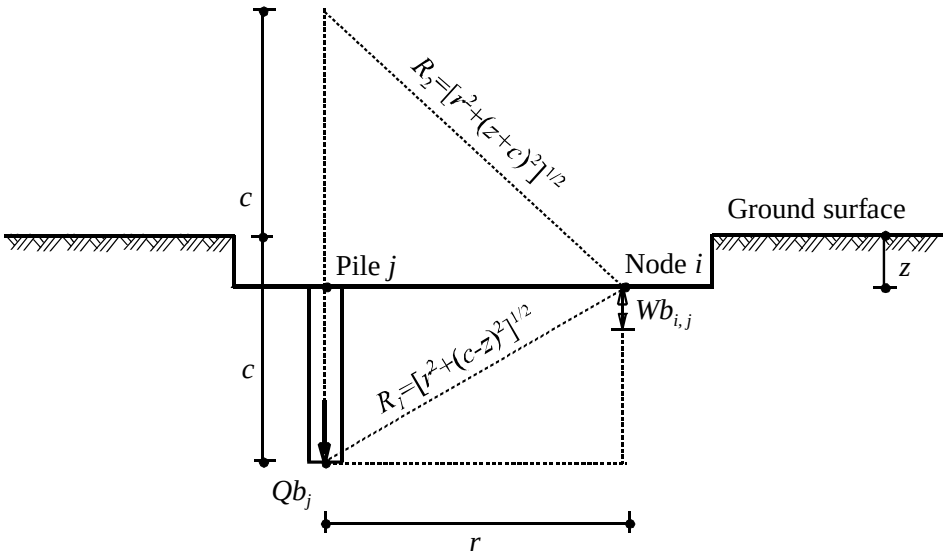


Figure 3-5 Settlement $Wb_{i,j}$ in a node *i* due to a tip force $Qb_j$ on the base of pile *j*

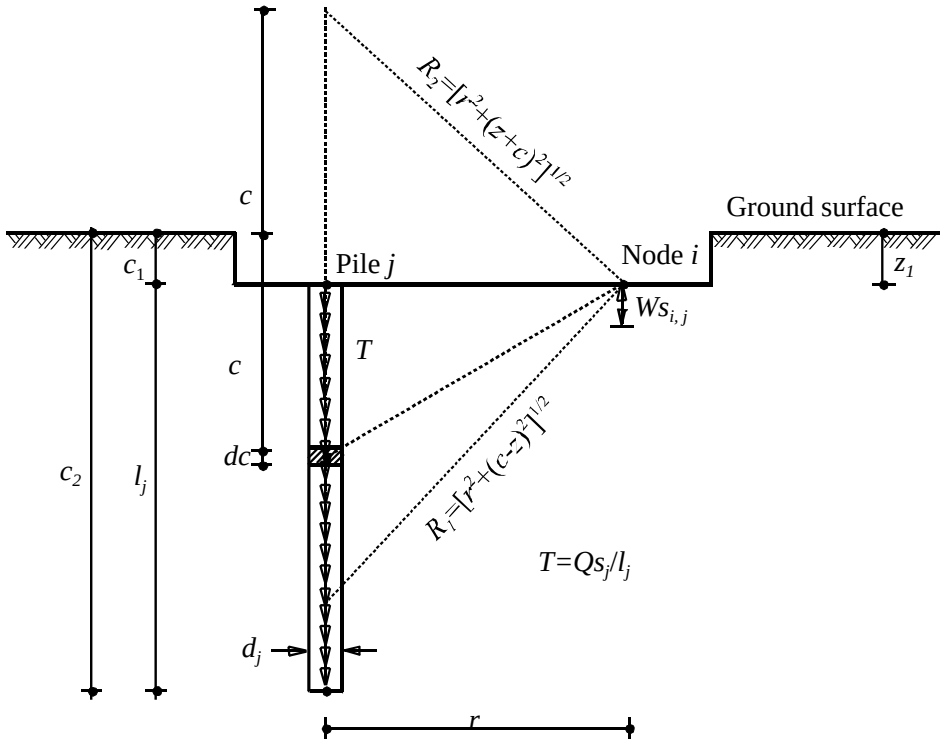


Figure 3-6 Settlement $Ws_{i,j}$ in a node *i* due to a skin force $Qs_j = T_j\, l_j$ on pile *j*

### 3.2.4 Raft-soil interaction

*Mindlin's* solution is used to evaluate the settlement in a point within the soil mass due to a load acting beneath the surface. Therefore, the solution is applied for pile problems. Also, *Mindlin's* solution is particularly convenient for analyzing raft in piled raft problems where the foundation level in most cases is relatively deep making contact forces acting deeply beneath the surface. In the present analysis, settlements in raft nodes due to contact forces on the raft may be determined from *Mindlin's* solution, in which flexibility coefficients for a contact force on the raft are obtained from Eq. (3.2). This can be carried out directly for all nodes except the loaded node. The reason is that at the loaded node $c = z$. Consequently, the first term in the Eq. (3.2) becomes singular when $r = 0$. In this case, Eq. (3.2) can be used but with replacing only the first term by another applicable for the loaded node. The replacement term in Eq. (3.2) is derived by converting the point load to an equivalent uniform load and carrying out the integration over the loaded area. The replacement term in Eq. (3.2) at the corner of a rectangular loaded area when $z = c \neq 0$ after integration becomes:

$$C_1 = \frac{3 - 4\,\nu_s}{2}\left(\frac{1}{a}\ln\frac{(m+a)}{(m-a)} + \frac{1}{b}\ln\frac{(m+b)}{(m-b)}\right) \tag{3.36}$$

where:
$a, b$ Sides of the loaded area [m]
and $m = \sqrt{a^2 + b^2}$

As *Mindlin's* solution with $c = 0$ is equivalent to *Boussinesq's* solution (1885), flexibility coefficient $C_{i,\,i}$ due to a rectangular uniform loaded area when $z = c = 0$ is obtained from *Boussinesq's* solution as follows:

$$C_{i,i} = \frac{1 - \nu_s^2}{2\,\pi\,E_s}\left(\frac{1}{a}\ln\frac{(m+a)}{(m-a)} + \frac{1}{b}\ln\frac{(m+b)}{(m-b)}\right) \tag{3.37}$$

When calculating the raft-soil flexibility coefficients, Eq. (3.37), Eq. (3.2) or Eq. (3.2) with the modified term in Eq. (3.36) is used. The settlement $Wr_{i,\,j}$ [m] in a node $i$ on the raft due to a contact force $Qr_j$ on node $j$ is given by:

$$Wr_{i,\,j} = Cr_{i,\,j}\,Qr_j \tag{3.38}$$

where:
$Cr_{i,\,j}$ Flexibility coefficient of node $i$ due to a contact force $Qr_j$ on node $j$ [m/kN]
$Cr_{i,\,j} = f_{i,\,j}$ for $i \neq j$
$Cr_{i,\,j} = C_{i,\,i}$ for $i = j$ and $z = c = 0$
$Cr_{i,\,j} = f_{i,\,j}$ with modified term $C_1$ for $i = j$ and $z = c \neq 0$

For a raft of $n_r$ nodes, the settlement in matrix form is expressed as:

$$\{Wr\} = [Cr]\{Qr\} \tag{3.39}$$

where:
$\{Wr\}$ $n_r$ vector of settlements in raft nodes due to contact forces on the raft
$[Cr]$ $n_r$* $n_r$ square matrix of raft flexibility coefficients due to unit contact forces on the raft
$\{Qr\}$ $n_r$ vector of contact forces on the raft

Equation (3.39) is rewritten as:

$$\{Qr\} = [Ks]\{Wr\} \tag{3.40}$$

where:
$[Ks]$ Soil stiffness matrix of the raft, $[Ks] = [Cr]^{-1}$

The total settlement in the raft due to all forces in the system of piled raft foundation is given by:

$$\{Wt\} = \{Wb\} + \{Ws\} + \{Wr\} \tag{3.41}$$

Substituting Eqns (3.34), (3.35) and (3.39) in Eq. (3.41), gives:

$$\{Wt\} = [Cb]\{Qb\} + [Cs]\{Qs\} + [Cr]\{Qr\} \tag{3.42}$$

where:
$\{Wt\}$ $n_r$ vector of total settlements in the raft due to all forces in the system of piled raft foundation

### 3.2.5 Formulation of soil equations

Let the vector $\{S\}$ represent the entire settlements in the raft mesh due to all forces in the system of piled raft foundation. This vector must have the dimension $n = n_p + n_r$ to include settlements in raft nodes and piles together. The vector of entire settlements can be obtained from:

$$\{S\} = \begin{Bmatrix} \{Sp\} \\ \{Wt\} \end{Bmatrix} \tag{3.43}$$

Substituting Eqns (3.31) and (3.42) in Eq. (3.43), gives:

$$\{S\} = \begin{Bmatrix} [Fb]\{Qb\} + [Is]\{Qs\} + [Cp]\{Qp\} + [Jr]\{Qr\} \\ [Cb]\{Qb\} + [Cs]\{Qs\} + [Cr]\{Qr\} \end{Bmatrix} \tag{3.44}$$

or

$$\{S\} = \begin{bmatrix} [Cp] & [0] \\ [0] & [Cr] \end{bmatrix} \begin{Bmatrix} \{Qp\} \\ \{Qr\} \end{Bmatrix} + \begin{Bmatrix} [Fb]\{Qb\} + [Is]\{Qs\} + [Jr]\{Qr\} \\ [Cb]\{Qb\} + [Cs]\{Qs\} \end{Bmatrix} \tag{3.45}$$

Equation (3.45) is written in a simplified form as:

$$\{S\} = [C]\{Q\} + \{Pr\} \tag{3.46}$$

where $\{Pr\}$ is given by:

$$\{Pr\} = \begin{Bmatrix} [Fb]\{Qb\} + [Is]\{Qs\} + [Jr]\{Qr\} \\ [Cb]\{Qb\} + [Cs]\{Qs\} \end{Bmatrix} \tag{3.47}$$

and the term $[C]\{Q\}$ is given by:

$$[C]\{Q\} = \begin{bmatrix} [Cp][0] \\ [0][Cr] \end{bmatrix} \begin{Bmatrix} \{Qp\} \\ \{Qr\} \end{Bmatrix} \tag{3.48}$$

where:
$\{Q\}$ $n$ vector of pile loads and contact forces
$[C]$ $n * n$ matrix of flexibility coefficients of piles and raft

Inverting the matrix of flexibility coefficients of piles and raft, Eq. (3.45) becomes:

$$\{Q\} = [Ks]\{S\} - [Ks]\{Pr\} \tag{3.49}$$

or

$$\{Q\} = [Ks]\{S\} - \{Pe\} \tag{3.50}$$

where $[Ks] = [C]^{-1}$ is the soil stiffness matrix of piles and raft and is given by:

$$[Ks] = \begin{bmatrix} [Kp][0] \\ [0][Kr] \end{bmatrix} \tag{3.51}$$

while the vector $\{Pe\}$ is given by:

$$\{Pe\} = [Ks]\{Pr\} \tag{3.52}$$

where $[Kr]$ represents soil stiffness of the raft alone.

### *3.2.5.1 Multi-layered soil*

Flexibility coefficients described previously can be applied only for isotropic elastic half-space soil medium. For finite layer, flexibility coefficients may be obtained as described by *Poulos/ Davis* (1980). As an example, for a point *k* in a layer of depth *h*, the flexibility coefficient is then:

$$f_{k,j}(h) = f_{k,j}(\infty) - f_{h,j}(\infty) \tag{3.53}$$

where:

$f_{k,j}(h)$ Flexibility coefficient for a point *k* in a layer of depth *h* due to a unit load on point *j* [m/kN]

$f_{k,j}(\infty)$ Flexibility coefficient for a point *k* due to a unit load on point *j* in a semi-infinite mass [m/kN]

$f_{h,j}(\infty)$ Flexibility coefficient for a point within the semi-infinite mass directly beneath *k*, at a depth *h* below the surface due to a unit load on point *j* [m/kN]

### *3.2.5.2 Reloading pressure effect*

To improve the deformation behavior of the soil, the total settlement of the piled raft is divided into two parts. In the first part the ground will settle according to the reloading modulus of compressibility *Ws* [kN/m$^2$] until the soil pressure reaches an overburden pressure *qv* [kN/m$^2$]. In the second part after reaching the load *qv* [kN/m$^2$] the ground will settle more under pressure *qe* according to the loading modulus of compressibility *Es* [kN/m$^2$] until reaching the average applied pressure *qo* [kN/m$^2$]. The reloading pressure effect may be taken into consideration by dividing the flexibility coefficient into two terms (Figure 3-7) such that:

$$f_{k,j} = \frac{qv}{qo} f_{k,j}(Ws) + \frac{qe}{qo} f_{k,j}(Es) \tag{3.54}$$

where:

$f_{k,j}(Ws)$ Flexibility coefficient calculated with *Ws* for a point *k* due to a unit load on point *j* [m/kN]

$f_{k,j}(Es)$ Flexibility coefficient calculated with *Es* for a point *k* due to a unit load on point *j* [m/kN]

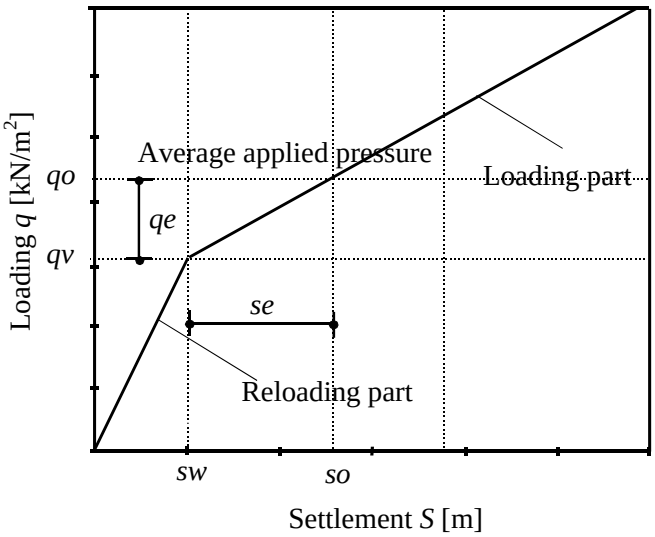


Figure 3-7 Loading-settlement diagram

### 3.2.6 Analysis of rigid piled raft

Figure 3-8 shows a rigid piled raft where in this case the settlement is defined by rigid body translation $w_o$ at the center of the raft and by two rotations $\theta_x$ and $\theta_y$ about *x*- and *y*-axes, respectively.

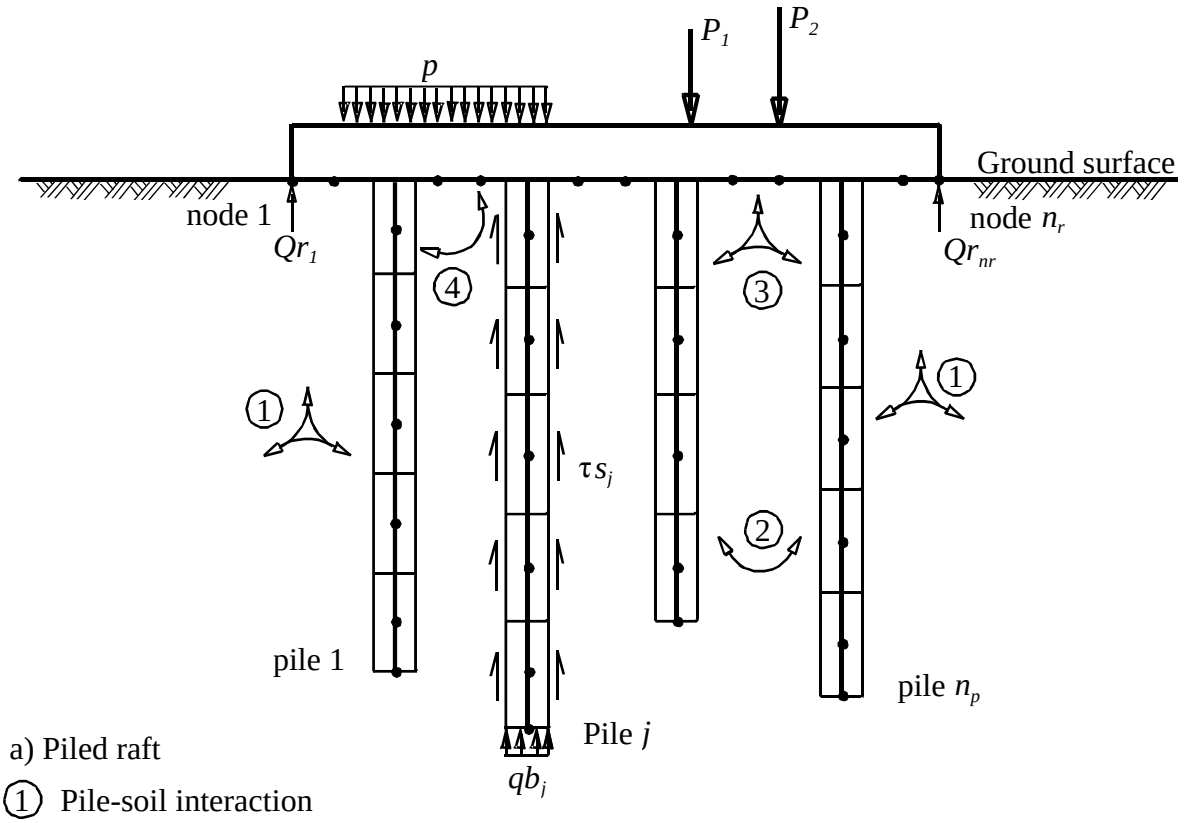


a) Piled raft

① Pile-soil interaction
② Pile-pile interaction
③ Raft-soil interaction
④ Pile-raft interaction

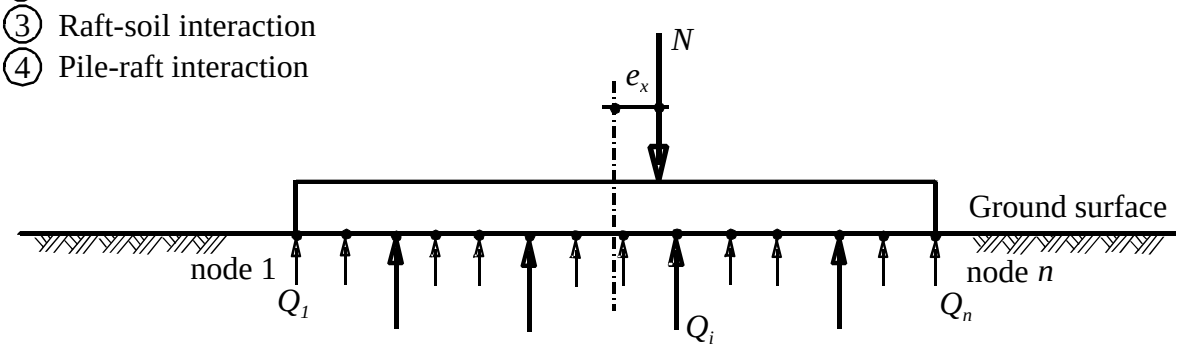


b) Equivalent statical system

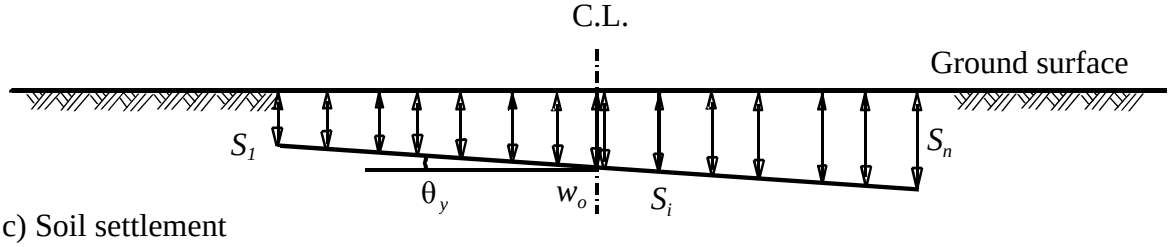


c) Soil settlement

Figure 3-8 Modeling rigid piled raft

Due to the piled raft rigidity, the following linear relation (plane translation) expresses the settlement $S_i$ at either a node in the raft or a pile that has coordinates ($x_i$, $y_i$) from the geometry centroid:

$$S_i = w_o + x_i \tan\theta_y + y_i \tan \tag{3.55}$$

Equation (3.55) is rewritten in matrix form for the entire piled raft system as:

$$\{S\} = [X]^T \{\Delta\} \tag{3.56}$$

where:
$\{\Delta\}$ 3 vector of translation $w_o$ and rotations tan $\theta_y$ and tan $\theta_x$
$[X]^T$ 3 * $n$ vector of coordinates $x$ and $y$

For equilibrium the following conditions must be satisfied:

- The resultant due to external vertical forces acting on the raft must be equal to the sum of contact forces and pile loads
- The moment due to that resultant about either $x$-axis or $y$-axis must be equal to the sum of moments due to contact forces and pile loads about that axis

Assuming $Q_i$ is a symbol representing either pile load $Qp$ or contact force $Qr$ on the mesh, gives:

$$\left.\begin{aligned} N &= Q_1 + Q_2 + Q_3 + ... + Q_n \\ N \,.\, e_x &= Q_1 \,.\, x_1 + Q_2 \,.\, x_2 + Q_3 \,.\, x_3 + ... + Q_n \,.\, x_n \\ N \,.\, e_y &= Q_1 \,.\, y_1 + Q_2 \,.\, y_2 + Q_3 \,.\, y_3 + ... + Q_n \,.\, y_n \end{aligned}\right\} \tag{3.57}$$

where:
$N$ Resultant of applied loads acting on the raft [kN]
$N\, e_x$ Moment due to resultant about $x$-axis, $M_x = N\, e_x$ [kN.m]
$N\, e_y$ Moment due to resultant about $y$-axis, $M_y = N\, e_y$ [kN.m]
$e_x$, $e_y$ Eccentricities of the resultant about $x$- and $y$-axes [m]
$x_i$, $y_i$ Coordinates of the load $Q_i$ [m]

Equation (3.57) is rewritten for the entire piled raft foundation in matrix form as:

$$\{N\} = [X]\{Q\} \tag{3.58}$$

where $\{N\}$ is the vector of resultant and moments.

Substituting Eqns (3.50) and (3.56) in Eq. (3.58), gives the following linear system of equations:

$$\{N\} = [X][Ks][X]^T \{\Delta\} - [X]\{Pe\} \tag{3.59}$$

Solving the above system of linear equations gives $w_o$, tan $\theta_x$, and tan $\theta_y$. Then, substituting these values in Eq. (3.56), after that in Eq. (3.60), gives the following equation to find the *n* unknown pile loads and contact forces.

$$\{Q\} = [Ks][X]^T \{\Delta\} - \{Pe\} \tag{3.60}$$

Substituting also the values $w_o$, tan $\theta_x$ and tan $\theta_y$ in Eq. (3.56), gives the *n* settlements.

### 3.2.7 Analysis of rigid pile group or flexible raft on rigid pile group

Analysis of a rigid pile group of $n_p$ piles using the described nonlinear relation is easier than that of rigid piled raft. In this case the contact forces $\{Qr\}$ and settlements on raft nodes $\{Wt\}$ are omitted from above equations. In this case, the vector $\{Pr\}$ of Eq. (3.47) is given by:

$$\{Pr\} = \{[Fb]\{Qb\} + [Is]\{Qs\}\} \tag{3.61}$$

and the term $[C]\{Q\}$ in Eq. (3.48) is given by:

$$[C]\{Q\} = [Cp]\{Qp\} \tag{3.62}$$

In the case of a flexible raft in which the group of piles acted on by known loads $\{Qp\}$ and $\{Qr\}$, Eq. (3.45) may be used directly to evaluate the settlement of each pile in the group.

### 3.2.8 Analysis of elastic piled raft

It is possible to treat the raft as an elastic plate on rigid piles. From the finite element analysis of the plate, the equilibrium of the raft is expressed as:

$$[Kg]\{\delta\} = \{P\} - \{Q\} \tag{3.63}$$

where:
$\{p\}$ $3 * n_r$ vector of applied loads and moments on the raft nodes
$[Kg]$ $3\ n_r * 3\ n_r$ plate stiffness matrix
$\{\delta\}$ $3 * n_r$ deformation vector of the raft

Substituting Eq. (3.50) in Eq (3.63), leads to:

$$[Kg]\{\delta\} = \{P\} - [Ks]\{S\} + \{Pe\} \tag{3.64}$$

Considering compatibility between piled raft displacement $\delta_i$ and soil settlement $s_i$, the following linear system of equations of the piled elastic raft can be obtained:

$$[[Ks] + [Kg]]\{\delta\} = \{P\} + \{Pe\} \tag{3.65}$$

### 3.2.9 Iteration method

In this paper, a proposed iteration method is developed to solve the system of linear equations, Eq. (3.59), of piled raft. The main idea of this method is that pile stiffness is determined from load-settlement relation due to self-settlement of pile. This pile stiffness is simply added to that of the raft. The piled raft is solved for each iteration cycle until the compatibility between settlements of raft, piles and soil is achieved. The iteration process of the method can be described in the following steps:

1 Generate the flexibility matrices due to pile-pile, pile-raft and raft-soil interactions: $[Fb]$, $[Is]$, $[Cb]$, $[Cs]$, $[Jr]$ and $[Cr]$

2 Find the soil stiffness matrix of the raft due to raft-soil interaction, $[Kr] = [Cr]^{-1}$

3 Using applied load on the raft, assume an average stress on raft nodes and piles, then find the initial loads on piles $\{Qp\}$ and the initial forces on raft nodes $\{Qr\}$

4 From the load-settlement curve according to DIN 4014 [5], find the values of:
- Soil stiffness matrix of the pile $[Kp]$
- Tip forces on piles $\{Qb\}$ due to pile loads $\{Qp\}$
- Skin forces on piles $\{Qs\}$ due to pile loads $\{Qp\}$

5 Generate the entire stiffness matrix of piles and raft $[Ks]$ by adding the soil stiffness of the pile $[Kp]$ computed in step 4 to the soil stiffness of the raft $[Kr]$

6 Determine the vector $\{Pr\}$ in Eq. (3.47) due to the contact forces and the computed tip and skin forces on piles in step 4. Then, find the vector $\{Pe\}$ from Eq. (3.52)

7 Carry out the analysis of piled raft, Eq. (3.59) for rigid piled raft or Eq. (3.65) for elastic piled raft, to get the pile settlements $\{Sv\}$ and contact forces $\{Qr\}$

8 Compare the settlement from cycle $i$ with that of cycle $i + 1$ to find the accuracy of the solution

9 If the accuracy from step 8 is less than a specified tolerance $\varepsilon$ then from the load-settlement curve according to DIN 4014 [5], determine the new pile loads $\{Qp\}$ due to computed settlements $\{Sv\}$ and go to step 4

The steps 4 to 9 are repeated until the accuracy reaches to a specified tolerance $\varepsilon$, which means that a sufficient compatibility between settlements of piles, raft and soil is achieved in the piles-raft-soil interface.

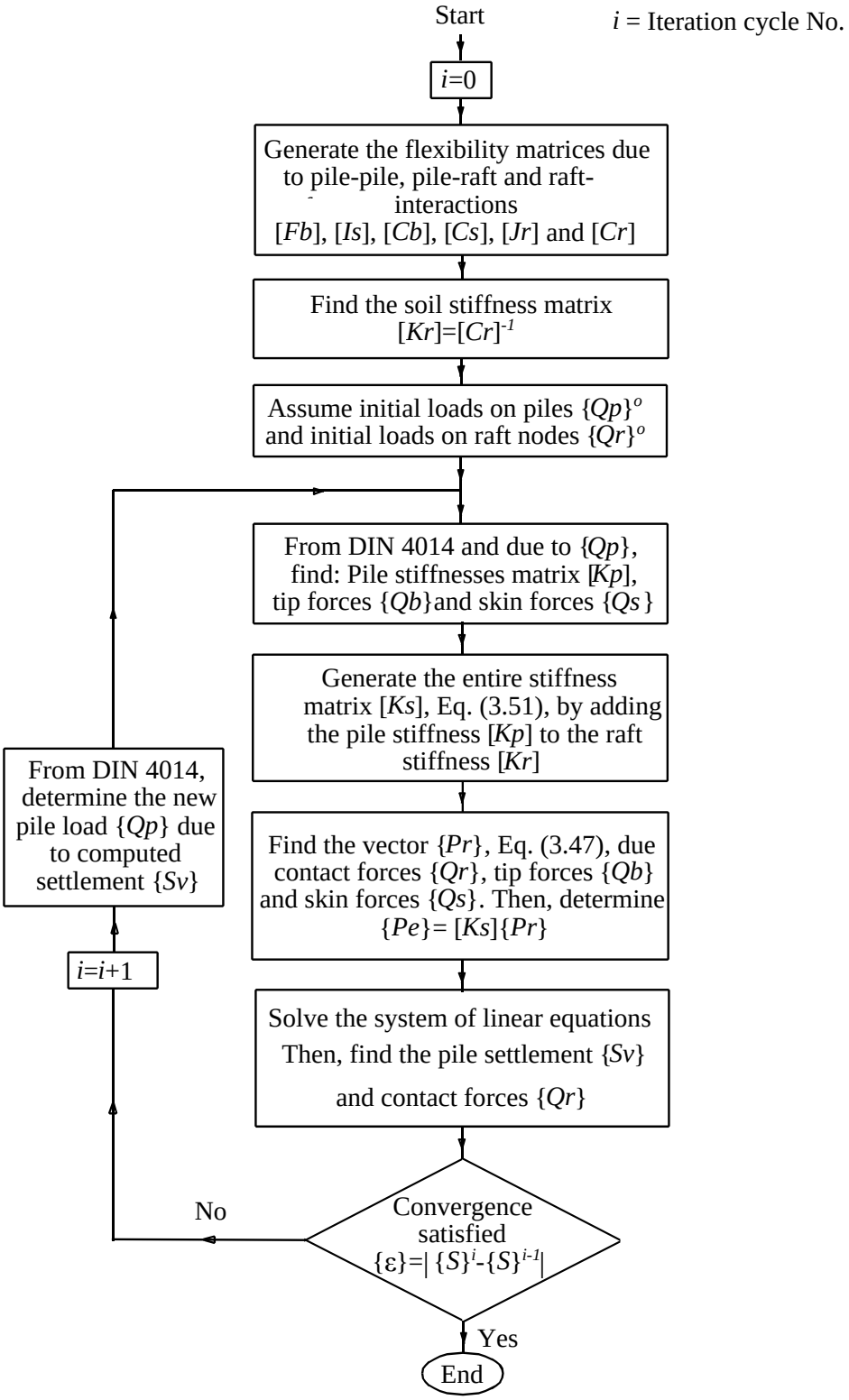


Figure 3-9 Flowchart of the iteration process in the program *ELPLA*

## 3.3 Case study: *Messeturm* piled raft

### 3.3.1 Description of the problem

*Messeturm* was the tallest high-rise building in Europe until 1997, Figure 3-10. The building lies in Frankfurt city in Germany. It is 256 [m] high and standing on a piled raft foundation.

Figure 3-10 *Messeturm*[1]

[1] http://de.wikipedia.org/wiki/Messeturm_(Frankfurt)

Using instruments installed inside this foundation, an extensive measuring program was established to monitor the behavior of the building. Because these instruments record raft settlements, raft contact pressures and loads on pile heads and along pile shafts, the building was a good chance for many authors to verify their analysis methods for piled raft. Since *Messeturm* was built many authors have studied its behavior. Some of them are *Sommer* (1989), *Sommer/ Katzenbach* (1990), *Thaher* (1991), *Sommer et al.* (1991), *EL-Mossallamy* (1996), *Katzenbach et al.* (2000), *Reul/ Randolph* (2003) and *Chow/ Small* (2005).

Figure 3-11 shows a layout of *Messeturm* with the piled raft according to *Chow/ Small* (2005). The building has a basement with two underground floors and 60 stories with a total estimated load of 1880 [MN]. The foundation is a square piled raft of 58.8 [m] side founded on Frankfurt clay at a depth 14 [m] under the ground surface. Raft thickness varies from 6 [m] at the middle to 3 [m] at the edge. A total of 64 bored piles with equal diameters of 1.3 [m], are arranged under the raft in 3 rings. Pile lengths vary from 26.9 [m] for the 28 piles in the outer ring to 30.9 [m] for the 20 piles in the middle ring and to 34.9 [m] for the 16 piles in the inner ring. The subsoil at the location of the building consists of gravels and sands up to 8 [m] below the ground surface underlay by layers of Frankfurt clay extending to great depth of more than 100 [m] below the ground surface. The groundwater level lies at 4.75 [m] under the ground surface.

The construction of *Messeturm* started in 1988 and finished in 1991. According to *Katzenbach et al.* (2000), the recorded settlement at the center of the raft in March 1990 was 8.5 [cm], while the last recorded settlement in December 1998 was 14.4 [cm] according to *Reul/ Randolph* (2003). If *Messeturm* stands on a raft only, the expected settlement would be between 35 [cm] and 40 [cm] based on geotechnical studies according to *Sommer* (1989). Therefore, to reduce the settlement, a piled raft was considered where the expected final settlement in this case would be between 15 [cm] and 20 [cm] according to *Sommer/ Katzenbach* (1990). Using the available data and results of the *Messeturm* piled raft, which have been discussed in details in the previous references, the present piled raft analysis is evaluated and verified. Thus by dealing the piled raft as a rigid foundation where the rigid analysis of piled raft is considered as an easy method to check results of any other complicated models.

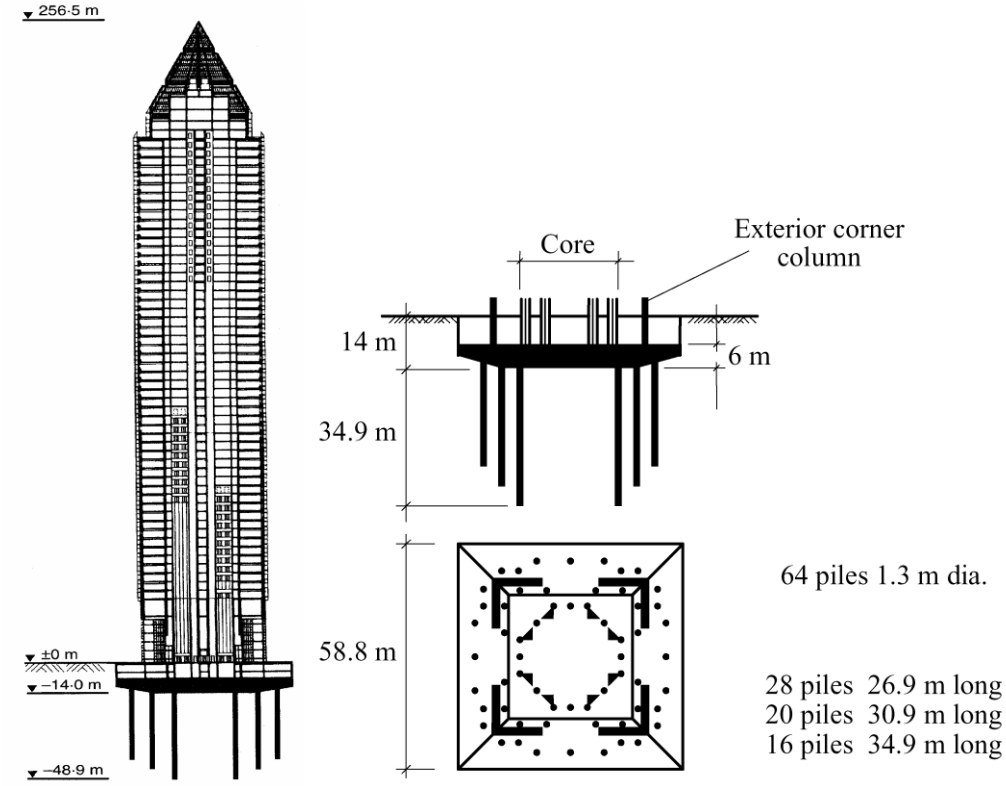


Figure 3-11 Layout of *Messeturm* with piled raft after *Chow/ Small* (2005)

### 3.3.2 Analysis of the piled raft

A series of comparisons are carried out to evaluate the nonlinear analysis of piled raft using DIN 4014 [5] for load-settlement relation. In which, results of other analytical solutions and measurements are compared with those obtained by the present analysis. In the comparisons the present analysis is termed NPRD.

Taking advantage of the symmetry in shape, soil and load geometry about both *x*- and *y*-axes, the analysis is carried out for a quarter of the piled raft. The raft is divided into elements with maximum length of 2.0 [m] as shown in Figure 3-12. Element sizes in *x*- and *y*-directions for a quarter of the raft are:

$$2 * 2.2 + 2.69 + 2 * 1.74 + 0.89 + 3 * 2.35 + 2.06 + 2.65 + 1.76 + 2 * 2.2 = 29.4 \text{ [m]}$$

Similarly, piles are divided into elements with 2.0 [m] in maximum length.

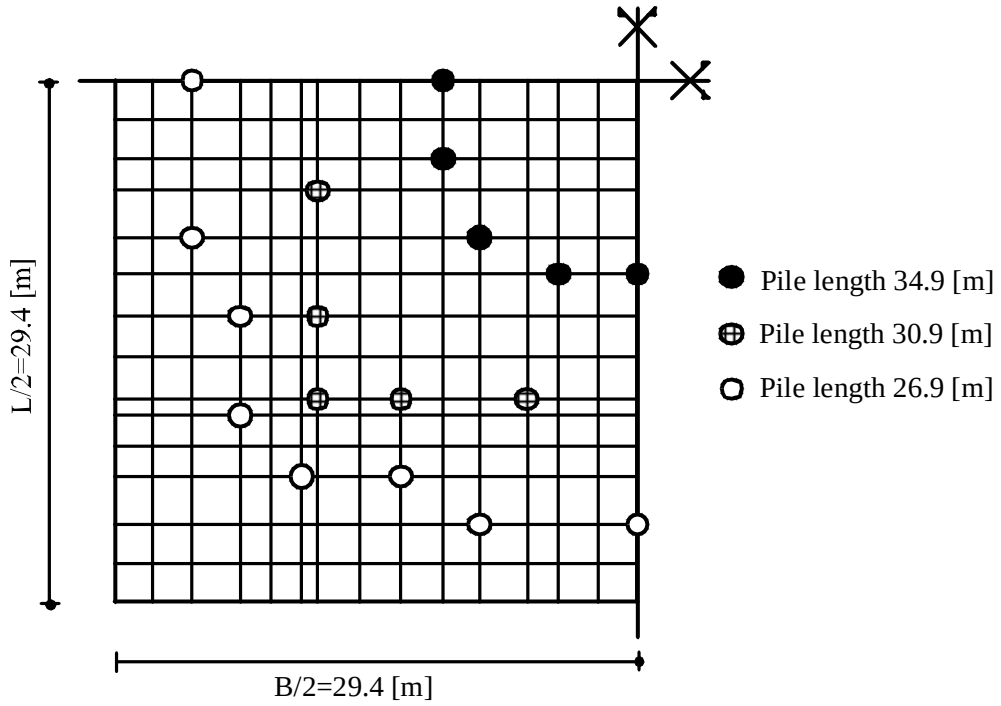


Figure 3-12 Mesh of *Messeturm* piled raft with piles (Max. element length = 2.0 [m])

### *a) Comparison with Randolph's analysis*

To examine NPRD for the *Messeturm* piled raft, results are compared with those using *Randolph's* analysis, which was carried out by *EL-Mossallamy* (1996). The raft is considered to be rigidly supported on equal rigid piles with an average length equal to 30.15 [m]. A soil layer of $H$ = 90 [m] with a constant elastic modulus is considered. Two cases of analyses are carried out with two different soil parameters as indicated in Table 3-1. For NPRD, the load-settlement relation is determined using an average undrained cohesion of $c_u$ = 300 [kN/m$^2$] in both cases. The uplift pressure on the raft due to groundwater is considered to be $P_w$ = 275 [kN/m$^2$]. Consequently, the total effective applied load on the raft including own weight of the raft and piles is assumed to be $N$ = 1600 [MN].

Table 3-2 summarizes the results of the immediate and total settlements for *Randolph's* analysis (1994) and NPRD while Table 3-3 summarizes the results of the bearing factors of piled raft for both of the analyses. Although the principles of both of the analyses are different, the results indicate a good agreement in settlement and a difference in bearing factor of piled raft ranges from 3.4 [%] to 7.7 [%].

Table 3-1 Soil properties used in *Randolph's* analysis and NPRD

| Case No. | Undrained conditions | | Drained conditions | |
|---|---|---|---|---|
| | $E_s$ [MN/m$^2$] | $\nu_s$ [-] | $E'_s$ [MN/m$^2$] | $\nu'_s$ [-] |
| Case 1 | 70.4 | 0.5 | 62.4 | 0.33 |
| Case 2 | 91.4 | 0.5 | 81.0 | 0.33 |

Table 3-2 Settlements *s* [cm] (*Randolph's* analysis vs. NPRD)

| Case No. | Immediate | | Total | |
|---|---|---|---|---|
| | *Randolph's* analysis | NPRD | *Randolph's* analysis | NPRD |
| Case 1 | 13.0 | 12.9 | 17.1 | 18.1 |
| Case 2 | 10.0 | 10.1 | 13.7 | 14.0 |

Table 3-3 Bearing factors of piled raft $\alpha_{kpp}$ [%] (*Randolph's* analysis vs. NPRD)

| Case No. | Immediate | | Total | |
|---|---|---|---|---|
| | *Randolph's* analysis | NPRD | *Randolph's* analysis | NPRD |
| Case 1 | 35.2 | 31.8 | 44 | 39 |
| Case 2 | 35.2 | 27.5 | 44 | 38 |

***b) Comparison with Thaher's analysis***

To analyze piled raft, *Thaher* (1991) had presented an analytical model using equivalent raft method, which was checked by the centrifuge model test results. He applied his model to the *Messeturm* piled raft to assess the rigid settlement.

### 3.3.3 Soil properties

The average clay properties used in *Thaher's* analysis can be described as follows:

*Modulus of compressibility*
Based on the back analysis presented by *Amann et al.* (1975), the distribution of modulus of compressibility for loading of Frankfurt clay with depth is defined by the following empirical formula:

$$E_s = E_{so}(1 + 0.35\,z) \tag{3.66}$$

while that for reloading is:

$$W_s = 70\left[\mathrm{MN/m^2}\right] \tag{3.67}$$

where:
$E_s$ Modulus of compressibility for loading [MN/m$^2$]
$E_{so}$ Initial modulus of compressibility, $E_{so}$ = 7 [MN/m$^2$]
$z$ Depth measured from the clay surface, [m]
$W_s$ Modulus of compressibility for reloading [MN/m$^2$]

*Undrained cohesion*
The undrained cohesion $c_u$ of Frankfurt clay increases with depth from $c_u$ = 100 [kN/m$^2$] to $c_u$ = 400 [kN/m$^2$] in 70 [m] depth under the clay surface according to *Sommer/ Katzenbach* (1990). To carry out NPRD, an average undrained cohesion of $c_u$ = 300 [kN/m$^2$] is considered.

*Poisson's ratio*
*Poisson's* ratio of Frankfurt clay is taken to be $\nu_s$ = 0.25 [-].

To carry out the analysis, the subsoil under the raft is considered as indicated in the boring log of Figure 3-13 that consists of 10 soil layers. The total depth under the ground surface is taken to be 102.83 [m].

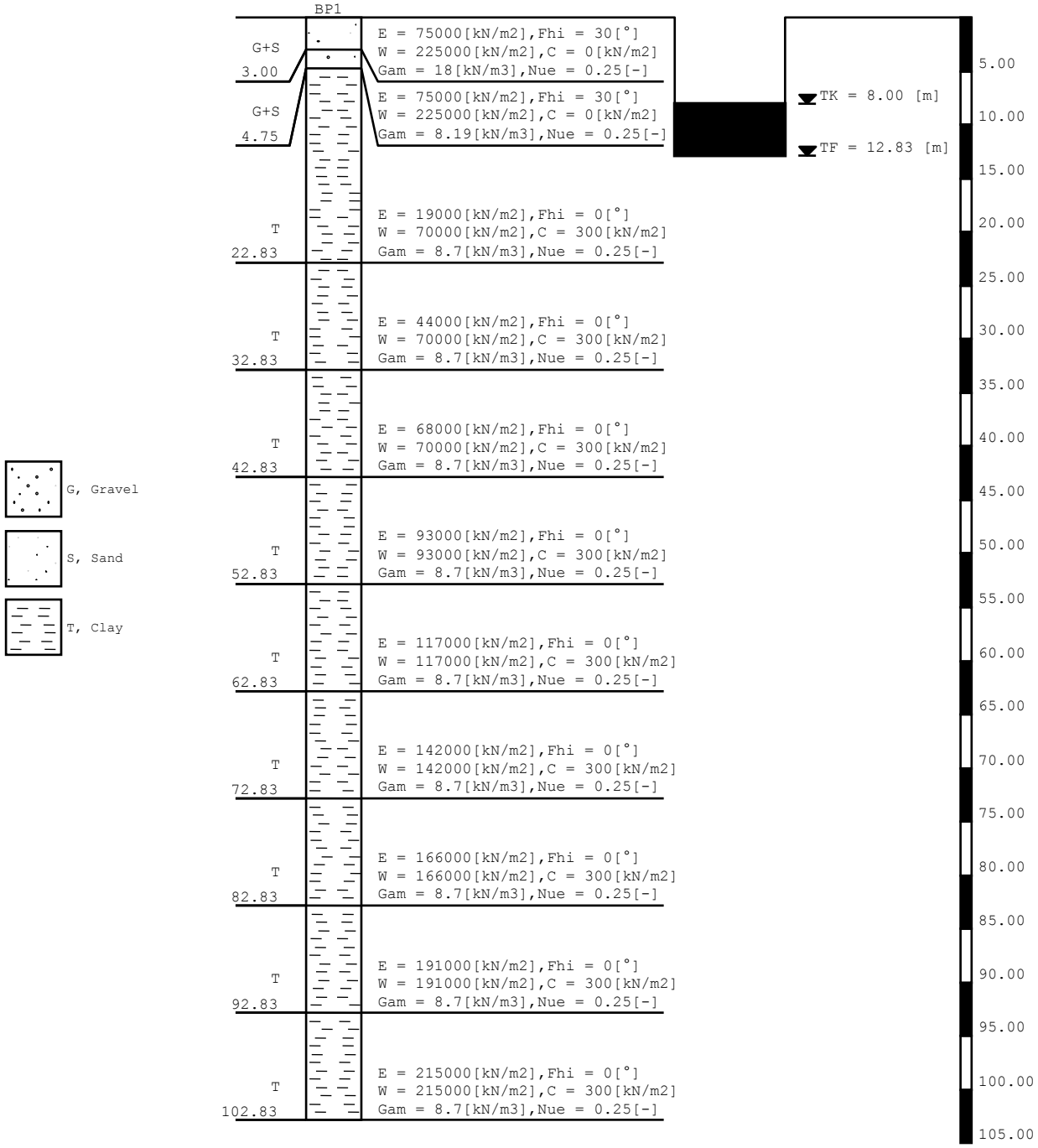


Figure 3-13 Boring log

Table 3-4 lists the results of settlement, bearing factor of piled raft and tip resistance obtained by NPRD compared with those obtained by *Thaher* (1991). The table shows that settlement and bearing factor of piled raft for the both analyses are nearly the same. Only a difference of 0.6 [MN/m$^2$] in the maximum tip resistance is found.

In Table 3-5, load on each pile in inner, middle and outer rings obtained by both NPRD and the centrifuge model test by *Thaher* (1991) are shown. Also, the table includes the measured total pile loads after the completion of the structural frame, presented by *Sommer et al.* (1991). The table indicates that results are in a good agreement.

Also, Table 3-5 shows that the piles transfer the load to the soil mainly by skin friction, as observed from the measurements (*Katzenbach et al.* (2000)). The measurements indicate that the load distribution within the pile group is quite homogeneous. This behavior is also noticed in NPRD not only for the pile load but also for the pile settlement.

As shown in Table 3-6, NPRD can introduce the individual settlement in the pile due to pile load itself or due to pile-pile and pile-raft interactions. Table 3-6 shows that the most of the settlement is due to self settlement of the pile compared with the settlement due to pile-pile and pile-raft interactions for loading or reloading. The self-settlement of the pile ranges between 52 and 55 [%] of the total settlement in the pile.

Table 3-4 Comparison between results obtained by *Thaher's* analysis and NPRD

| Analysis | Settlement $s_r$ [cm] | Bearing factor $\alpha_{kpp}$ [%] | Min. tip resistance [MN/m$^2$] | Max. tip resistance [MN/m$^2$] |
|---|---|---|---|---|
| *Thaher's* analysis | 19.00 | 40.00 | 1 | 1.5 |
| *NPRD* | 18.77 | 40.44 | 1 | 2.1 |

Table 3-5 Pile load for NPRD, centrifuge model test and measured results

| Pile ring | NPRD | | | Total pile load from centrifuge model test [MN] | Measured total pile load [MN] |
|---|---|---|---|---|---|
| | Tip force [MN] | Shaft force [MN] | Total pile load [MN] | | |
| Inner ring | 2.71 | 8.55 | 11.26 | 14 | 11 |
| Middle ring | 2.74 | 7.57 | 10.31 | 13 | 13 |
| Outer ring | 2.72 | 6.59 | 9.31 | 10 | 10 |

Table 3-6 Settlement in piles

| Pile ring | Self settlement $s_p$ [cm] | Settlement due to pile-pile and pile-raft interactions | | Total settlement $s_r$ [cm] | Self/ Total $s_p/s_r$ [%] |
|---|---|---|---|---|---|
| | | Loading $s_e$ [cm] | Reloading $s_w$ [cm] | | |
| Inner ring | 9.75 | 4.97 | 4.05 | 18.77 | 52 |
| Middle ring | 10.29 | 4.78 | 3.70 | 18.77 | 55 |
| Outer ring | 9.86 | 5.10 | 3.81 | 18.77 | 53 |

**Comments**

The maximum difference between the settlements in step *i* and next step *i* + 1 is considered as an accuracy number. In this case study, the accuracy number was chosen to be 0.0001 [cm].

For a single run of analysis, the results were obtained in relatively short time (17 [Sec] for analysis *a* and 1.2 [Min] for analysis *b* using Pentium 4 PC with 512 MB RAM). This is related to the following parameters:

- Flexibility coefficients due to pile-pile interaction are determined only for two forces: shaft and base forces

- As the settlement due to load on pile itself is determined from DIN 4014 [5], flexibility coefficients can be determined without numerical problems using closed form equations instead of equations that must be evaluated by numerical integration

- There is no need to determine a global stiffness matrix for the soil since the flexibility matrix is generated every step in the iteration cycle

- Instead of determining flexibility coefficients due to pile-pile interaction from settlement equations, the coefficients are determined from the load-settlement relation according to DIN 4014 [5]

This case study shows that NPRD is not only an acceptable method to analyze piled raft but also a practical one for analyzing large piled raft problems. Beside that NPRD gives a good agreement with previous theoretical and empirical nonlinear analyses of piled raft, it takes less computational time compared with other complicated models using three dimension finite element analyses. As further comparative example to proof that an analysis of *Messeturm* using three dimensional finite element analysis after *Randolph* (1994) and *Reul/ Randolph* (2003) gave a settlement of 17.4 [cm] at the center while that of NPRD gave 18.77 [cm].

## 3.4 References


[1] *Amann, P./ Breth, H./ Stroh, D.* (1975): Verformungsverhalten des Baugrundes beim Baugrubenaushub und anschließendem Hochhausbau am Beispiel des Frankfurter Ton Mitteilungen der Versuchsanstalt für Bodenmechanik und Grundbau der Technischen Hochschule Darmstadt, Heft 15

[2] *Basile, F.* (1999): Non-Linear analysis of pile groups
Proc. Instn Civ. Engrs Geotech. Engng, 137, 105-115

[3] *Basile, F.* (2003): Analysis and design of pile groups
Numerical Analysis and Modelling in Geomechanics,
Spon press (eds J. W. Bull), London, Chapter 10, pp 278-315

[4] *Chow, H./ Small J.* (2005): Behaviour of Piled Rafts with Piles of Different Lengths and Diameters under Vertical Loading
GSP 132 Advanced in Deep Foundations, ASCE

[5] DIN 4014: Bohrpfähle Herstellung, Bemessung und Tragverhalten
Ausgabe März 1990

[6] *Duncan, J./ Chang, C.* (1970): Non-linear analysis of stress and strain in soils
Journal of Soil Mechanics and Foundation Engineering Division
Proceedings of the American Society of Civil Engineers, 96, No. SM5, pp. 1121-1124

[7] ECP 197: Egyptian Code for Soil Mechanics-Design and Construction of Foundations
Part 4, Deep Foundations (in Arabic) (1995)

[8] *El Gendy, M./ Hanisch, J./ Kany, M.* (2006): Empirische nichtlineare Berechnung von Kombinierten Pfahl-Plattengründungen
Bautechnik 9/06

[9] *Kany, M./ El Gendy, M./ El Gendy, A.* (2006): Benutzerhandbuch für das Programm *ELPLA* (eingebunden in das Programmsystem GEOTEC), Zirndorf

[10] *Katzenbach, R./ Arslan, U./ Moormann, C.* (2000): Piled raft foundation projects in Germany
Chapter 13 in: Design application of raft foundations
Edited by Hemsley, Thomas Telford

[11] *Mandolini, A./ Viggiani, C.* (1997).: Settlement of piled foundations
Géotechnique, 47, No. 4, 791-816

[12] *Mindlin, R.* (1936): Force at a point in the interior of a semi-infinite-solid
Physics 7, S. 195-202

[13] *EL-Mossallamy, Y.* (1996): Ein Berechnungsmodell zum Tragverhalten der Kombinierten Pfahl-Plattengründung
Dissertation, Technische Hochschule Darmstadt, Darmstadt, D17

[14] *Poulos, H./ Davis, E.* (1980): Pile Foundation Analysis and Design
John Wiley & Sons, Inc.

[15] *Randolph, M.F.* (1994): Design methods for pile groups and pile rafts
XXX ICSMFE New Dehli, India, Rotterdam Balkema Vol. 4, S. 61-82

[16] *Reul, O./ Randolph, M.F.* (2003): Piled rafts in overconsolidated clay: comparison of in situ measurements and numerical analyses
Géotechnique 53, No. 3, 301-315

[17] *Russo, G.* (1998): Numerical analysis of piled raft
Int. J. Numer. Anal. Meth. Geomech., 22, 477-493

[18] *Sommer, H.* (1989): Entwicklung der Hochhausgründungen in Frankfurt/ Main
Festkolloquium 1989, 20 Jahre Grundbauinstitut, Darmstadt

[19] *Sommer, H./ Katzenbach, R.* (1990): Last-Verformungsverhalten des Messeturmes Frankfurt/ Main
Vorträge der Baugrundtagung 1990 in Karlsruhe, Seite 371-380

[20] *Sommer, H./ Tamaro, G./ DeBenedittis, C.* (1991): Messe Turm, foundation for the tallest building in Europe
4th International Conference on Piling and Deep Foundations, Italy, 139-145

[21] *Thaher, M.* (1991): Tragverhalten von Pfahl-Platten-Gründungen im bindigen Baugrund, Berechnungsmodelle und Zentrifugen-Modellversuche
Dissertation, Institut für Grundbau der Ruhr-Universität, Bochum, Heft 15

[22] *Viggiani, C.* (1998): Pile groups and pile raft behaviour
Proc. of the 3rd int. Geot. Sem. on Deep Foundations on Bored and Auger Piles
Ghent, Belgien 19.-21- Oct.
Balkema Rotterdam, S. 77-91

[23] *Witzel, M./ Kempfert, H. G.* (2005): A simple approach to predict the load settlement behavior of precast driven piles with due consideration of the driving process
GSP 132 Advanced in Deep Foundations, Proceeding of Sessions of the Geo-Frontiers Congress, Austin, Texas, ASCE

[24] Richtlinie für den Entwurf, die Bemessung und den Bau von Kombinierten Pfahl-Plattengründungen (KPP) - (KPP-Richtlinie)
Hrg.: Arbeitskreis "Pfähle" der Deutschen Gesellschaft für Geotechnik e.V., Juli 2001

Enthalten in: Kombinierte Pfahl-Plattengründungen
Hrg.: *Hanisch, J./ Katzenbach, R./ König, G.* (2002)
Ernst & Sohn

# Chapter 4

# Analyzing friction piles in clay soil

Table of Contents Page

**4 Analyzing friction piles in clay soil** 4- 3

4.1 Introduction 4- 3

4.2 Numerical Modeling 4- 5
4.2.1 Formulation of stress coefficients 4- 5
4.2.2 Modeling single pile 4-13
4.2.3 Modeling pile groups and piled raft 4-16

4.3 Numerical Results 4-19
4.3.1 Test example: Verification of a piled raft on a deeply extended clay layer 4-19
4.3.2 Case study 1: Piled raft of *Stonebridge Tower* 4-21
4.3.3 Case study 2: Piled raft of *Dashwood House* 4-25

4.4 References 4-28

# 4 Analyzing friction piles in clay soil

## 4.1 Introduction

Settlements of a foundation may be calculated using either flexibility or stress coefficients-technique. Analyzing foundation on elastic soil layers may be carried out using flexibility coefficients-technique, while that on consolidated soil is preferred to be carried out by stress coefficients-technique. In this case, compression index of the soil is used to define the consolidation characteristics of the clay. It is known that the compression index *Cc*, which is obtained from the *e*-log σ curve (*e*: void ratio, σ: consolidation pressure) of the consolidation test, will be the same for any stress range on the linear part of the curve, while the coefficient of volume change *mv* (inverse of the modulus of compressibility *Es* = 1/*mv*) will vary according to the stress range (Figure 4-1). Therefore, to calculate the real consolidation settlement for a thick clay layer and because the stress from the foundation varies with depth, a variable modulus of compressibility must be obtained, even for homogenous layer.

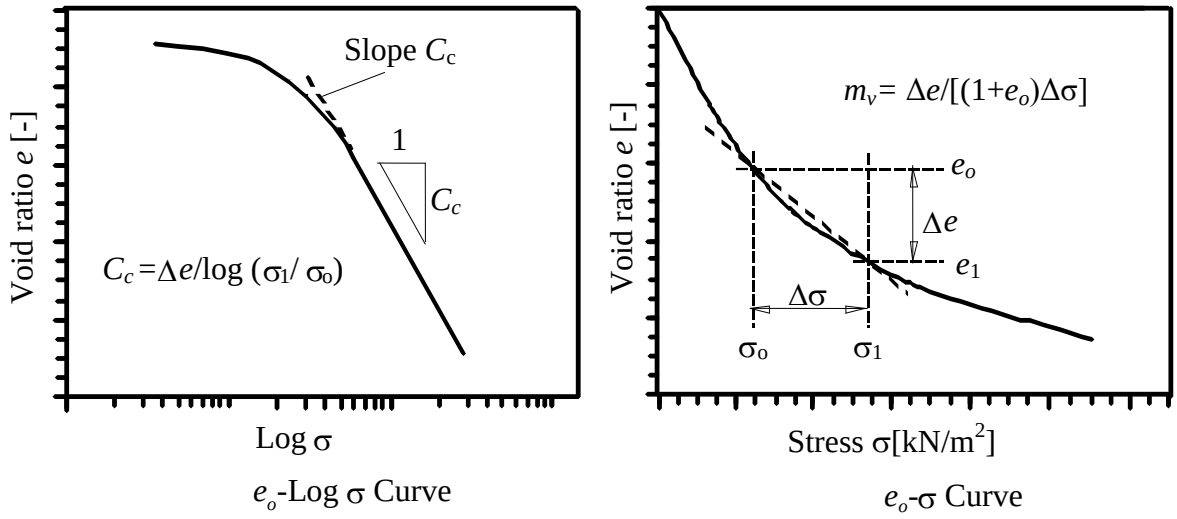


Figure 4-1 Void ratio-stress relationship

The problem when analyzing a foundation on clay layer is the determination of the non-linear increment of the vertical stress on the layer due to the unknown contact pressure at the soil-pile interface. *Griffths* (1984) presented charts for average vertical stress increment beneath a corner of a uniformly loaded rectangular area based on numerical integration of existing solutions. *Masih* (1993) and (1994) considered the effect of settlement caused by cohesive soil consolidation on the structure. The analysis dealt with elastic speared footings using one-point method. *El Gendy* (2003) introduced an analysis of a rigid circular raft on a clay layer by calculating the stress at mid-depth of soil element. The increment of vertical stress is obtained by numerical integration. *El Gendy* (2006) developed stress coefficients for triangular loaded elements and point load acting on the entire clay sub-layer through closed form equations. These coefficients can be used for any irregular shape of foundations on multi-clay layers. Analyses carried out by the methods mentioned previously were applied on spared footings and rafts on clay.

The problem of raft on clay soil taking into account soil-structure interaction is a complicated nonlinear problem as shown by *El Gendy* (2006). It will be more complicated for piled raft. This is because the increment of stress in soil depends on the unknown contact pressure at the soil-pile-raft interface. In rigid piled raft, the contact pressure distribution at the soil-pile-raft interface on a homogenous soil layer is independent from elastic properties of the soil. This advantage reduces considerably the analysis if the contact pressure is obtained from other available solution. In this case half of the problem is solved. Consequently, using the known contact pressure from other analyses enables to derive a practical solution for single pile, pile groups and piled raft on clay soil.

*El Gendy* (2007) presented a numerical procedure to determine the final consolidation settlement of friction piles in clay soil using stress coefficients-technique. He derived closed form equations for determining the increment of non-linear stress in clay layers caused by contact forces generated at the pile-soil interface. Using these stress coefficients, an analysis for single pile, pile groups and piled raft on clay soil to predict the consolidation settlement may be carried out. In the analysis, the contact pressure is obtained from the elastic solution of the problem. This enables to determine the nonlinear increment of stress in the soil layers. Consequently, the consolidation settlement can be calculated using the compression index and void ratio parameters. The computation may be carried out only at one point on the raft to get the settlement.

This chapter described stress coefficients developed by *El Gendy* (2007) to determine the final of consolidation settlement of friction piles in clay soil. Friction pile is analyzed as a single pile or as a member in pile groups or piled raft. However, these coefficients can be applied on elastic or rigid piled raft, only the rigid piled raft will be used to show the validity of the method. Furthermore, piled raft is usually used for high structure with high rigidity. Analysis of an elastic piled raft may be carried out similar to that of rafts on clay layers proposed by *El Gendy* (2006).

## 4.2 Numerical Modeling
### 4.2.1 Formulation of stress coefficients

In the analysis, the pile is divided into a number of shaft elements with *m* nodes and a circular base as shown in Figure 4-2a. To carry out the analysis, pile shaft elements are represented by line elements as indicated in Figure 4-2b. All stresses acting on shaft elements and on the base are replaced by a series of concentrated forces acting on line nodes.

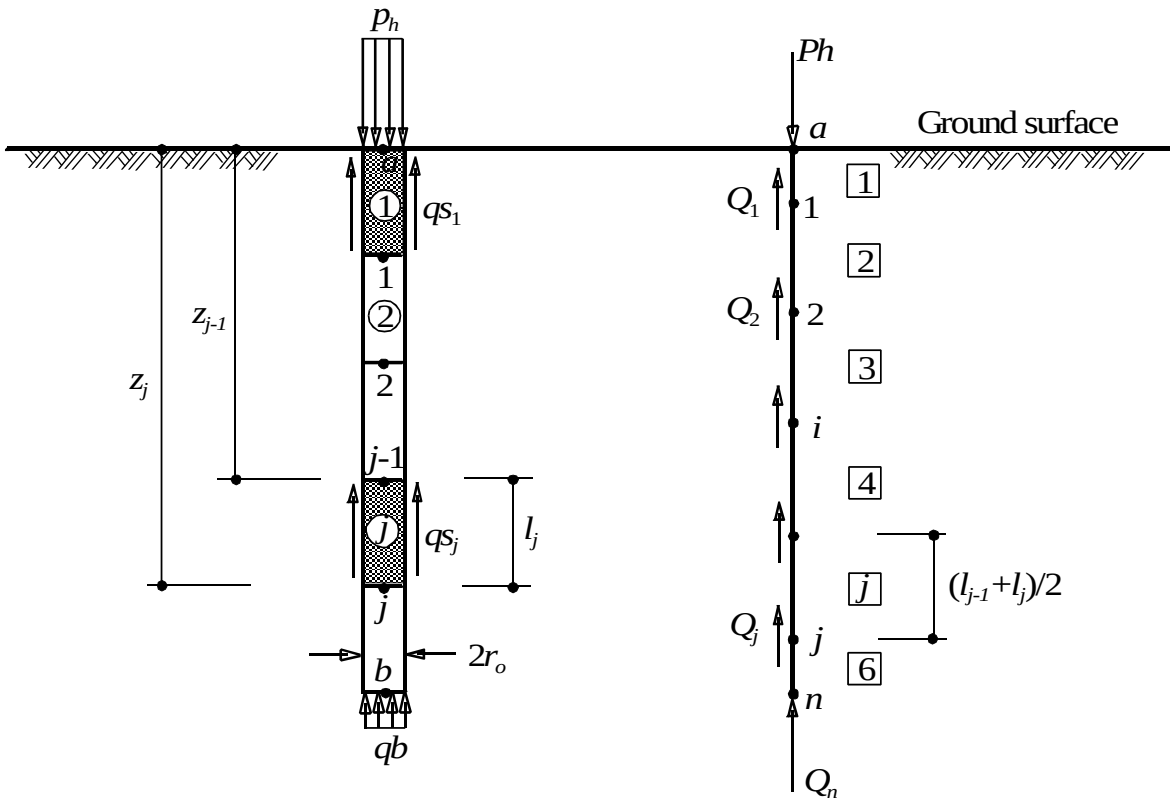


a) Pile shaft elements b) Pile line elements

Figure 4-2 Pile geometry and elements

Pioneer authors of pile analysis such as *Poulos/ Davis* (1968) and *Butterfield/ Banerjee* (1971) integrated numerically coefficients of flexibility using *Mindlin's* solution for point load within a semi-infinite mass. Analysis of pile using numerical coefficients increases computation time significantly, especially in large pile problems. However, the present analysis depends on stress coefficients determined from elastic theory using *Mindlin's* solution an analytical derivation of coefficients of stresses is presented. Closed form equations for these coefficients are derived in the next paragraphs.

#### *4.2.1.1 Stress coefficient $c_{i,j}(k)$ of layer k at point i due to a unit force on point j*

It is convenient when calculating consolidation settlement to consider the stress occurs on the vertical direction only. In this case *Poisson's* ratio of the soil may be eliminated from stress equations. Stress coefficient can be derived from *Mindlin's* equation for determining the displacement when omitting *Poisson's* ratio from this equation. The displacement at point *i* due to a point load acting at point *j* beneath the surface in a semi-infinite mass (Figure 4-3) is expressed as:

$$w(z)_i = \frac{Q_j}{E_s} I_{i,j}(z) \tag{4.1}$$

where:

$E_s$ Modulus of elasticity of the soil [kN/m$^2$]
$Q_j$ Point load acting at point *j* in the soil mass [kN]
$w(z)_i$ Displacement in point *i* at depth *z* under the surface [m]
$I_{i,j}(z)$ Displacement factor of a node *i* at depth *z* under the surface due to a load at point *j* [1/m]

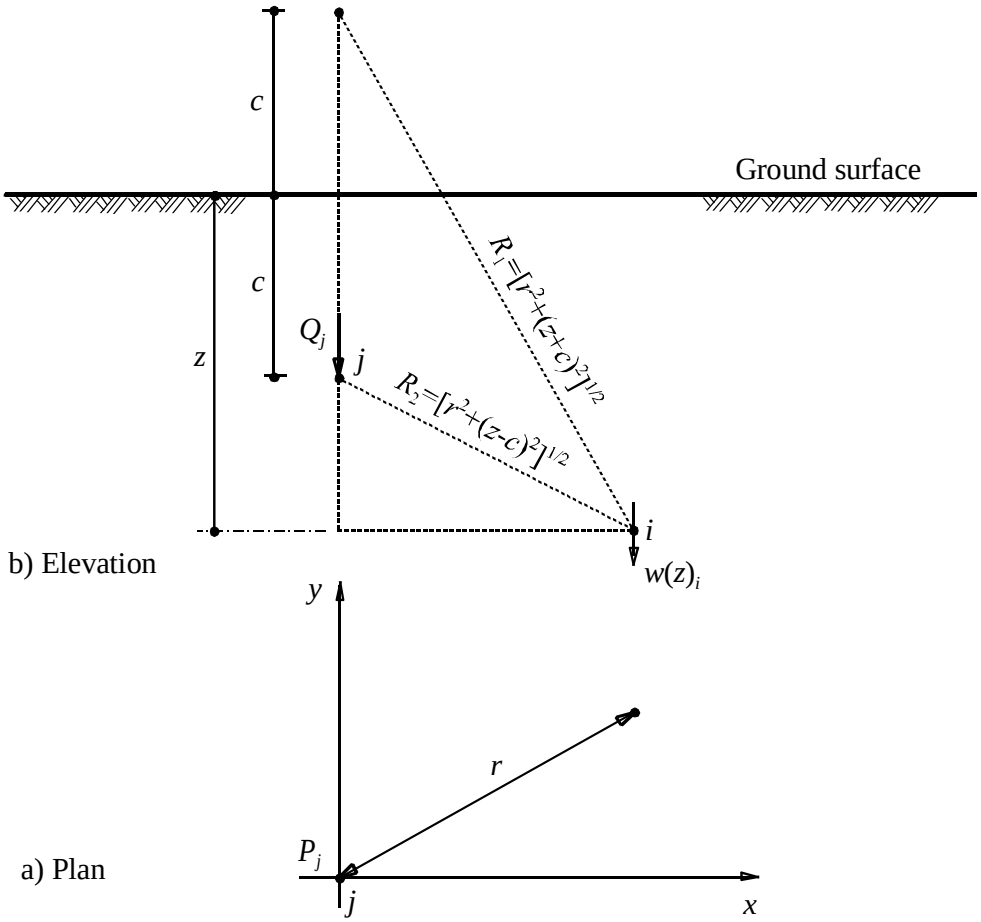


Figure 4-3 Geometry of *Mindlin's* problem

The displacement factor $I_{i,j}(z)$ when eliminating *Poisson's* ratio is given by:

$$I_{i,j}(z) = \frac{1}{8\pi}\left(\frac{3}{\sqrt{r^2+(z-c)^2}} + \frac{5}{\sqrt{r^2+(z+c)^2}} + \frac{(z-c)^2}{\left(r^2+(z-c)^2\right)^{\frac{3}{2}}} + \frac{3\,(z+c)^2 - 2cz}{\left(r^2+(z+c)^2\right)^{\frac{3}{2}}} + \frac{6\,c\,z\,(z+c)^2}{\left(r^2+(z+c)^2\right)^{\frac{5}{2}}}\right) \tag{4.2}$$

where:

| | |
|---|---|
| $c$ | Depth of the point load $Q_j$ from the surface [m] |
| $z$ | Depth of the studied point $i$ from the surface [m] |
| $r$ | Radial distance between points $i$ and $j$ [m] |

For a finite layer $k$ (Figure 4-4), the displacement in the entire layer may be obtained from:

$$w(k)_i = w(z_1)_i - w(z_2)_i \tag{4.3}$$

where:

| | |
|---|---|
| $w(k)_i$ | Displacement in a layer $k$ beneath $i$ [m] |
| $w(z_1)_i$ | Displacement in semi-infinite mass beneath $i$, at a depth $z_1$ under the surface [m] |
| $w(z_2)_i$ | Displacement in semi-infinite mass beneath $i$, at a depth $z_2$ under the surface [m] |
| $z_1$ | Start depth of the soil layer $k$ from the surface [m] |
| $z_2$ | End depth of the soil layer $k$ from the surface [m] |

Displacement in a soil layer $k$ may be also expressed as:

$$w(k)_i = \frac{1}{E_s}\,\delta\sigma_{i,j}(k)\,h \tag{4.4}$$

where:

| | |
|---|---|
| $\delta\sigma_{i,j}(k)$ | Stress in a soil layer $k$ beneath $i$ due to a load at point $j$ [kN/m$^2$] |
| $h$ | Thickness of the soil layer $k$ [m] |

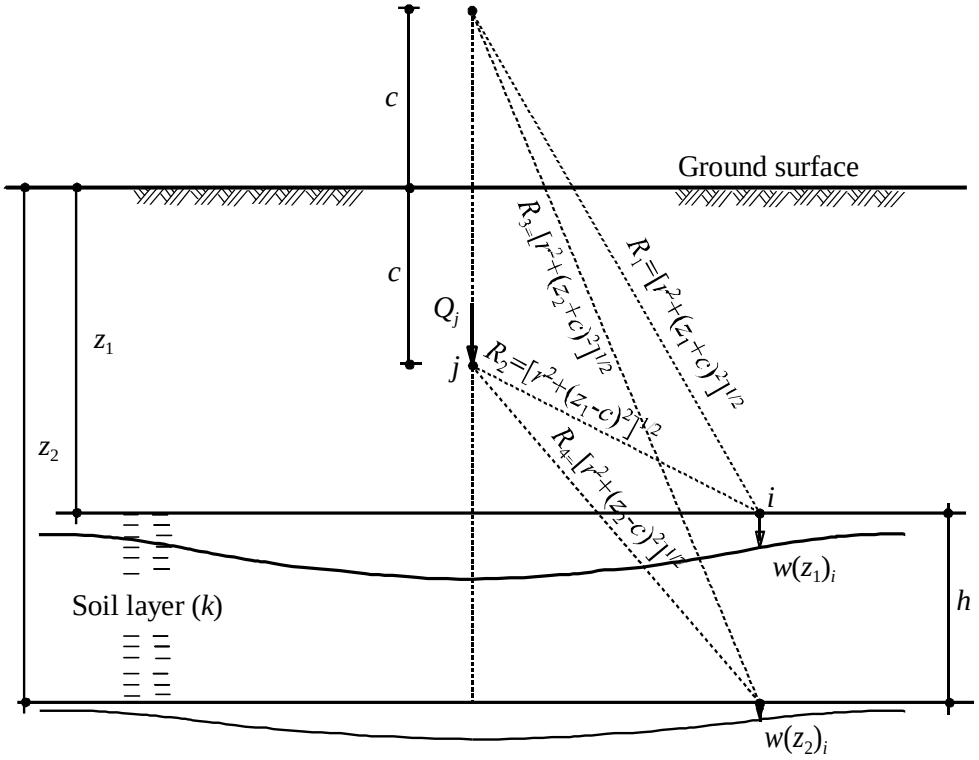


Figure 4-4 Settlement in a soil layer ($k$)

The stress $\delta\sigma_{i,j}(k)$ in the soil layer can be obtained by equating Eq. (4.3) to Eq. (4.4), which leads to:

$$\delta\sigma_{i,j}(k)=\frac{Q_j}{h}\frac{1}{8\pi}\left(\frac{3}{\sqrt{r^2+(z_1-c)^2}}+\frac{5}{\sqrt{r^2+(z_1+c)^2}}+\frac{(z_1-c)^2}{\left(r^2+(z_1-c)^2\right)^{\frac{3}{2}}}\right.$$
$$+\frac{3\,(z_1+c)^2-2cz_1}{\left(r^2+(z_1+c)^2\right)^{\frac{3}{2}}}+\frac{6\,c\,z_1\,(z_1+c)^2}{\left(r^2+(z_1+c)^2\right)^{\frac{5}{2}}}-\frac{3}{\sqrt{r^2+(z_2-c)^2}}-\frac{5}{\sqrt{r^2+(z_2+c)^2}} \qquad (4.5)$$
$$\left.-\frac{(z_2-c)^2}{\left(r^2+(z_2-c)^2\right)^{\frac{3}{2}}}-\frac{3\,(z_2+c)^2-2cz_2}{\left(r^2+(z_2+c)^2\right)^{\frac{3}{2}}}-\frac{6\,c\,z_2\,(z_2+c)^2}{\left(r^2+(z_2+c)^2\right)^{\frac{5}{2}}}\right)$$

Equation (4.5) is rewritten in a simple form as:

$$\delta\sigma_{i,j}(k)=\frac{1}{h}\left[I_{i,j}(z_1)-I_{i,j}(z_2)\right]Q_j \qquad (4.6)$$

or

$$\delta\sigma_{i,j}(k)=c_{i,j}(k)\,Q_j \qquad (4.7)$$

where:

$I_{i,j}(z_1)$ Displacement factor due to a load at point $j$ in semi-infinite mass beneath $i$, at a depth $z_1$ under the surface [1/m$^2$]

$I_{i,j}(z_2)$ Displacement factor due to a load at point $j$ in semi-infinite mass beneath $i$, at a depth $z_2$ under the surface [1/m$^2$]

$c_{i,j}(k)$ Stress coefficient for a layer $k$ beneath $i$ due to a unit load at point $j$ [1/m$^2$]

The stress coefficient $c_{i,j}(k)$ is given by:

$$c_{i,j}(k) = \frac{1}{8\pi h}\left( \frac{3}{\sqrt{r^2 + (z_1 - c)^2}} + \frac{5}{\sqrt{r^2 + (z_1 + c)^2}} + \frac{(z_1 - c)^2}{\left(r^2 + (z_1 - c)^2\right)^{\frac{3}{2}}} + \frac{3\,(z_1 + c)^2 - 2cz_1}{\left(r^2 + (z_1 + c)^2\right)^{\frac{3}{2}}} + \frac{6\,c\,z_1\,(z_1 + c)^2}{\left(r^2 + (z_1 + c)^2\right)^{\frac{5}{2}}} - \frac{3}{\sqrt{r^2 + (z_2 - c)^2}} - \frac{5}{\sqrt{r^2 + (z_2 + c)^2}} - \frac{(z_2 - c)^2}{\left(r^2 + (z_2 - c)^2\right)^{\frac{3}{2}}} - \frac{3\,(z_2 + c)^2 - 2cz}{\left(r^2 + (z_2 + c)^2\right)^{\frac{3}{2}}} - \frac{6\,c\,z_2\,(z_2 + c)^2}{\left(r^2 + (z_2 + c)^2\right)^{\frac{5}{2}}} \right) \tag{4.8}$$

#### *4.2.1.2 Stress coefficient $f_{i,b}(k)$ of a layer k at node i due to a unit force on the base b*

Replacing the radial distance $r$ in Eq. (4.8) by the radius of the base $r_o$ [m] gives the stress coefficient $f_{i,b}(k)$ of a layer $k$ at node $i$ due to a unit force $Q_b = 1$ [kN] acting on the base $b$.

#### *4.2.1.3 Stress coefficient $f_{b,b}(k)$ of a layer k at the base b due to a unit force on the base itself*

The base $b$ of the pile has a circular loaded area of radius $r_o$ [m] and a uniform load $q = Q_b / \pi r_o^2$ [kN/m$^2$] as shown in Figure 4-5. The stress coefficient $f_{b,b}(k)$ of a layer $k$ at the base center $b$ due to a unit load $Q_b = 1$ [kN] at the base itself can be obtained from:

$$f_{b,b}(k) = \frac{1}{\pi r_o^2}\int_0^{2\pi}\int_0^{r_o} \frac{1}{h}\left[I_{i,j}(z_1) - I_{i,j}(z_2)\right] r\,dr\,d\theta \tag{4.9}$$

The integration of the stress coefficient can be obtained analytically as:

$$f_{b,b}(k) = \frac{1}{4\pi r_o^2 h}\left( 5\left[\sqrt{r_o^2 + 4c^2} - 2c\right] + 10c^2\left[\frac{1}{2c} - \frac{1}{\sqrt{r_o^2 + 4c^2}}\right] - \frac{8c^4}{\left(r_o^2 + 4c^2\right)^{3/2}} - 5\left[\sqrt{r_o^2 + 4h^2} - 2h\right] - 10h^2\left[\frac{1}{2h} - \frac{1}{\sqrt{r_o^2 + 4h^2}}\right] + \frac{8h^4}{\left(r_o^2 + 4h^2\right)^{3/2}} \right) \tag{4.10}$$

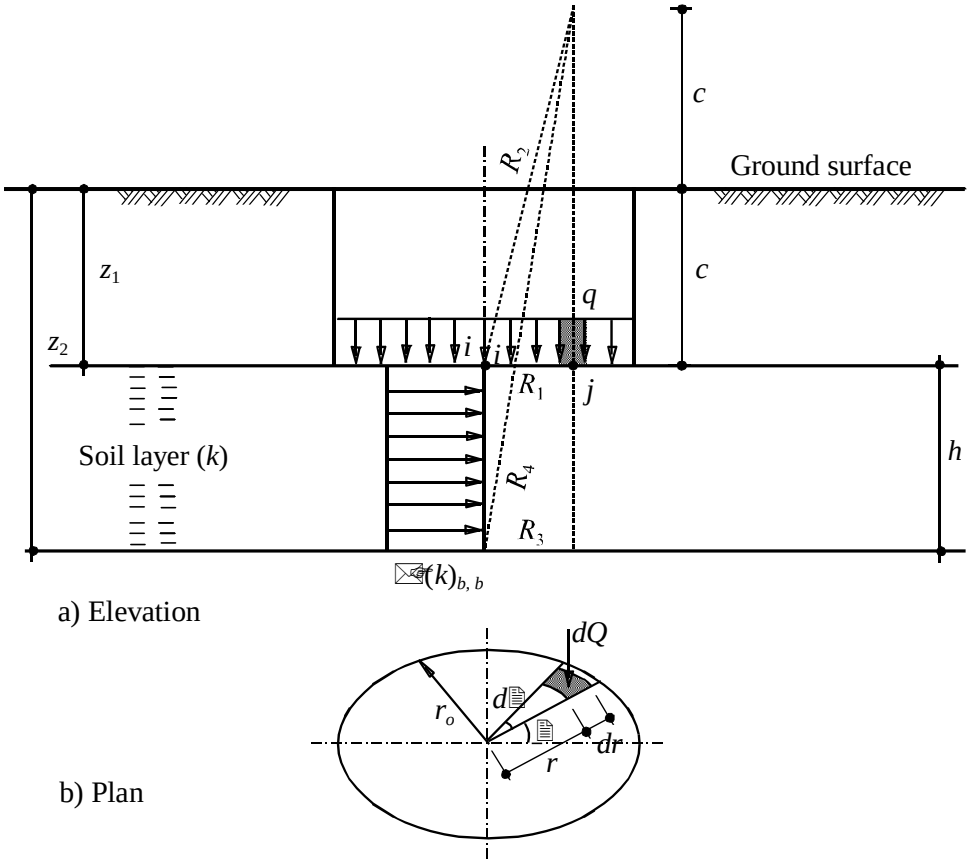


Figure 4-5 Geometry of the base to find the stress coefficient $\delta(k)_{b,b}$ at the center

#### *4.2.1.4 Stress coefficient $f_{i,j}(k)$ of a layer k at node i due to a unit shear force on a node shaft j*

To avoid the significant computations when determining the stress coefficients due to shaft stress, the shaft stress $\tau$ [kN/m$^2$] is replaced by an equivalent line load. The shaft element *j* of the pile has a length *l* [m] and a line load $T = Qs_j / l$ [kN/m] as shown in Figure 4-6. The stress coefficient $f_{i,j}(k)$ for a layer *k* at a node *i* due to a unit load $Qs_j = 1$ [kN] at a shaft element *j* can be obtained from:

$$f_{i,j}(k) = \frac{1}{l} \int_{l_1}^{l_2} \frac{1}{h} \left[ I_{i,j}(z_1) - I_{i,j}(z_2) \right] dc \tag{4.11}$$

The integration yields to:

$$f_{i,j}(k) = \frac{1}{8\pi l h} \left( I_1 + I_2 + I_3 + I_4 + I_5 \right) \tag{4.12}$$

where terms $I_1$ to $I_5$ are given by:

$$I_1 = 3 \ln \left[ \frac{\sqrt{r_1^2 + (z_1 - l_2)^2} - (z_1 - l_2)}{\sqrt{r_1^2 + (z_1 - l_1)^2} - (z_1 - l_1)} \right] - 3 \ln \left[ \frac{\sqrt{r_1^2 + (z_2 - l_2)^2} - (z_2 - l_2)}{\sqrt{r_1^2 + (z_2 - l_1)^2} - (z_2 - l_1)} \right] \tag{4.13}$$

$$I_2 = 5\ln\left[\frac{\sqrt{r_1^2+(z_1+l_2)^2}+(z_1+l_2)}{\sqrt{r_1^2+(z_1+l_1)^2}+(z_1+l_1)}\right]-5\ln\left[\frac{\sqrt{r_1^2+(z_2+l_2)^2}+(z_2+l_2)}{\sqrt{r_1^2+(z_2+l_1)^2}+(z_2+l_1)}\right] \tag{4.14}$$

$$\begin{aligned} I_3 = {} & \ln\left[\frac{\sqrt{r_1^2+(z_1-l_2)^2}-(z_1-l_2)}{\sqrt{r_1^2+(z_1-l_1)^2}-(z_1-l_1)}\right]+\frac{z_1-l_2}{\sqrt{r_1^2+(z_1-l_2)^2}}-\frac{z_1-l_1}{\sqrt{r_1^2+(z_1-l_1)^2}} \\ & -\ln\left[\frac{\sqrt{r_1^2+(z_2-l_2)^2}-(z_2-l_2)}{\sqrt{r_1^2+(z_2-l_1)^2}-(z_2-l_1)}\right]-\frac{z_2-l_2}{\sqrt{r_1^2+(z_2-l_2)^2}}+\frac{z_2-l_1}{\sqrt{r_1^2+(z_2-l_1)^2}} \end{aligned} \tag{4.15}$$

$$\begin{aligned} I_4 = {} & 3\left(\ln\left[\frac{\sqrt{r_1^2+(z_1+l_2)^2}+(z_1+l_2)}{\sqrt{r_1^2+(z_1+l_1)^2}+(z_1+l_1)}\right]-\frac{(z_1+l_2)}{\sqrt{r_1^2+(z_1+l_2)^2}}+\frac{(z_1+l_1)}{\sqrt{r_1^2+(z_1+l_1)^2}}\right) \\ & -2z_1\left(\frac{1}{\sqrt{r_1^2+(z_1+l_1)^2}}-\frac{1}{\sqrt{r_1^2+(z_1+l_2)^2}}+\frac{z_1(z_1+l_1)}{r_1^2\sqrt{r_1^2+(z_1+l_1)^2}}-\frac{z_1(z_1+l_2)}{r_1^2\sqrt{r_1^2+(z_1+l_2)^2}}\right) \\ & -3\left(\ln\left[\frac{\sqrt{r_1^2+(z_2+l_2)^2}+(z_2+l_2)}{\sqrt{r_1^2+(z_2+l_1)^2}+(z_2+l_1)}\right]-\frac{(z_2+l_2)}{\sqrt{r_1^2+(z_2+l_2)^2}}+\frac{(z_2+l_1)}{\sqrt{r_1^2+(z_2+l_1)^2}}\right) \\ & +2z_2\left(\frac{1}{\sqrt{r_1^2+(z_2+l_1)^2}}-\frac{1}{\sqrt{r_1^2+(z_2+l_2)^2}}+\frac{z_2(z_2+l_1)}{r_1^2\sqrt{r_1^2+(z_2+l_1)^2}}-\frac{z_2(z_2+l_2)}{r_1^2\sqrt{r_1^2+(z_2+l_2)^2}}\right) \end{aligned} \tag{4.16}$$

$$\begin{aligned} I_5 = {} & \frac{6z_1\left[r_1^4-z_1(z_1+l_2)^3\right]}{3r_1^2\left[r_1^2+(z_1+l_2)^2\right]^{3/2}}-\frac{6z_1\left[r_1^4+z_1(z_1+l_1)^3\right]}{3r_1^2\left[r_1^2+(z_1+l_2)^2\right]^{3/2}}-\frac{6z_1}{\sqrt{r_1^2+(z_1+l_2)^2}}+\frac{6z_1}{\sqrt{r_1^2+(z_1+l_1)^2}} \\ & -\frac{6z_2\left[r_1^4-z_2(z_2+l_2)^3\right]}{3r_1^2\left[r_1^2+(z_2+l_2)^2\right]^{3/2}}+\frac{6z_2\left[r_1^4+z_2(z_2+l_1)^3\right]}{3r_1^2\left[r_1^2+(z_2+l_2)^2\right]^{3/2}}+\frac{6z_2}{\sqrt{r_1^2+(z_2+l_2)^2}}-\frac{6z_2}{\sqrt{r_1^2+(z_2+l_1)^2}} \end{aligned} \tag{4.17}$$

where:

$l_1$ Start depth of the line load $T$ or the shear stress $\tau$ from the surface [m]
$l_2$ End depth of the line load $T$ or the shear stress $\tau$ from the surface [m]
$l$ Length of the line load $T$ or the shear stress $\tau$ [m]
$r_1$ Radial distance between point $i$ and $j$ [m]

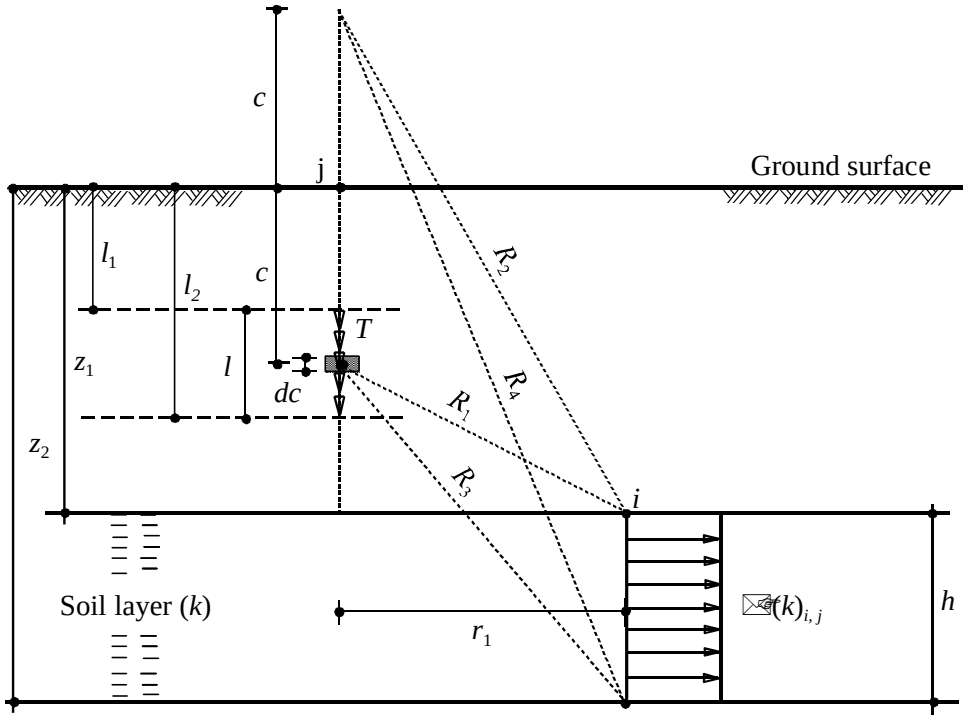


Figure 4-6 Geometry of the line load to find the stress coefficient $\delta(k)_{i,j}$ at the center

#### *4.2.1.5 Stress coefficient $f_{b,j}(k)$ of a layer k at the base b due to a unit shear force on a node shaft j*

The pile has a radius $r_o$ [m], while the shaft element $j$ has a length $l$ [m] and a shear stress $\tau = Qs_j / 2\,\pi\, r_o\, l$ [kN/m$^2$] as shown in Figure 4-7. The stress coefficient $f_{b,j}(k)$ of a layer $k$ at the base center $b$ due to a unit load $Qs_j = 1$ [kN] at a shaft element $j$ can be obtained from:

$$f_{b,j}(k) = \frac{1}{2\,\pi\, l} \int_0^{2\pi} \int_{l_1}^{l_2} \frac{1}{h} \left[ I_{i,j}(z_1) - I_{i,j}(z_2) \right] dc\, d\theta \qquad (4.18)$$

The integration yields to:

$$f_{b,j}(k) = \frac{1}{8\,\pi\, l} \left( J_1 + J_2 + J_3 + J_4 + J_5 \right) \qquad (4.19)$$

Replacing $r_1$ by $r_o$ in Eqns (4.13) to (4.17) gives terms $J_1$ to $J_5$.

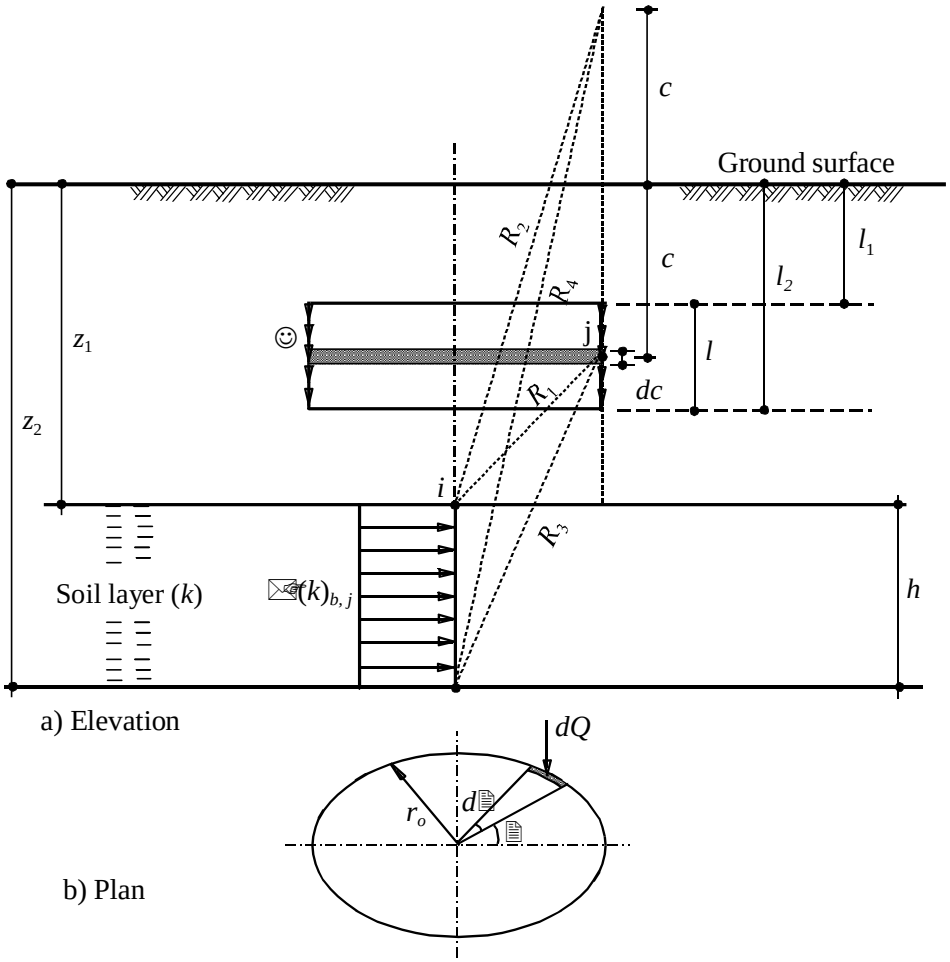


Figure 4-7 Geometry of cylindrical surface stress to find the stress coefficient at the center

### 4.2.2 Modeling single pile

#### *4.2.2.1 Increment of vertical stress*

A deeply extended clay layer is considered to simulate the half-space soil medium. The layer is subdivided into *l* sub-layers of equal thickness as shown in Figure 4-8. The increment of vertical stress in a soil layer *k* at a point *i* is attributed to stresses caused by all contact forces on that layer.

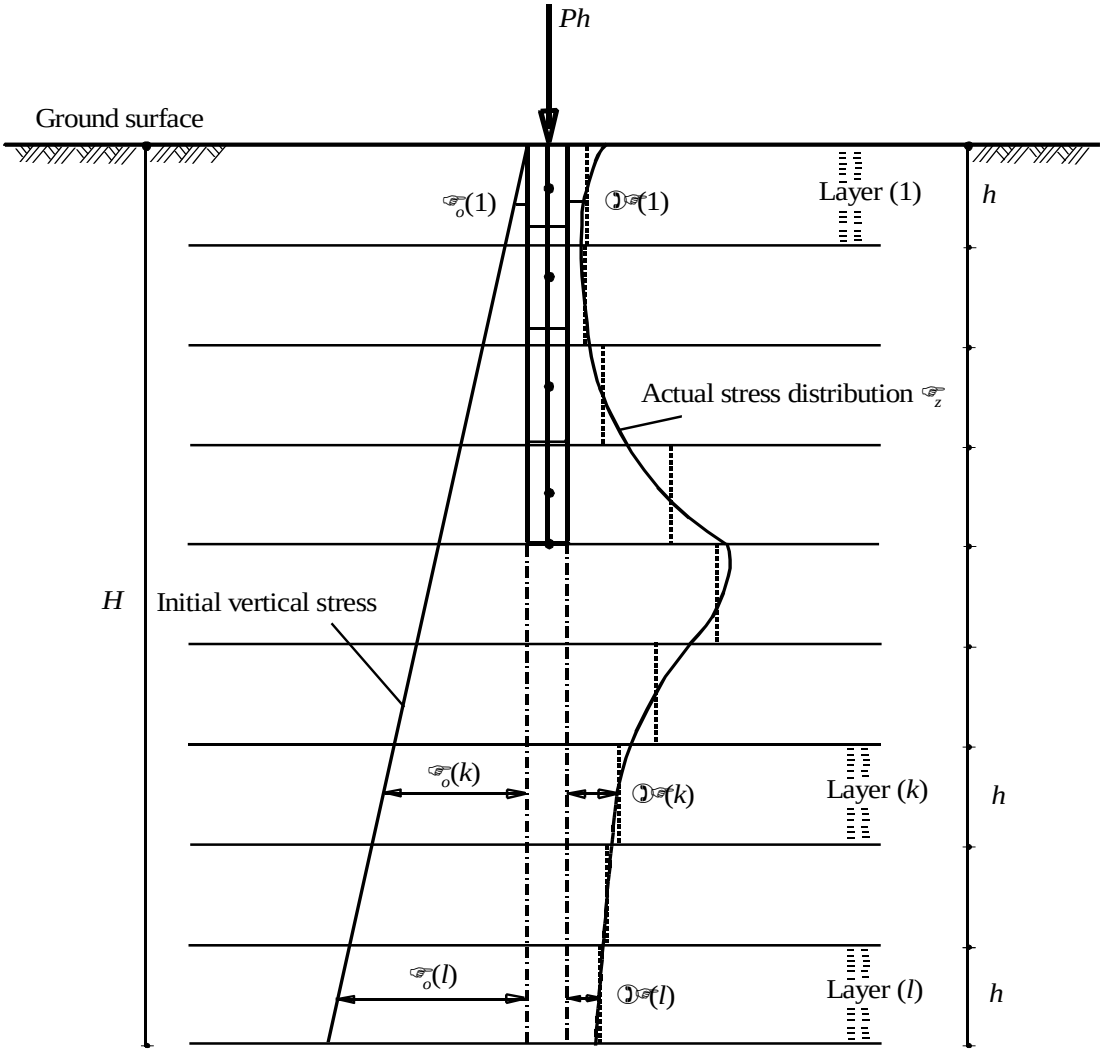


Figure 4-8 Pile in a deeply extended clay layer

Considering a point *i* that lies on the pile axis, the increment of vertical stress in a soil layer *k* due to shear forces $Qs_j$ on all *m* nodes and due to the base force *Qb* is expressed as:

$$\Delta\sigma(k) = \sum_{j=1}^{m} f_{i,j}(k)\, Qs_j + f_{i,b}(k)\, Qb \qquad (4.20)$$

where:

| | |
|---|---|
| *j*-1 and *j* | Node number of element *j* |
| $\Delta\sigma(k)$ | Increment of vertical stress in a soil layer *k* at pile *i* [kN/m$^2$] |
| $Qs_j$ | Shear force on node *j* [kN] |
| *Qb* | Force on the base *b* [kN] |

#### *4.2.2.2 Consolidation settlement*

Using clay properties $C_c$ and $e_o$, the consolidation settlement due to all contact forces on a pile is given by:

$$Sc = \frac{C_c\, h}{1+e_o} \sum_{k=1}^{l} \log\left( \frac{\sigma_o(k) + \Delta\sigma(k)}{\sigma_o(k)} \right) \tag{4.21}$$

where:

| | |
|---|---|
| $Sc$ | Consolidation settlement of the pile $i$ [m] |
| $C_c$ | Compression index [-] |
| $e_o$ | Initial void ratio [-] |
| $\sigma_o(k)$ | Initial overburden pressure in a layer $k$ [kN/m$^2$] |
| $l$ | Number of clay layers |

#### *4.2.2.3 Contact pressure along the pile*

Due to the natural geometry of the pile where the length is much greater than the diameter, the pile in vertical direction can be considered as a rigid body. In rigid body motion, points on the rigid body move downward with a constant displacement. Many authors solved the problem of contact pressure distribution that gives a constant displacement in the half-space medium at all points in a rigid pile. Some of them are *Poulos/ Davis* (1968) and *Butterfield/ Banerjee* (1971). It is found that the contact pressure is independent on the elastic constants of the half-space medium. *El Gendy* (2003) showed that the contact pressure distribution under a rigid raft on a finite clay layer is independent from the soil properties. *El Gendy* (2006) showed also that the distribution of contact pressure for rafts on deeply extended clay layer is quite similar to that on half-space medium of elastic layer. This concept is used to determine the consolidation settlement on an extended clay layer. The stress causing a constant elastic displacement in the half-space medium must also cause a constant consolidation settlement in a deeply extended clay layer. Therefore, the formula used to determine the contact pressure distribution along a rigid pile on elastic medium is also valid for a rigid pile on consolidated medium using the soil properties $C_c$ and $e_o$. Consequently, the contact pressure becomes known for the problem. In this case, problem unknowns are considerably reduced to only the uniform consolidation settlement. Available formula used to determine the contact pressure along a rigid pile is presented by *El Gendy* (2007). The contact force on a pile of $n$ nodes, Figure 4-2, is given by:

$$Q_i = \frac{Ph \sum_{j=1}^{n} k_{i,j}}{\sum_{i=1}^{n}\sum_{j=1}^{n} k_{i,j}} \tag{4.22}$$

where:

| | |
|---|---|
| $Q_i$ | Contact force on node $i$ [kN] |
| $Ph$ | Force on the pile head [kN] |
| $k_{i,j}$ | Stiffness matrix coefficient |

The stiffness matrix coefficients in Eq. (4.22) depend only on the geometry of pile elements and soil layers. To get these coefficients, soil flexibility matrix is generated first with omitting soil elastic properties from flexibility equations by replacing modulus of elasticity by 1.0 and *Poission's* ratio by 0.0. Then, inverting flexibility matrix, gives the soil stiffness matrix, which contains the required coefficients.

### 4.2.3 Modeling pile groups and piled raft

Only piled raft analysis is presented. Freestanding raft is a special case of piled raft without contacting between raft and soil. It can be analyzed in the same manner of piled raft. Consider the piled raft of a centric load shown in Figure 4-9 where the settlement in this case is defined by the rigid body translation *Sc* at the center ($x_c$, $y_c$) of the raft.

#### *4.2.3.1 Increment of vertical stress*

Equation (4.20) for the increment of vertical stress in a soil layer *k* under the center ($x_c$, $y_c$) of the piled raft may be rewritten in general form as:

$$\Delta\sigma_c(k) = \sum_{j=1}^{n} I_{i,j}(k)\, Q_j \tag{4.23}$$

where:

$\Delta\sigma_c(k)$ Increment of vertical stress in a soil layer *k* under the center of the raft [kN/m$^2$]
$Q_j$ Contact force on node *j* [kN]
*n* Total number of contact nodes on the piled raft
$I_{i,j}(k)$ Stress coefficient for layer *k* under node *i* on the raft due to a unit force on node *j* [1/m$^2$]

For pile-pile interaction or pile-raft interaction the stress coefficients $I_{i,j}(k)$ are determined from Eq. (4.8) to Eq. (4.19), while those for raft-raft interaction or raft-pile interaction are determined according to *El Gendy* (2006).

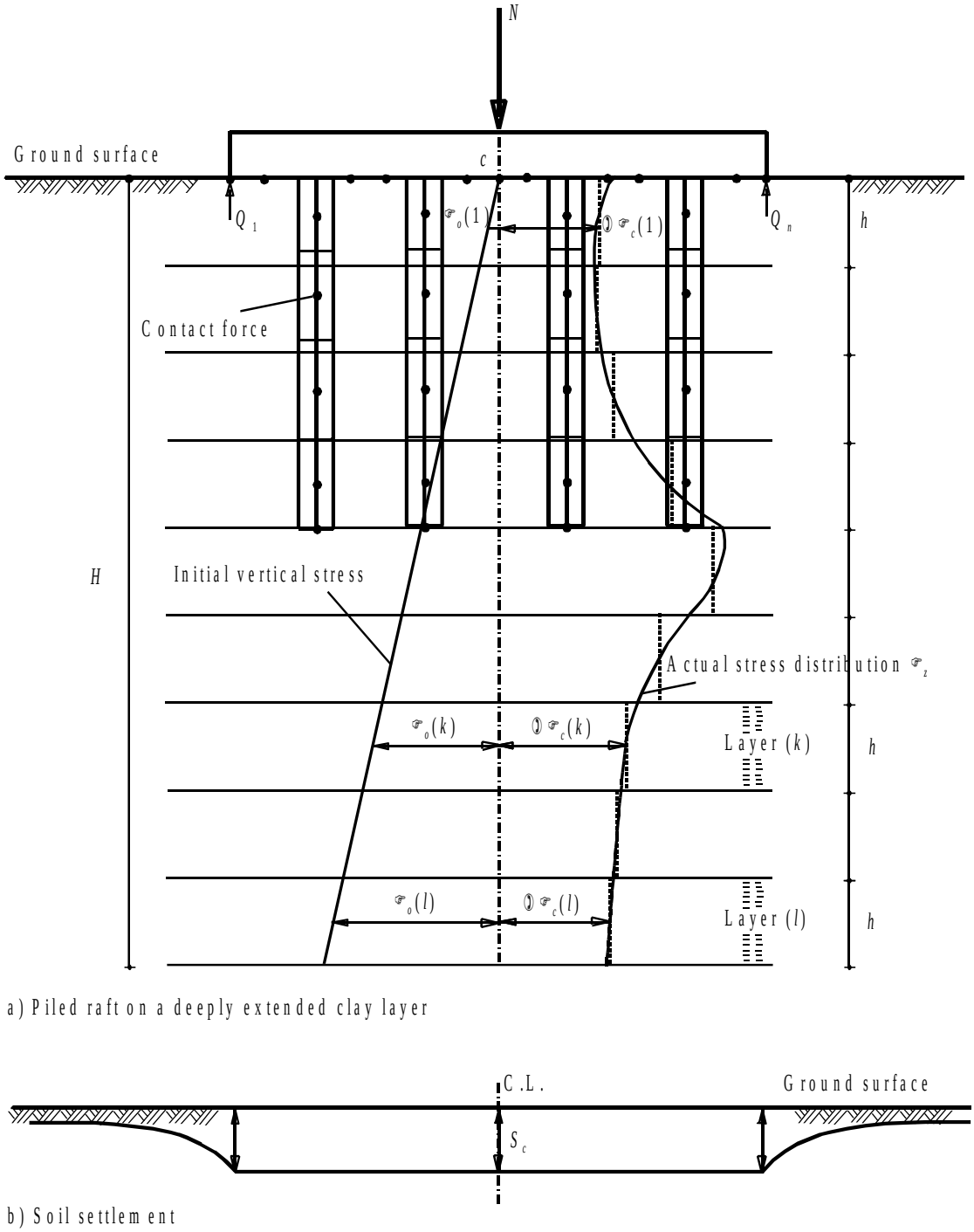


Figure 4-9 Modeling piled raft

#### *4.2.3.2 Consolidation settlement*

The consolidation settlement due to all contact forces on the piled raft under the center of the raft is given by:

$$Sc = \frac{C_c\, h}{1+e_o} \sum_{k=1}^{l} \log\left( \frac{\sigma_o(k) + \Delta\sigma_c(k)}{\sigma_o(k)} \right) \tag{4.24}$$

#### *4.2.3.3 Contact pressure on the piled raft nodes*

Similar to Eq. (4.22), the contact force on a node *i* of the piled raft is given by:

$$Q_i = \frac{N \sum_{j=1}^{n} k_{i,j}}{\sum_{i=1}^{n} \sum_{j=1}^{n} k_{i,j}} \tag{4.25}$$

where $N$ [kN] is the resultant of applied loads acting on the raft.

## 4.3 Numerical Results

### 4.3.1 Test example: Verification of a piled raft on a deeply extended clay layer

A square raft of a side $L$ = 10.0 [m] on a deeply extended clay layer is chosen to verify the present analysis of a piled raft on a clay layer. The raft is supported by 25 piles. Each pile is 10.0 [m] long and 0.5 [m] in diameter. Piles are spaced at centers on a 2.0 [m] square grid as shown in Figure 4-10. The raft is subjected to a centric vertical load of $N$ = 15 [MN]. To check the accuracy of the analysis, the raft with piles is analyzed for two different cases:

1. Freestanding raft (pile groups)
2. Piled raft

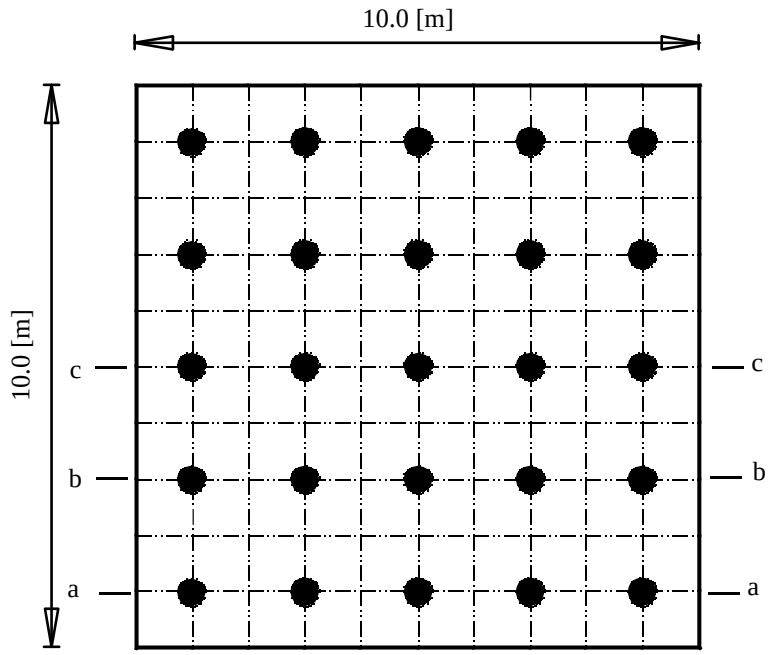


Figure 4-10 Mesh of raft with piles

#### *4.3.1.1 Clay properties*

The clay is assumed to have the following properties:

| | | | |
|---|---|---|---|
| Term of compression index and initial void ratio | $C_c / (1 + e_o)$ | = 0.001 | [-] |
| Dry unit weight of the clay | $\gamma_s$ | = 18.5 | [kN/m$^3$] |

### *4.3.1.2 Analysis of the raft*

The raft is subdivided into 100 square elements; each is 1.0 [m] side, while the pile is subdivided into 5 line elements of each 2.0 [m] length. The contact pressure distribution along piles and under the raft is obtained with the assumption of a semi-infinite soil layer using the elastic analysis. In consolidation settlement calculation, the clay layer is considered as semi-infinite soil layer when the clay has a deep thickness of $z$ = 100 [m]. The clay layer is subdivided into sub-layers each of thickness $h$ = 20.0 [m]. Definition of rigid body movement can be used to verify the analysis. For a rigid body subjected to a vertical centric load, the body moves downward with a uniform displacement. Therefore, the consolidation settlement for the freestanding and piled rafts must be uniform on all points on rafts. In the analysis of raft as rigid body, computing the consolidation settlement at the raft centroid is sufficient. But to check the linearity of the consolidation settlement, settlements are determined for all points on raft.

### *4.3.1.3 Results and discussions*

Consolidation settlements at sections a to c (Figure 4-10) for the freestanding raft are shown in Figure 4-11, while those for piled raft are shown in Figure 4-12. Although the consolidation settlement is determined under all points on the raft, the consolidation settlement is distributed linearly under the raft with maximum difference 4 [%] in case of a freestanding raft and 3 [%] in case of piled raft in respect to fitting curves. The piled raft bearing factor is found to be $\alpha_{kpp}$ = 90 [%], this is related to arranging piles in narrow distances. Consequently, the difference in consolidation settlements for both cases is small.

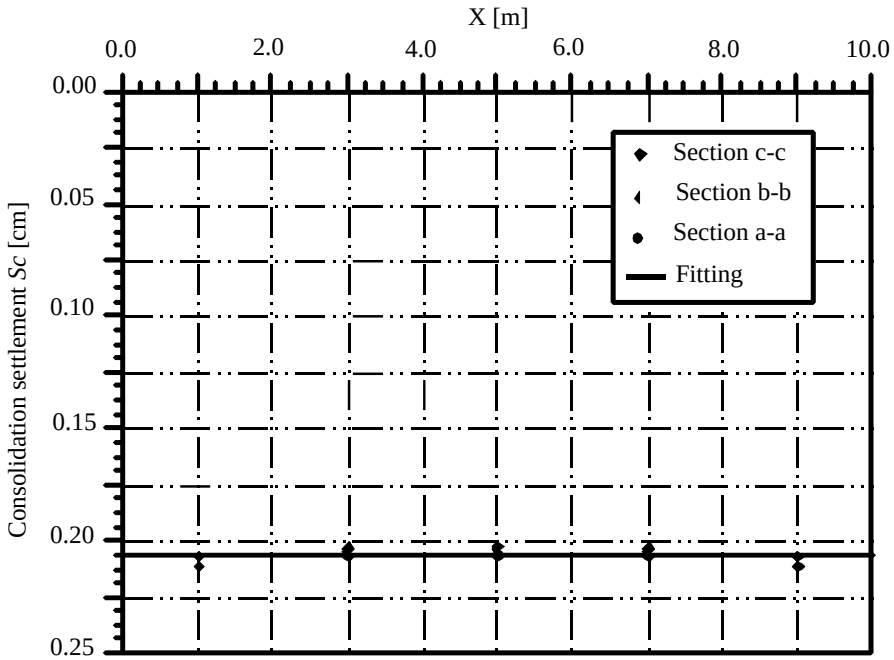


Figure 4-11 Consolidation settlement at sections a to c for freestanding raft

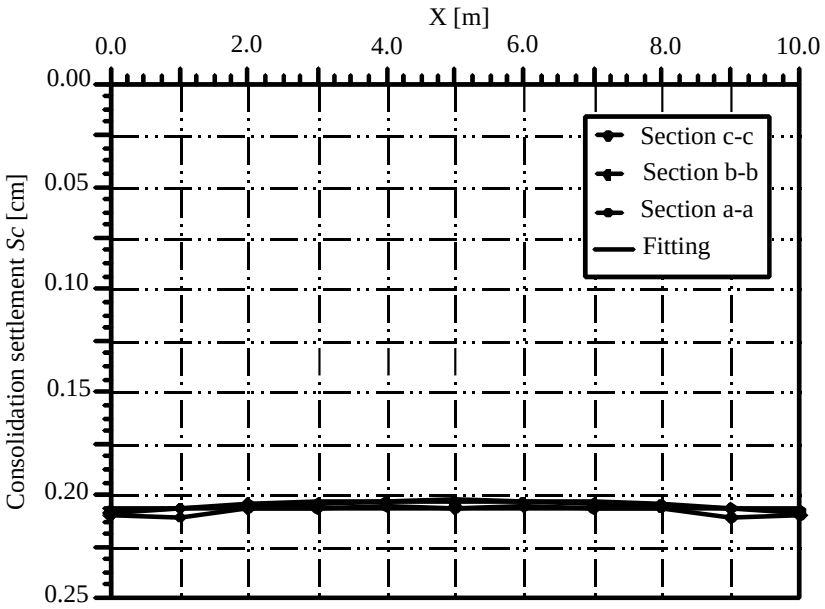


Figure 4-12 Consolidation settlement at sections a to c for piled raft

### 4.3.2 Case study 1: Piled raft of *Stonebridge Tower*

*Stonebridge Tower* piled raft analysis and measurements discussed by *Hemsley* (2000) and reported by *Cooke et al.* (1981) are considered to check the accuracy of the present analysis. *Stonebridge* is a tower of 16-storey floors at Stonebridge Park in North London, England. The tower is 43 [m] high. The foundation is a rectangular piled raft of area 43.3 [m] by 19.2 [m]. The estimated total load on the raft gives an average applied uniform load of 187 [kN/m$^2$]. Raft thickness is 0.9 [m]. A total of 351 bored piles are located under the raft. All piles have a length of $l$ = 13 [m] and a diameter of $D$ = 0.45 [m]. Piles are arranged on 1.6 [m] by 1.5 [m] grid. Figure 4-13 shows a mesh of *Stonebridge Tower* raft with piles. The tower is founded on a thick layer of London clay which, at this site, extends to the ground surface. As the building has no underground floors, raft is located close to the ground surface.

The tower was constructed between 1973 and 1975, the recorded average settlement of the raft was about 1.8 [cm] after four years from the end of construction. Later measurements indicate that differential raft settlement is small, because the stiffness of the cross-wall superstructure is high. *Padfield/ Sharrock* (1983) modeled the raft by plate-bending finite elements, with an equivalent raft thickness of 4.5 [m] to take account of the stiffness of the superstructure. The soil is treated as a multi-layered elastic half-space subjected to loads both at the surface and at depth at the pile locations. Raft-pile interaction is neglected and an iterative process is used to match raft and soil settlement. They obtained a good agreement between the observed and computed results. The foundation of *Stonebridge Tower* is an ideal case study to verify the present analysis because conditions of this piled raft coincide with the assumptions of the present analysis. The piled raft is a full rigid on a deeply extended clay layer. Using available data and results of *Stonebridge Tower* piled raft the present analysis is evaluated and verified for analyzing a piled raft on clay soil.

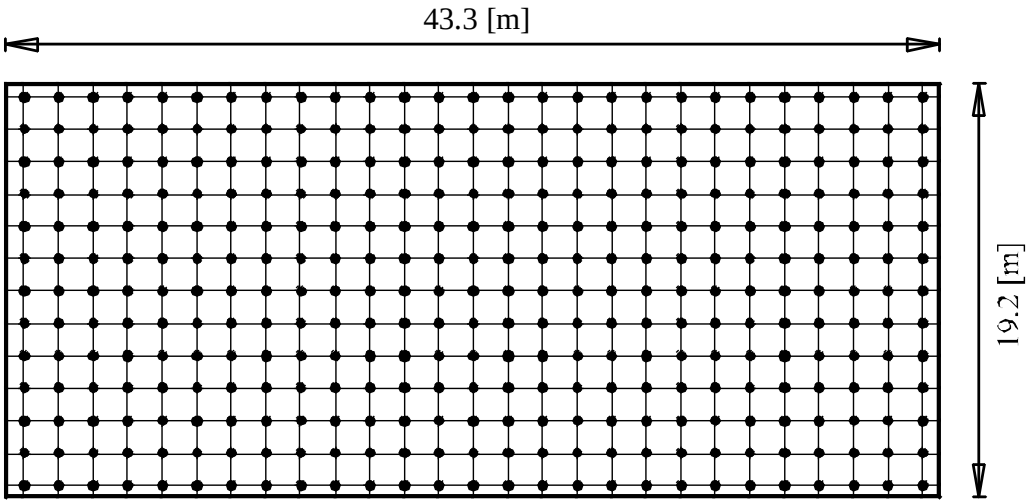


Figure 4-13 Mesh of *Stonebridge Tower* raft with piles

To show the difference between results when analyzing piled raft of *Stonebridge Tower* by methods that use variable soil modulus, piled raft of *Stonebridge Tower* is analyzed by the following methods:

- **N**onlinear analysis of **p**iled **r**aft using **D**IN 4014 (NPRD)
- **N**onlinear analysis of **p**iled **r**aft using **h**yperbolic function (NPRH)
- **L**inear analysis of **p**iled **r**aft (LPR)

The method NPRD was developed by *El Gendy et al.* (2006), while those of NPRH and LPR were developed by *El Gendy* (2007).

#### *4.3.2.1 Soil properties*

The following section describes all soil parameters and constants, those used to carry out the present analysis and other selected methods for comparison. London clay is classified as overconsolidated clay. The undrained cohesion of London clay increases with depth and can be approximated according to *Hong et al.* (1999) by the following linear relation:

$$c_u = 150 + 6.67z \tag{4.26}$$

where:
$c_u$ Undrained cohesion of London clay [kN/m$^2$]
$z$ Depth measured from the clay surface [m]

*Hong et al.* (1999) used a ratio of 200 between the shear modulus $G$ and the undrained cohesion $C_u$ to get a variable shear modulus of the soil.

$$G = 200c_u = 200\left(150 + 6.67z\right) \tag{4.27}$$

The relationship between the shear modulus $G$ and modulus of elasticity $E$ is given by:

$$G = \frac{E}{2\,(1+\nu_s)} \tag{4.28}$$

Substituting Eq. (4.27) into Eq. (4.28) and taking *Poisson's* ratio of the clay $\nu_s$ = 0.25 [-] leads to:

$$E = E_o\,(1 + 0.0445\,z) \tag{4.29}$$

where:
$G$ Shear modulus [kN/m$^2$]
$E$ Modulus of elasticity of London clay [kN/m$^2$]
$\nu_s$ *Poisson's* ratio of the soil [-]
$E_o$ Initial modulus of compressibility, $E_{so}$ = 75000 [kN/m$^2$]

A relationship between the modulus of compressibility, compression index and initial void ratio for overconsolidated clay ($\sigma_o + \Delta\sigma_{av} > \sigma_c$) may be expressed as (*Mayne/ Poulos* (1999)):

$$E_s = \frac{(1+e_o)}{C_r}(\sigma_v)\ln(10) \tag{4.30}$$

or

$$E_s = \left(\frac{1-\nu_s}{1-\nu_s-2\nu_s^2}\right)E = = \frac{(1+e_o)}{C_r}(\sigma_v)\ln(10) \tag{4.301}$$

where:
$E_s$ Modulus of compressibility of London clay [kN/m$^2$]
$C_r$ Recompression index [-]
$\sigma_v$ Stress in soil, $\sigma_v = \sigma_o + \Delta\sigma_{av}$ [kN/m$^2$]
$\sigma_c$ Preconsolidation pressure [kN/m$^2$]
$\Delta\sigma_{av}$ Average vertical stress increase in the clay [kN/m$^2$]

The term of recompression index and initial void ratio can be obtained by equating Eq. (4.30) to Eq. (4.29) directly under piles at $z$ = 15 [m]. The average vertical stress which increases at this depth may be approximated by distributing the raft pressure in the soil with a slope of 1:2.

Term of recompression index and initial void ratio for the whole layer is given by:

$$\frac{C_r}{(1+e_o)} = 0.0045 \tag{4.32}$$

To carry out the analysis by the NPRD method, an average undrained cohesion of $c_u$ = 200 [kN/m$^2$] is considered. *Russo* (1998) suggested limited shaft friction not less than 180 [kN/m$^2$] meeting undrained shear strength of 200 [kN/m$^2$]. To carry out the analysis by the LPR method, a limit shaft friction of $ql$ = 180 [kN/m$^2$], which gives a limiting pile load of $Ql$ = 3817 [kN] is assumed. Groundwater in typical London clay lies within 1.0 [m] from the ground surface (*Rickard et al.* (1985)). The groundwater level is assumed to lie directly below the raft. Dry unit weight of the clay is taken to be $\gamma_s$ = 18.5 [kN/m$^3$].

#### *4.3.2.2 Pile material*

To take the weight of the piles in the analysis, the unit weight of the pile material is taken to be $\gamma_b = 25$ [kN/m$^3$].

#### *4.3.2.3 Analysis of the piled raft*

As piles are narrow to each other, pile-raft interaction may be neglected and the foundation is analyzed as freestanding raft. Comparisons are carried out to evaluate the present analysis. Settlements computed from methods that use variable soil modulus and field measurements are compared with that obtained by the present analysis. Piles are subdivided into line elements, each of 3.75 [m] length. The effective depth of the soil layers under the raft is taken to be $H$ = 100 [m] for all methods. In the analysis by NPRD, NPRH and LPR methods, the total layer is subdivided into 10 sub-layers to take the variety of the soil modulus with depth. In the present analysis, the average vertical stress increase is determined in sub-layers of the clay, each of 20 [m] thickness.

#### *4.3.2.4 Comparison with measured settlement*

To examine the present analysis for *Stonebridge Tower* piled raft, the computed consolidation settlement is compared with the measured settlement in Table 4-1. The computed settlement was determined at the raft centroid. The table shows a small difference between computed and measured settlements.

Table 4-1 Comparison between measured and computed settlements

| Item | Measured settlement | Computed settlement | Difference |
|---|---|---|---|
| Consolidation settlement $S_c$ [cm] | 1.8 | 2.1 | + 0.3 |

#### *4.3.2.5 Comparison with methods using variable soil modulus*

Figure 4-14 shows the consolidation settlement of piled raft obtained by the present analysis and those obtained by methods using variable soil modulus. Also, the figure includes the measured settlement.

LPR gives the smallest settlements among the others. This was expected, because the settlement from nonlinear analysis is greater than that obtained from linear analysis. However, the contact pressures for the present analysis and LPR are the same where they are independent from soil properties but settlements of them are not the same. It can be noticed that the consolidation settlement of the present analysis has a good agreement not only with measured settlement but also with computed settlement of nonlinear analyses using variable soil modulus.

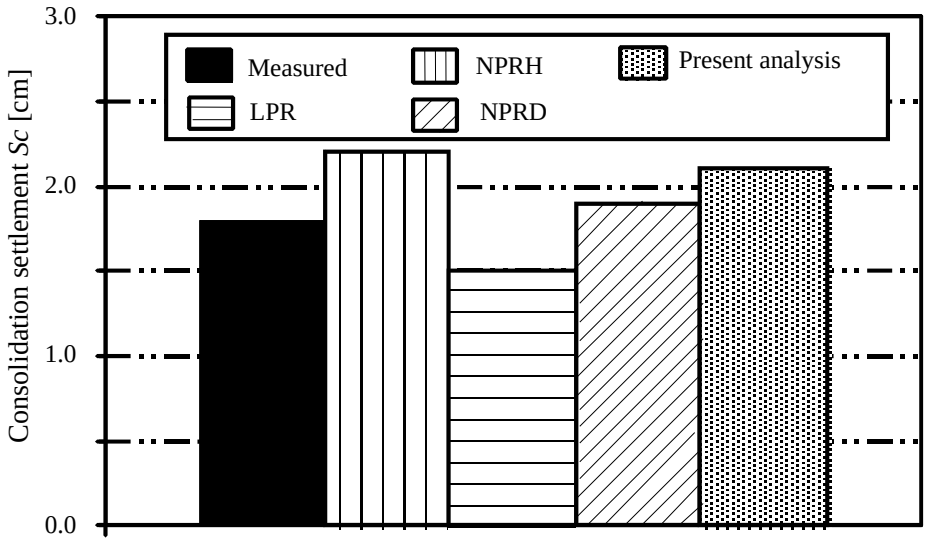


Figure 4-14 Comparison between measured and computed settlements (case study 1)

### 4.3.3 Case study 2: Piled raft of *Dashwood House*

*Hong et al.* (1999) applied a method for the analysis of large vertically loaded pile groups using load-transfer curves (NPRLT) on the piled raft of *Dashwood House*. They compared the computed settlement with that of the field measurement reported by *Hooper* (1979). In this case study, the computed and measured settlement of this piled raft is used to verify the present analysis.

*Dashwood House* is a high building of 15-storey floors with a single storey basement located in North London, England. The building is 61 [m] high. The foundation of *Dashwood House* is a rectangular piled raft of area 43 [m] by 31.5 [m]. The building load including the raft weight is 274 [MN]. A total of 462 bored piles are located under the raft. All piles have a length of $l$ = 15 [m] and a diameter of $D$ = 0.485 [m]. Piles are arranged on a square grid of 1.5 [m] interval. Figure 4-15 shows the mesh of the raft with piles. The subsoil at the building location consists of 8 [m] of fill, sand and gravel, followed by London clay. The raft is founded on gravel about 1 [m] above the upper clay surface. In their analysis for simplicity, *Hong et al.* (1999) considered the raft resets on the London clay directly.

#### *4.3.3.1 Analysis of the piled raft*

*Dashwood House* has the same conditions of *Stonebridge Tower* in respect to the soil, statical system of the structure and piled raft. Considering the same properties of London clay presented in case study 1, the piled raft is analyzed by the present analysis and the selected previously methods. Piles are divided into line elements each of 3.25 [m] length.

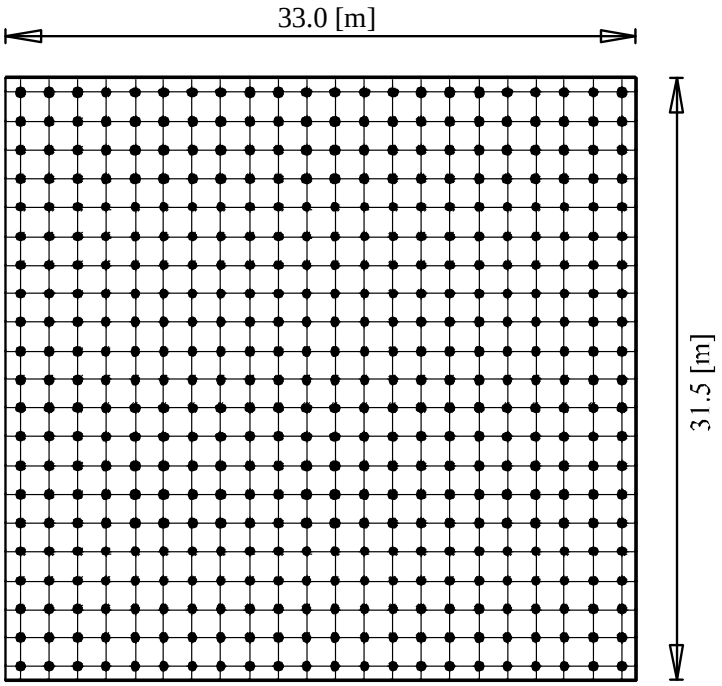


Figure 4-15 Mesh of *Dashwood House* raft with piles

#### *4.3.3.2 Comparison with measured settlement*

The consolidation settlement is compared with the measured settlement in Table 4-2. The table shows a small difference between computed and measured settlements.

Table 4-2 Comparison between measured and computed settlements

| Item | Measured settlement | Computed settlement | Difference |
|---|---|---|---|
| Consolidation settlement $S_c$ [cm] | 3.3 | 2.9 | - 0.4 |

#### *4.3.3.3 Comparison with methods using variable soil modulus*

Figure 4-16 shows the consolidation settlement of piled raft obtained by the present analysis and those obtained by methods using variable soil modulus. Also, the figure includes the measured settlement and the computed settlement by the NPRLT method. From this figure, the same conclusions, which are presented in case study 1, are achieved.

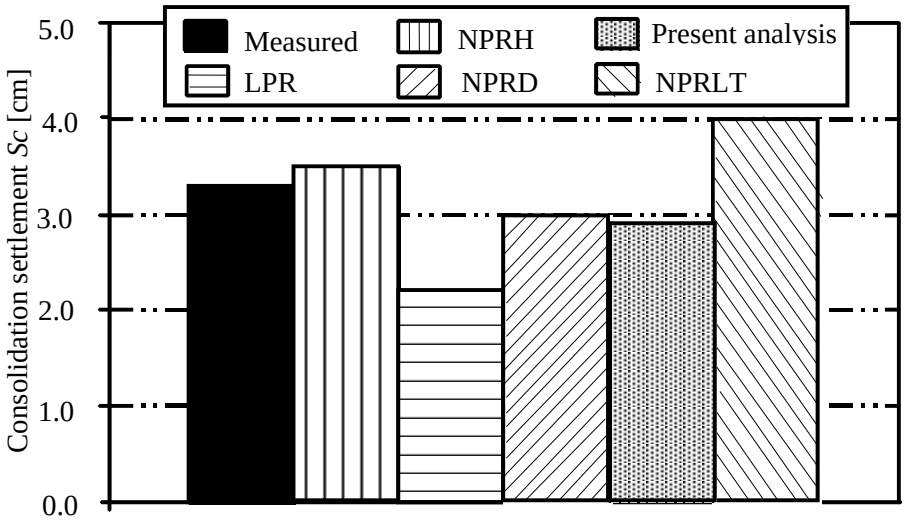


Figure 4-16 Comparison between measured and computed settlements (case study 2)

## 4.4 References


[1] *Butterfield, R./ Banerjee, P.* (1971): The problem of pile group-pile cap interaction
Géotechnique, Vol. 21, No. 2, 351-371

[2] *Cook, W./ Bryden-Smith, W./ Gooch, N., Sillett, F.* (1981): Some observation of the foundation loading and settlement of a multi-storey building on a piled raft foundation in London Clay
Proce. Instn. Civ. Engrs. Part1

[3] *El Gendy, M.* (2003): Numerical Modeling of Rigid Circular Rafts on Consolidated Clay Deposits
Int. Workshop on Geotechnics of Soft Soils-Theory and Practice
Vermeer, Schweiger, Karstunen & Cudny (eds.)

[4] *El Gendy, M.* (2006): Developing stress coefficients for raft-deformation on a thick clay layer
Scientific Bulletin, Faculty of Engineering, Ain Shams University, Cairo, Egypt
Vol. 41, No. 3, September 2006, pp. 73-108

[5] *El Gendy, M.* (2007): Formulation of a composed coefficient technique for analyzing large piled raft
Scientific Bulletin, Faculty of Engineering, Ain Shams University, Cairo, Egypt
Vol. 42, No. 1, March 2007, pp. 29-56

[6] *El Gendy, M.* (2007): Deriving equations for analyzing friction piles in clay soil
Scientific Bulletin, Faculty of Engineering, Ain Shams University, Cairo, Egypt
Vol. 42, No. 1, March 2007, pp. 1-27

[7] *El Gendy, M./ Hanisch, J./ Kany, M.* (2006): Empirische nichtlineare Berechnung von Kombinierten Pfahl-Plattengründungen
Bautechnik 9/ 06

[8] *Griffiths, D.* (1984): A chart for estimating the average vertical stress increase in an elastic foundation below a uniformly loaded rectangular area
Can. Geotech. J. 21, 710-713

[9] *Hemsley J.* (2000): Design application of raft foundations
Thomas Telford, London, Section 18

[10] *Hong, D./ Chow, Y./ Yong, K.* (1999): A method for analysis of large vertically loaded pile groups
Int. J. Numer. Anal. Meth. Geomech., 23, 243-262

[11] *Hooper, J.* (1979): Review of behaviour of piled raft foundation
CIRIA Report 83, pp. 45-54

[12] *Masih R.* (1993): Structural Stiffness Influence on Soil Consolidation
Journal of Geotechnical Engineering; 119 (1), pp. 168-172

[13] *Masih R.* (1994): Foundation Uniform Pressure and Soil-Structure Interaction
Journal of Geotechnical Engineering; 120 (11), pp. 2064-2071

[14] *Mayne, P./ Poulos, H.* (1999): Approximate displacement influence factors for elastic shallow foundations
Journal of Geotechnical and Geoenviromental Engineering, 453-459

[15] *Padfield, J./ Sharrock, J.* (1983): Settlement of structures on clay soils
Construction Industry Research and Information Associate, London
CIRIA Spec. Publn 27

[16] *Poulos, H./ Davis, E.* (1968): The settlement behaviour of single axially loaded incompressible piles and piers
Géotechnique, Vol. 18, 351-371

[17] *Rickard,C./ Manie, B./ Price, G./ Simons, N./ Waedel, I./ Clayton, C.* (1985): Interaction of a piled raft foundation at Basildon, UK
11th Int. Conf. Soil Mechanics and Foundation Engineering, San Francisco, USA
[18] *Russo, G.* (1998): Numerical analysis of piled rafts
Int. J. Numer. Anal. Meth. Geomech., 22, 477-493

**Case study 5**

# Piled raft of *Westend 1* in Frankfurt

**Content**

Page

**5 Case study 5: *Westend 1* piled raft ..... 3**

5.1 General ..... 3

5.2 Analysis of the piled raft ..... 5

5.3 FE-Net ..... 5

5.4 Loads ..... 6

5.5 Pile and raft material ..... 6

5.6 Soil properties ..... 7

5.7 Results ..... 11

5.8 Measurements and other results ..... 11

5.9 Evaluation ..... 11

5.10 References ..... 16

# 5 Case study 5: *Westend 1* piled raft

## 5.1 General

*Westend 1* is 208 [m] high skyscraper and standing on a piled raft. The tower lies in Frankfurt city, Germany. It was completed in 1993. The tower was the third tallest skyscraper in Frankfurt and also in Germany until 1993, Figure 5-1.

Using instruments installed inside the foundation of *Westend 1*, an extensive measuring program was established to monitor the behavior of the building. Because these instruments record raft settlements, raft contact pressures and loads on pile heads and along pile shafts, the building was a good opportunity to verify analysis methods for piled raft foundation and compare them with the recorded data Extensive studies were carried out by *Poulos et al.* (1997) *Poulos* (2001), *Reul* and *Randolph* (2003) and *Chaudhary* (2010) on analyzing the piled raft by methods of *Poulos and Davis* (1980), *Poulos* (1991), *Poulos* (1994), *Ta and Small* (1996), *Sinha* (1996), *Franke et al.* (1994), Randolph (1983) and *Clancy and Randolph* (1993).

The building has a basement with three underground floors and 51 stories with an average estimated applied pressure of 412 [kN/m$^2$]. The foundation area is about 2900 [m$^2$] founded on Frankfurt clay at a depth of 14·5 [m] under the ground surface. Raft thickness varies from 4·65 [m] at the middle to 3 [m] at the edge. A total of 40 bored piles, 30 [m] length by 1.3 [m] diameter. Piles are arranged in 2 rings under the heavy columns of the superstructure. The subsoil consists of gravels and sands up to 8 [m] below the ground surface underlay by layers of Frankfurt clay extended to more than 100 [m] below the ground surface. The groundwater level lies at 4.75 [m] under the ground surface.

Figure 5-1 *Westend 1* [1]

[1] https://en.wikipedia.org/wiki/Westendstrasse_1

Figure 5-2 shows a layout of *Westend 1* with the piled raft according to *Reul and Randolph* (2003).

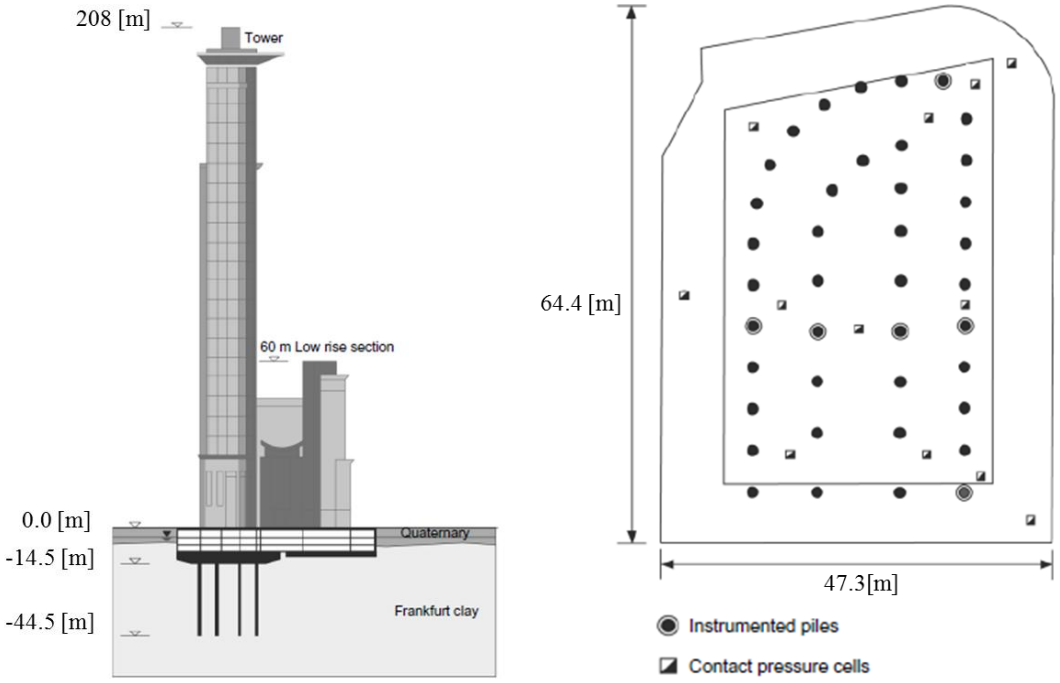


Figure 5-2 Layout of *Westend 1* with piled raft after *Reul* and *Randolph* (2003)

## 5.2 Analysis of the piled raft

Using the available data and results of the *Westend 1* piled raft the nonlinear analyses of piled raft in *ELPLA* are evaluated and verified using the following load-settlement relations of piles, *El Gendy et al.* (2006) and *El Gendy* (2007):

1- Hyperbolic function.
2- German standard DIN 4014.
3- German recommendations EA-Piles (lower values).
4- German recommendations EA-Piles (upper values).

The foundation system is analyzed as rigid or elastic piled rafts. In which, the raft is considered as either rigid or elastic plate supported on equally rigid piles.

A series of comparisons are carried out to evaluate the nonlinear analyses of piled raft for load-settlement relations of piles. Results of other analytical solutions and measurements are compared with those obtained by *ELPLA*.

## 5.3 FE-Net

The raft is divided into triangular elements with a maximum length of 2.0 [m] as shown in Figure 5-3. Similarly, piles are divided into elements with 2.0 [m] length.

## 5.4 Loads

The uplift pressure on the raft due to groundwater is $P_w$ = 81 [kN/m$^2$]. Consequently, the total effective applied load on the raft including own weight of the raft and piles is $N$ = 950 [MN]. The load is defined by a uniform load of 412 [kN/m$^2$] on the entire raft.

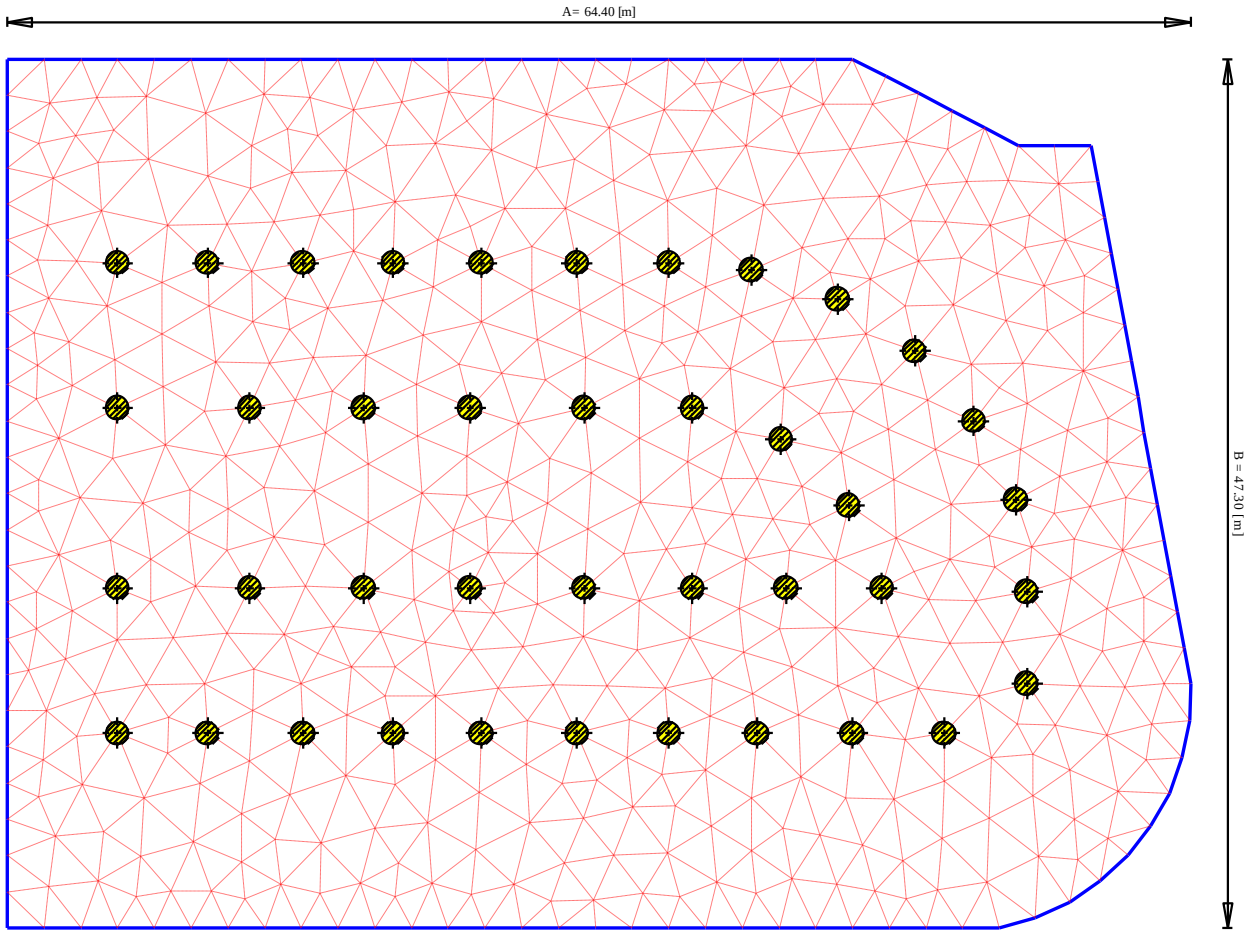


Figure 5-3 Mesh of *Westend 1* piled raft with piles of element length = 2.0 [m]

## 5.5 Pile and raft material

The average raft thickness is 4.2 [m]. All piles are 30 [m] length and 1.3 [m] diameter. The following values are used for pile and raft material:

| | | | | |
|---|---|---|---|---|
| For the raft: | | | | |
| Modulus of elasticity | $E_p$ | = | 34 000 | [MN/m$^2$] |
| *Poisson's ratio* | $\nu_p$ | = | 0.25 | [-] |
| Unit weight | $\gamma_b$ | = | 0.0 | [kN/m$^3$] |
| For piles: | | | | |
| Modulus of elasticity | $E_p$ | = | 22 000 | [MN/m$^2$] |
| Unit weight | $\gamma_b$ | = | 0.0 | [kN/m$^3$] |

## 5.6 Soil properties

The average clay properties used in the analysis can be described as follows:

*Modulus of compressibility*
Based on the back analysis presented by *Amann et al.* (1975), the distribution of modulus of compressibility for loading of Frankfurt clay with depth is defined by the following empirical formula:

$$E_s = E_{so}(1 + 0.35\,z) \tag{3.1}$$

while that for reloading is:

$$W_s = 70\left[\mathrm{MN/m^2}\right] \tag{3.2}$$

where:

$E_s$ Modulus of compressibility for loading [MN/m$^2$]
$E_{so}$ Initial modulus of compressibility, $E_{so}$ = 7 [MN/m$^2$]
$z$ Depth measured from the clay surface, [m]
$W_s$ Modulus of compressibility for reloading [MN/m$^2$]

*Undrained cohesion $c_u$*
The undrained cohesion $c_u$ of Frankfurt clay increases with depth from $c_u$ = 100 [kN/m$^2$] to $c_u$ = 400 [kN/m$^2$] at 70 [m] depth under the clay surface according to *Sommer/ Katzenbach* (1990). To carry out the analyses using German standards and recommendations, an average undrained cohesion of $c_u$ = 200 [kN/m$^2$] is considered.

*Limit pile load Ql*
*Russo* (1998) suggested a shaft friction of 180 [kN/m$^2$] for undrained shear strength of 200 [kN/m$^2$]. To carry out the analysis using a hyperbolic function, a shaft friction of $\tau$ = 180 [kN/m$^2$] is assumed, which results in pile shaft capacity of $Q_l$ = 22 [MN] as shown in equation 2.3

$$Q_l = \tau * \pi * D * l = 180 * \pi * 1.3 * 30 = 22054\,[\mathrm{kN}] = 22\,[\mathrm{MN}] \tag{2.3}$$

where:
$Q_l$ Limit pile load, [MN]
$\tau$ Limit shaft friction, $\tau$ = 180 [kN/m$^2$]
$D$ Pile diameter, [m]
$l$ Pile length, [m]

*Poisson's ratio*
*Poisson's* ratio of gravels and sands is taken to be $\nu_s$ = 0.25 [-].

The boring log for the subsoil under the raft consists of 12 soil layers as shown Figure 5-4. The total depth under the ground surface is 108 [m].

Figure 5-5 to Figure 5-8 show the load settlement relations for the different analyses.

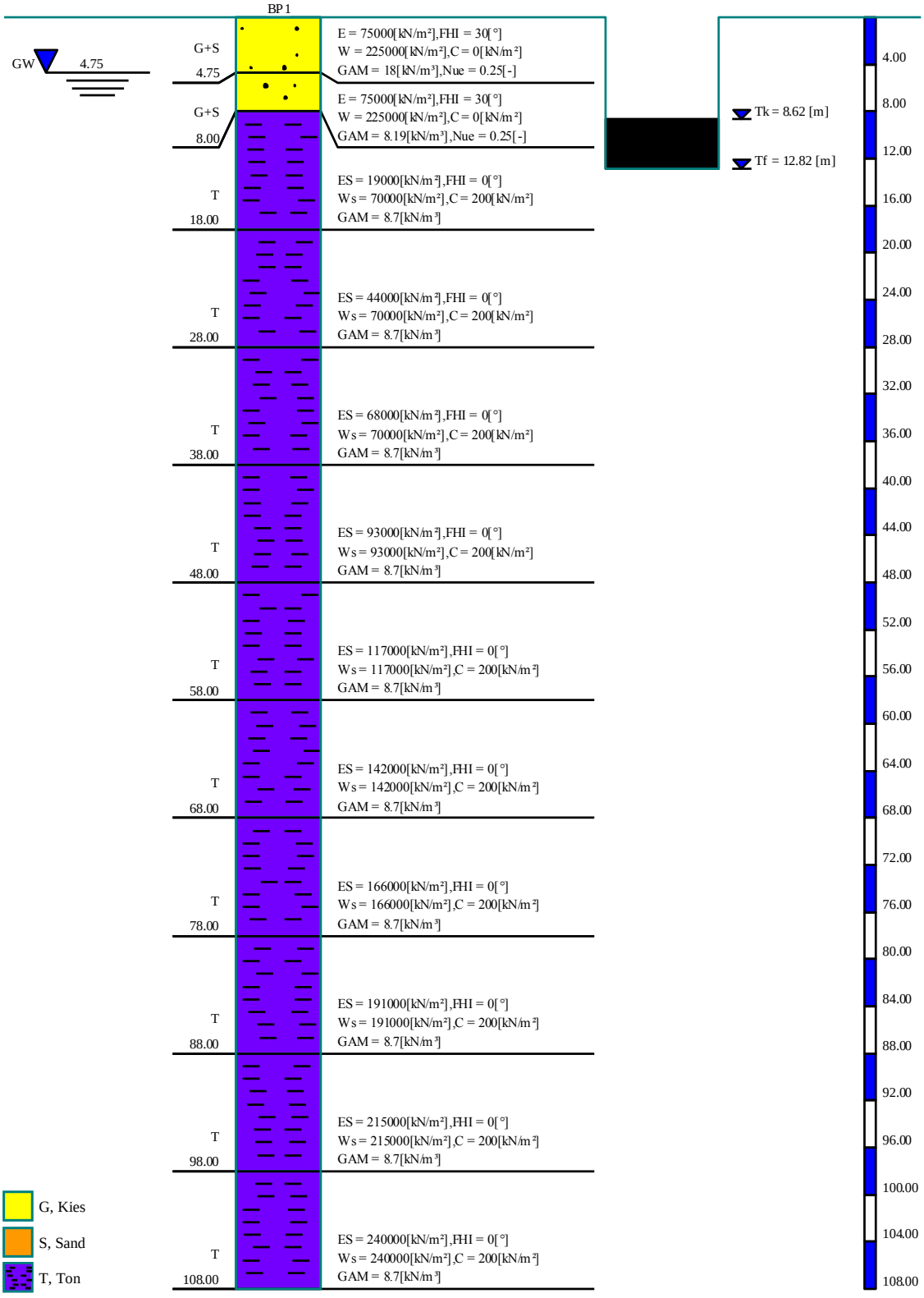


Figure 5-4 Boring log

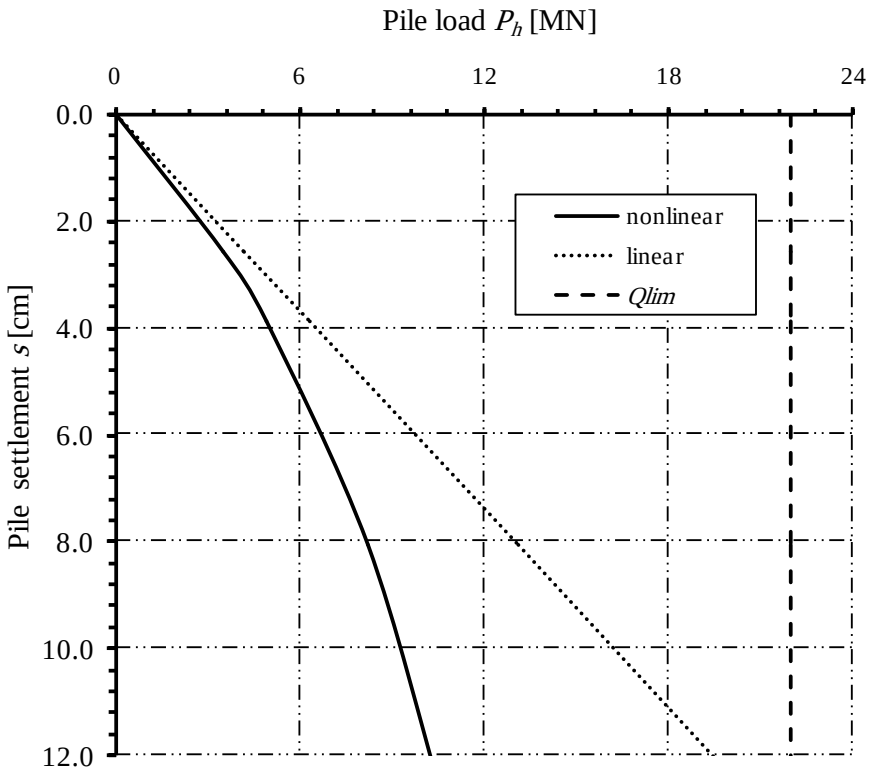


Figure 5-5 Load-settlement (hyperbolic function)

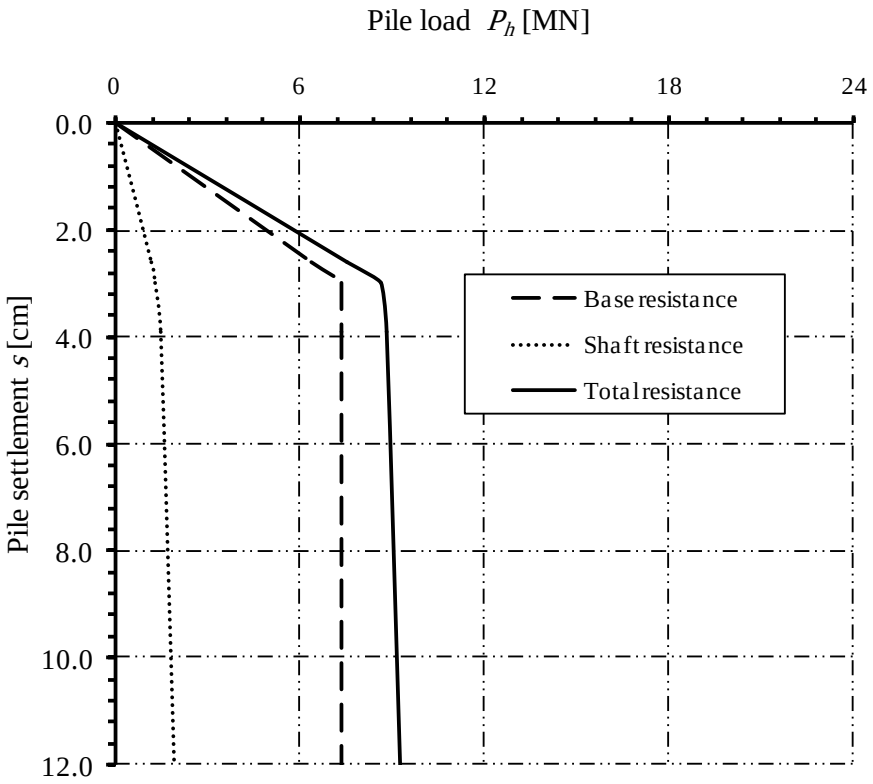


Figure 5-6 Load-settlement (DIN 4014)

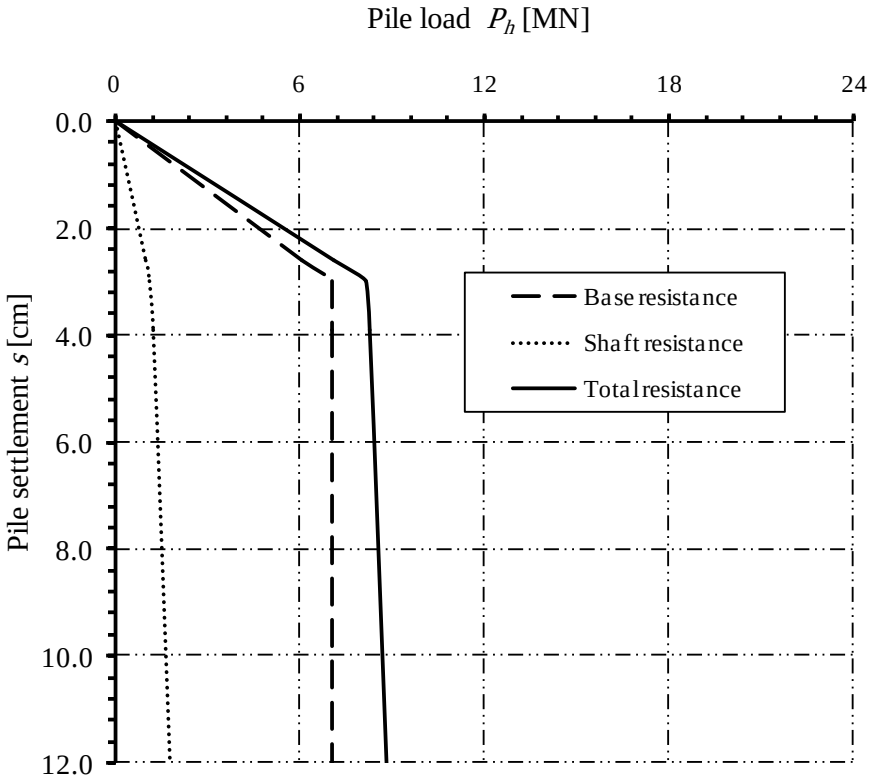


Figure 5-7 Load-settlement (EA-Piles, lower values)

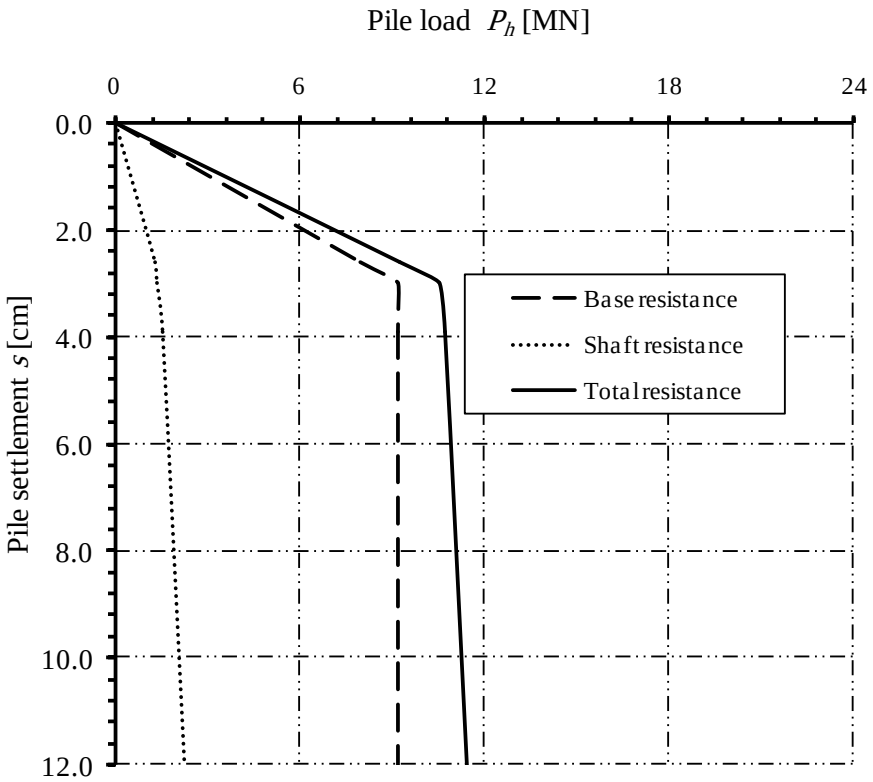


Figure 5-8 Load-settlement (EA-Piles, upper values)

## 5.7 Results

For a sample of the results for the different analyses by *ELPLA*, Figure 5-9 and Figure 5-10 show the settlement for both rigid and elastic piled rafts using German recommendations EA-Piles for upper and lower values, while Figure 5-11 and Figure 5-12 show the pile load for both rigid and elastic piled rafts using the hyperbolic function.

## 5.8 Measurements and other results

The construction of *Westend 1* started in 1990 and finished in 1993. According to *Lutz et al.* (1996), the recorded settlement at the center of the raft 2·5 years after completion of the shell of the building is 12 [cm]. The bearing factor from the measured pile loads is $\alpha_{kpp}$= 0.49. The measured minimum and maximum pile loads of 9·2 [MN] and 14·9 [MN] respectively are according to *Franke and Lutz* (1994).

Figure 5-13 compares the settlement, bearing factor of piled raft and min and max pile load values calculated by *ELPLA* with those of measurements. For more comparison, Figure 5-14 shows the rest of the results for the different methods presented by *Reul* and *Randolph* (2003). 999

## 5.9 Evaluation

This case study shows that ELPLA is a practical tool for analyzing large piled raft problems in significantly lowered computational time.

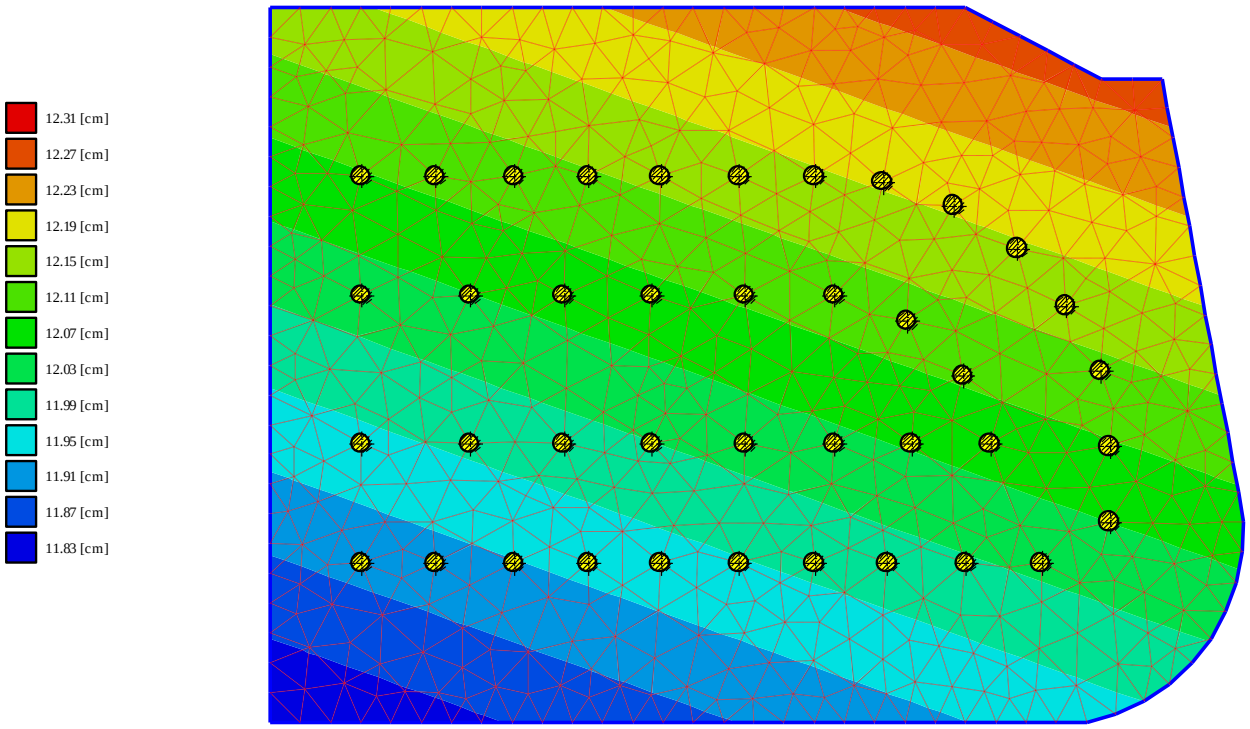


Figure 5-9 Settlement for rigid piled raft using German recommendations EA-Piles for lower values

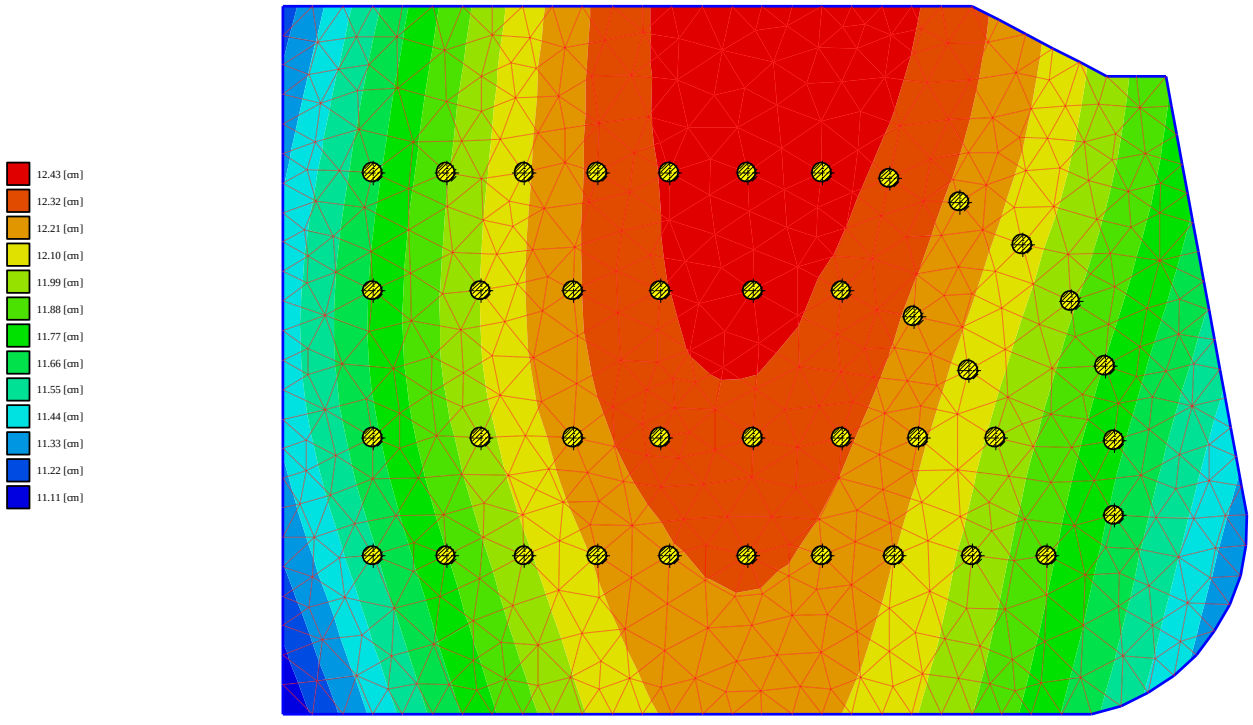


Figure 5-10 Settlement for elastic piled raft using German recommendations EA-Piles for lower values

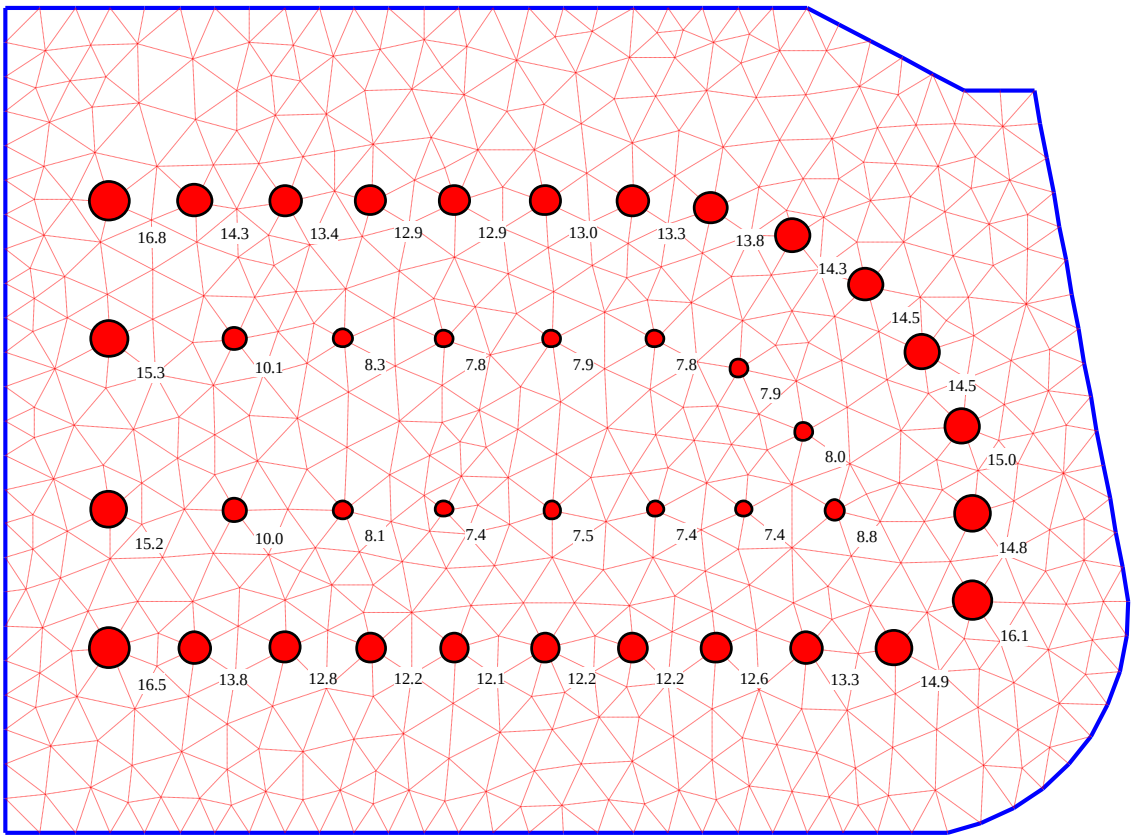


Figure 5-11 Pile load [MN] for rigid piled raft using hyperbolic function

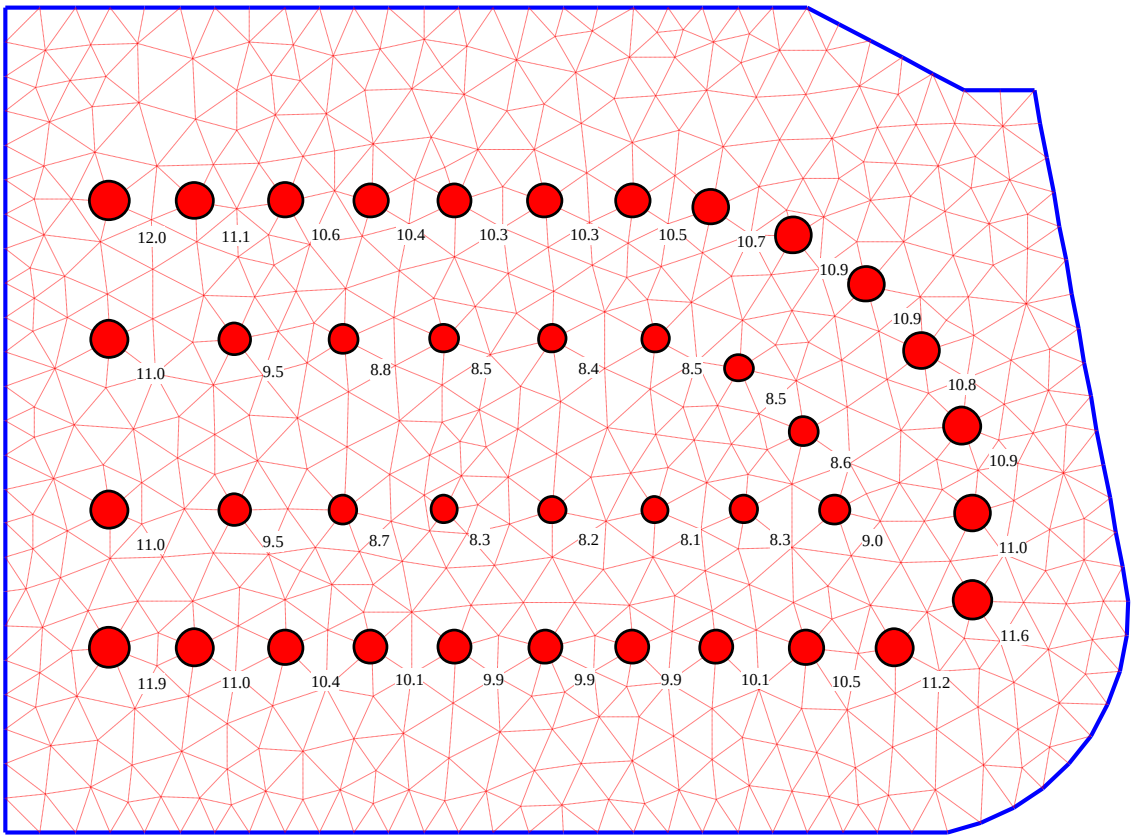


Figure 5-12 Pile load [MN] for elastic piled raft using hyperbolic function

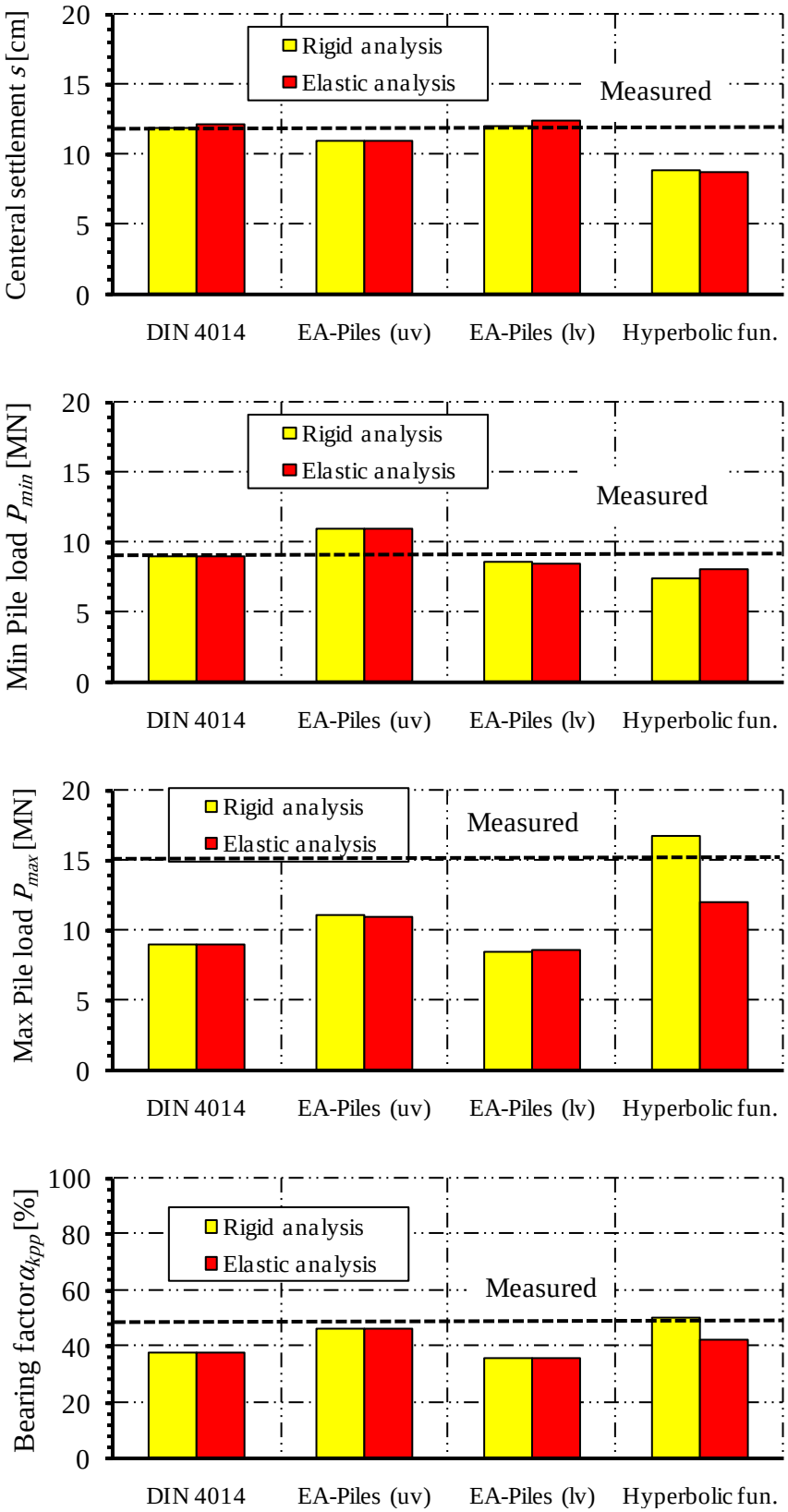


Figure 5-13 Results obtained from measurements and *ELPLA*

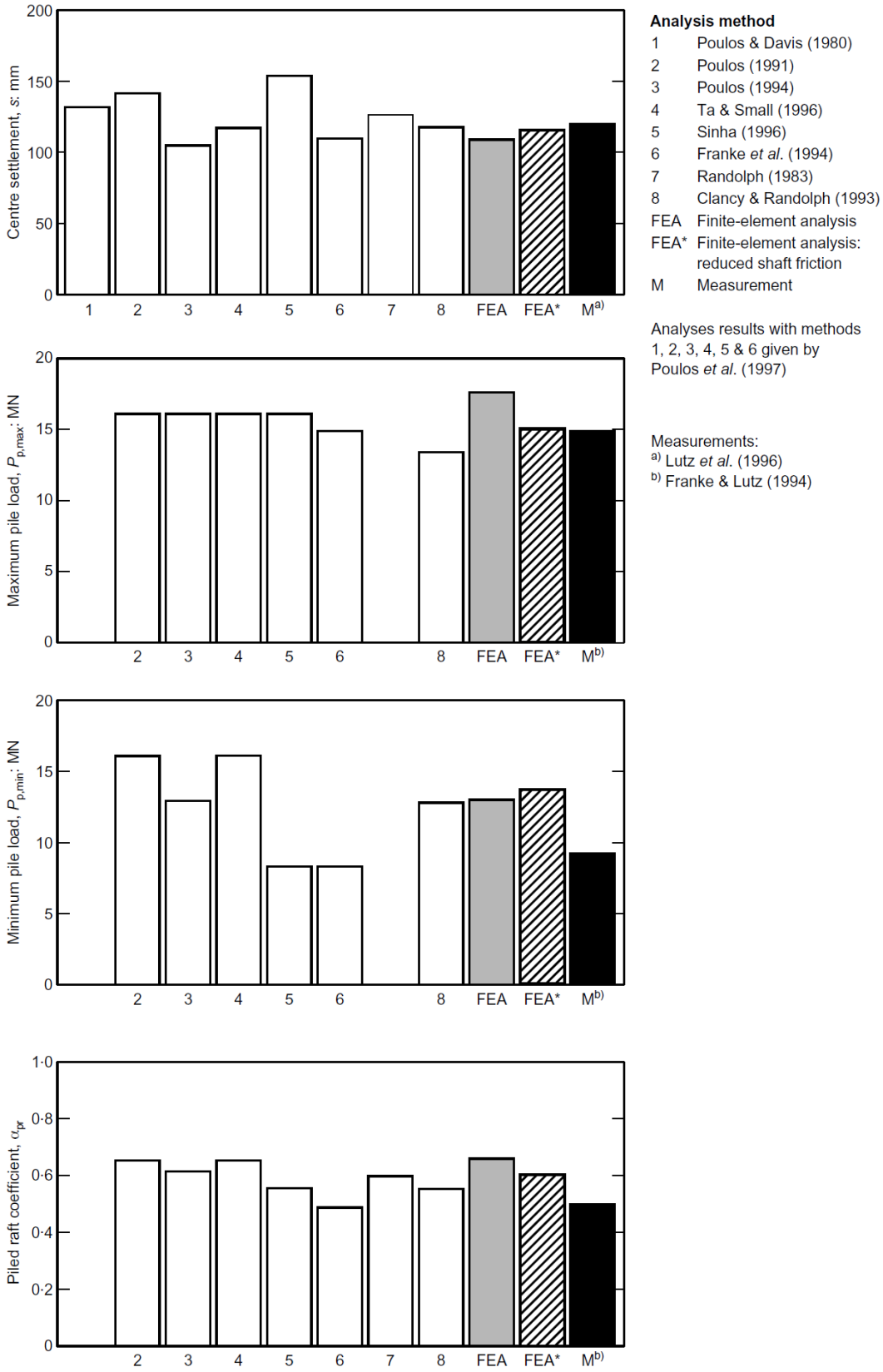


Figure 5-14 Comparison of different methods and measurements (*Reul* and *Randolph* (2003))

## 5.10 References


[1] *Abate, S.* (2009): Analysis and Parametric Study of Piled Raft Foundation Using Finite Element Based Software.
Msc thesis, Addis Ababa University.

[2] *Amann, P./ Breth, H./ Stroh, D.* (1975): Verformungsverhalten des Baugrundes beim Baugrubenaushub und anschließendem Hochhausbau am Beispiel des Frankfurter Ton Mitteilungen der Versuchsanstalt für Bodenmechanik und Grundbau der Technischen Hochschule Darmstadt, Heft 15.

[3] *Cecilia, B.* (2015): Serviceability and safety in the design of rigid inclusions and combined pile-raft foundations.
PhD thesis, Technical University Darmstadt.

[4] *Clancy, P. & Randolph, M.* (1993): An approximate analysis procedure for piled raft foundations.
Int. J. Numer. Anal. Methods Geomech. 17, 849–869.

[5] *Chaudhary, K.* (2010): Reconsiders for soil-structure interaction problems with significant material stiffness contrast.
PhD thesis, National University of Singapore.

[6] DIN 4014: Bohrpfähle Herstellung, Bemessung und Tragverhalten
Ausgabe März 1990

[7] *EA-Pfähle* (2007): Empfehlungen des Arbeitskreises "Pfähle" EA-Pfähle; Arbeitskreis Pfähle (AK 2,1) der Deutschen Gesellschaft für Geotechnik e.V., 1. Auflage, Ernst & Sohn, Berlin.

[8] *Franke, E., Lutz, B. & El-Mossallamy, Y.* (1994): Measurements and numerical modelling of high rise building foundations on Frankfurt Clay. Proceedings of a conference on vertical and horizontal deformations of foundations and embankments.
ASCE Geotechnical Special Publication No. 40, Vol. 2, pp. 1325–1336.

[9] *Franke, E., Lutz, B.* (1994): Pfahl-Platten-Gründungs-Messungen..
Report for the German Research Council (DFG) No. Fr60-1/11.

[10] *El Gendy, M./ Hanisch, J./ Kany, M.* (2006): Empirische nichtlineare Berechnung von Kombinierten Pfahl-Plattengründungen
Bautechnik 9/06

[11] *El Gendy, M.* (2007): Formulation of a composed coefficient technique for analyzing large piled raft.
Scientific Bulletin, Faculty of Engineering, Ain Shams University, Cairo, Egypt. Vol. 42, No. 1, March 2007, pp. 29-56

[12] *El Gendy, M./ El Gendy, A.* (2018): Analysis of raft and piled raft by Program *ELPLA*
GEOTEC Software Inc., Calgary AB, Canada.

[13] *Lutz, B. / Wittmann, P. / El Mossallamy, Y./ Katzenbach, R.* (1996): Die Anwendung von Pfahl-Plattengründungen: Entwurfspraxis, Dimensionierung und Erfahrungen mit Gründungen in überkonsolidierten Tonen auf der Grundlage von Messungen.
Vorträge der Baugrundtagung 1996 in Berlin, pp. 153–164. Essen: DGGT.

[14] *Poulos, H./ Davis, E.* (1980): Pile Foundation Analysis and Design
John Wiley & Sons, Inc.

[15] *Poulos, H.* (1991): Analysis of piled strip foundations.
Proceedings of the conference on computer methods and advances in geomechanics.
pp. 183–191, Rotterdam: Balkema.

[16] *Poulos, H.* (1994): An approximate numerical analysis of pile–raft interaction.
Int. J. Numer. Anal. Methods Geomech. 18, 73–92.

[17] *Poulos, H. G., Small, J. C., Ta, L. D., Sinha, J. & Chen, L.* (1997): Comparison of some methods for analysis of piled rafts..
Proc. 14th Int. Conf. Soil Mech. Found. Engng, Hamburg 2, 1119-1124.

[18] *Poulos, H.* (2001): Piled raft foundations: design and applications.
Géotechnique 51, No. 2, 95-113

[19] *Randolph, M.* (1983): Design of piled raft foundations.
Proceedings of the international symposium on recent developments in laboratory and field tests and analysis of geotechnical problems, Bangkok, pp. 525–537.

[20] *Reul, O./ Randolph, M.* (2003): Piled rafts in overconsolidated clay: comparison of in situ measurements and numerical analyses
Géotechnique 53, No. 3, 301-315

[21] *Russo, G.* (1998): Numerical analysis of piled raft
Int. J. Numer. Anal. Meth. Geomech., 22, 477-493

[22] *Small , J.* (2002): Soil-Structure interaction.
Australian Geomechanics Journal.

[23] *Sommer, H./ Katzenbach, R.* (1990): Last-Verformungsverhalten des Messeturmes Frankfurt/ Main
Vorträge der Baugrundtagung 1990 in Karlsruhe, Seite 371-380

[24] *Sinha, J.* (1996): Piled raft foundations subjected to swelling and shrinking soils.
PhD thesis, University of Sydney, Australia.

[25] *Ta, L./ Small, J.* (1996): Analysis of piled raft systems in layered soils.
Int. J. Numer. Anal. Methods Geomech. 20, 57–72.

**Case study 6**

# Piled raft of *Skyper* in Frankfurt

**Content**

Page

**6 Case study: *Skyper* piled raft ..... 3**

6.1 General ..... 3

6.2 Analysis of the piled raft ..... 5

6.3 FE-Net ..... 6

6.4 Loads ..... 6

6.5 Pile and raft material ..... 7

6.6 Soil properties ..... 7

6.7 Results ..... 10

6.8 Measurements and other results ..... 10

6.9 Evaluation ..... 10

6.10 References ..... 15

# 6 Case study: *Skyper* piled raft foundation

## 6.1 General

*Skyper* is 154 [m] high-rise building supported on a piled raft foundation. The tower was one of the tallest three skyscrapers in Frankfurt, Germany when it was completed in 2004, Figure 6-1.

The tower has a basement with three underground floors and 38 stories with an average estimated applied load of 426 [kN/m$^2$]. The raft of the *Skyper* tower has a uniform thickness of 3.5 [m] supported by 46 bored piles with a diameter 1.5 [m]. Piles are arranged under the core structure in 2 rings; external ring has 20 piles, 31 [m] long while the internal ring has 26 piles, 35 [m] in length. The raft has an irregular plan shape with an area of 1900 [m$^2$]. The raft founded on a typical Frankfurt clay at a depth 13.4 [m] below ground surface. The subsoil at the location of the building consists of gravels and sands up to 7.4 [m] below ground surface underlay by layers of Frankfurt clay extending to a depth of 56.4 [m] below ground surface followed by incompressible Frankfurt Limestone layer. The groundwater level is 5 [m] below ground surface.

Extensive studies using different calculation methods were carried out by *Saglam* (2003), *El-Mossallamy et al.* (2009), *Sales et al.* (2010), *Richter and Lutz* (2010), *Vrettos, C.* (2012), *Bohn* (2015) to evaluate the ***Skyper*** piled raft foundation design


Figure 6-1 *Skyper* [1]

[1] https://en.phorio.com/file/703520609/

Figure 6-2 shows a layout of the *Skyper* piled raft foundation.

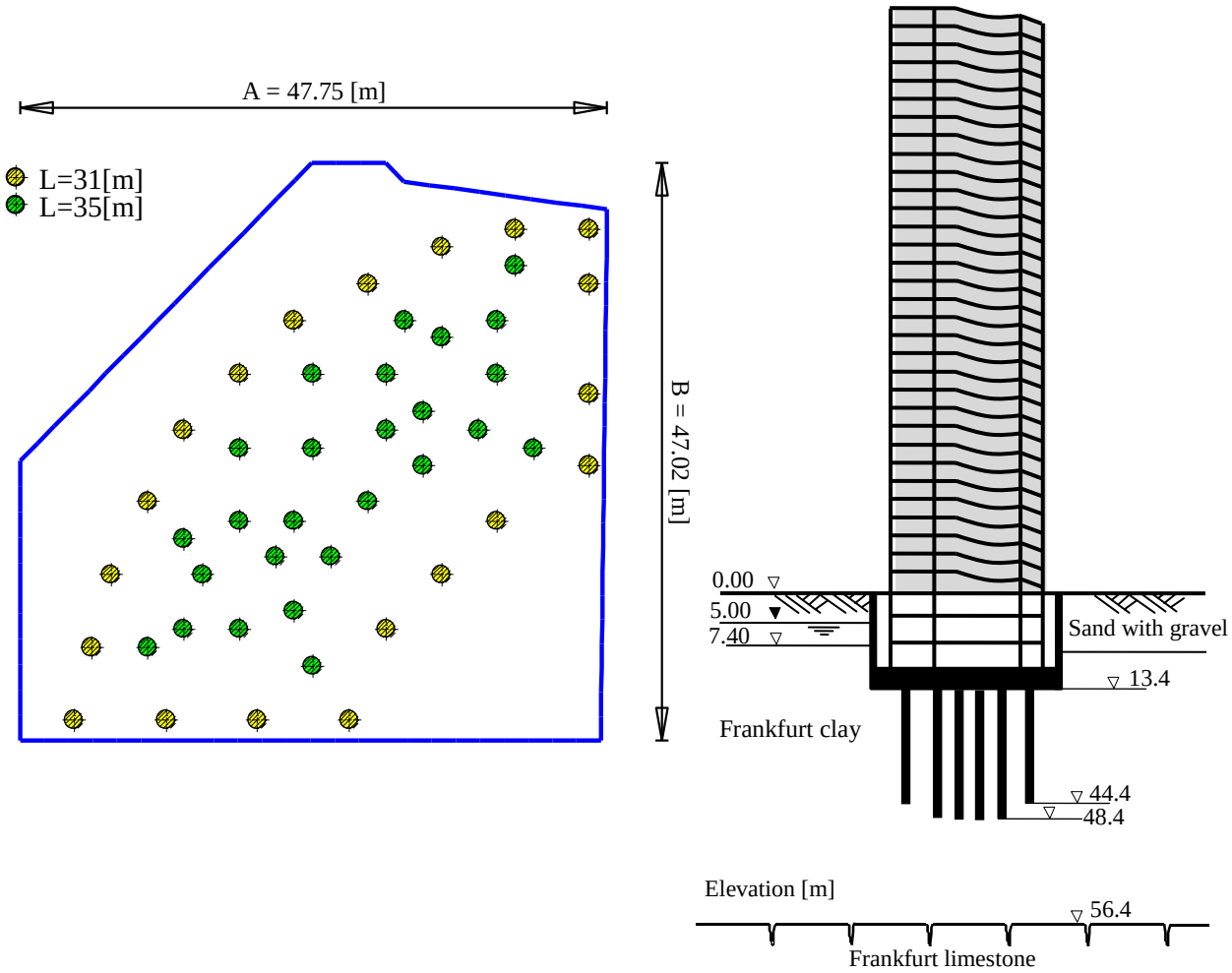


Figure 6-2 Layout of the *Skyper* piled raft foundation

## 6.2 Analysis of the piled raft

Using the available data and results of the *Skyper* piled raft, the nonlinear analyses of piled raft in *ELPLA* are evaluated and verified using the following load-settlement relations of piles, *El Gendy et al.* (2006) and *El Gendy* (2007):

1- Hyperbolic function.
2- German standard DIN 4014.
3- German recommendations EA-Piles (lower values).
4- German recommendations EA-Piles (upper values).

The foundation system is analyzed as rigid or elastic piled rafts. In which, the raft is considered as either rigid or elastic plate supported on rigid piles.

A series of comparisons are carried out to evaluate the nonlinear analyses of piled raft for load-settlement relations of piles. In which, results of other analytical solutions and measurements are compared with those obtained by *ELPLA*.

## 6.3 FE-Net

The raft is divided into triangular elements with maximum length of 2.0 [m] as shown in Figure 6-3. Similarly, piles are divided into elements with 2.0 [m] length.

## 6.4 Loads

The uplift pressure on the raft due to groundwater is $P_w$ = 160 [kN/m$^2$]. Consequently, the total effective applied load on the raft including own weight of the raft and piles is $N$ = 810 [MN].

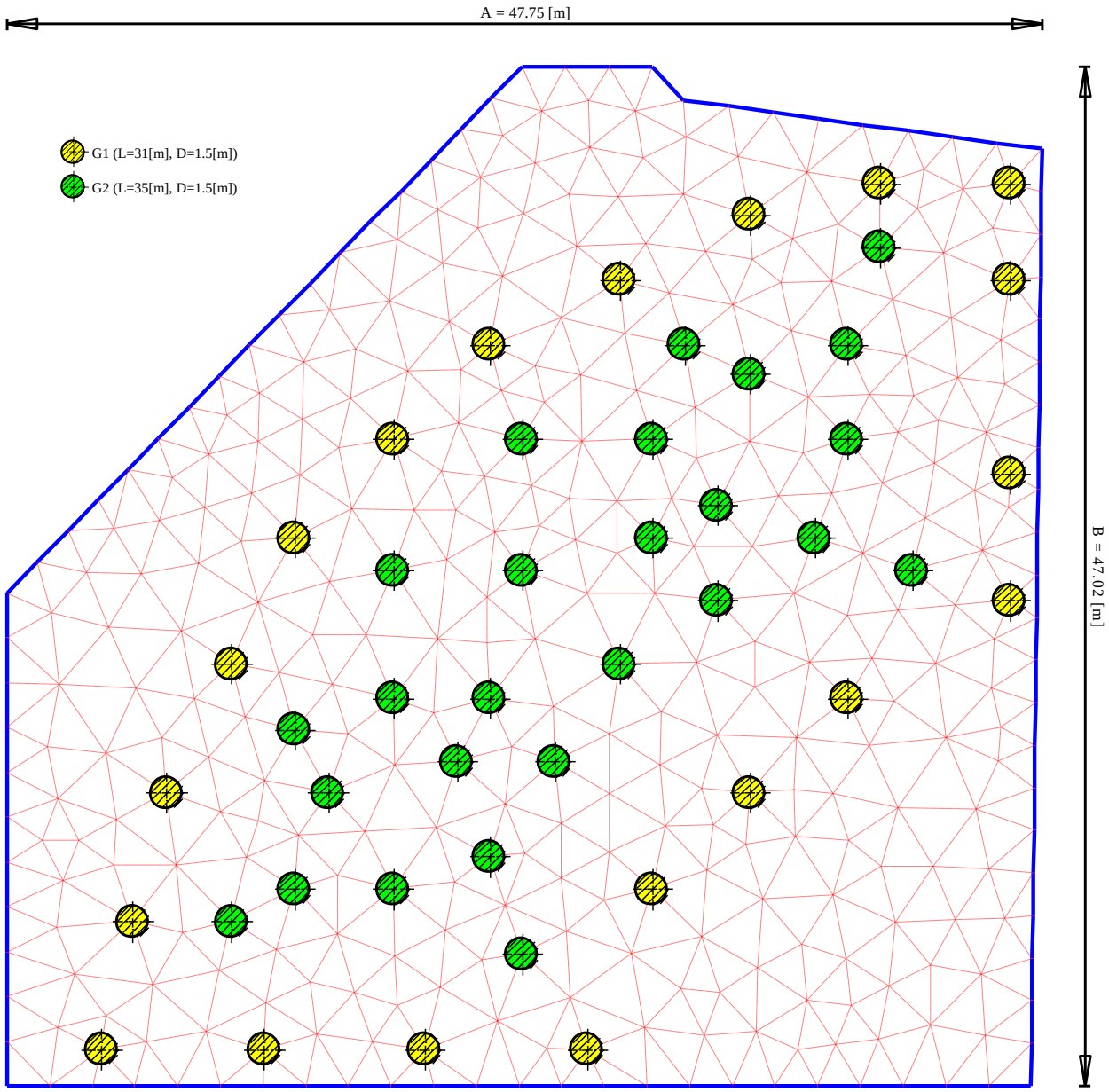


Figure 6-3 Mesh of *Skyper* piled raft with piles

## 6.5 Pile and raft material

The raft thickness is 3.5 [m]. The piles are 1.5 [m] in diameter and 31 [m] and 35 [m] in length. The following values were used for pile and raft material:

| | | | | |
|---|---|---|---|---|
| For the raft: | | | | |
| Modulus of elasticity | $E_p$ | = | 34 000 | [MN/m$^2$] |
| *Poisson's ratio* | $\nu_p$ | = | 0.25 | [-] |
| Unit weight | $\gamma_b$ | = | 0.0 | [kN/m$^3$] |
| For piles: | | | | |
| Modulus of elasticity | $E_p$ | = | 22 000 | [MN/m$^2$] |
| Unit weight | $\gamma_b$ | = | 0.0 | [kN/m$^3$] |

## 6.6 Soil properties

The clay properties used in analysis can be described as follows:

*Modulus of compressibility*
Based on the back analysis presented by *Amann et al.* (1975), the distribution of modulus of compressibility for loading of Frankfurt clay with depth is defined by the following empirical formula:

$$E_s = E_{so}(1 + 0.35\,z) \tag{3.1}$$

while that for reloading is:

$$W_s = 70\left[\mathrm{MN/m^2}\right] \tag{3.2}$$

where:
$E_s$ Modulus of compressibility for loading [MN/m$^2$]
$E_{so}$ Initial modulus of compressibility, $E_{so}$ = 7 [MN/m$^2$]
$z$ Depth measured from the clay surface, [m]
$W_s$ Modulus of compressibility for reloading [MN/m$^2$]

*Undrained cohesion $c_u$*
The undrained cohesion $c_u$ of Frankfurt clay increases with depth from $c_u$ = 100 [kN/m$^2$] to $c_u$ = 400 [kN/m$^2$] in 70 [m] depth under the clay surface according to *Sommer/ Katzenbach* (1990). To carry out the analyses using German standard and recommendations, an average undrained cohesion of $c_u$ = 200 [kN/m$^2$] is considered.

*Limit pile load Ql*
*Russo* (1998) suggested a limiting shaft friction not less than 180 [kN/m$^2$] meeting undrained shear strength of 200 [kN/m$^2$]. To carry out the analysis using a hyperbolic function, a limit shaft friction of $\tau$ = 180 [kN/m$^2$] is assumed. The limit pile load for pile group 1 is calculated from:

$$Q_{l1} = \tau * \pi * D * l = 180 * \pi * 1.5 * 31 = 26295\,[\mathrm{kN}] = 26\,[\mathrm{MN}] \tag{2.3}$$

while that for pile group 2 from:

$$Q_{l2} = \tau * \pi * D * l = 180 * \pi * 1.5 * 35 = 29688\,[\mathrm{kN}] = 30\,[\mathrm{MN}] \tag{2.4}$$

where:
$Q_l$ Limit pile load, [MN]
$\tau$ Limit shaft friction, $\tau = 180$ [kN/m$^2$]
$D$ Pile diameter, [m]
$l$ Pile length, [m]

*Poisson's ratio*
*Poisson's* ratio of gravels and sands is taken to be $\nu_s = 0.25$ [-].

To carry out the analysis, the subsoil under the raft is considered as indicated in the boring log of Figure 6-4 that consists of 7 soil layers. The total depth under the ground surface is taken to be 56.4 [m].

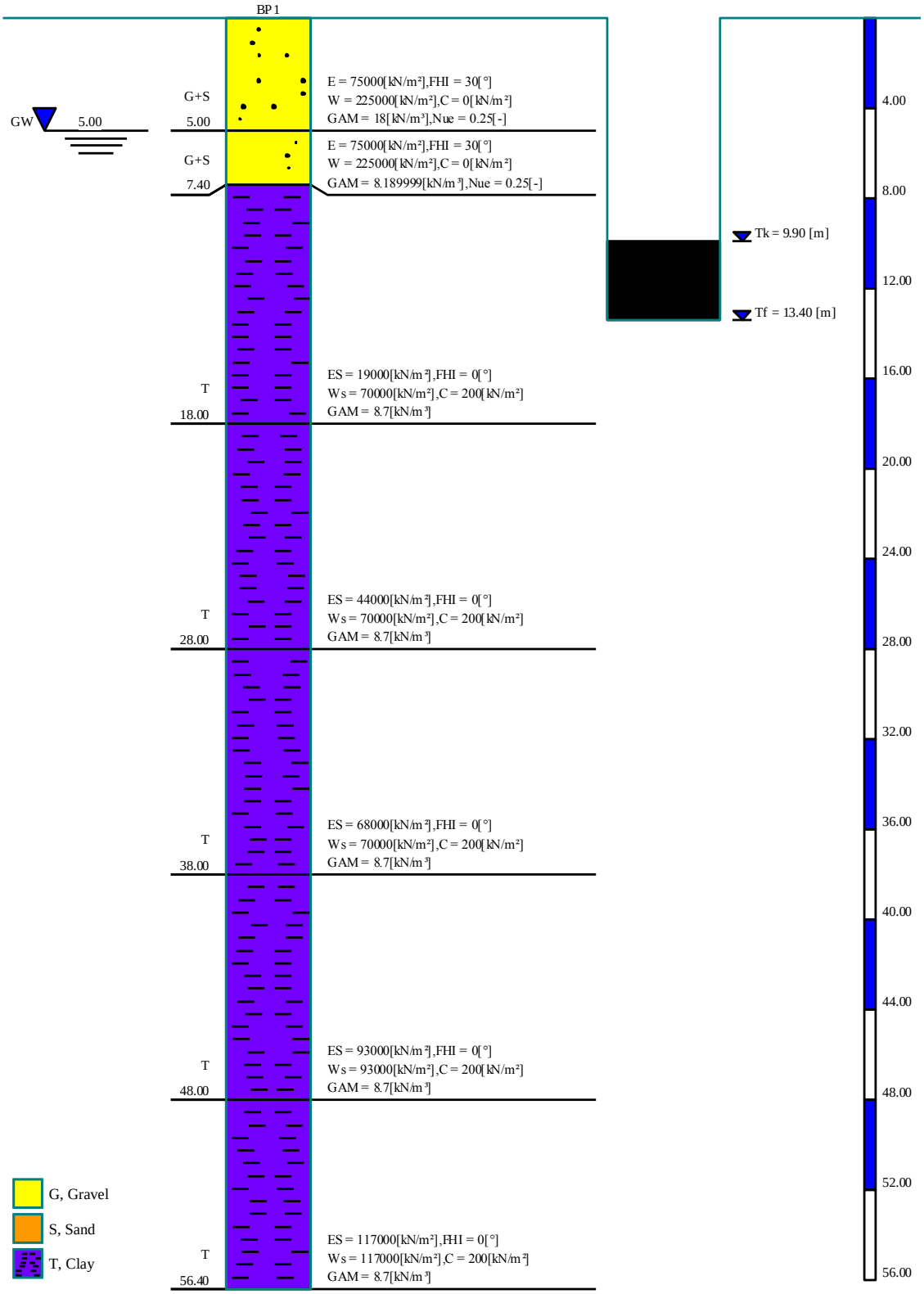


Figure 6-4 Boring log

## 6.7 Results

As examples for results of different analyses by *ELPLA*, Figure 6-5 and Figure 6-6 show the settlement, while Figure 6-7 and Figure 6-8 show the pile load for both rigid and elastic piled rafts using German recommendations EA-Piles for upper values.

## 6.8 Measurements and other results

The construction of *Skyper* started in 2003 and finished in the first half of 2004. According to *Richter and Lutz* (2010), all calculations resulted in a predicted settlement of 5 up to 7.5 [cm] for the tower, while according to *El-Mossallamy et al.* (2009) the bearing factor of piled raft $\alpha_{kpp}$ was computed in a range of 60% to 85%. The observed settlement was 5.5 [cm] directly after the completion of the shell only. After *Lutz et al.* (2006) with $\alpha_{kpp} \approx 0.6$, the average max. pile forces ranges between 12 to 14 [MN], while min. pile forces ranges between 10 to 11[MN].

Figure 6-9 compares results of settlement, bearing factor of piled raft and min and max pile loads obtained by *ELPLA* with the predicted results from the other methods. For more comparison, Table 6-1 shows the other results for another different methods presented by *Richter* and *Lutz* (2010). Based on settlement measurements 4 years after construction, the maximum settlement under the foundation is about 5 to 5.5 [cm]. Using the three-dimensional finite element method, a settlement of 6.3 [cm] was calculated according to *Richter and Lutz* (2010).

## 6.9 Evaluation

It can be concluded from Figure 6-9 that results obtained from different analyses available in *ELPLA* can present rapid and acceptable estimation for settlement, bearing factor of the piled raft and pile loads. This case study shows also that analyses available in *ELPLA* are practical for analyzing large piled raft problems. Because of they are taking less computational time compared with other complicated models using three dimension finite element analyses.

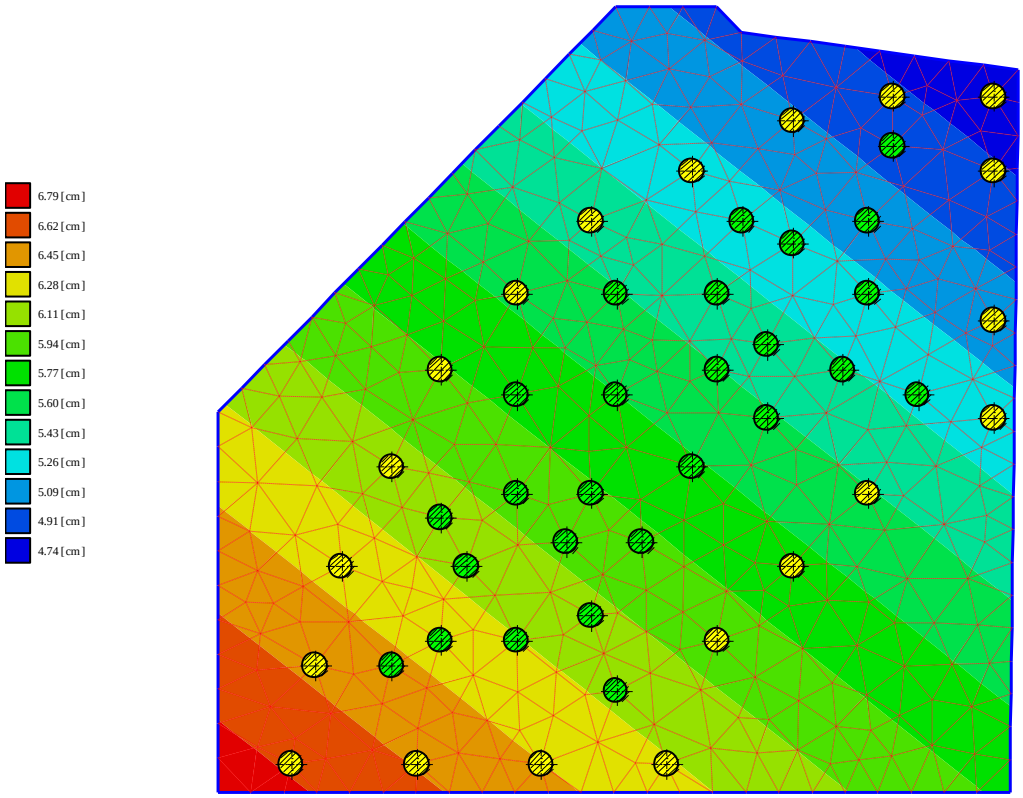


Figure 6-5 Settlement for rigid piled raft using German recommendations EA-Piles for upper values

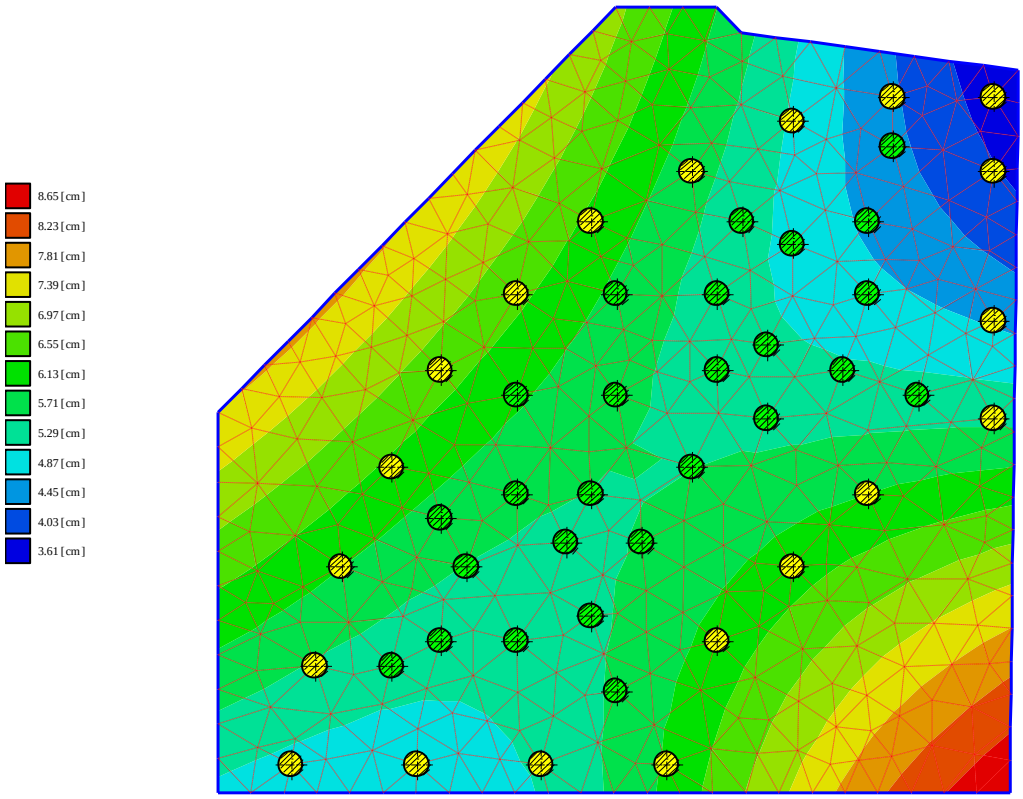


Figure 6-6 Settlement for elastic piled raft using German recommendations EA-Piles for upper values

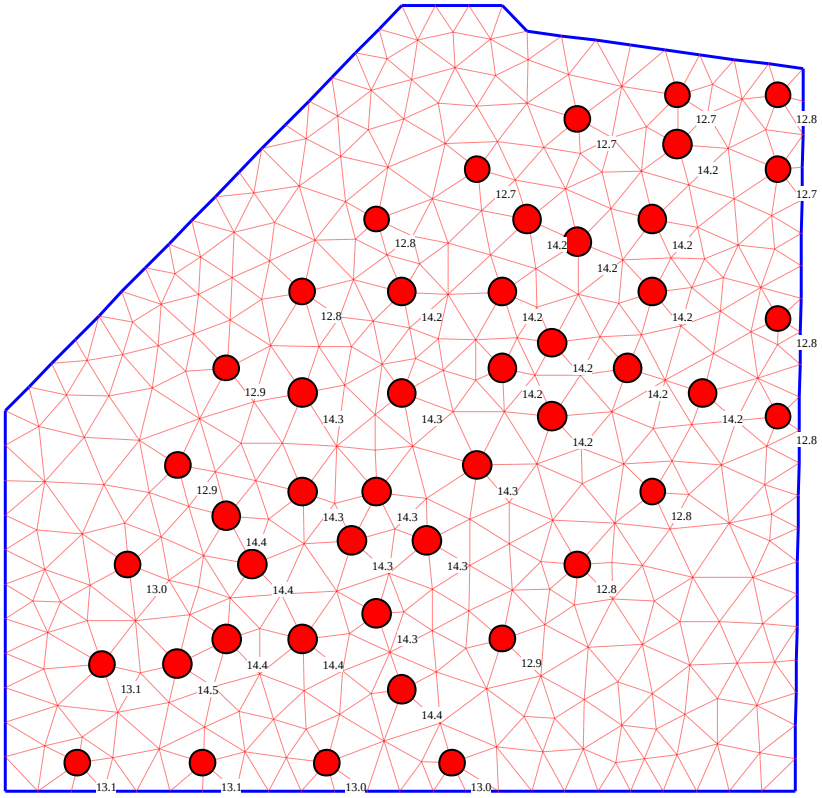


Figure 6-7 Pile load [MN] for rigid piled raft using German recommendations EA-Piles for upper values

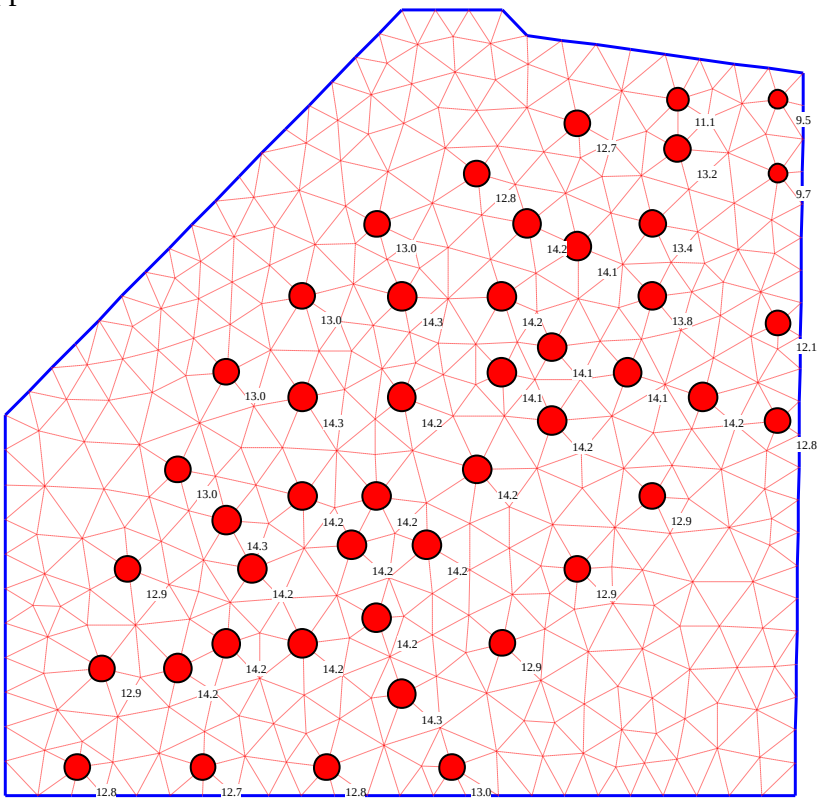


Figure 6-8 Pile load [MN] for elastic piled raft German recommendations EA-Piles for upper values

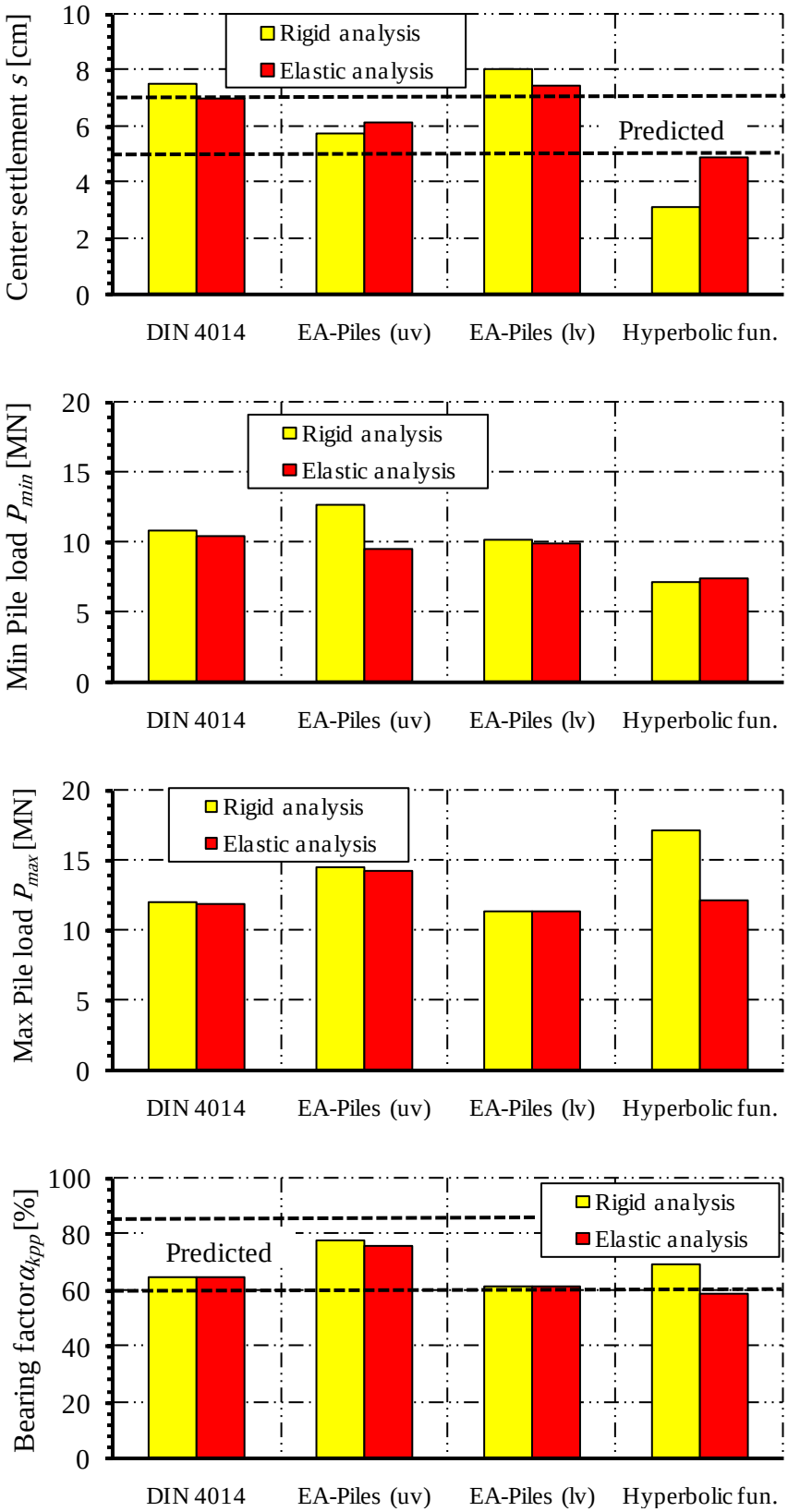


Figure 6-9 Results obtained from measurements and *ELPLA*

Table 6-1 Overview of calculation results of other models after *Richter* and *Lutz* (2010)

| Method | | | BEM | FEM | Elast. half space | Measured |
|---|---|---|---|---|---|---|
| Average settlement | $S_{kpp}$ | [cm] | 4.8 | 6.3 | 5.0-7.3 (9.5) | |
| Max. settlement | $S_{max}$ | [cm] | 6.0 | 7.5 | - | 5.5* |
| Bearing factor | $\alpha_{kpp}$ | [%] | 71 | 82 | 59-79 | |
| Modulus of subgrade | $k_s$ | [MN/m$^3$] | about 2.0 | | 1.6-2.8 | |
| Average pile load | $Q_p$ | [MN] | 12.5 | 14.3 | 10.3-13.9 | |
| Min. pile load | $Q_{p,min}$ | [MN] | 9.9 | 11.6 | 8.5-10.1 | |
| Max. pile load | $Q_{p,max}$ | [MN] | 16.1 | 17.6 | 13.8-20.5 | |
| Average pile stiffness | $k_p$ | [MN/m] | 261 | 301 | 125-280 | |

* Directly after the completion of the shell only

## 6.10 References


[1] *Amann, P./ Breth, H./ Stroh, D.* (1975): Verformungsverhalten des Baugrundes beim Baugrubenaushub und anschließendem Hochhausbau am Beispiel des Frankfurter Ton
Mitteilungen der Versuchsanstalt für Bodenmechanik und Grundbau der Technischen Hochschule Darmstadt, Heft 15

[2] *Bohn, C.* (2015): Serviceability and safety in the design of rigid inclusions and combined pile-raft foundations. PhD thesis, Technical University Darmstadt.

[3] DIN 4014: Bohrpfähle Herstellung, Bemessung und Tragverhalten
Ausgabe März 1990

[4] *EA-Pfähle* (2007): Empfehlungen des Arbeitskreises "Pfähle" EA-Pfähle; Arbeitskreis Pfähle (AK 2,1) der Deutschen Gesellschaft für Geotechnik e.V., 1. Auflage, Ernst & Sohn, Berlin.

[5] *El Gendy, M./ Hanisch, J./ Kany, M.* (2006): Empirische nichtlineare Berechnung von Kombinierten Pfahl-Plattengründungen
Bautechnik 9/06

[6] *El Gendy, M.* (2007): Formulation of a composed coefficient technique for analyzing large piled raft.
Scientific Bulletin, Faculty of Engineering, Ain Shams University, Cairo, Egypt. Vol. 42, No. 1, March 2007, pp. 29-56

[7] *El Gendy, M./ El Gendy, A.* (2018): Analysis of raft and piled raft by Program *ELPLA*
GEOTEC Software Inc., Calgary AB, Canada.

[8] *El-Mossallamy, Y., Lutz, B. and Duerrwang, R.* (2009): Special aspects related to the behavior of piled raft foundation. Proceedings of the 17th International Conference on Soil Mechanics and Geotechnical Engineering, M. Hamza et al. (Eds.).

[9] *Richter, T and Lutz, B.* (2010): Berechnung einer Kombinierten Pfahl-Plattengründung am Beispiel des Hochhauses „Skyper“ in Frankfurt/Main.
Bautechnik 87 (2010), Heft 4.

[10] *Russo, G.* (1998): Numerical analysis of piled raft
Int. J. Numer. Anal. Meth. Geomech., 22, 477-493

[11] *Sales, M., Small, J. and Poulos, H.* (2010): Compensated piled rafts in clayey soils: behaviour, measurements, and predictions.
Can Geotech. J. 47: 327-345.

[12] *Saglam, N.* (2003): Settlement of piled rafts: A critical review of the case histories and calculation methods.
M.Sc. thesis, The middle east technical university.

[13] *Sommer, H./ Katzenbach, R.* (1990): Last-Verformungsverhalten des Messeturmes Frankfurt/ Main
Vorträge der Baugrundtagung 1990 in Karlsruhe, Seite 371-380

[14] *Vrettos, C.* (2012): Simplified analysis of piled rafts with irregular geometry.
Int. Conf. Testing and Design Methods for Deep Foundations, Kanazawa.

**Case study 7**

# Analysis of Piled raft of *Burj Khalifa* in Dubai by the program *ELPLA*

*O. El Gendy*
*M. El Gendy*

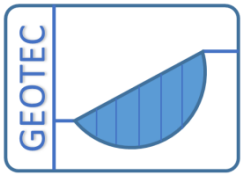



GEOTEC Software Inc.
PO Box 14001 Richmond Road PO, Calgary AB, Canada T3E 7Y7
Tele.:+1(587) 332-3323
geotec@geotecsoftware.com
www.geotecsoftware.com

**16-11-2018**

**Content**

Page

**7 Case study 7: *Burj Khalifa* piled raft ..... 3**

7.1 General ..... 3

7.2 Analysis of the piled raft ..... 5

7.3 FE-Net ..... 5

7.4 Loads ..... 5

7.5 Pile and raft material ..... 6

7.6 Soil properties ..... 7

7.7 Results ..... 11

7.8 Measurements and other results ..... 15

7.8.1 Measured settlement ..... 15

7.8.2 Calculated final settlement ..... 17

7.8.3 Calculated final pile loads ..... 19

7.9 Conclusion ..... 22

7.10 References ..... 22

# 7 Case study 7: *Burj Khalifa* piled raft

## 7.1 General

*Burj Khalifa* is a 163-storey skyscraper in Dubai, United Arab Emirates. The total height of the building is 829.8 [m], with a podium development at its base, including a 4 to 6-story garage. With a total height of 829.8 [m] and a roof height (excluding antenna) of 828 [m], *Burj Khalifa* has been the tallest structure and building in the world since its topping out in late 2008, Figure 7-1.

The *Burj Khalifa* is located on a 42 000 [$m^2$] site. The tower is founded on a 3.7 [m] thick raft supported on 192 bored piles, 1.5 [m] in diameter, extending 47.45 [m] below the base of the raft; podium structures are founded on a 0.65 [m] thick raft (increased to 1 [m] at column locations) supported on 750 bored piles, 0.9 [m] in diameter, extending 30–35 [m] below the base of the raft. The tower raft consists of three wings each is 50 [m] long and 25 [m] wide forming an area of 3305 [$m^2$]. Figure 7-2 shows an isometric view of *Burj Khalifa* Tower foundation system and a plan for pile locations.

Extensive studies using different calculation methods were carried out by *Poulos* and *Bunce* (2008), *Badelow & Poulos* (2016) and *Russo etc. al.* (2013).

Figure 7-1 Burj Khalifa [1]

[1] https:// tadalafilforsale.net/group/burj-khalifa-images/#photo_27

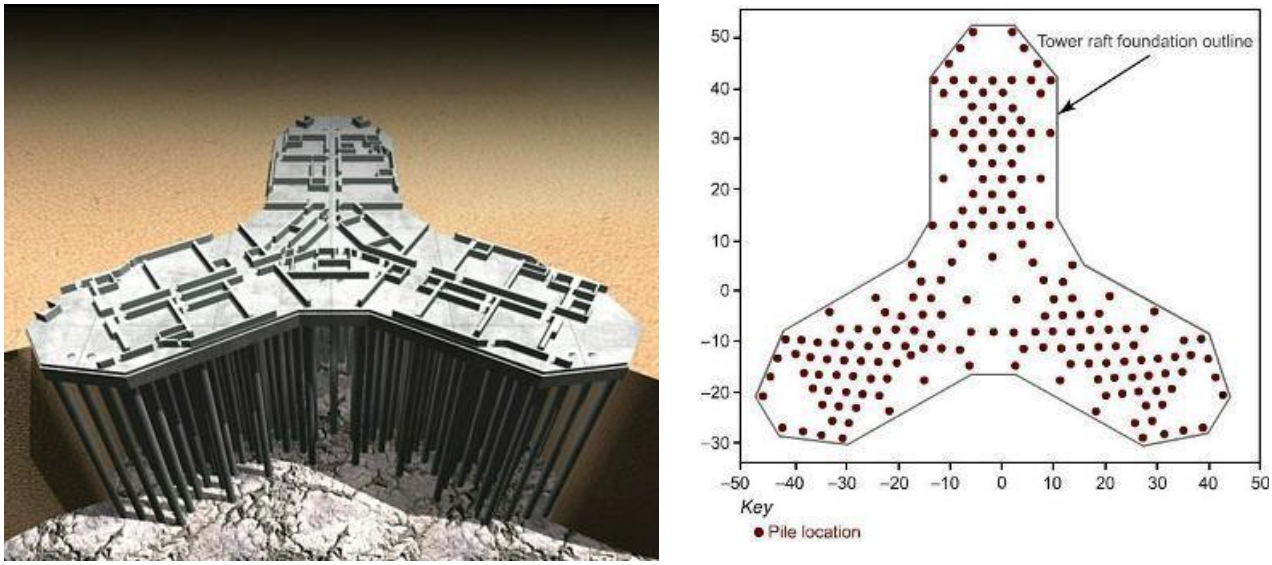


Figure 7-2 *Burj Khalifa* Tower Foundation system

## 7.2 Analysis of the piled raft

Using the available data and results of the *Burj Khalifa* piled raft, which have been discussed in detail in the previous references, the nonlinear analyses of piled raft in *ELPLA* are evaluated and verified using the following load-settlement relations of piles, *El Gendy et al.* (2006) and *El Gendy* (2007):

1- Hyperbolic Function for Load-Settlement Curve.
2- Given Load-Settlement Curve.

The foundation system is analyzed as an elastic piled raft in which the raft is considered as an elastic plate supported on equal rigid piles.

A series of comparisons are carried out to evaluate the nonlinear analyses of piled raft for load-settlement relations of piles. In which, results of other analytical solutions and measurements are compared with those obtained by *ELPLA*.

## 7.3 FE-Net

The raft is divided into triangular elements with a maximum length of 2.0 [m] as shown in Figure 7-3. Piles are divided into five elements with 9.49 [m] length.

## 7.4 Loads

Only long-term conditions have been considered, and for most of the early analyses, an average load per pile of 23.21 [MN] has been used (this is a representative of the design dead and live loads) and has been applied as an uniformly distributed load on the tower raft of about 1250 [kPa].

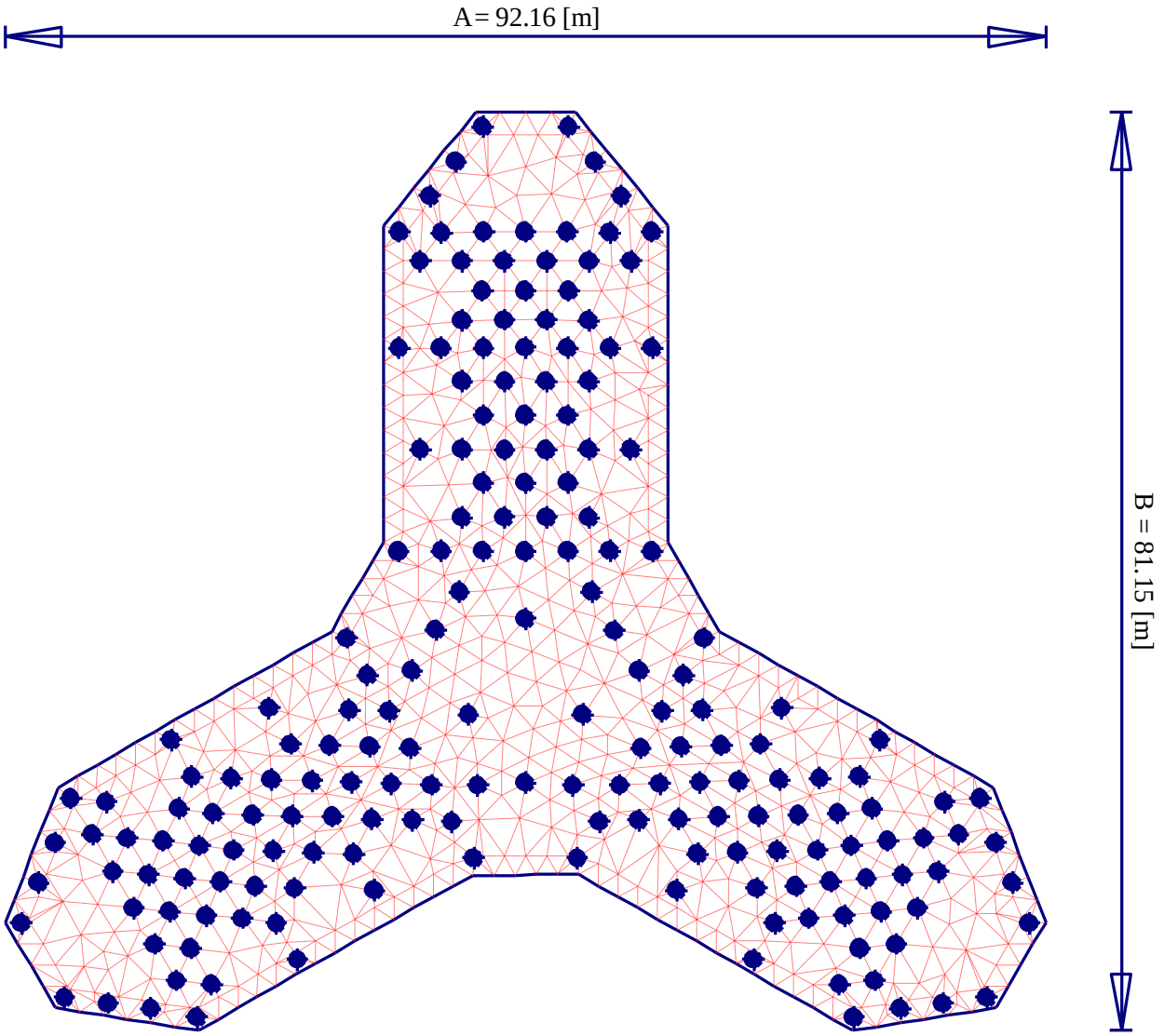


Figure 7-3 Mesh of *Burj Khalifa* piled raft with piles of element length = 2.0 [m]

## 7.5 Pile and raft material

The raft is 3.7 [m] thick and was poured utilizing C50 (cube strength) self-consolidating concrete. The Tower raft is supported by 192 bored cast-in-place piles. The C60 self-consolidating concrete piles are 1.5 [m] in diameter and 47.45 [m] long.
The following values were used as pile and raft material:

| | | | | |
|---|---|---|---|---|
| For the raft: | | | | |
| Modulus of elasticity | $E_p$ | = | 33234 | [MN/m$^2$] |
| *Poisson's ratio* | $\nu_p$ | = | 0.167 | [-] |
| Unit weight | $\gamma_b$ | = | 23.60 | [kN/m$^3$] |
| | | | | |
| For piles: | | | | |
| Modulus of elasticity | $E_p$ | = | 36406 | [MN/m$^2$] |
| Unit weight | $\gamma_b$ | = | 23.60 | [kN/m$^3$] |

## 7.6 Soil properties

The ground conditions comprise a horizontally stratified subsurface profile which is complex and highly variable, due to the nature of deposition and the prevalent hot arid climatic conditions. Medium dense to very loose granular silty sands (Marine Deposits) are underlain by successions of very weak to weak sandstone interbedded with very weakly cemented sand, gypsiferous fine grained sandstone/siltstone and weak to moderately weak conglomerate/calcisiltite.

Groundwater levels are generally high across the site and excavations were likely to encounter groundwater at approximately 2.5 [m] below ground level.

The drilling was carried out using cable percussion techniques with follow-on rotary drilling methods to depths between 30 [m] and 140 [m] below ground level.

The ground profile and derived geotechnical design parameters assessed from the investigation data are summarized in Table 7-1.

Table 7-1 Summary of Geotechnical Profile and Parameters

| Strata | Sub-Strata | Subsurface Material | Level at top of stratum [m DMD] | Thickness $H$ [m] | UCS $q_s$ [MPa] | Undrained Modulus $E_u$ [MPa] | Ult. Comp. Shaft Frict. $f_s$ [kPa] |
|---|---|---|---|---|---|---|---|
| 1 | 1a | Medium dense silty Sand | +2.50 | 1.50 | - | 34.5 | - |
| | 1b | Loose to very loose silty Sand | +1.00 | 2.20 | - | 11.5 | - |
| 2 | 2 | Very weak to moderately weak Calcarenite | -1.20 | 6.10 | 2.0 | 500 | 350 |
| 3 | 3a | Medium dense to very dense Sand/ Silt with frequent sandstone bands | -7.30 | 6.20 | - | 50 | 250 |
| | 3b | Very weak to weak Calcareous Sandstone | -13.50 | 7.50 | 1.0 | 250 | 250 |
| | 3c | Very weak to weak Calcareous Sandstone | -21.00 | 3.00 | 1.0 | 140 | 250 |
| 4 | 4 | Very weak to weak gypsiferous Sandstone/ calcareous Sandstone | -24.00 | 4.50 | 2.0 | 140 | 250 |
| 5 | 5a | Very weak to moderately weak Calcisiltite/ Conglomeritic Calcisiltite | -28.50 | 21.50 | 1.30 | 310 | 285 |
| | 5b | Very weak to moderately weak Calcisiltite/ Conglomeritic Calcisiltite | -50.00 | 18.50 | 1.70 | 405 | 325 |
| 6 | 6 | Very weak to weak Calcareous/ Conglomerate strata | -68.50 | 22.50 | 2.50 | 560 | 400 |
| 7 | 7 | Weak to moderately weak Claystone/ Siltstone | -91.00 | >46.79 | 1.70 | 405 | 325 |

To carry out the analysis, the subsoil under the raft is considered as indicated in the boring log of Figure 7-4 that consists of 12 soil layers. The total depth under the ground surface is taken to be 140 [m].

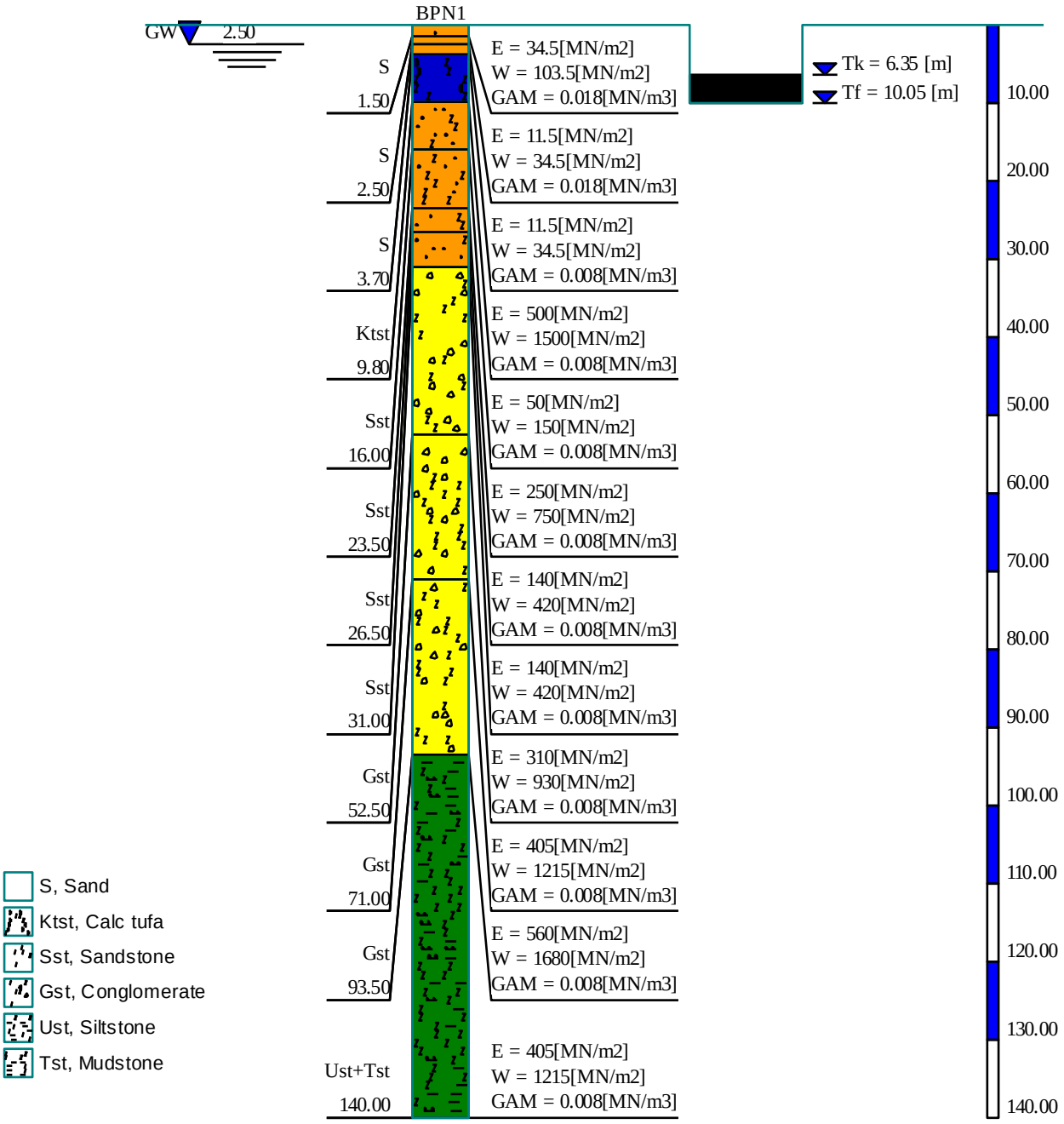


Figure 7-4 Boring log

Figure 7-5 to Figure 7-6 show load-settlement relations for the different analyses.

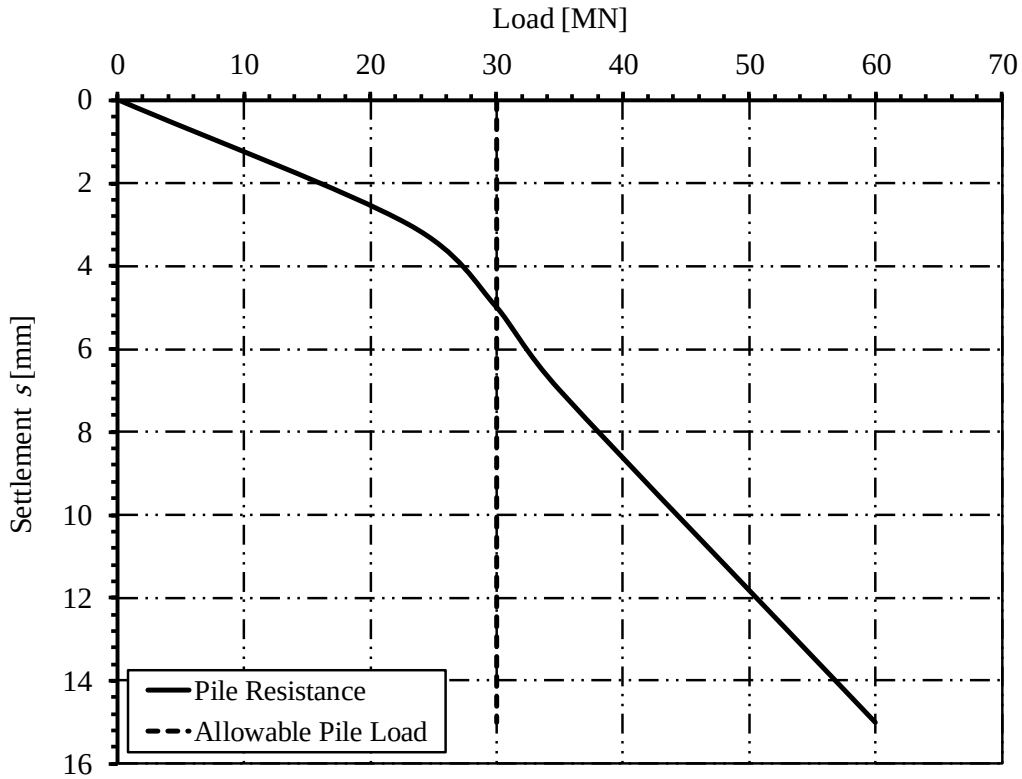


Figure 7-5 Load-settlement relation from pile load test

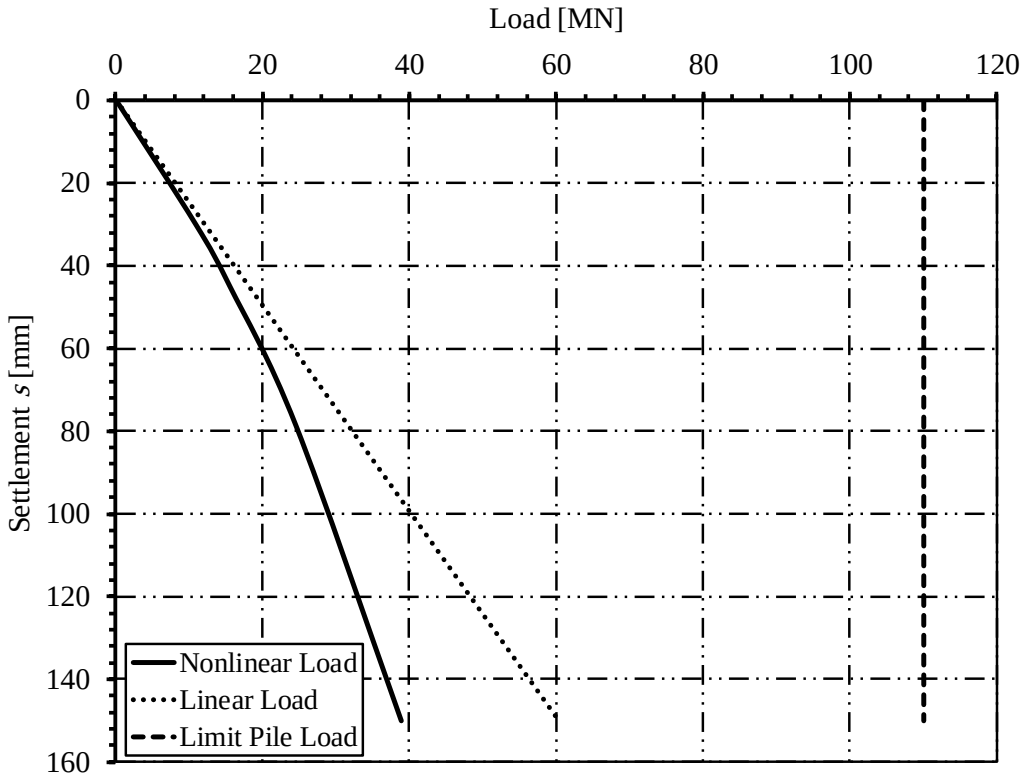


Figure 7-6 Load-settlement relation according to a hyperbolic function

## 7.7 Results

As examples for results of different analyses by *ELPLA*, Figure 7-8 and Figure 7-7 show the settlement for elastic piled raft of *Burj Khalifa* using methods: "Hyperbolic Function for Load-Settlement Curve" and "Given Load-Settlement Curve from pile-load test", respectively. Besides, Figure 7-9, Figure 7-10 and Figure 7-11 show self-settlement $S_v$, interaction settlement $S_{rv}$ and total settlement $S_r$ of piles using the method "Given Load-Settlement Curve from pile-load test".

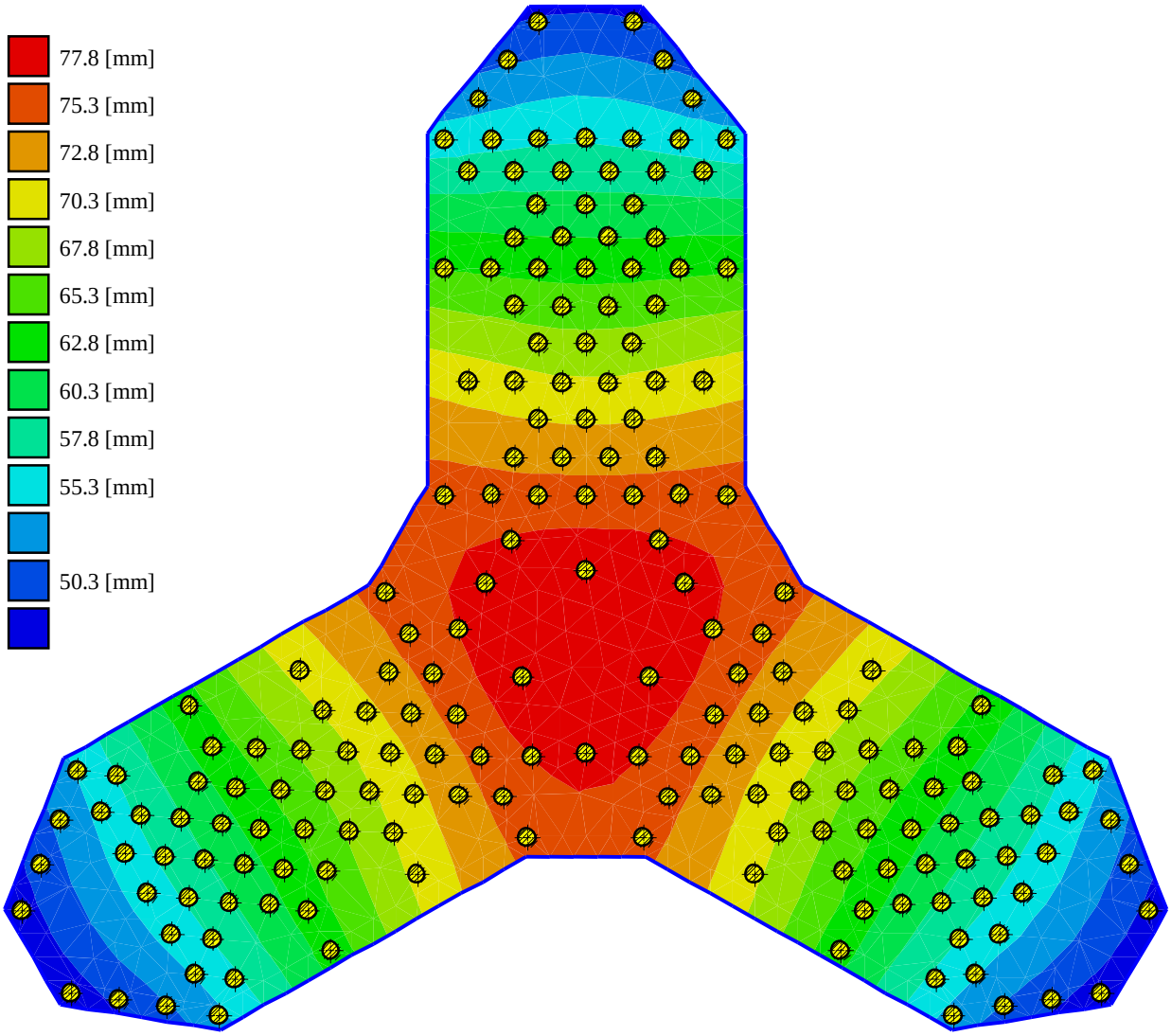


Figure 7-7 Settlement using the method "Hyperbolic Function for Load-Settlement Curve"

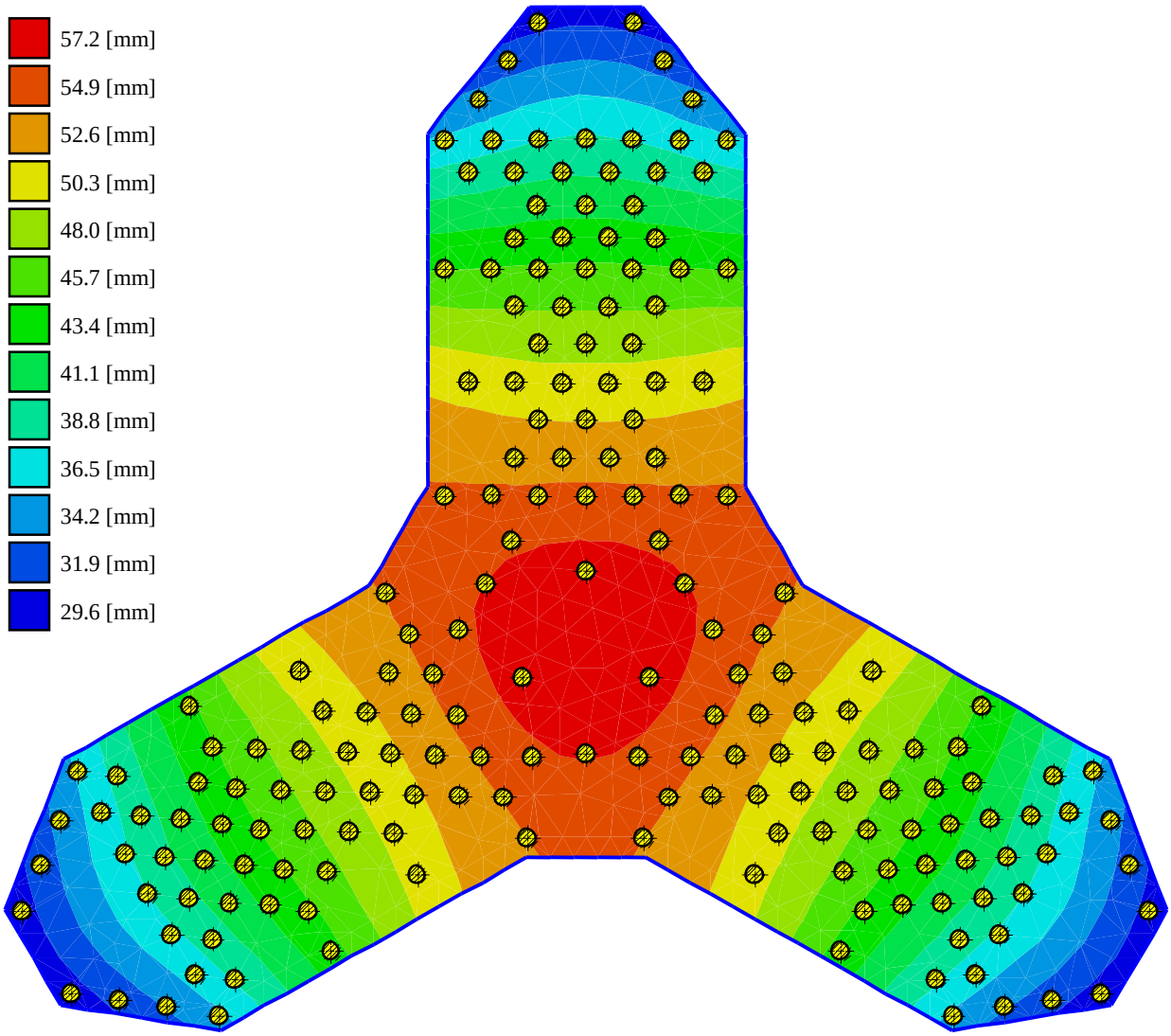


Figure 7-8 Settlement using the method "Given Load-Settlement Curve"

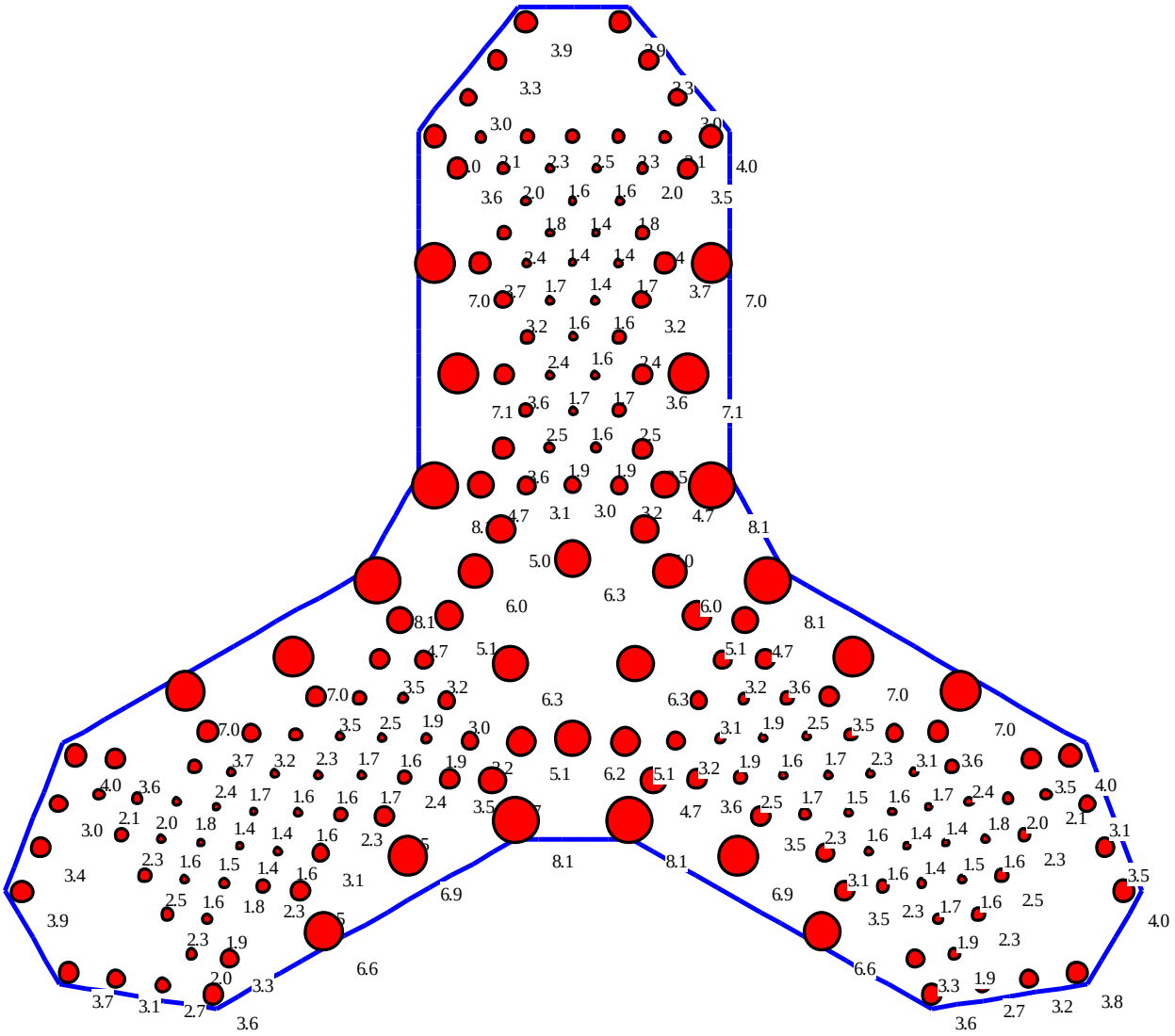

Figure 7-9 Self settlement of piles $S_v$ [mm] using the method "Given Load-Settlement Curve"

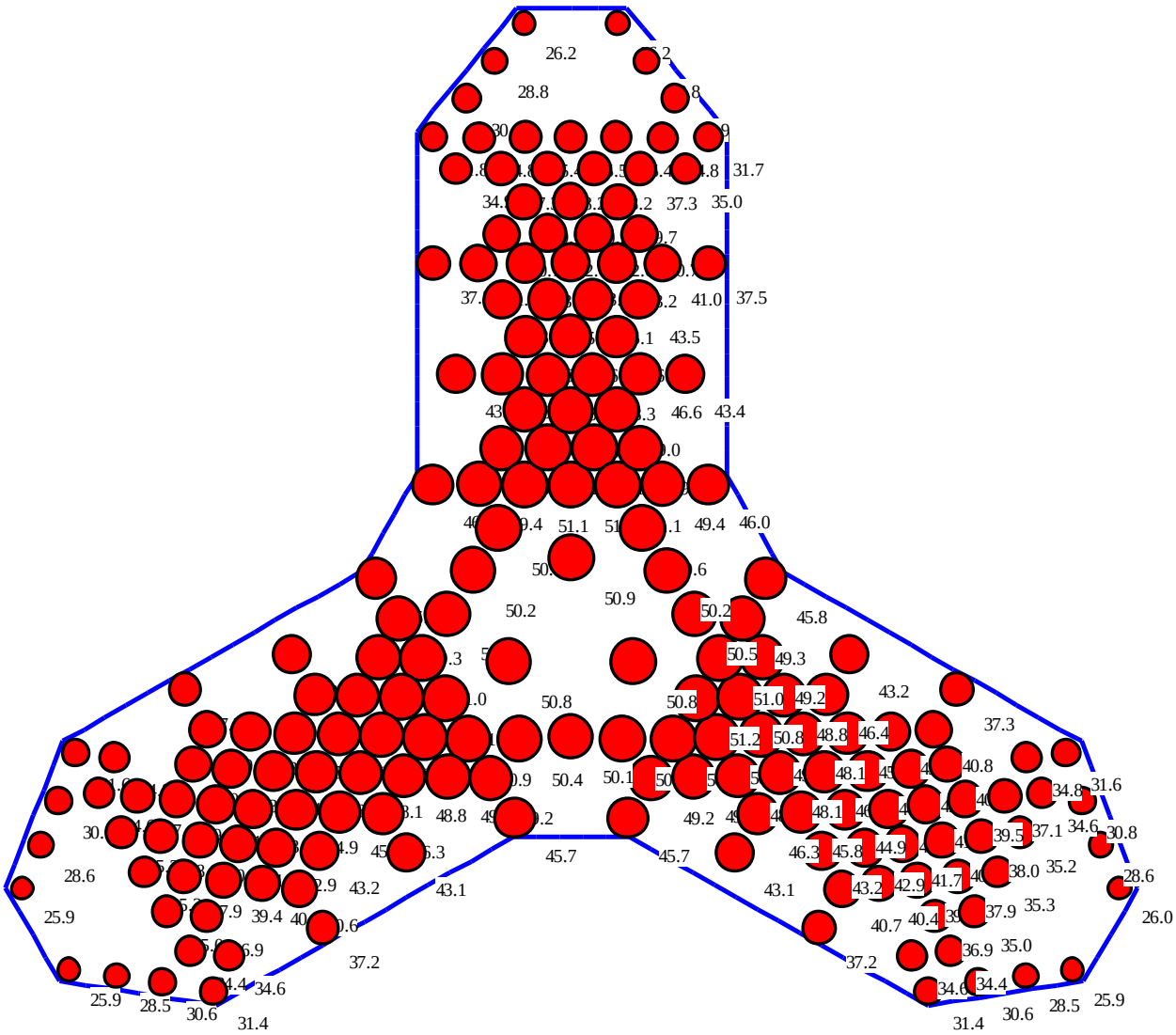


Figure 7-10 Interaction settlement of piles $S_{rv}$ [mm] using the method "Given Load-Settlement Curve"

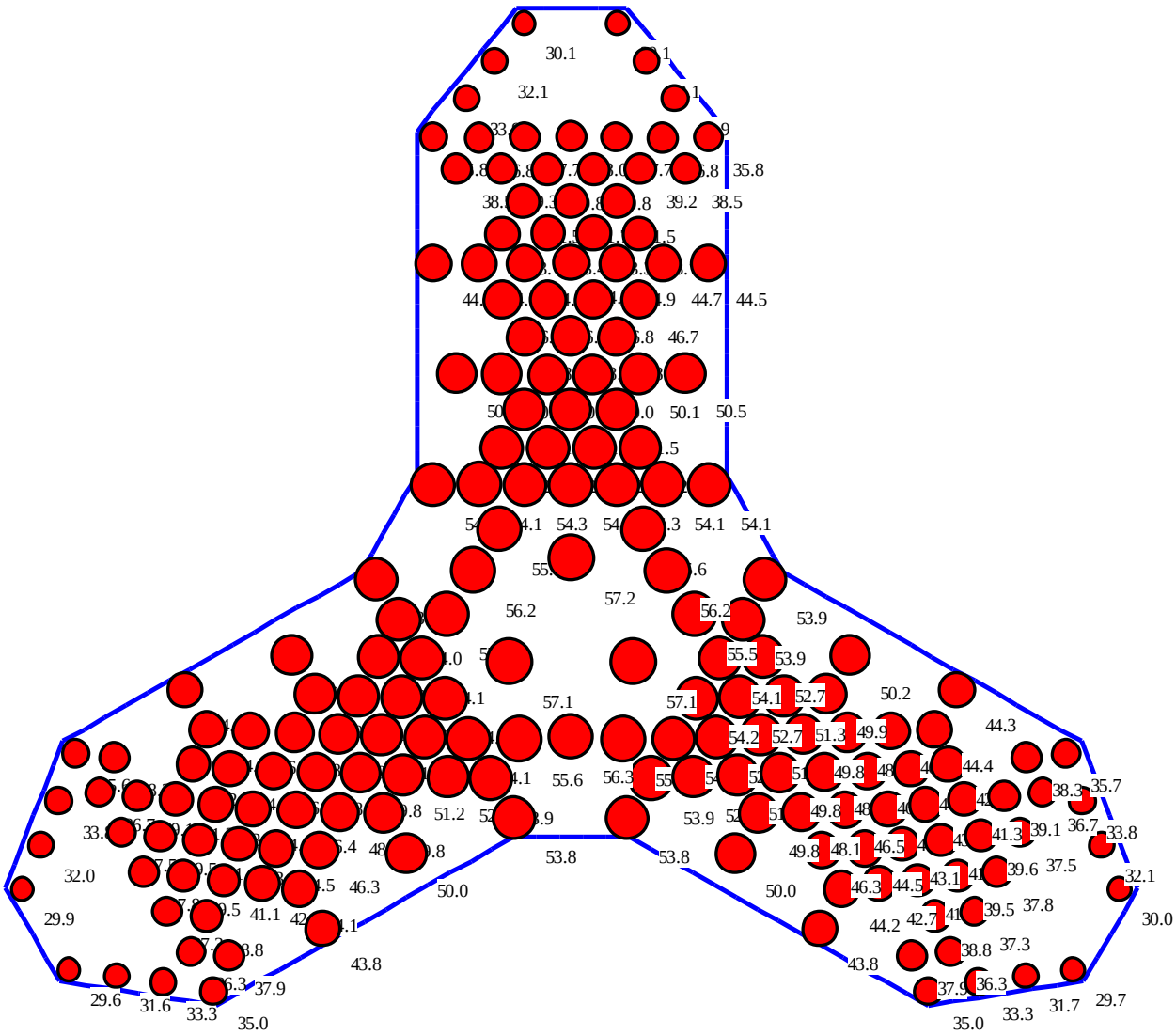


Figure 7-11 Total settlement of piles $S_r$ [mm] using the method "Given Load-Settlement Curve"

## 7.8 Measurements and other results

### 7.8.1 Measured settlement

The construction of *Burj Khalifa* began on 6 January 2004, with the exterior of the structure completed on 1 October 2009. According to *Badelow & Poulos* (2016) the settlement of the tower raft was monitored from completion of concreting till 18 February 2008. The recorded maximum settlement at 18 February 2008 was 43 [mm] under nearly 80 % of the building load.

A comparison is presented between the measured settlement on 18 February 2008 under 80% of the total load and that computed by *ELPLA* using Method: "Given Load-Settlement Curve". Figure 7-12 shows a comparison between measured settlement (Feb. 2008) and computed settlement under 80 % of the total load at a cross section of the Wing c, while 0 shows a comparison between extreme values of measured settlement and that calculated for the same case.

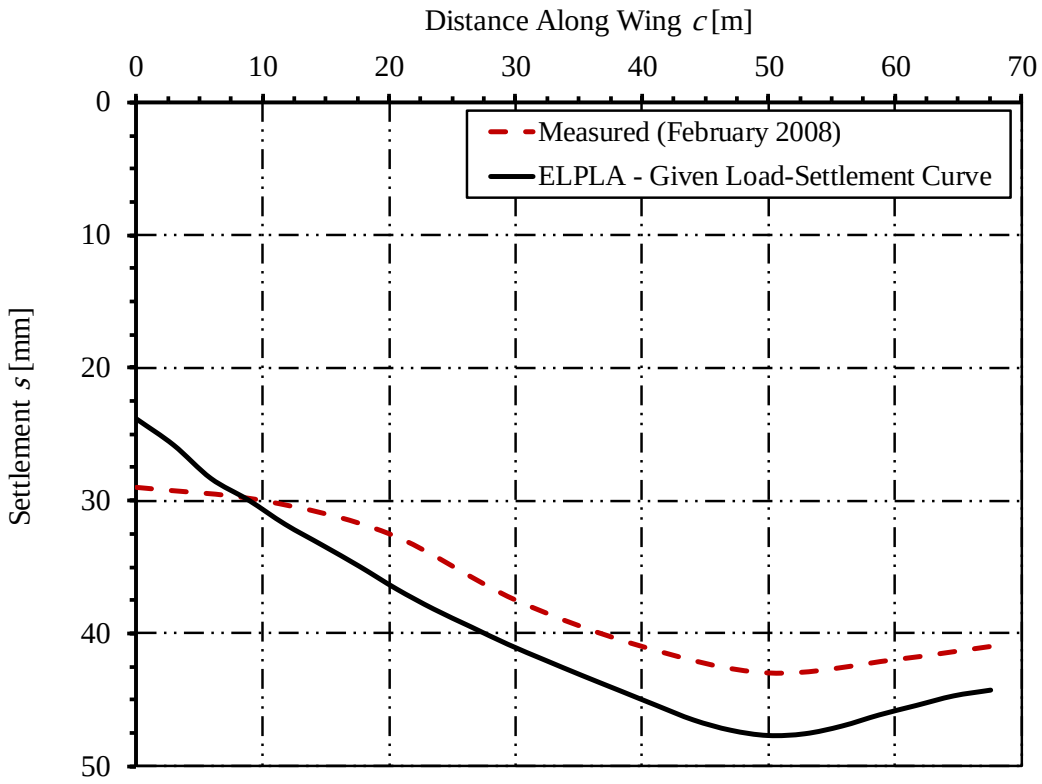


Figure 7-12 Measured settlement (Feb. 2008) and computed settlement under 80 % of total load

Table 7-2 Comparison between measured settlement at February 2008 and that calculated by *ELPLA* under 80 % of the total load

| Method | $S_{max.}$ [mm] | $S_{min.}$ [mm] | $S_{Diff.}$ [mm] |
|---|---|---|---|
| Measured (18 February 2008) | 43 | 29 | 14 |
| *ELPLA* – Method: "Given Load-Settlement Curve" | 48 | 24 | 24 |

Figure 7-13 shows contours of measured settlement [mm] at February 2008 and that calculated by *ELPLA* under 80 % of the total load using method "Given Load-Settlement Curve"

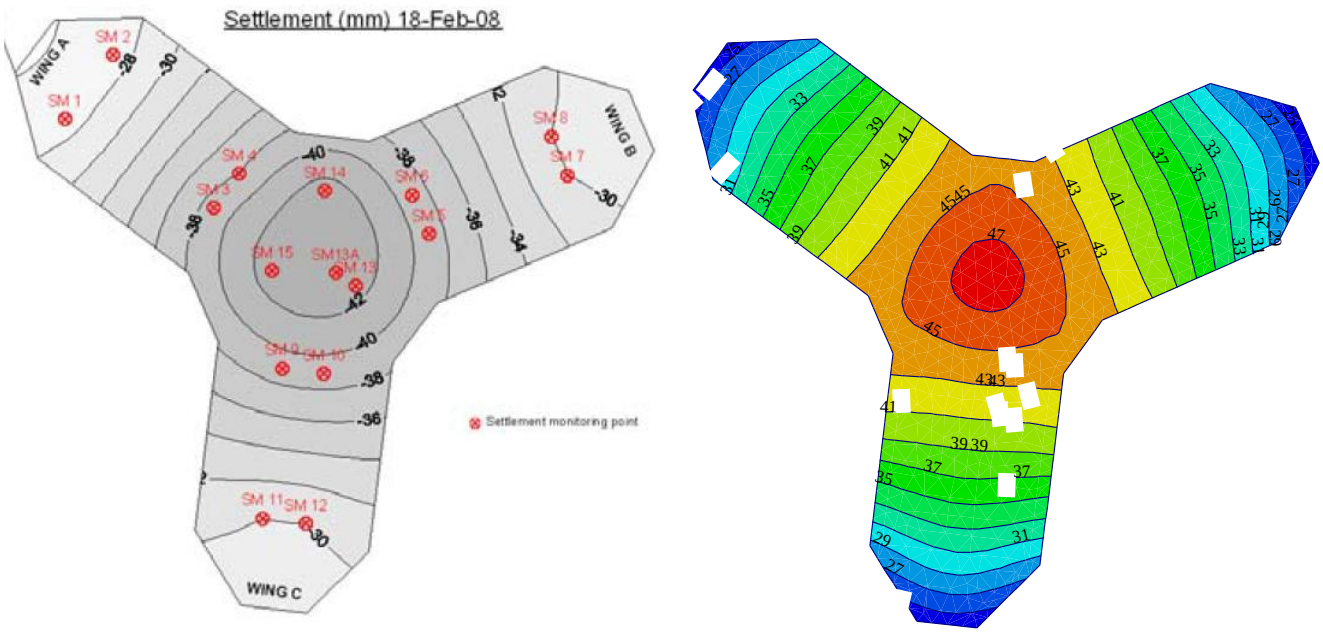


Figure 7-13 Contours of measured settlement [mm] at February 2008 and that calculated by *ELPLA* under 80 % of the total load using method "Given Load-Settlement Curve"

The above comparison of the piled raft under 80 % of the total load illustrates that the maximum and minimum results of *ELPLA* are in good agreement with the measured settlement with difference not exceed 1 [cm]. The measured differential settlement is considerably smaller than that computed because the building stiffness is not considered in *ELPLA* analysis in this case, which would reduce the differential settlement.

### 7.8.2 Calculated final settlement

Several analyses were used to assess the response of the foundation for the *Burj Khalifa* Tower and Podium. The main design model was developed using a Finite Element (*FE*) program *ABAQUS* run by a specialist company *KW Ltd*, based in the UK. Other models were developed to validate and correlate the results from the *ABAQUS* model using other software programs. The design values of settlement were presented by *Poulos* and *Bunce* (2008).

*Russo etc. al.* (2013) deals with the re-assessment of foundation settlements for the *Burj Khalifa* Tower in Dubai. Re-assessment was carried out using the computer program Non-linear Analysis of Piled Rafts *NAPRA* with neglecting the structure stiffness effect on raft settlement.

A comparison is presented between the computed settlement in other references and the computed settlement by *ELPLA* using different Nonlinear analysis methods. The comparison is presented as a cross section at Wing c and tables as in Figure 7-14 and Table 7-3, respectively.

The comparison shows that the results of two methods in *ELPLA* are in good agreement with the calculated results of *Russo etc. al.* (2013). The second method (Load-Settlement relation as a Hyperbolic Function for Load-Settlement Curve) results are closer to the design results presented by *Poulos* and *Bunce* (2008).

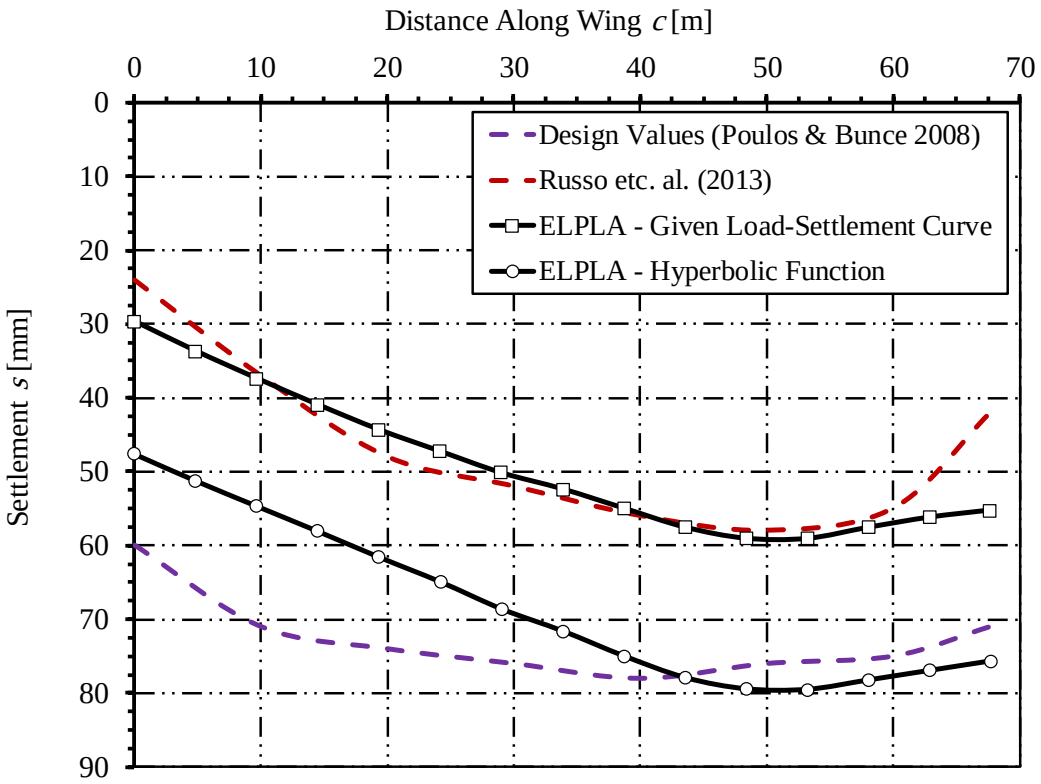


Figure 7-14 Final settlement for elastic piled raft using different analysis models

Table 7-3 Comparison between various calculated settlement profiles

| Method | $S_{max.}$ [mm] | $S_{min.}$ [mm] | $S_{Diff.}$ [mm] |
|---|---|---|---|
| Design Values (*Poulos* and *Bunce* 2008) | 78 | 60 | 18 |
| *Russo* etc. al. (2013) | 58 | 24 | 34 |
| *ELPLA* – Given Load-Settlement Curve | 58 | 29 | 29 |
| *ELPLA* – Hyperbolic Function for Load-Settlement Curve | 79 | 47 | 32 |

### 7.8.3 Calculated final pile loads

The maximum and minimum pile loads were obtained from the three-dimensional finite element analysis for all loading combinations by *Poulos* and *Bunce* (2008). The maximum loads were at the corners of the three “wings” and were of the order of 35 [MN], while the minimum loads were within the center of the group and were of the order of 12-13 [MN].

Figure 7-15 and Figure 7-16 show pile loads obtained by *ELPLA* using method: "Hyperbolic Function for Load-Settlement Curve" and method "Given Load-Settlement Curve from pile-load test", while Table 7-4 compares results of max and min pile loads obtained by *ELPLA* with those of *Poulos* and *Bunce* (2008).

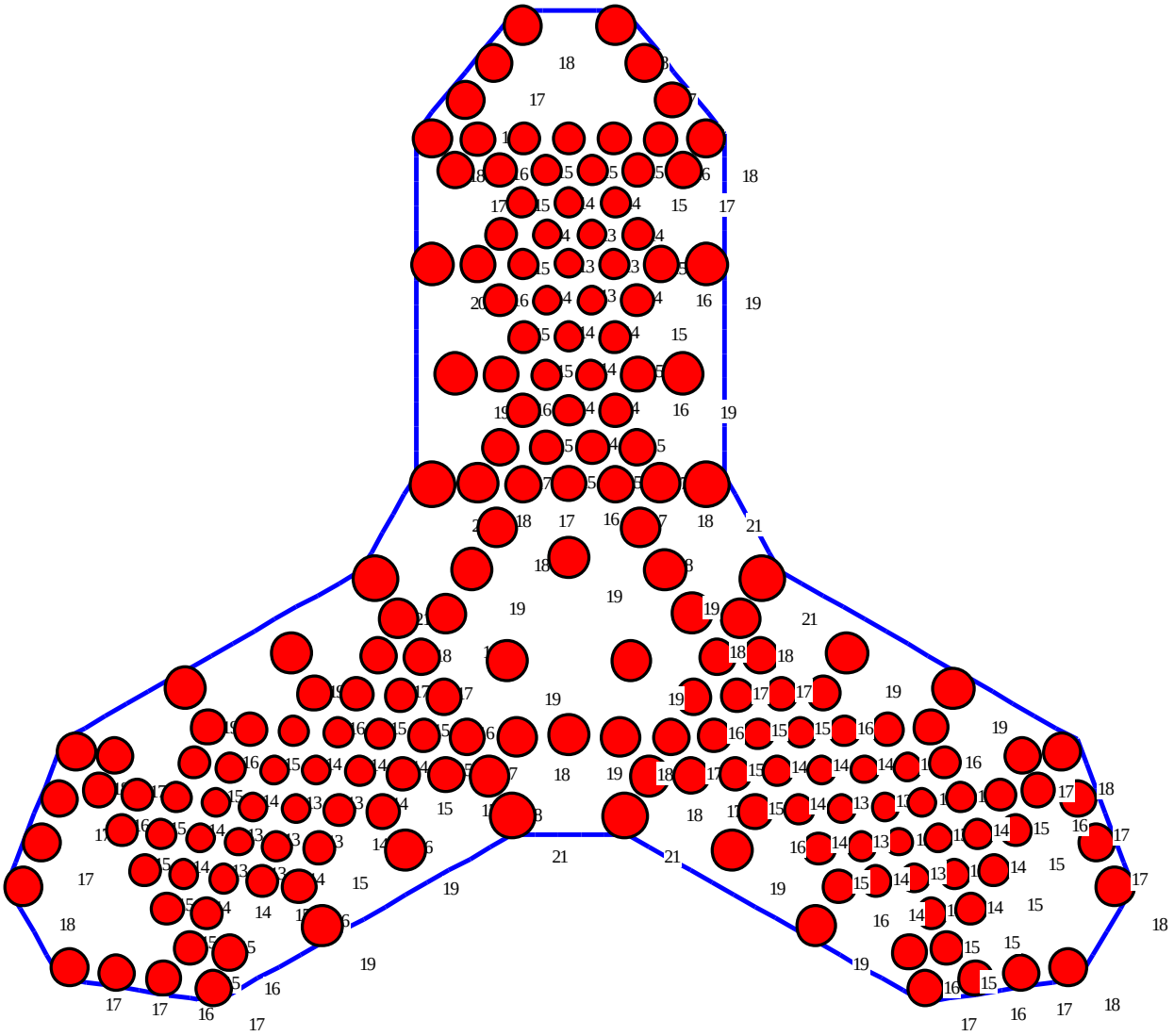

Figure 7-15 Pile load [MN] using the method "Hyperbolic Function for Load-Settlement Curve"

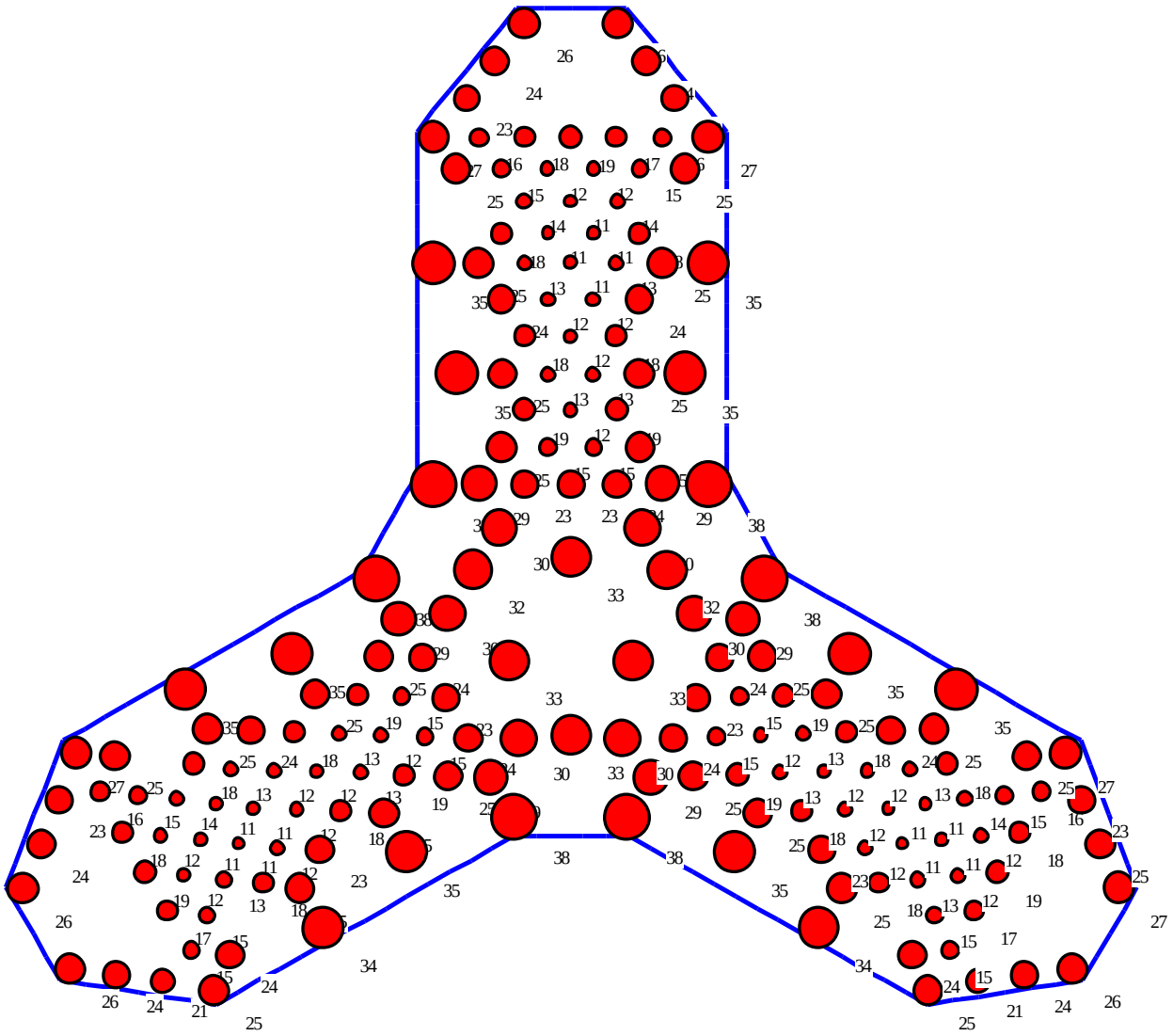

Figure 7-16 Pile load [MN] using the method "Given Load-Settlement Curve"

Table 7-4 Comparison between various calculated pile loads

| Method | $P_{max.}$ [MN] | $P_{min.}$ [MN] |
|---|---|---|
| FEA (*Poulos* and *Bunce* 2008) | 35 | 12-13 |
| *ELPLA* – Given Load-Settlement Curve | 38 | 11 |
| *ELPLA* – Hyperbolic Function for Load-Settlement Curve | 21 | 13 |

## 7.9 Conclusion

This case study shows that ELPLA is a practical tool for analyzing large piled raft problems in significantly lowered computational time.

## 7.10 References

[1] *El Gendy, M. / Hanisch, J./ Kany, M.* (2006): Empirische nichtlineare Berechnung von Kombinierten Pfahl-Plattengründungen.
Bautechnik 9/06

[2] *El Gendy, M.* (2007): Formulation of a composed coefficient technique for analyzing large piled raft. Scientific Bulletin, Faculty of Engineering, Ain Shams University, Cairo, Egypt. Vol. 42, No. 1, March 2007, pp. 29-56

[3] *El Gendy, M./ El Gendy, A.* (2018): Analysis of raft and piled raft by Program *ELPLA* GEOTEC Software Inc., Calgary AB, Canada.

[4] *Poulos, H. / Bunce, G.* (2008): Foundation Design for the Burj Khalifa, Dubai – the World's Tallest Building.
6th International Conference on Case Histories in Geotechnical Engineering, Arlington, VA, August 11-16, 2008.

[5] *Russo, G./ Abagnara, V./ Poulos, H. & Small, J.* (2013): Re-assessment of foundation settlements for the Burj Khalifa, Dubai. Acta Geotechnica (2013) 8:3–15.

[6] *Badelow, F./ Poulos, H.* (2016): Geotechnical foundation design for some of the world's tallest buildings.
The 15th Asian Regional Conference on Soil Mechanics and Geotechnical Engineering

**Case study 8**

# Analysis of Piled Raft of *Shanghai* Tower in Shanghai by the Program *ELPLA*

*M. El Gendy*
*A. El Gendy*
*O. El Gendy*

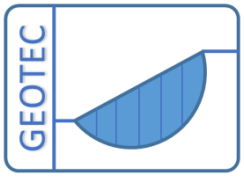



GEOTEC Software Inc.
PO Box 14001 Richmond Road PO, Calgary AB, Canada T3E 7Y7
Tele.:+1(587) 332-3323
geotec@geotecsoftware.com
www.geotecsoftware.com

**22-11-2018**

**Content**

Page

**8 Case study 8: *Shanghai* Tower piled raft ..... 3**

8.1 General ..... 3

8.2 Analysis of the piled raft ..... 5

8.3 FE-Net ..... 5

8.4 Loads ..... 6

8.5 Pile and raft material ..... 7

8.6 Load settlement curve ..... 8

8.7 Soil properties ..... 8

8.8 Results ..... 11

8.9 Measurements and other results ..... 16

8.9.1 Measured settlement ..... 16

8.9.2 Calculated final settlement ..... 16

8.10 Conclusion ..... 16

8.11 References ..... 17

# 8 Case study 8: *Shanghai* Tower piled raft

## 8.1 General

The *Shanghai* Tower is a mega tall skyscraper in Lujiazui, Pudong, Shanghai, Figure 8-1. It is considered the second-tallest building in the world after *Burj Khalifa*. The height of the tower is 632 meters. It consists of a 124-storey tower, a 7-storey podium and a 5-storey basement.

The tower has a 5-storey basement, and its foundation depth is 31.4 [m]. The thickness of the raft under the tower is 6 [m] and the area of the raft is 8945 [$m^2$]. The raft of *Shanghai* tower is supported by 955 bored piles with a diameter 1.0 [m]. The spacing between the piles is 3 [m] and the piles are distributed in different foundation arrangements where the entire raft area is divided into four sub areas *A*, *B*, *C* and *D* as shown in Figure 8-2. The length of the pile in area *A* is 56 [m], while the length of the pile in other zones is 52 [m].

Extensive studies with different calculation methods were carried out by *Sun etc. al.* (2011), *Xiao etc. Al.* (2011), *Tang* and *Zhao* (2014), (2014), *Su etc. al.* (2013), (2014) and *Zhao, X.* and *Liu, S.* (2017).

Figure 8-1 *Shanghai* Tower [1]

[1] https://upload.wikimedia.org/wikipedia/commons/3/32/Shanghai_Tower_2015.jpg

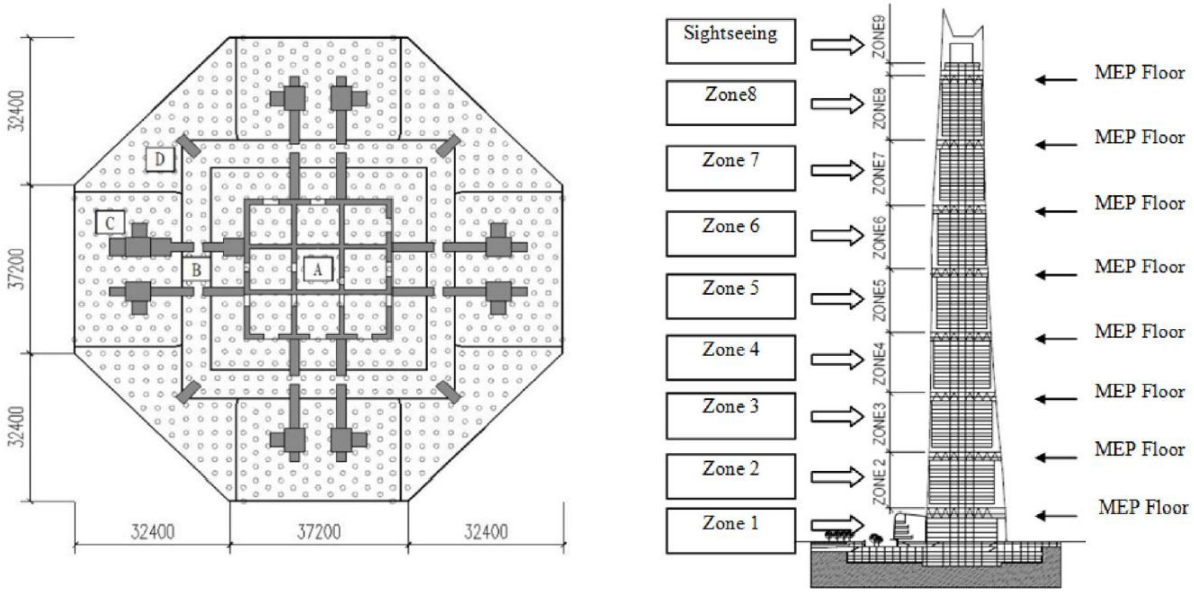


Figure 8-2 *Shanghai* Tower Foundation system and vertical zoning of the Tower (*Zhao, X.* and *Liu, S.* (2017))

## 8.2 Analysis of the piled raft

Using the available data and results of the *Shanghai* piled raft, which have been discussed in detail in the references, the nonlinear analysis of piled raft in *ELPLA* according to *El Gendy et al.* (2006) and *El Gendy* (2007) is evaluated and verified using the load-settlement relation of piles from the pile load test given by *Xiao etc. Al.* (2011).

For simplicity, the piled raft is considered double symmetric and only a quarter of the foundation system is analyzed. The foundation system is analyzed as an elastic raft supported on unequal rigid piles.

## 8.3 FE-Net

The raft is divided into triangular elements with a maximum length of 1.5 [m] as shown in Figure 8-3. Piles are divided into five elements with 14 [m] length.

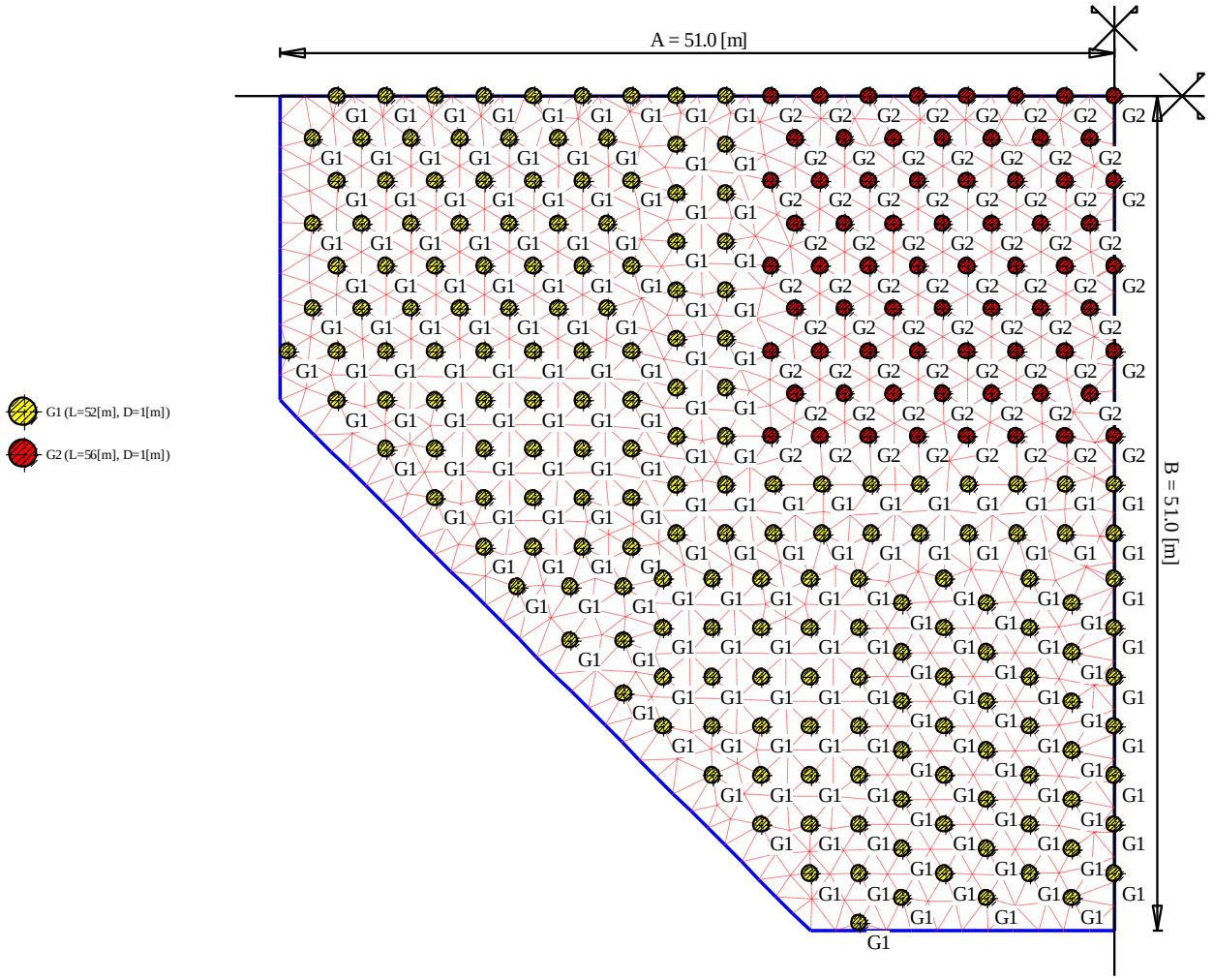


Figure 8-3 FE-mesh of *Shanghai* tower piled raft with piles

## 8.4 Loads

According to *Tang* and *Zhao* (2014), the tower foundation carries a total dead and live loads of 6710 [MN] and 963 [MN], respectively. The total vertical load used in calculating the settlement is 7672 [MN]. The column and wall sections and loads are listed in Table 8-1The system of loading acting on the piled raft is shown in Figure 8-4.

Table 8-1 Section and load of columns and walls

| | Section | Average load [MN] | Distributed load [MPa] |
|---|---|---|---|
| Horizontal super columns | 5.3×3.7[m] | 4×450.16 | 22.96 |
| Vertical super columns | 3.7×5.3[m] | 4×461.75 | 23.55 |
| Diagonal columns | 5.5×2.4[m] | 4×231.22 | 17.52 |
| Core walls | $t_{flange}$ = 1.2[m], $t_{web}$ = 0.9[m] | 3099.87 | 16.50 |

| | | | |
|---|---|---|---|
| Total load | | 7672.387 | |

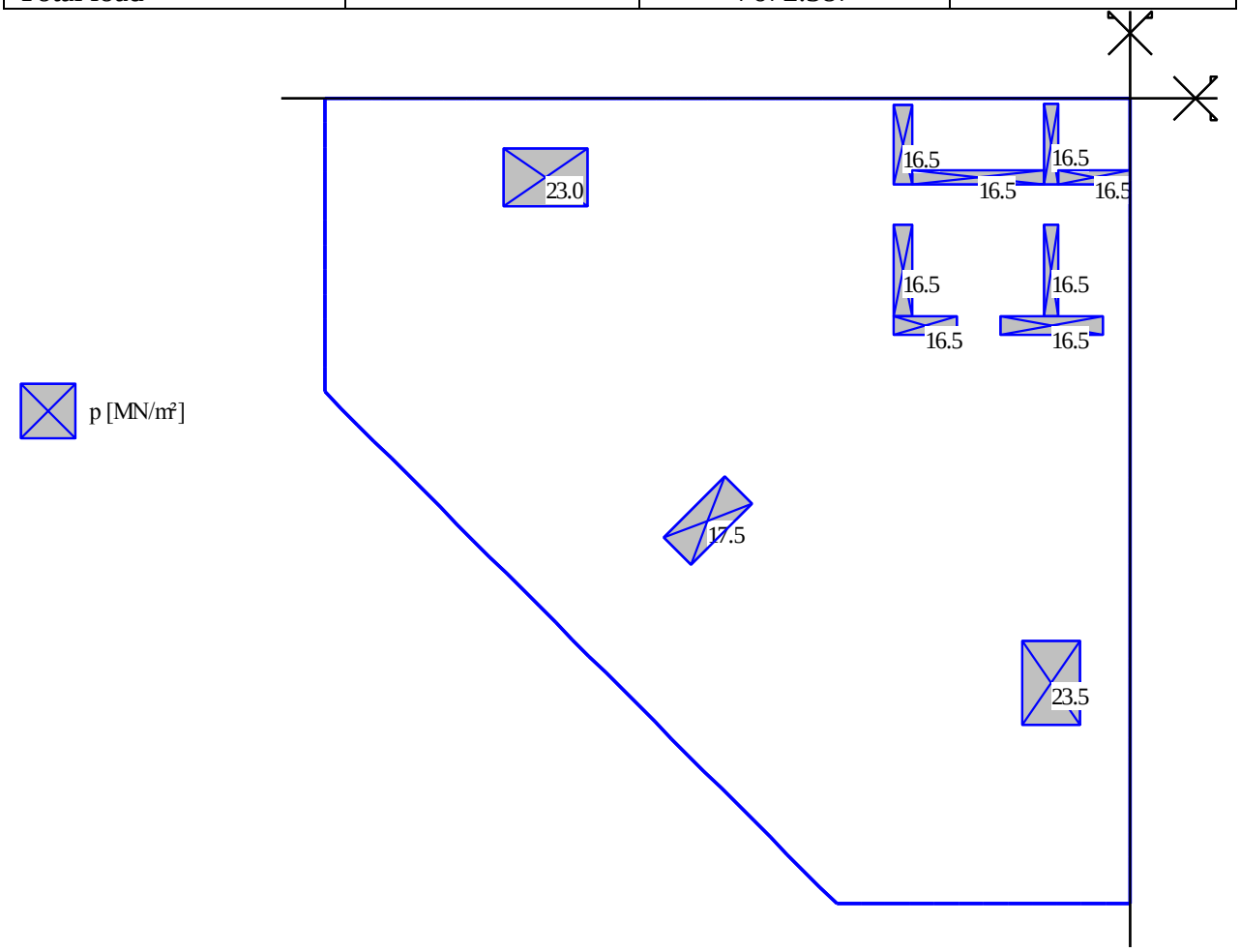


Figure 8-4 System of loading acting on the piled raft

## 8.5 Pile and raft material

The concrete grade of the raft and piles is C50. The following values were used as pile and raft material:

| | | | | |
|---|---|---|---|---|
| Modulus of elasticity | $E_p$ | = | 33234 | [MN/m$^2$] |
| *Poisson's ratio* | $\nu_p$ | = | 0.167 | [-] |
| Unit weight | $\gamma_b$ | = | 23.60 | [kN/m$^3$] |

## 8.6 Load settlement curve

Figure 8-5 shows the load-settlement relation resulted from the pile load test given by *Xiao etc. Al.* (2011).

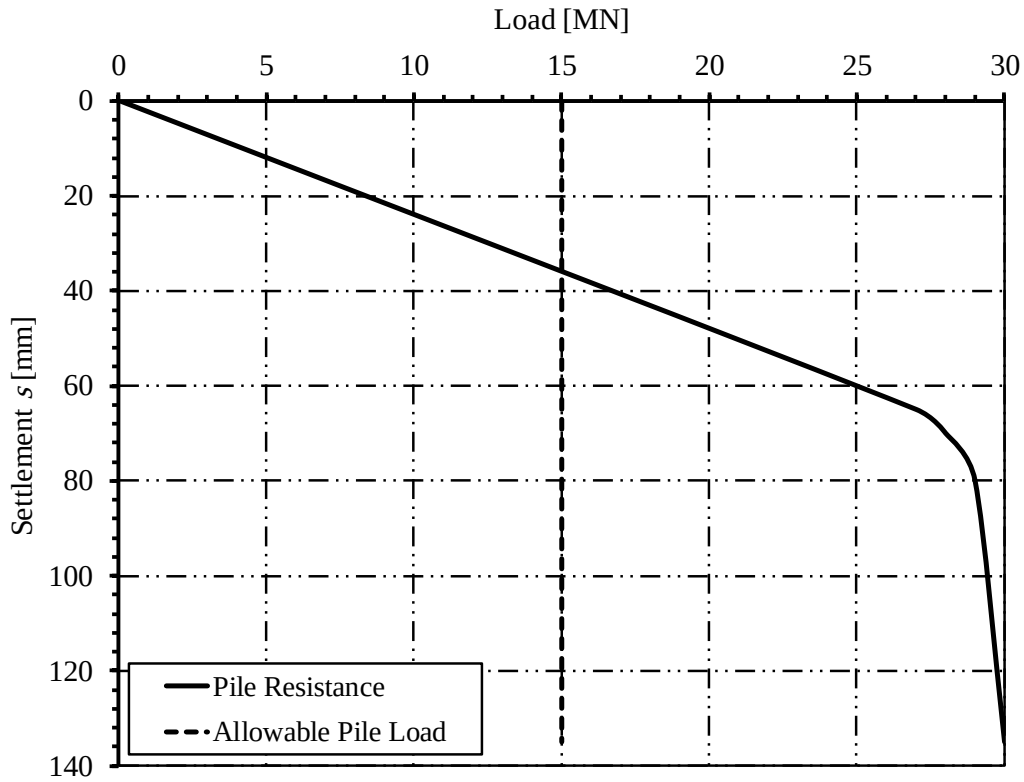


Figure 8-5 Load-settlement relation from pile load test

## 8.7 Soil properties

The site for the *Shanghai* Tower is in the new *Pudong* development district of Shanghai. The groundwater level is about 0.5~1.5 [m] below ground level. The foundation depth of the tower is 31.4 [m] below ground level.

Geotechnical investigation indicates that the ground conditions comprise horizontally stratified subsurface profile which is complex and highly variable. The subsoil below the ground level is composed of clay, silty clay and sand, underlain by a completely decomposed granite. According to the soil type and physical properties, the subsoil is divided into nine layers and fourteen sub-layers. The top layer is the bearing layer for shallow foundation while the fifth, seventh and ninth layers are the end-bearing layers for piles.

The soil profile and geotechnical parameters are summarized in Table 8-2. The subsoil layer under the raft up to 105 [m] deep are indicated in the boring log shown in Figure 8-6.

Table 8-2 Summary of geotechnical profile and parameters

| Strata | Sub-strata | Subsurface Material | Level at top of stratum $z$ [m] | Modulus of compressibility $E_s$ [MPa] | Bulk Density $\gamma_{Bulk}$ [kN/m$^3$] |
|---|---|---|---|---|---|
| 1 | | Fill | 4.5 | 0 | |
| 2 | | Plastic to soft-plastic silty clay | 2.7 | 3.97 | 18.4 |
| 3 | | Flow plastic muddy silty clay interspersed with sandy silt | 1.5 | 3.84 | 17.7 |
| 4 | | Flow plastic muddy clay | -3.0 | 2.27 | 16.7 |
| 5 | 1-a | Soft plastic clay | -11.5 | 3.56 | 17.6 |
| | 1-b | Soft plastic to plastic silty clay | -15.5 | 5.29 | 18.4 |
| 6 | | Hard plastic clay | -20.0 | 6.96 | 19.8 |
| 7 | 1 | Medium dense to dense silty sand with sandy silt | -24.0 | 11.45 | 18.7 |
| | 2 | Dense silty sand | -30.8 | 75 | 19.2 |
| | 3 | Dense silty sand with sandy silt and clay | -59.1 | 60 | 19.1 |
| 8 | | absent | | | |
| 9 | 1 | Dense sandy silt | -63.4 | 70 | 19.1 |
| | 2-1 | Dense silty sand with coarse and gravelly sand and clay | -71.7 | 80 | 20.2 |
| | 2t | Hard plastic to plastic silty clay with clayed silt | -82.7 | 35 | 20.0 |
| | 2-2 | Dense silty sand with fine sand and sandy silt | -84.0 | 85 | 19.3 |
| | 3 | Dense fine sand | -96.0 | 90 | 19.7 |
| | 3t | Hard plastic to plastic silty clay with clayed silt | -100.5 | 35 | 19.1 |

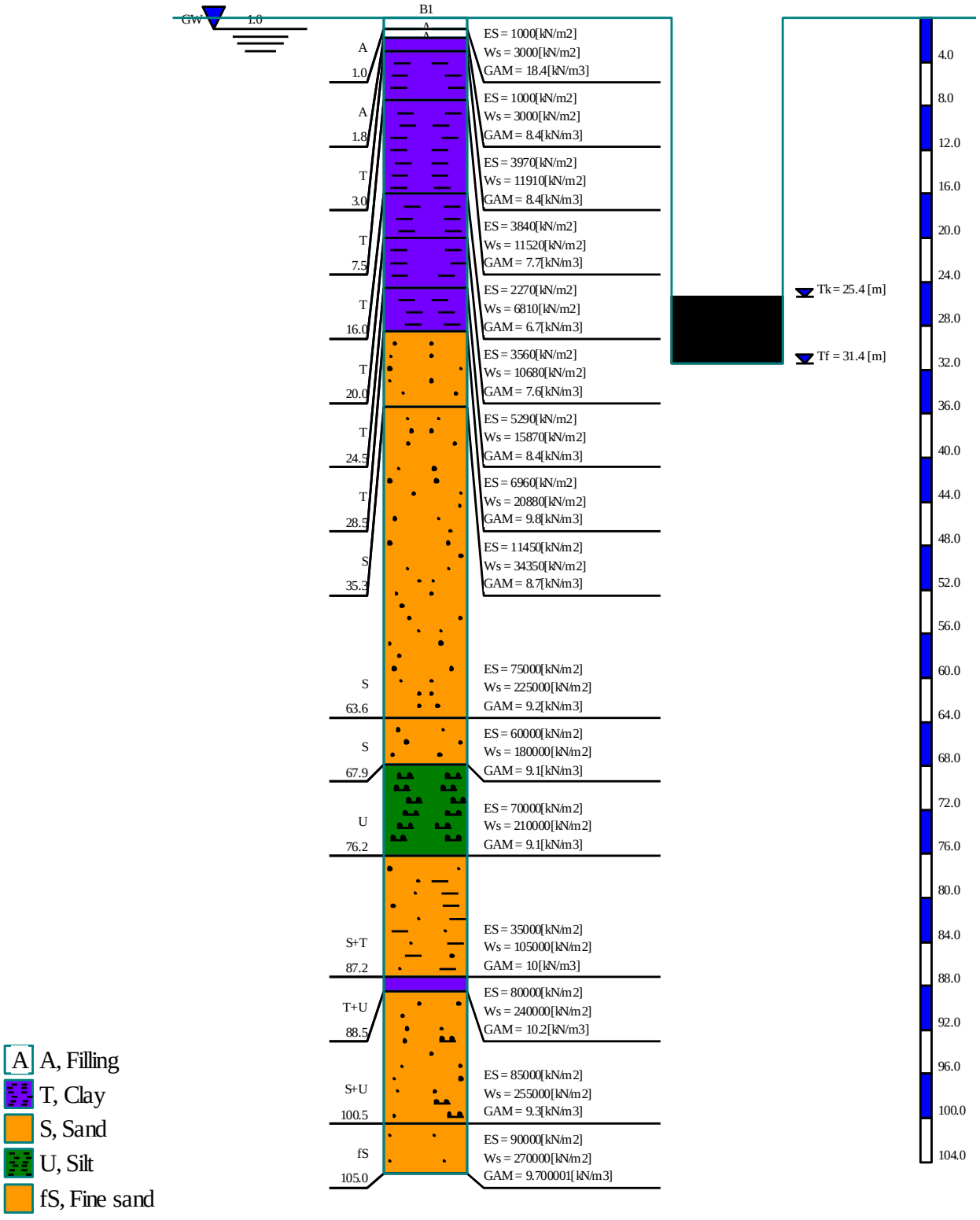


Figure 8-6 Boring log used in *ELPLA* analysis

## 8.8 Results

Figure 8-7 to Figure 8-11 show the settlement and pile reactions for the piled raft analyzed using the "Given load-settlement curve from pile load test" method.

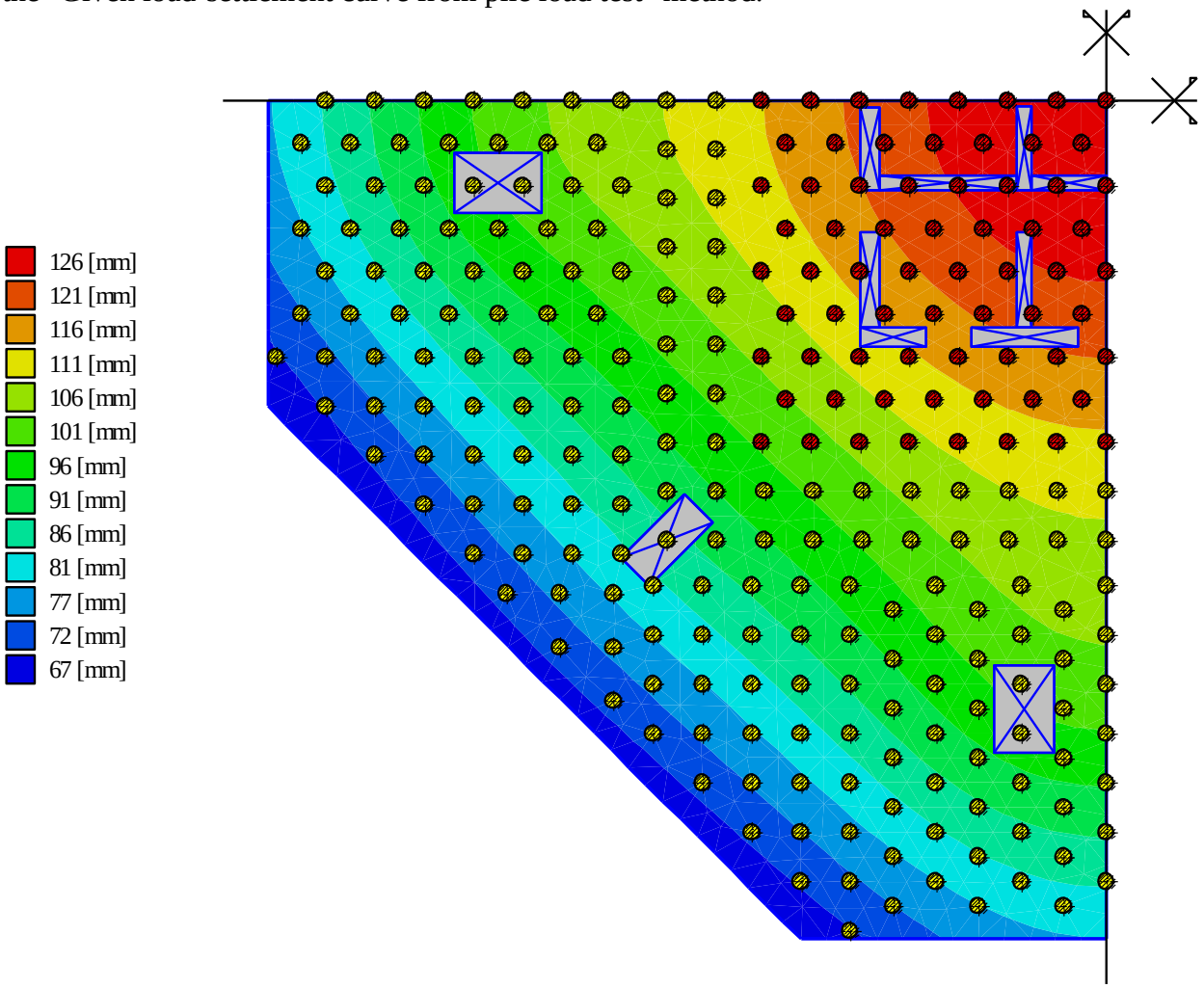


Figure 8-7 Settlement under the piled raft

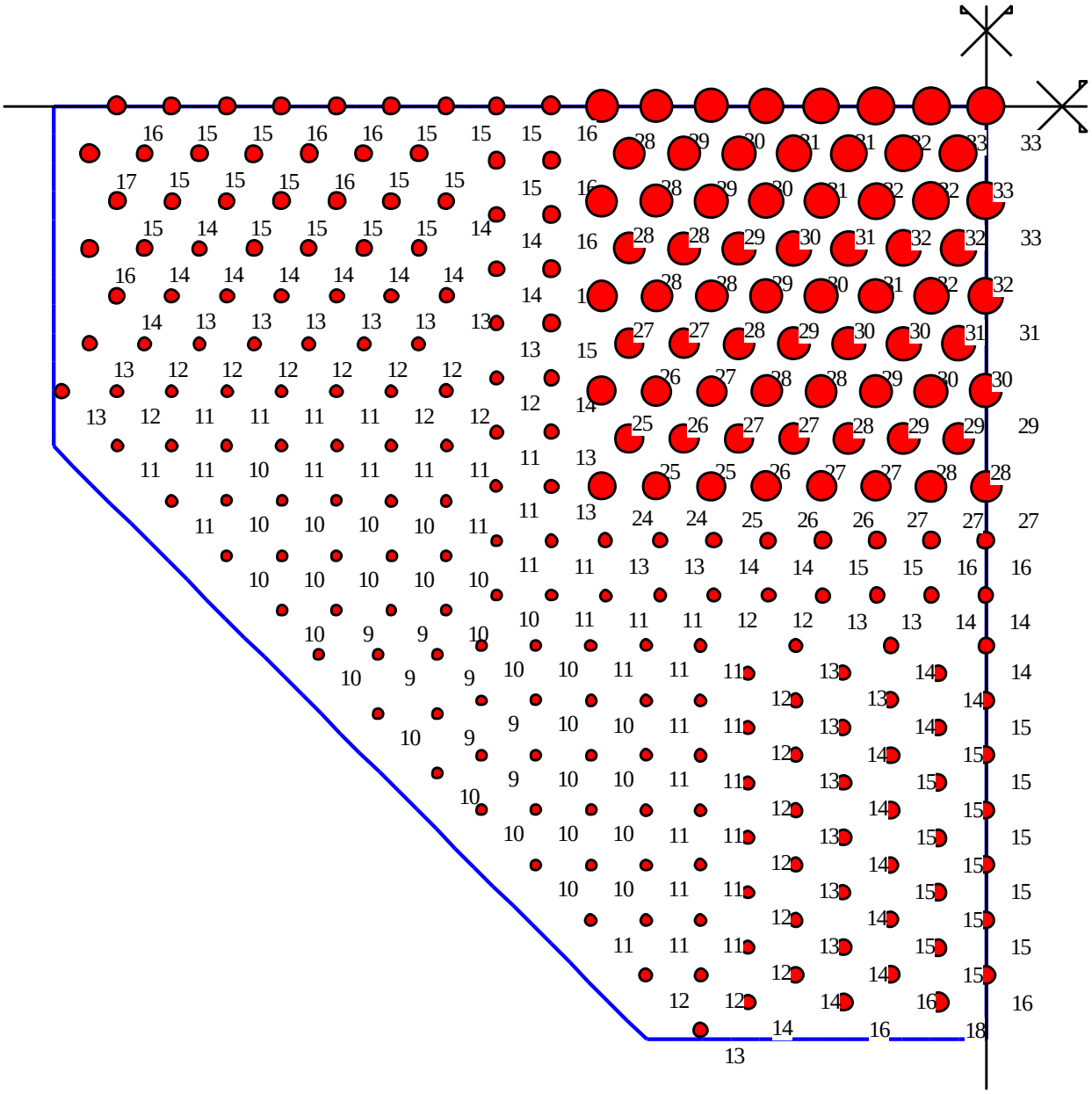

Figure 8-8 Self settlement of piles $S_v$ [mm]

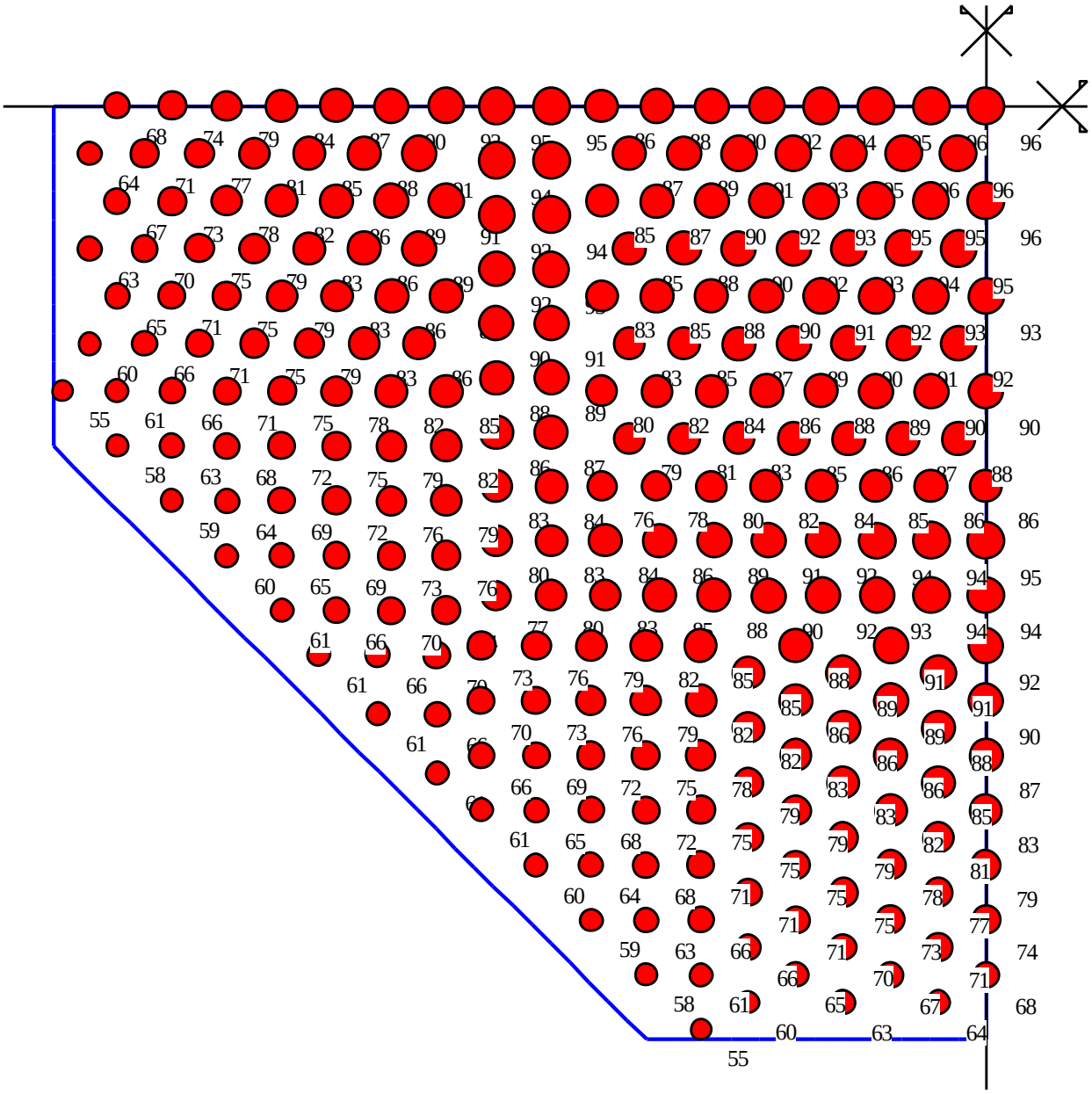

Figure 8-9 Interaction settlement of piles $S_{rv}$ [mm]

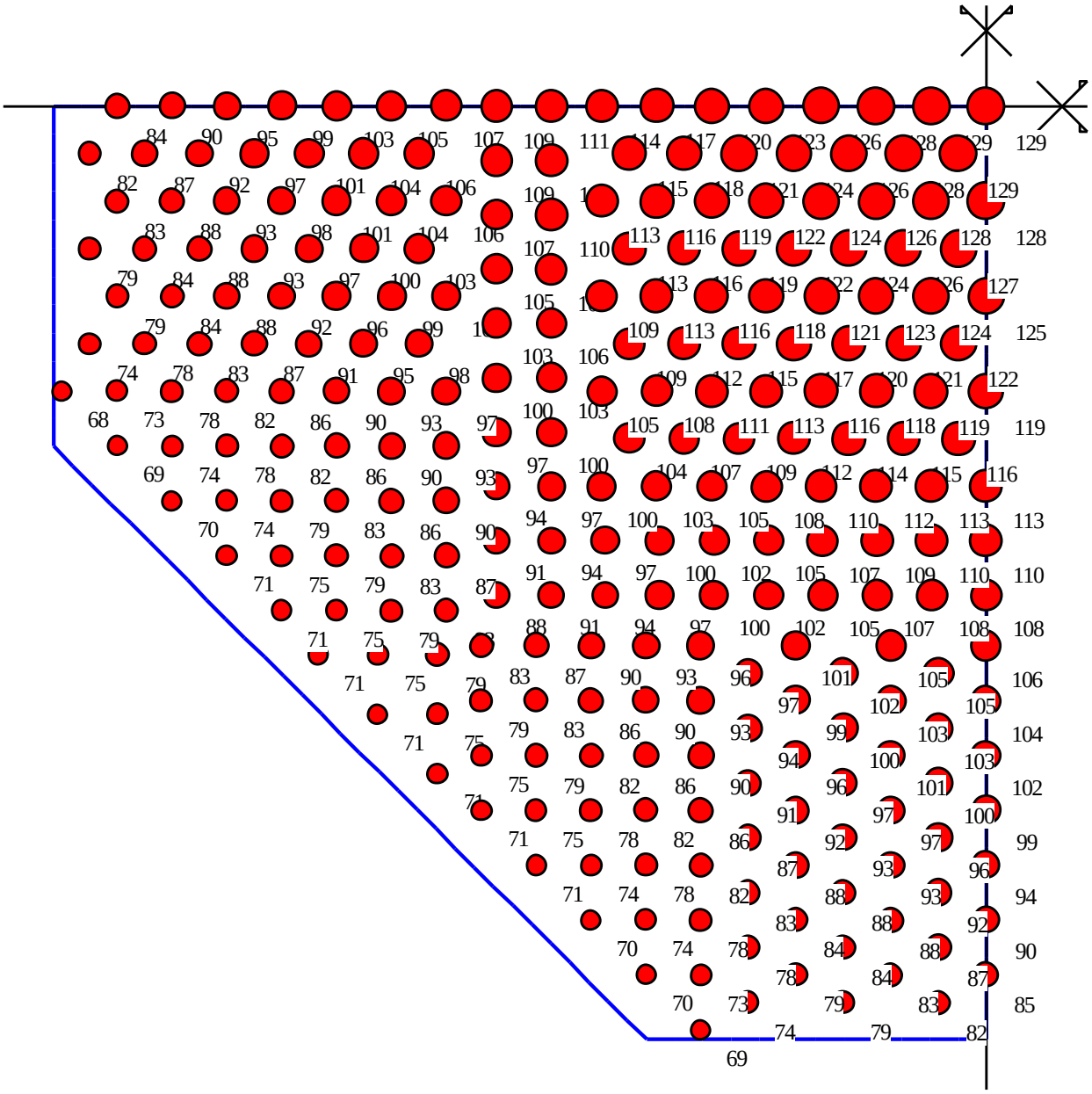

Figure 8-10 Total settlement of piles $S_r$ [mm]

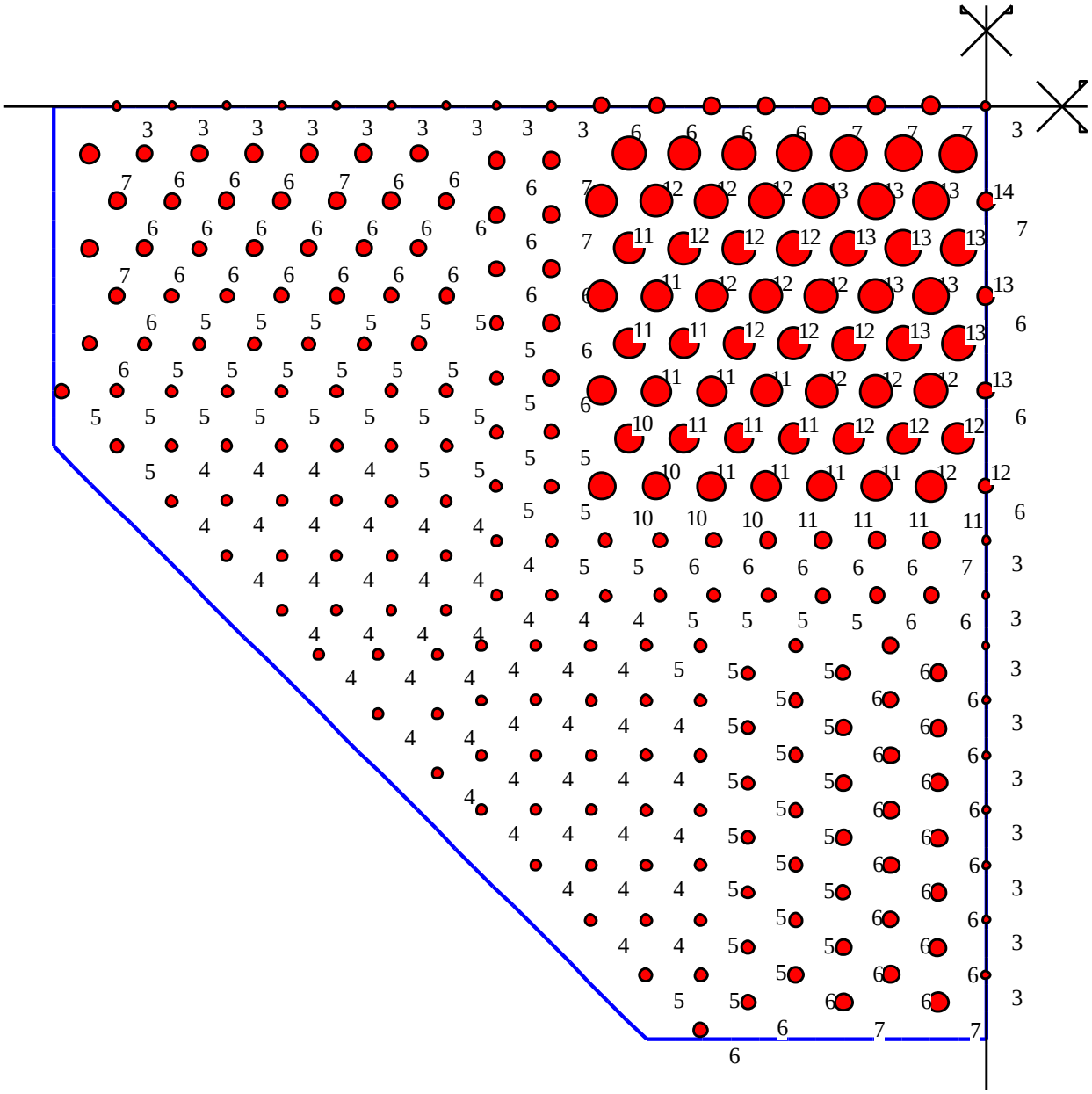

Figure 8-11 Pile reactions [MN]

## 8.9 Measurements and other results

### 8.9.1 Measured settlement

The construction of *Shanghai* started 29 November 2008 and finished on 6 September 2014. According to *Su etc. al.* (2014), the settlement of the core and mega columns reached 60 and 45 [mm], respectively; on 30 April 2013 under nearly 75% of the building load. As expected, these values are less than the computed values because it doesn't consider the long term settlement due to the consolidation of the clay layers. The soil below the tower will continue to consolidate until reaching the final settlement therefore calculation methods need to take consolidation effect into account.

### 8.9.2 Calculated final settlement

Several analyses were used to assess the response of the foundation for the *Shanghai* Tower. According to *Sun etc. al.* (2011), the computed values of maximum settlement ranges between 101 and 143 [mm].

A comparison between the computed settlement obtained by *ELPLA* and that obtained by other methods is presented in Table 8-3.

Table 8-3 Comparison between *ELPLA* results and those of other methods

| Method | $S_{max.}$ [mm] | $S_{min.}$ [mm] | $S_{Diff.}$ [mm] |
|---|---|---|---|
| *ELPLA* | 129 | 64 | 65 |
| *Xiao etc. al.* (2011) - Computed | 143 | 44 | 99 |
| *Xiao etc. al.* (2011) - Predicted | 112 | 68 | 44 |
| *Tang and Zhao* (2014) - Hybrid Method | 107 | 90 | 17 |
| *Tang and Zhao* (2014) - Empirical Formula | 121 | - | - |
| *Tang and Zhao* (2014) - Predicted Method | >120 | - | - |
| *Sun etc. al.* (2011) - Computed | 101 | 37 | 64 |

## 8.10 Conclusion

This case study shows that ELPLA is a practical tool for analyzing large piled raft problems in significantly lowered computational time.

## 8.11 References


[1] *El Gendy, M.* (2007): Formulation of a composed coefficient technique for analyzing large piled raft. Scientific Bulletin, Faculty of Engineering, Ain Shams University, Cairo, Egypt. Vol. 42, No. 1, March 2007, pp. 29-56

[2] *El Gendy, M./ El Gendy, A.* (2018): Analysis of raft and piled raft by Program *ELPLA* GEOTEC Software Inc., Calgary AB, Canada.

[3] *El Gendy, M./ Hanisch, J./ Kany, M.* (2006): Empirische nichtlineare Berechnung von Kombinierten Pfahl-Plattengründungen Bautechnik 9/06.

[4] *Su, J./ Xia, Y./ Xu, Y./ Zhao, X./ Zhang, Q.* (2014): Settlement Monitoring of a Supertall Building Using the Kalman Filtering Technique and Forward Construction Stage Analysis. Advances in Structural Engineering Vol. 17 No. 6 2014.

[5] *Su, J.Z./ Xia, Y./ Chen, L./ Zhao, X./ Zhang, Q.L./ Xu, Y.L./ Ding, J.M./ Xiong, H.B./ Ma, R.J./ Lv, X.L./ Chen, A.R.* (2013): Long-term structural performance monitoring system for the Shanghai Tower. Journal of Civil Structural Health Monitoring, Vol. 3, No. 1, pp. 49–61.

[6] *Sun, H.H./ Zhao, X./ Li, X.P./ Ding, J.M./ Zhou, Y.* (2011): Performance analysis of basement fin wall of the Shanghai tower based on the interaction between pile-raft foundation and superstructure. Procedia Engineering, Vol. 14, pp. 1367–1375.

[7] *Tang, Y. J/ Zhao, X. H.* (2014): 121-story Shanghai Center Tower foundation re-analysis using a compensated pile foundation theory. Structural Design of Tall and Special Buildings 23: 854–879.

[8] *Tang, Y. J/ Zhao, X. H.* (2014): Deformation of compensated piled raft foundations with deep embedment in super-tall buildings of Shanghai. Struct. Design Tall Spec. Build. (2014).

[9] *Xiao, J. H/ Chao, S./ Zhao, X.H.* (2011): Foundation design for Shanghai Center Tower. Advanced Materials Research 248–249: 2802–2810.

[10] *Zhao, X./ Liu, S.* (2017): Foundation Differential Settlement Included Time-dependent Elevation Control for Super Tall Structures. International Journal of High-Rise Buildings March 2017, Vol 6, No 1, 83-89.